Summer 2024

Optimization of Fire Emergency Preparedness in Underground Mining Environments: An Agent-Based Evacuation Approach

Oluwafemi Babatunde Salami
Missouri University of Science and Technology

Department: Mining Engineering

OPTIMIZATION OF FIRE EMERGENCY PREPAREDNESS IN UNDERGROUND MINING ENVIRONMENTS: AN AGENT-BASED EVACUATION APPROACH

by

OLUWAFEMI BABATUNDE SALAMI

A DISSERTATION

Presented to the Graduate Faculty of the

MISSOURI UNIVERSITY OF SCIENCE AND TECHNOLOGY

In Partial Fulfillment of the Requirements for the Degree

DOCTOR OF PHILOSOPHY

in

MINING ENGINEERING

2024

Approved by:

Dr. Guang Xu, Advisor
Dr. Lana Alagha
Dr. Catherine Johnson
Dr. Liming Yuan
Dr. Ashish Ranjan Kumar

PUBLICATION DISSERTATION OPTION

This dissertation consists of the following four articles, formatted in the style used by the Missouri University of Science and Technology:

Paper I, found on pages 9–77, has been published in *Process Safety and Environmental Protection Journal*.

Paper II, found on pages 78–122, has been published in *Process Safety and Environmental Protection Journal*.

Paper III, found on pages 123–171, has been submitted for publication to *Tunneling and Underground Space Technology Journal.*

Paper IV, found on pages 172–215, is intended for submission to *Tunneling and Underground Space Technology Journal.*

ABSTRACT

Underground mining environments present a complex interplay of thermal and non-thermal hazards, with fires constituting a significant risk due to the release of heat smoke from incomplete combustion. The propagation of these hazards through the ventilation networks underscores the critical need for understanding fire scenarios and their interaction with the underground environment. Existing knowledge regarding past mine fire disasters, and quantification of associated hazards and risks are insufficient for optimizing emergency evacuation strategies in the event of an underground fire emergency.

This research endeavors to bridge this gap by developing advanced quantitative risk assessment and evacuation models tailored specifically for underground mine fires. The primary goal of this work is to establish a robust integrated system for evaluating and optimizing emergency evacuation strategies by leveraging the capabilities of computational fluid dynamics (CFD) and agent-based model (ABM) simulations.

Furthermore, this study aims to investigate critical factors that significantly influence fire safety and emergency preparedness in underground mining environments. By identifying these critical factors, this work seeks to optimize the management of emergency evacuation plans, offering an enhanced fire safety solutions for underground mining environments.

ACKNOWLEDGMENTS

First and foremost, I am grateful to God for the grace to complete this study. Indeed, it was a journey more of perseverance, and faith than intelligence or brilliance. Secondly, I am deeply appreciative of the writing skills my advisor thought me. I have always believed that education is about brilliance, passing examinations, and solving complex mathematical problems. Dr. Xu changed my perspective, and I am glad he introduced me to academic writing, and I will forever be grateful for that. Additionally, I want to thank him immensely for providing me with the funding to embark on this program, and for his prompt responses throughout my PhD journey.

Also, I would also like to thank myself for the humility and courage to finish this program. My PhD journey was a great test of my humility and endurance, and I am glad I came, saw, and conquered.

One of the main reasons I endured this program is because of my former students. They go everywhere and speak about my intelligence and brilliance. If I ever thought of quitting, I will most likely have to continue because of them. I am immensely thankful for their “hype”, encouraging comments, as well as there well wishes. This dissertation is dedicated to them.

Moreso, I would like to also acknowledge all my committee members for their invaluable advice and criticism during my comprehensive examination to improve this work. Finally, I am deeply grateful for my family and friends for their support and best wishes throughout this program. They endured my unavailability without complaints, and I most appreciative of their unconditional love and moral support.

TABLE OF CONTENTS

LIST OF ILLUSTRATIONS

SECTION Page

LIST OF TABLES

1. INTRODUCTION

1.1. PROBLEM STATEMENT

Fire disasters remain one of the leading disasters in underground mines. They occur mainly due to the presence of combustible fuels underground mines (Tang et al., 2021). They pose a serious threat to underground mine workers and efforts to eliminate the occurrence of fire in mining environments are still far from realization. Fires in underground mines have been a leading historical cause of mass fatalities in the mining industry (Stewart, 2021; Tang et al., 2021). Data from the literature indicate that about 177 fire accidents occurred in the USA mines between 2009 and 2018 (Tang et al., 2021). The most recent mine fire happened in September 2022 at a Utah mine and caused no injuries but lasted for weeks. Additionally, report from the National Institute of Occupational Safety and Health (NIOSH) on mine disasters showed that fire accidents are the second most rampant mine accidents in terms of fatalities in US mines (NIOSH, 2021a). Although there were more fatalities due to explosion accidents, most explosions eventually resulted in fires. The threat of mine fires is not restricted to US mines; similar concerns have also been reported in Australia and China (Hansen, 2018; Zhu et al., 2019). In Australia, for instance, a total of 128 fires were reported in underground metalliferous mines between 2008-2012 (Hansen, 2018). While in China, statistical analysis has shown that explosions and fires were the major disasters in underground coal mines (Zhu et al., 2019).

When fires occur in underground mines, heat and toxic gases are produced, which are then dispersed in confined spaces through the ventilation network (Zhou, 2009b). The dispersed smoke poses a major challenge to safe evacuation. Poor visibility due to smoke

makes evacuation more difficult. The limited number of evacuation routes constrained pathways, and the long-distance miners must navigate to reach a safe zone add to the complexity of any evacuation mission. According to studies, most of mine fire fatalities are brought on by the absorption of noxious fumes, principally carbon monoxide. (Oluwafemi Babatunde Salami, Guang Xu, et al., 2023; Zhou, 2009b). Thus, it is critical to understand how the evolution of fires and the mechanism of thermal plume dispersion characterize mine fire hazards.

Modeling and characterization of mine fire behavior are critical for effective fire monitoring and early warning, evacuation of personnel, rapid response, and successful firefighting. To date, CFD has been successfully applied in conjunction with experiments to evaluate fires hazards, fire suppression performance, and product of combustion dispersion in tunnels and underground mine drift with reasonable accuracy (Edwards & Hwang, 1999; Fernández-Alaiz, Castañón, et al., 2020b; Hwang & Edwards, 2001; Li & Chow, 2003; Yuan & Smith, 2015).

Even more recently, Agent-Based Modeling (ABMs) has gained much attention in mine fire research (Edrisi et al., 2021; Nguyen et al., 2013; Tan et al., 2015). In a study, Li et al (Li et al., 2015), developed an agent-based cellular automata model that could intuitively describe the spatial-temporal development process of a fire source ignition and smoke spread in an underground mine fire disaster and the model was verified in an underground mine. This type of simulation approach exhibited superiority over traditional ventilation network fire simulation techniques in that it could visualize the hazard area and the extent of the hazard in the fire disaster can be obtained. Another advantage of the ABMs

is that they could mimic occupants' evacuation from fires when coupled with CFD fire models such as Fire Dynamic Simulator (FDS).

Most of our knowledge on fire and toxic gases spread in underground mines environment is based on previous studies using straight tunnel fires or model scale tests which is a major setback to fully glimpse fire evolution in real underground mines. By using model scale tests, it is impossible to preserve all the dimensionless terms derived by the scaling theory (Li & Ingason, 2012). The thermal properties of the material used for building the model scale tunnel is another factor that may influence the temperature and heat transfer and some studies have evaluated that using different insulating materials such as Promatect, concrete, rock, and fiber has a significant effect on maximum temperature obtained from tunnel fires (Li & Ingason, 2012). The heat transfer of rock was found to be higher than other non-metal tunnel walls. Also, the generation of toxic carbon monoxide (CO) and the mechanism of thermal plume spread has been neglected in most tunnel fire studies. However, this is very important to know in underground mines environment as it is the chief cause of miners' fatalities. Although some researchers have developed evacuation models for buildings and transport tunnels (Hu et al., 2012; Hu et al., 2014; Erica D Kuligowski, 2008; Mossberg et al., 2021b; Poon, 1994; Shen, 2005; Yuan, Fang, Yin, Lo, et al., 2009), analogous studies for underground mines are only at their preliminary stage due to the complexity and ever-changing nature of the mining environments. In addition, current evacuation strategies are based on static evacuation plans. This evacuation method only offers a rigid evacuation path and does not consider changes in the topology of the evacuation network or changes in the evacuation path caused by hazard dynamics. Hence, there is a need to develop a robust evacuation model for underground fire

emergency planning. The proposed evacuation model should take into consideration the mine configuration (i.e., the geometrical parameters), fire field data (mainly the heat release rate, smoke spread behavior, flame characteristics, and nature of fuel), behavioral rules governing miners' evacuation such as miners' age, sex, education, and experience, and finally the agent population which in this case is the number of miners expected to be underground. This can be achieved by direct coupling of fire dynamics simulation with agent-based evacuation models such as pathfinder.

1.2. OBJECTIVE OF THE STUDY

The objective of this work is to develop a quantitative risk assessment evacuation model for underground mine fire that takes full advantage of CFD simulations and evacuation modeling. This was achieved by establishing an integrated underground fire emergency evacuation evaluation and optimization system that will inform how miners are trained and what interventions might help overcome barriers to safe self-escape from fire hazards. Full-scale underground mine fire experiments were conducted, and the results was used to calibrate the CFD models. Furthermore, an agent-based model was developed for evaluating and optimizing the emergency evacuation plans in the event of a mine fire. The model used the CFD results as environmental inputs to represent the actual fire dynamics a mine worker would encounter in the event of a mine fire. Through this integrated approach, the developed system could evaluate the impact of critical factors that could substantially increase fire safety, thus optimizing the management of emergency evacuation plans. The framework of this research is depicted in Figure 1.1.

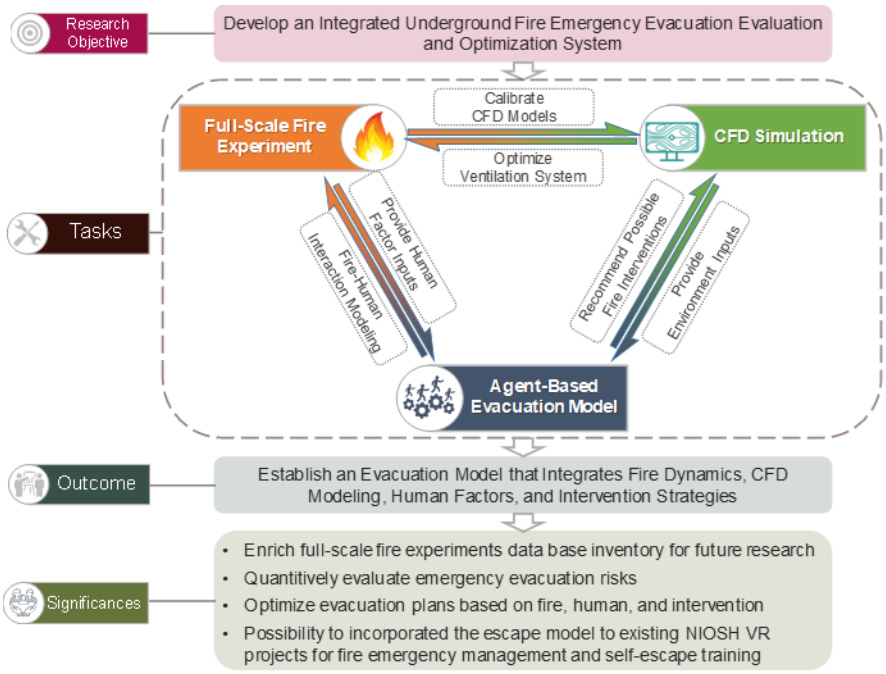

Figure 1.1. Project flow chart

1.3. SCOPE OF WORK

The scope of this study is summarized as follow:

1) Full-scale investigation of underground mine fires

The objective of this task is to investigate the interactive influence of ventilation conditions induced by ceiling smoke extraction and fire size on temperature attenuation, maximum excess gas temperature, and toxic gas spread in an underground mine. Full-scale fire tests using different pool sizes (small, medium, and large) of diesel was performed in the drift of the experimental mine to evaluate the effect of varying ventilation conditions on temperature and toxic gases distribution.

2) Develop computational fluid dynamics (CFD) fire models and validate with experiment.

The objective of this task is to develop a CFD model for mine fire hazard quantification and risk assessment. Environmental factors from full-scale fire tests in sub-task 1 was used as input for the CFD models and the models' accuracy was evaluated using observed results of heat release rate (HRR), temperature, smoke evolution, and thermal plume spread from the experiments.

3) Establish an agent-based evacuation model that couples with CFD fire dynamics and miners' behavior during evacuation. The goal of this task is to develop an agent-based evacuation model (ABM) that integrates the result from the CFD fire simulation model completed in sub-task 2.

1.4. STRUCTURE OF THE DISSERTATION AND RESEARCH SIGNIFICANCE

As per the delineated research objectives, this dissertation focuses on four topics and consists of four papers. The four topics include: 1) A state of art review of current emergency evacuation strategies in underground mining environments and way forward (Paper I); 2) Full-scale experimental studies of mine fires to obtain fire-smoke temperature and toxic gas concentration (Paper II); 3) Numerical modeling of mine fire using computational fluid dynamics (CFD) (Paper III); and 4) Analysis of impact of fire and smoke on evacuation time of crew for improved emergency planning (Paper IV). The literature review is summarized in first papers and distributed in the introduction section of each paper.

In Paper I, a comprehensive review of mine fire hazards and mine fire disaster was presented, the existing techniques of mine fire studies and the available tools for mine fire numerical simulation, the current methodology of developing evacuation plans in

underground mines was also presented. Furthermore, major research efforts that should be made in the future to develop an agent-based evacuation approach that incorporates fire-field parameters and human behavior into the evacuation model was proposed.

In Paper II, full-scale fire tests were carried out and empirical model of temperature attenuation were developed. Exiting model for maximum ceiling smoke temperature were analyzed and recommendations was made about selecting the appropriate model based on ventilation criteria. Suggestions and discussions regarding the determination of fire lame height was presented and the generation of toxic gases mainly carbon monoxide in the underground environment was presented as well.

Paper III examined an equipment fire scenario in an underground mine using computational fluid dynamics. The simulation results were verified using experiment and discussion about the impact of auxiliary ventilation on fire smoke stratification and smoke turbulence was presented. The study also investigated the impact of longitudinal ventilation velocity on smoke back flow due to fire in an underground development heading and recommendations were made for future design to improve safety protocols.

In Paper IV an agent-based evacuation model was developed to analyze the impact of fire smoke on evacuation time of crew. Fire smoke greatly impact visibility in the underground and in this study, a speed reduction factor based on the measured visibility was incorporated into the evacuation model to optimize evacuation efficiency.

The culmination of this study holds promise in significantly advancing emergency preparedness within underground mining environments. Its broader implications extend to enhancing our understanding of fire hazards and their quantification in various confined

underground spaces like subways, and tunnels. In conclusion, these insights promise to bolster emergency rescue preparedness, mitigating potential fatalities in underground mining environments.

PAPER

I. UNDERGROUND MINING FIRE HAZARDS AND OPTIMIZATION OF EMERGENCY EVACUATION STRATEGIES: THE ISSUES, EXISTING METHODOLOGY AND LIMITATIONS, AND WAY FORWARD

Salami O.B[a], Guang Xu[a]*Ashish Ranjan Kumar[b], Robert Ilango Pushparaj[a]

[a] Department of Mining and Explosives Engineering, Missouri University of Science and Technology, Rolla, Missouri, 65401, USA

[b] Department of Energy and Mineral Engineering, Penn State University Park, PA 16802, USA

ABSTRACT

Underground mine fires are associated with thermal and non-thermal hazards. Thermal hazards are primarily characterized by the release of heat into the underground confined space. The non-thermal hazards are noxious gases primarily carbon monoxide produced from incomplete combustion which may be circulated to other parts of the sub-surface environments through the ventilation network. Consequently, it is paramount to understand the interaction of possible fire scenarios and the underground ventilation system due to the hazards fire poses in such environments to design an appropriate emergency evacuation plan. This work aims to present a comprehensive review of the status of underground mine fire studies, techniques for emergency evacuation planning, the merits and limitations of the existing methods, the current best practices, and the way forward to develop an integrated smart solution for improved safety practices in underground environments. In addition, this study further identifies critical factors based on

experimental and numerical fire studies that could substantially improve fire safety and emergency preparedness in underground confined environments, thus optimizing the management of emergency evacuation plans in such environments.

Keywords: Underground Mines Fire Hazards, Computational Fluid Dynamics, Emergency Evacuation, Agent-Based Models, Smart Evacuation.

1. MINE FIRE DISASTER AND EVACUATION CHALLENGES

Mine fires have been a leading historical cause of mass fatalities in the mining industry (Stewart, 2021; Tang et al., 2021). They pose a serious threat to underground mine workers. Effective efforts to eliminate the potential of fires in a mining environment are still far from realization. Mine fires may occur from equipment leakages, tire fires, conveyor belt fires (Yuan & Smith, 2015), or oxidation and explosion in coal gobs (Xiang et al., 2021). Data from the literature show that about 177 fires occurred in the US mines between 2009 and 2018 (Tang et al., 2021). One of the most recent mine fires occurred in September 2022 at a Utah mine and caused no injuries but lasted for weeks (KSL.com, 2022). A report from the National Institute of Occupational Safety and Health (NIOSH) on mine disasters showed that fire accidents are the second most rampant mine accidents in terms of fatalities in all underground mines (including metals, non-metals, coal, and stone) in the US (NIOSH, 2021a). Mine fire accidents are not restricted just to the US mines; similar concerns have also been reported in Australia and China (Hansen, 2018; Zhu et al., 2019). In Australia, for instance, a total of 128 fires were reported in underground hard-rock mines between 2008-2012 (Hansen, 2018). While in China, statistical analysis has

shown that explosions and fires were the major disasters in underground coal mines (Zhu et al., 2019).

One of the major challenge miners faces during evacuation is caused by smoke roll-back. The event of smoke roll-back otherwise called back-layering, as shown in Figure1, can pose a serious challenge to safe evacuation (Zhou, 2009a). Back-layering occurs when smoke and hot combustion products that were created close to the tunnel ceiling flow against the ventilation stream. This circumstance arises when the airflow velocity is below the minimum (critical) velocity of airflow required to prevent smoke roll-back. The smoke roll-back could be catastrophic in underground mines because of its high toxicity, which might impair the miners while attempting self-escape (Fan et al., 2018; Lin & Chuah, 2008; Wu et al., 2018). Numerous studies have investigated smoke rollback length and have developed methodologies to combat it. The studies have demonstrated that a minimum ventilation velocity is critical to designing safe tunnels and underground systems (Fernández-Alaiz, Castañón, et al., 2020a; C. Hwang & J. Edwards, 2005; Ingason & Li, 2010; Tsai et al., 2010).

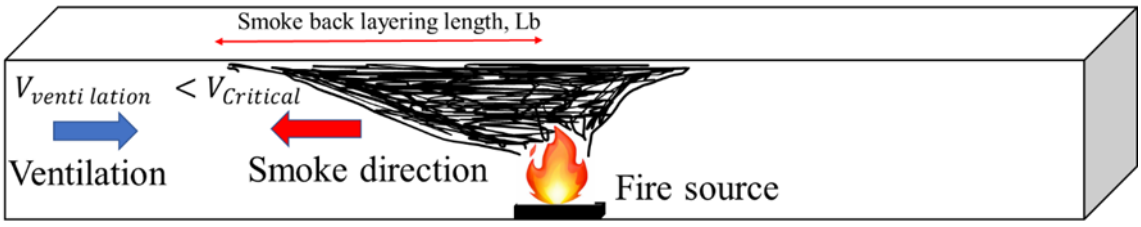

Figure 1. Schematic representation of smoke back-layering.

Poor preparedness is another major challenge that could significantly impact a safe and timely evacuation from underground fires (Brnich et al., 2010; Chasko et al., 2005; Conti, 2005; Jinzhang & Fengxiao, 2022; Onifade, 2021; Queensland-Government, 2022;

Singh et al., 2021). This may arise from human perspective preparedness such as the inability of miners to locate the emergency exit quickly, deploy appropriate PPEs, or due to poor stress management skills of the personnel and other unforeseen circumstances. On the other hand, it may arise from delays in facility preparedness such as the readiness of the egress system which includes the escape shaft, ventilation door, etc., or the overall response capability of the mine operators. Previous research has shown that severe fatalities occurred in underground mines due to the inability of the miners to find a self-escape route quickly which could prolong the evacuation time. According to a study (Brnich et al., 2010), the findings indicated that over 80 % of miners who lost their lives in a mine disaster survived the initial incidents but perished while trying to self-escape. It was observed that miners were not aware of the self-escape route and decided to make use of familiar but unsafe exit ways during a fire. A more recent survey conducted by another group of mine rescue services showed that more frequent preparation such as physical capacity tests, quarterly refresher tests, and training of miners about fire rescue skills could enhance mine rescue missions (Onifade et al., 2022). The complicated geometry and the limited numbers of evacuation routes, and the long-distance miners must navigate through to reach a safe zone are some other factors that could contribute to the complexity of any evacuation mission. For this reason, emergency preparation such as the Queensland level 1 mine emergency exercise which was adopted in Australia has continued to make preparedness the focal point to enhance self-escape in the yearly exercise that began in 1998 to date (Halim & Brune, 2019; Queensland-Government, 2022).

Therefore, it is imperative to prepare an emergency evacuation plan to reduce fatalities that may occur due to underground fire hazards. Such techniques could enable

miners self-escape during a fire accident as mine rescuers may sometimes be able unable to evacuate miners who are trapped in a refuge chamber (Halim & Brune, 2019). This can be achieved by developing an appropriate evacuation model. Such evacuation models incorporate the capability of evaluating an emergency evacuation process by computing the risk factor and the chances of a safe escape to the surface or underground refuge chambers. Although many works have illustrated how this alternative approach can be deployed in underground mines, the development of such practical and reliable self-escape models is nonetheless far from perfect. Several researchers have worked on the development of safe evacuation models for buildings and transport tunnels (Hu et al.; Hu et al., 2014; Erica D. Kuligowski, 2008; Mossberg et al., 2021a; Shen, 2005; Yuan, Fang, Yin, & Lo, 2009). They have demonstrated that developing an emergency plan before a disaster occurs is crucial to a successful evacuation. However, analogous studies for underground mines are only at their preliminary stage due to the complexity and dynamic nature of the mining environments.

This paper's goal is to present the status of experimental and numerical studies on underground fires to understand their hazards and give insight into ways to improve emergency evacuation planning. Figure 2 shows the structural flow chart of this paper. Firstly, we present an overview of mine fire disasters and the major causes of underground fire hazards. Then, the methods for fire studies using laboratory and full-scale experiments are presented, followed by the discussion of the quantification of major fire characteristics which includes the heat release rate (HRR), flame characteristics, and smoke spread behavior. The experimental findings provide inputs for fire simulation studies, which are presented in Section 5. The goal of experimental and numerical fire studies is to enable

more elaborate quantification of fire risk for dynamic reconstruction and visualization of underground fire scenarios, thereby helping to improve safe emergency planning. Finally, in Section 6 we addressed the merits and shortcomings of the existing methodologies for emergency evacuation planning and propose a robust agent-based approach. This paper is valuable in helping researchers and the mining/underground construction industry understand the onus of the available evacuation strategies and how they can be best applied to different underground fire hazard scenarios.

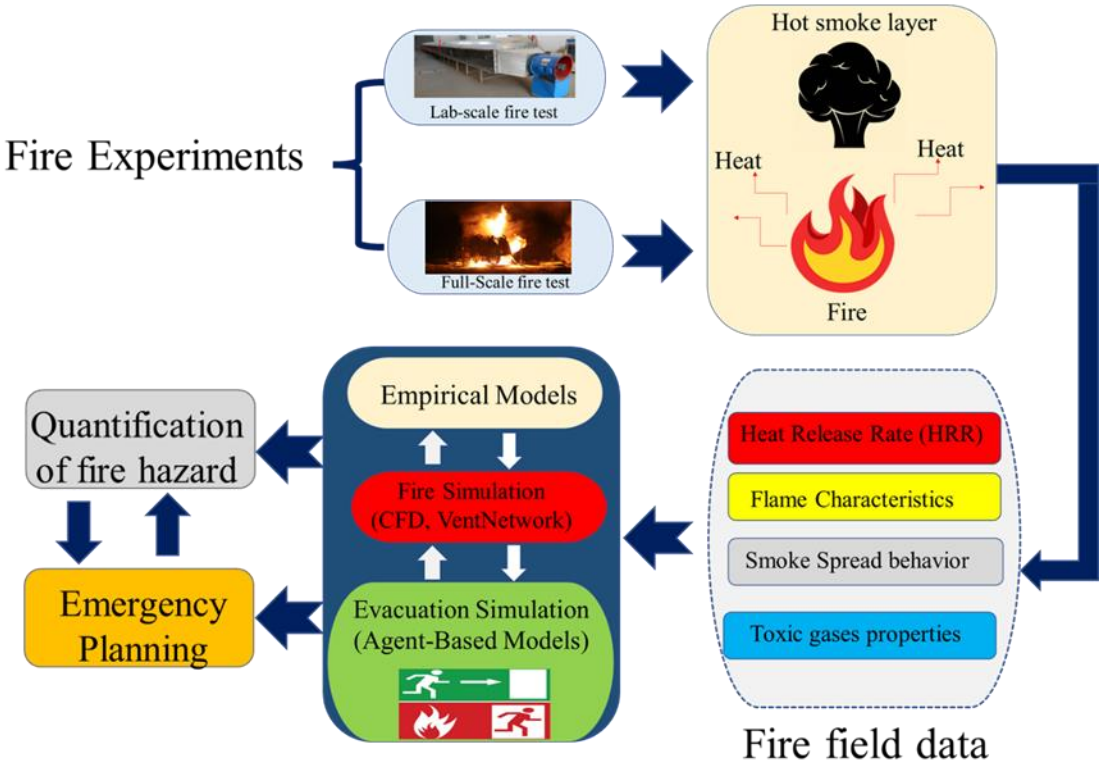

Figure 2. Graphical abstract of this study.

2. MINE FIRE EXPERIMENTAL STUDIES

Generally, experimental methods or numerical simulations are used for mine fire studies. Fire experiments could be conducted using laboratory models or reduced-scaled tunnels (Cheng et al., 2001; Ingason & Li, 2010), or full-scale fire experiments performed in real underground mines/tunnels (Hansen, 2019b; Hansen & Ingason, 2013a, 2013c).

2.1. OVERVIEW OF MINE FIRE STUDIES

In the US, the 1951 Orient Mine Disaster, which claimed the lives of 119 miners, caused the Bureau of Mines to conduct in-depth research on the fire resistance of cables, hydraulic fluids, and conveyor belts in other to assess the fire risks (Smith & Thimons, 2009). The Bureau produced an acceptance standard for conveyor belts in US mines in 1955 as a result, marking a notable advancement in the field. With the successful creation of the MFIRE ventilation code in the 1970s, mine fire research was furthered. By 1962, the Bureau of Mines had finished its first ventilation studies using the fluid network analyzer for contaminant dispersion. The NIOSH Lake Lynn Laboratory (LLL) started operations in 1980. By 1984, the facility had a fire gallery that enabled full-scale flammability testing of the mine conveyor belt. Mine fires study continued to experience tremendous growth in the 1990s. The Bureau of Mines created a software program that could evaluate the danger of spontaneous combustion in underground mining operations (Smith & Thimons, 2009). In 1995, the Bureau of mines was closed, and some of its functions were transferred to NIOSH. By 2001, NIOSH and the Mine Safety and Health Administration (MSHA) began a collaboration to further understand the characteristics of mine fires to identify the

capabilities as well as the limitations of the mine fire suppression technologies. Since then, NIOSH researchers and MSHA technical specialists have worked together on the science of mine fires, mine fire control, and suppression technology (Trevits et al., 2009).

2.2. LABORATORY EXPERIMENTS

The key parameters that characterize fire experiment classification are the pool size and the tunnel size. The size of the pool affects how fire behaves and how quickly heat is released. Studies have shown that the heat release rate (HRR) is linearly related to the pool size (Marková et al., 2020). Even though there is no generally acceptable classification of fire pools based on their sizes and earlier classification of fire pools was based on whether the fire is radiatively or convectively dominated, some researchers have tried to categorize fire pools with respect to the pool diameter. For instance, fires in pools of diameter < 0.2 m are generally classified as small pool fires while pool sizes of between 10.0 – 100.0 m are regarded as large pools for fire research (Steinhaus et al., 2007). Pool fires can be divided into three categories, according to Palacios et al. (Palacios et al., 2020): large-scale pools ($D \geq 1.0$ m), medium-scale pools ($0.1\ m \leq D < 1.0$ m), and small-scale pools ($D < 0.1$ m). Whereas another study defined pool diameters larger than 0.2 m as large pool fires (Babrauskas, 1983). In a different study, pool areas are used in defining pool sizes, with 10.0 m2, 25.0 m2, and 50.0 m2 considered as small, medium, and large pools respectively (R. O. Carvel et al., 2001).

Laboratory fire experiments are generally conducted in reduced-scale model tunnels which are usually made of fireproof materials, and as such could be limited to small or medium size pool fires. Typical instrumentation of a laboratory fire experiment and

thermocouple instrumentation for five measuring stations (S1-S5) separated 1.0 m apart is shown in Figure 3. The setup consists of two gas monitors denoted as G, and two monitoring cameras upstream and downstream of the fire to capture the real-time evolution of the fire in the tunnel. Sometimes, fire experiments are conducted under artificial ventilation conditions, while in other cases, they are conducted under free burn conditions. Stainless steel (Li et al., 2010) and transparent Promatect H board (Ingason & Li, 2010) are the popular materials used for tunnel construction. The size of the tunnel generally ranges from a few meters to about 100.0 m depending on the available facilities and experimental design. For instance, a previous study (Li et al., 2010), examined back-layering length and critical ventilation velocity using a 12.0 m long model stainless steel tunnel while a 10.0 m long model tunnel built for a laboratory experiment was used to investigate HRR and other fire characteristics under differing ventilation conditions in another similar study (Ingason & Li, 2010).

The Froude formulae is used to determine the corresponding value of the fire characteristics on a full-scale based on the results obtained from laboratory tests. Although these correlations have been widely used by many researchers, they are only theoretical calculations and still require a series of validation studies.

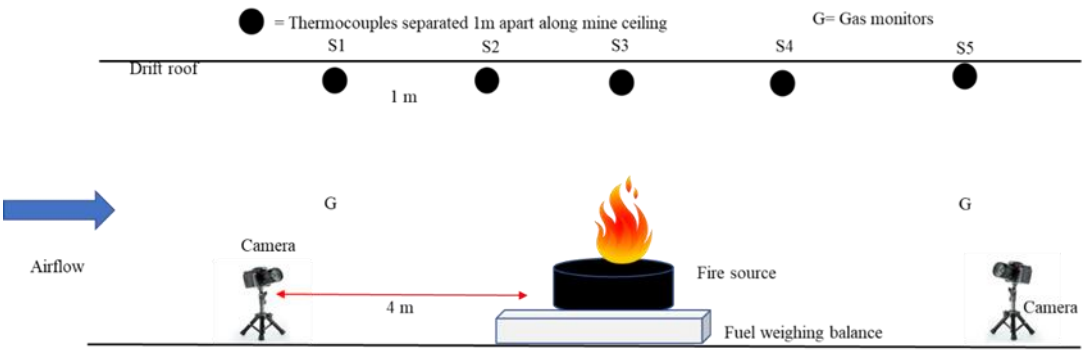

Figure 3. Typical instrumentation of laboratory fire experiments.

Table 1. Scaling correlation of laboratory and full-scale fire parameters

Parameter	Scaling correlation
Heat release rate (HRR), kW	$\dot{Q}_F = \dot{Q}_M \left(\frac{L_F}{L_M}\right)^{5/2}$
Velocity, m/s	$V_F = V_M \left(\frac{L_F}{L_M}\right)^{1/2}$
Time, s	$t_F = t_M \left(\frac{L_F}{L_M}\right)^{1/2}$
Energy, kJ	$E_F = E_M \left(\frac{L_F}{L_M}\right)^{3} \left(\frac{\Delta H_{c,M}}{\Delta H_{c,F}}\right)$
Mass, kg	$M_F = M_F \left(\frac{L_F}{L_M}\right)^{3}$
Temperature, k	$T_F = T_F$

Table 1 itemizes the scaling formulae used for determining the corresponding full-scale fire properties based on laboratory experiments. (In Table 1, L = length, Q = heat release rate, V = velocity, t = time, E = energy, M = mass, T = temperature while subscripts F and M denote full-scale values and model tunnel scale values respectively) (Chow et al., 2010; Ingason & Li, 2010b; Li et al., 2011; Oka & Atkinson, 1995).

2.3. FULL-SCALE FIRE EXPERIMENTS

On-site fire experiments are also called full-scale fire experiments. The experimental instrumentation for them is analogous to the laboratory setup presented in Figure 3. The major difference is that the experiments are conducted in the actual underground airways or tunnels (see Figure 4). They involve conducting real fire

experiments mostly by burning diesel, and gasoline pools, or sometimes burning abandoned/damaged machinery such as dozers or drilling machines in an underground mine. Experiments conducted in massive laboratories such as the NIOSH LLL that mimic real mining conditions could also be considered full-scale fire experiments. These kinds of tests are difficult to repeat due to their high expense and time requirements, yet they continue to be the most trustworthy method of validating current mine fire modeling software (Hansen, 2019b; Hansen & Ingason, 2013a).

Figure 4. A picture of full-scale fire tests in the Missouri S&T experimental mine.

Previous researchers have established the importance of performing full-scale experiments to evaluate and analyze simulation results from computer models produced from computational fluid dynamics (CFD) and ventilation network analysis. In a scenario, a full-scale fire study was conducted to investigate the CO spread in an underground mine, and the results were compared to verify MFIRE capability (Zhou et al., 2018). In the study, the simulated CO concentration was compared to the measured data at three different

locations in the NIOSH Safety Research Coal Mine (SRCM) laboratory, and findings from the study indicate that a full-scale experiment could help validate simulation models. Sometimes, conducting full-scale fire tests may be the only feasible solution because simulation tools such as CFD are only effective to model a portion of a mine and cannot accurately model complicated mine networks (Yuan et al., 2016).

Evaluation of fire characteristics and their effect on fire safety is also done using full-scale fire testing. In one investigation, a full-scale fire experiment that involved burning mining vehicles in an underground mine was carried out to examine how quickly various underground mining vehicles generate heat (Hansen, 2019b; Hansen & Ingason, 2013a). The fire tests involved an underground wheel loader unit and a drill rig. The drilling rig reached its maximum HRR of 29.4 MW after 21.0 minutes of combustion, while the wheel loader reached its maximum HRR of 15.9 MW about 11.0 minutes after ignition (Hansen & Ingason, 2013a). The study is important because the information gathered can be used for estimating the overall heat release rate of mining trucks. It could also be used to generate HRR curves for specific mining vehicles. The findings from the study remain a major milestone in the history of mine fire studies as the study is one of the few attempts to investigate the fire dynamics of burning mining vehicles in the underground. Some of the other important mine fire experimental studies that have significantly contributed to our knowledge of mine fire dynamics are presented in Table 2.

Table 2 A list of some important full-scale fire experimental studies on heat and POC spread.

Reference	Fire source	Location	Method of determination of HRR	Estimated HRR Value
(Newman, 1984)	Heptane Coal with Kerosene Neoprene (Conveyor belt) with coal and methanol	Not stated	Not stated	10.0 KW -20.0 MW
(Hansen & Ingason, 2013a)	UG wheel loader/LHD unit and development drilling rig (Jumbo)	Underground facilities of Björka Mineral AB on the outskirts of Sala, Sweden	Oxygen consumption calorimetry (OCC)	Peak heat = 15.9 MW for the loader, and = 29.4 MW for drilling rig
(Zhou et al., 2018)	Diesel pool and conveyor belt	Safety Research Coal Mine at NIOSH, USA	Fuel mass loss rate	Max of 90.0 kW for belt fire and 350.0 kW for diesel fire
(Laage & Yang, 1991)	Wood and diesel pool	Waldo Mines, USA	Convective heat flux	Max HRR=50KW for diesel. No report on HRR for wood.
(Cafaro & Bertola, 2010)	Gasoline pool	Colli Berici tunnel, Italy	Fuel mass loss rate	2 -4.5MW
(Lönnermark et al., 2012)	Commuter train	Brunsberg tunnel, Sweden	OCC	76.7 -77.4 MW
(Ingason et al., 2015)	Diesel pool and HGV trailer mock-up	Runehamar tunnel, Norway	OCC	66 – 202 MW
(Haack, 1998)	Vehicles (Passenger car, Bus, HGV, Railway coaches)	EUREKA Project (Repparfjord Tunnel, Norway)	OCC	3 – 100 MW
(Lemaire & Kenyon, 2006)	Fire pools (heptane and toluene) and vehicles	Second Benelux Tunnel, Netherlands	Mass loss rate	0 -25 MW

3. INFLUENCE OF IMPORTANT PARAMETERS FOR UNDERGROUND MINE FIRE HAZARDS STUDIES

3.1. IMPACTS OF VENTILATION

Ventilation is a critical factor that influences fire dynamics in confined spaces and may cause significant changes to the fire evolution and product of combustion spread (Beard et al., 1999; Hansen, 2019b). An earlier investigation (R. O. Carvel et al., 2001) to examine the effect of forced longitudinal ventilation on HRR for vehicle fires in tunnels using a Bayesian estimate affirmed this proposition. It was shown that a velocity of about 3.0 m/s may cause the fire size to increase by a factor of up to 5.0 if no mechanical ventilation is used for heavy goods vehicles (HGV) (R. Carvel et al., 2001). In a similar vein, increasing ventilation for large pool fires in tunnels or mine airways may increase the heat release rate by up to 50.0 % at a velocity of 10.0 m/s (R. Carvel et al., 2001). Small pool fires, on the other hand, show a stark difference. For small pool fires, increasing the ventilation will tend to reduce the size of the fire, and this may be attributed to the fact that small pool fires are fundamentally fuel-controlled (Beard et al., 1999; R. Carvel et al., 2001).

Generally, two major ventilation systems, namely the forcing and the exhausting are common in fire studies experiments. Although most laboratory investigations of fire behavior with longitudinal ventilation adopted the forcing ventilation technique (Beard et al., 1999; R. Carvel et al., 2001; R. O. Carvel et al., 2001), a few fire experiments used the exhausting ventilation system. Regardless of the ventilation system adopted, the goal is to prevent smoke back-layering by operating the fan to achieve air flows above the critical velocity (Beard et al., 1999; Kong et al., 2021; Tsai et al., 2010). Even though the primary

aim of longitudinal ventilation is to help prevent smoke roll-back, experiments have shown that certain increases in the longitudinal ventilation will only cause the fire to burn faster and increase the fire growth rate (Beard et al., 1999). Most fire experiments in mines and tunnels are designed based on the configuration and already existing situation in the mines, and only a limited adjustment can be made to the mine layout, thereby restricting the choices of fan selection for experimental purposes.

3.2. BACK-LAYERING LENGTH

Smoke back-layering is a non-thermal hazard from mine fires (Khan et al., 2016), and the extent of the back-layering length is another critical parameter for underground space/tunnel fire safety design. Numerous studies have shown strong dependence between ventilation velocity and back-layering length. The critical velocity on one hand has been proven to be dependent on the fire size and applying appropriate longitudinal ventilation could help mitigate the effect of smoke roll-back. In one case study of smoke control strategy in a confined space, a fire of about 4.0 MW was found to require a ventilation velocity up to 1.1 m/s to prevent back-layering (Deckers et al., 2013). Likewise, in another study involving a model tunnel (4.0 m long, 0.6 m wide, and 0.6 m high), with multiple fire sources, a velocity of 0.57 m/s was found to be critical for a 6.0 KW fire (Weng et al., 2015).

The size of the fire, the rate of heat release, the size of the mine drift, the placement of the fire, and the existence or absence of a smoke extraction point are other factors that affect the back-layering length. The combination of some or all these factors has led to the development of different empirical and numerical models for predicting smoke back-

layering length. In one of the studies, an analytical model for predicting smoke rollback was developed for a tunnel taking into account both longitudinal ventilation and point extraction ventilation (Wang et al., 2018). Their model considered both the mass flow rate of the smoke and the separation between the fire and the smoke vent. The HRR, the longitudinal velocity, the velocity at the exhaust, and the dimension (width and height) of the tunnel were also considered. The key findings from their studies indicate that minimizing the separation between the smoke vent and the fire could decrease the back-layering length and the effect becomes more pronounced for higher vent velocity.

Furthermore, the effect of tunnel inclination was modeled, and a new model to predict back-layering length for tilted tunnels was developed (Zhang et al., 2021). The study used a fire dynamic simulator (FDS) to simulate nine different tunnel slopes from 0.0 – 8.0 % to investigate smoke flow characteristics in the tilted tunnels under natural ventilation. It was observed that the length of the smoke back-layering in the downhill direction decreased with increasing tunnel slope. A similar study investigated a model tunnel with a 4.0 % slope and obtained analogous results (Kong et al., 2021). Their established model suggests that the dimensionless smoke rollback length is logarithmically related to the downstream length to the cubic power, and the predicted values agreed with the simulations' results for a tunnel slope of 3.5 – 7.5 %. In the same vein, a more robust model which incorporates the effect of the vertical shaft for inclined tunnels was developed by the Wan research group (Wan et al., 2019). The research attempted to unravel the phenomenon of plug-holing for tunnels with a slope from 5.0 - 25.0 % and the results indicated that plug-holing decreases as the slope of the drift increases. Summarily, back-layering lengths have been generally observed to show an exponential relationship with

tunnel slope for inclined tunnels (Kong et al., 2022), and numerous empirical models have been proposed to quantify back-layering length in underground mine drift/tunnels. From the critical review above, the existing models can be classified based on the parameters in Table 3.

Table 3 Classification of back-layering model based on tunnel configuration.

Parameter	Subclass	
Tunnel inclination	Horizontal	Inclined
Ventilation	Natural	Longitudinal
Smoke Exhaust shaft	Present	Absent

The most commonly used back-layering length model was developed by Li et al. (Li et al., 2010) for longitudinally ventilated tunnel and it is given by equation 1:

$$L_b{}^* = \begin{cases} 18.5\, In\left(0.81\, {Q^*}^{\frac{1}{3}} / V^*\right), Q^* \le 0.15 \\ 18.5 In\left(\frac{0.43}{V^*}\right), Q^* > 0.15 \end{cases} \quad (1)$$

While the slope effect for black layering can be expressed as shown in equation 2 (Kong et al., 2021; Oka et al., 2013).

$$\frac{L_b}{Q^{2/5}} = 3.18\theta^{-0.56} \quad (2)$$

Models for other scenarios of mine configuration and the location of the smoke extraction point can be derived by combining the above equations to measure the back-layering length. In the Runehamar tunnel fire tests for instance, the results show that smoke back-layering length could be up to 100 m or more for an HRR between 66 MW to 202

MW with a longitudinal ventilation velocity of about 2.0 m/s (Ingason et al., 2015). Another full-scale study involving a commuter train in a Swedish tunnel successfully measured the arrival time of smoke which could help to determine back-layering length due to fires in tunnels (Lönnermark et al., 2012). On the other hand, some other researchers have applied a numerical approach to measuring back-layering length. In one study, it was observed that the back-layering length could be up to 15.0 m in a 72.0 m long tunnel for HRR values between 40-160 KW, and longitudinal ventilation velocity of 0.2-0.8 m/s (Wu et al., 2018), while the observed back-layering length was about 9.0 m when the same tunnel configuration was used in another similar study where a ceiling smoke extraction system was present in the tunnel (Chen et al., 2015). Overall, the literature points out that the measured back-layering length depends on several factors principal of which are HRR, ventilation, and tunnel geometry.

3.3. IMPACTS OF COMBUSTIBLE MATERIALS

The nature of the combustible material is a crucial property that affects fire behavior. In most fire experimental studies, diesel and gasoline are the most used combustible materials (Babrauskas, 1983; Beard et al., 1999; Cafaro & Bertola, 2010; R. Carvel et al., 2001; Cheng et al., 2001; Chow et al., 2008; P. H. Thomas, 1963; Yuan et al., 2016; Zhang, 2012). Some extreme cases involve the burning of abandoned mining vehicles underground (Hansen & Ingason, 2013a; Li et al., 2010). Other materials have also been used including wooden cribs, belts, coal, etc. For instance, wooden cribs were used by Ingason and Li (Ingason & Li, 2010) in a series of twelve tests to examine the effect of longitudinal ventilation on tunnel fires. Another similar experimental study used

a heptane pool of diameter 0.35 - 0.70 m to investigate fire pool characteristics (Poulsen & Jomaas, 2012). Zhou et al. (Zhou et al., 2018) conducted fire tests for diesel pool cases and a belt to perform a validation study on the capability of MFIRE in modeling carbon monoxide for underground mine fires. In the study, a pan (32 in. by 44 in.) was used to burn 7.6 l (2.0 gal.) of diesel for the diesel test while the conveyor belt was cut into 48 pieces sized 7.6 cm × 7.6 cm for the conveyor fire test during the experiments.

4. FIRE CHARACTERISTICS AND CALCULATION PROCEDURES

After fire experiments are conducted, fire characteristics are further analyzed by the determination of some key factors. This section presents the methodologies used for such calculations and analyses.

4.1. HEAT RELEASE RATE (HRR)

The heat release rate is the most important parameter used to describe the behavior of fire and could be calculated by using different calorimetry methods or mass loss rate techniques (Brohez et al., 2000; Huggett, 1980; Khan et al., 2016; Tewarson, 1980). However, two major approaches have been mostly adopted for calculating HRR for mine fires. The first approach is based on oxygen consumption calorimetry (OCC) proposed by Hugget (Huggett, 1980) and has been adopted in a couple of fire research studies (Hansen & Ingason, 2013a). The OCC has been successfully adopted to measure HRR in mine fire experiments for both full-scale and small-scale experiments. This approach assumed that

the local gas temperature and the local gas concentration can be related as shown in equations 3 and 4.

$$\dot{Q} = \frac{13100 \times \rho_0 \times \mu_0 \times A \times (\frac{M_{O2}}{M_a}) \times (1 - X_{H_2O,0})}{\frac{0.1}{X_{O2,0}} + \frac{1 - X_{O2,avg} \times (\frac{X_{O2,avg}}{1 - X_{CO2,avg}})}{X_{O2,0} - (X_{O2,avg} \times (\frac{1 - X_{CO2,0}}{1 - X_{CO2,avg}}))}} \quad (3)$$

$$\mu_0 = \mu_{avg} \times \left(\frac{T_0}{T_{avg}}\right) \quad [m/s] \quad (4)$$

where T_0 is the ambient temperature [K], T_{avg} is the average temperature in a mine airway [K], A is the cross-sectional area [m^2], M_{O2} is the molecular weight of oxygen, and μ_0 represents the cold gas velocity in a mine airway [m/s] and μ_{avg} is the average longitudinal velocity in a mine drift [m/s]. The molecular weight of air is M_a. $X_{H2\ O,\ 0}$ represents the mole fraction of water in the surrounding air, $X_{O2,\ avg}$ represents the average oxygen content, and $X_{CO2,\ avg}$ represents the average carbon dioxide concentration. The mole fractions of oxygen and carbon dioxide in the surrounding air are $X_{O2,\ 0}$ and $X_{CO2,\ 0}$ respectively. The second technique of calculating the heat release rate is by measuring the changes in the mass of the fuel with the burning time (Zhang, 2012; Zhou et al., 2018). This technique is frequently used to measure the HRR in underground fire experimental studies. The mass loss rate is measured by using a digital scale that can continuously record the weight of fuel during the experiment. The HRR can then be calculated as given in Equation 5.

$$Q = m'' \Delta H_{c,eff} \left(1 - e^{-k\beta D}\right) \quad (5)$$

where D is the diameter of the burning area (in m), kβ is the empirical constant (in m^{-1}), and m" symbolizes the burning rate or mass loss rate per unit area per unit time ($kgm^{-2}s^{-1}$),

$\Delta H_{c,\,eff}$ represents the effective heat of combustion ($kJ.kg^{-1}$). Eliminating the element in parenthesis from the equation would simplify it further, and the HRR could be calculated from the mass loss rate of the combustion product as shown in (Yuan et al., 2016).

4.2. FLAME HEIGHT

(Bubbico et al., 2016; P. H. Thomas, 1963; Zhen & Xiaolin, 2014) describe the correlation that is most frequently employed to determine the height of the flame. The method calculates the flame height by using a relationship between the diameter of the pool and the fuel-burning rate.

Table 4. List of empirical correlations for flame height determination.

Reference	Empirical correlation	Definition of parameters
(Bubbico et al., 2016; Marková et al., 2020; P. H. Thomas, 1963; Zhen & Xiaolin, 2014)	$\frac{H}{D} = 42\left(\frac{m''}{\rho_a\sqrt{gD}}\right)^{0.61}$	H= flame height (m) D= pool diameter (m) m''= burning rate ($kgm^{-2}s^{-1}$) ρ_a= density of air (kg/m3) g=acceleration due to gravity (m/s2) Q= heat release rate. (kW)
(Marková et al., 2020)	$\frac{H}{D} = 0.235\frac{Q^{2/5}}{D} - 1.02$	
(Marková et al., 2020; Miao et al., 2014)	$\frac{H}{D} = 1.73 + 0.33D^{-1}$	

Other methods include a correlation developed by Heskestad in 1995 (Marková et al., 2020), which employs the relationship between the heat release rate and pool diameter while Miao et al. (Miao et al., 2014) developed an even simpler correlation that only

requires the pool diameter to determine the flame height. A list of the widely used correlation for determining the flame height is presented in Table 4. One may refer to (Lam & Weckman, 2015; Salvagni et al., 2019; Salvagni et al., 2020) for further reading on flame characteristics and determination.

4.3. FLAME LENGTH

The flame length could be defined as the horizontal distance from the center of the fire source to the flame tip (Ingason & Li, 2010). Only a few attempts have been made to determine an empirical correlation for flame length. The method that is frequently employed to determine flame length is based on the work of Rew and Deaves (Rew & Deaves, 1999). They primarily used information from the Channel Tunnel Fire in 1996, as well as findings from the HGV-EUREKA 499 fire test and the Memorial Tests. The empirical correlation derived is stated in equation 6 where Q and V denote the HRR and ventilation velocity respectively (Ingason & Li, 2010).

$$L_f = 20\left(\frac{Q}{120}\right)\left(\frac{V}{10}\right)^{-0.4} \tag{6}$$

Although the above equation is suitable to be applied in mine fire scenarios since most of the equipment in the underground are HGVs, however, this equation has a drawback in that it does not consider any geometrical parameter. This limitation makes it impossible to apply the correlation in predicting the flame length in other tunnels due to the different geometries of tunnels and fire sources associated with underground mines.

4.4. HEAT FLUX

According to (Ingason & Li, 2010; Ingason & Wickström, 2007), the heat flux to an object at a given position from fire in mines can be calculated from the equation given below:

(7)

$$q''_{inc} = \frac{\varepsilon_{PT} \times \sigma \times T_{PT}^4 + (h_{PT} + K_{cond}) \times (T_{PT} - T_0) + \rho_{st} \times c_{st} \times \delta \times \frac{\Delta T_{PT}}{\Delta t}}{\varepsilon_{PT}} \; [kW/m^2]$$

where σ is the Stefan-Boltzmann constant, 5.67·10-11 kW/m^2·K^4, ε_{PT} denotes the surface emissivity of the plate thermometer, which was estimated to be 0.8 (Hansen & Ingason, 2013a), T_0 is the temperature of the surrounding air[K], ρ_{st} denotes the density of steel assumed as 8100 kg/m^3, c_{st} represents the specific heat capacity of steel [J/kg·K], which was set to 460 J/kg·K, δ is the thickness of steel plate [m], given as 0.0007 m (Ingason & Wickström, 2007), and t is the time [s]. T_{PT} represents the temperature of the plate thermometer [K], h_{PT} is the coefficient of the plate thermometer for convective heat transfer, [W/m^2·K], which is given as 10.0 W/m^2·K (Ingason & Wickström, 2007), K_{cond} is a conduction correction factor [W/m^2·K], which was estimated to be 22.0 W/m^2·K (Hansen & Ingason, 2013a).

5. MINE FIRE SIMULATION AND HAZARD ANALYSIS METHODS

Mine fire simulation and hazard analysis techniques could be classified into three categories as shown in Figure 5: 1D mine ventilation network fire simulation,

computational fluid dynamics (CFD) fire simulation, and hybrid fire simulation that combines the above two methods (Vermesi et al., 2017).

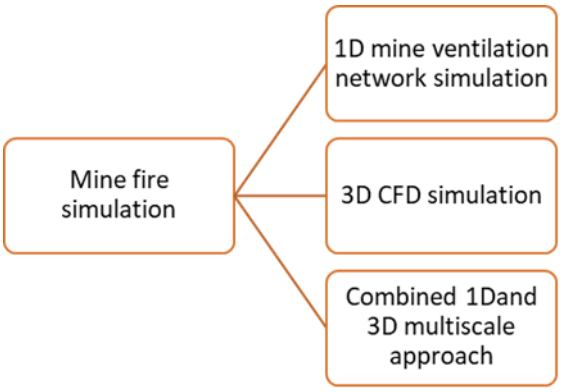

Figure 5. Classification of mine fire simulation technique.

5.1. 1 D MINE FIRE SIMULATION

Fires simulation using 1D ventilation networks such as MFIRE is well documented in the literature (Chang et al., 1990; Cheng et al., 2001; Hardy & Heasley, 2006; Laage & Yang, 1995; Zhou, 2009a; Zhou et al., 2016; Zhou et al., 2018).

Mine fires could be simulated using 1D mine ventilation network analysis tools. These tools are simple to use, quick to run and computationally inexpensive. The most popular 1D mine fire simulation package is the MFIRE program. Others include VnetPC and Ventsim. The MFIRE mine ventilation network analysis could be used to simulate fire accidents in underground mines (Cheng et al., 2001; Laage & Yang, 1995), and the development of analog computers in the 1950s and 60s led to a more robust analysis of mine ventilation network. Although, the first attempt to simulate the interaction between mine fires and ventilation network could be traced to (Greuer, 1977) and by 1981, a computer program that could solve mine fires and ventilation interaction problems using

steady-state analysis was developed (Laage & Yang, 1995; Zhou, 2009a). The program named MTU/BOM was developed by a group of researchers at the Michigan Technological University in conjunction with the U.S bureau of mines. Since the development of MFIRE, it has undergone several modifications, and the latest one is called MFIRE 2.30 which was later developed by (Zhou, 2009a).

The current version of MFIRE, MFIRE 2.30 is more sophisticated and has better predictive capability compared to the previous version developed. It introduced a t-squared fire model to account for the variability of the heat release rate of mine fires. In addition, it also accounted for the effect of smoke roll back and heat release from moving source such as the conveyor belt. Perhaps the greatest improvement of the MFIRE 2.30 was the recoding of the original MFIRE program in object-oriented C++. The previous version of the program was written in FORTRAN to run on a DOS environment, and it was in danger of being incompatible with the latest computers that run on the Windows Vista environment (Chang et al., 1990; Zhou et al., 2016; Zhou & Smith, 2012).

MFIRE could be used to plan for emergency evacuation in an event of a fire accident in underground mines. It could be used to predict the spread of carbon monoxide in an underground mine thereby helping in fire emergency planning (Yuan et al., 2016; Zhou et al., 2020). Carbon monoxide is a major threat to the life of miners in the underground and studies have validated that MFIRE could accurately predict the spread of carbon monoxide in underground mines (Yuan et al., 2016; Zhou et al., 2018). Aside from modeling CO spread in the mine, it could also be used to predict the peak temperatures and heat flow to air and rock with a single fixed heat input from a study conducted at Waldo mines (Laage & Yang, 1991). Furthermore, MFIRE could help predict the emergency

ventilation technique during a fire outbreak in the underground. (Cheng et al., 2001) employed MFIRE to simulate a hypothetical fire outbreak in the Taipei Mass Rapid Transit System (TMRTS) and proposed that a push–pull ventilation will efficiently exhaust the high-temperature air and smoke out of the underground facilities once the fire breaks out.

Recently, the Ventsim program has continued to gain popularity compared to MFIRE mainly because it possesses better visualization and modeling capabilities for underground mine ventilation analysis (Nematollahi Sarvestani et al., 2023). It is one of the best-selling mine ventilation software which has gained the trust and approval of mines operators, government representatives, researchers, and consultants in the mining industry (Duy Huy et al., 2022). Haghighat and Gillies (Haghighat & Gillies, 2015) applied Ventsim to study the fire and airflow behavior when a Bobcat vehicle is ignited at the working face of a mine. In their analysis, they were able to determine the concentration of CO gas at the closest station to the fire to be about 3000 ppm if all the ventilation fans were turned off. In addition, the investigation identified the most perilous part of the mine based on the fire scenario and this could aid future emergency preparedness. In another study by (Brakea et al., 2015), they analyzed the survivability criteria based on the toxic gas concentration, temperature, and visibility that could impede safe evacuation. They found out that the visibility, wet bulb temperature (WB), and dry bulb temperature (DBT) could significantly impact the survival chances of miners even if they wear the self-contained self-rescuer (SCSR) device.

Liang et al (Liang et al., 2018) employed Ventsim to examine the spontaneous combustion of coal in an underground coal mine. The study which sought to investigate the air leakage problem in the long-wall operated in multi-seam and under shallow cover

at the Bulianta colliery discovered that spontaneous combustion could be mitigated by isolating and pressurizing active long-wall panels. Additionally, the authors found that differential pressure in the colliery could be adjusted by varying the performance of the auxiliary fans and the resistance of the ventilation regulator. These recommendations were made for future field implementation in the Bulianta coal mine. Several other researchers have also used Ventsim for various mine ventilation and fire emergency planning. For example, (Stewart et al., 2015) examined the capability of Ventsim to simulate back-layering phenomena in mines by using a splitting algorithm to create a high-density three-dimensional mesh within the ventilation airway. Previously, (Wei et al., 2011) used Ventsim to design a ventilation management system for a deep underground mine by identifying areas of the mine with large resistance, thus making recommendations for effective management of airflow. Some other researchers have also employed Ventsim in the design and optimization of mine ventilation systems such as the simulation and analysis of multiple fire scenarios conducted by (Brakea et al., 2015), and the modeling of fires in an underground room-and-pillar mine by (Nematollahi Sarvestani et al., 2023).

However, despite the extensive work that has been done with Ventsim and other 1D network models such as MFIRE for mine fire evacuation planning, they are still faced with some major setbacks. One major shortcoming of this simulation is that it cannot be used to predict the behavior of smoke and heat in complex situations. 1D network analysis only considers airflow along one pathway between the ventilation network nodes thereby restricting the smoke, heat, and other product of combustion to one-directional flow which is not practical in real fire scenarios (Stewart et al., 2015). The spread of smoke and toxic gases generated creates a bi-directional flow in the mine or tunnel and may impede

firefighting or mine rescue missions. This limitation could be overcome by using CFD because CFD models are more accurate than 1D models and could predict the behavior of smoke and heat in complex tunnels.

5.2. COMPUTATIONAL FLUID DYNAMICS METHOD

The fact that CFD simulations produce more detailed data, such as airflow velocity, pressure, gas concentration, heat flux, temperature, etc., is one of the main benefits of CFD in mine fire safety (Yuan et al., 2016). Therefore, as compared to numerical 1D ventilation network simulation techniques, CFD fire models offer a deeper understanding of complex thermal gas flow and heat transfer concerns. The fire dynamic simulator (FDS), created by NIST primarily to address low-speed flows with a focus on heat and smoke transport from flames, is the most popular CFD software for mine fire research. Below is a discussion of some of the important parameters for CFD fire simulation.

5.2.1. Effect of Geometry and Obstructions. Experimental measurements and modeling predictions have indicated that blockage/obstructions can greatly influence the critical velocity and temperature distribution along the mine drift (Shafee & Yozgatligil, 2018). For instance, when there is a blockage or obstruction, the corresponding critical ventilation velocity decreases (Gannouni & Maad, 2015; Han et al., 2021; Lee & Tsai, 2012; Meng et al., 2018; Oka & Atkinson, 1995). The reduction is seen to rely on where the obstacles are located on the tunnel floor. When the gap between the obstacle's bottom and the tunnel floor widens, it becomes slightly larger. This phenomenon also accounts for the smaller back-layering length observed in tunnels with obstacles when compared to empty tunnels. In one study, three types of vehicular obstructions were used in a 7.0 m-

long tunnel. It was observed that the reduction ratio for the critical velocity approximately equals the vehicle blockage ratio (Lee & Tsai, 2012). Also, Huang et al. (Huang et al., 2018) demonstrated through numerical studies that sealing off the entrance of the tunnel is a good tactic for firefighting and improving safety. Because less oxygen is provided when the tunnel is sealed off, their tests demonstrated that the longitudinal ceiling temperature lowers as the tunnel entrance sealing ratio increases. A scenario involving a mine truck fire and miners using brattice obstruction to escape from the underground can be depicted in Figure 6.

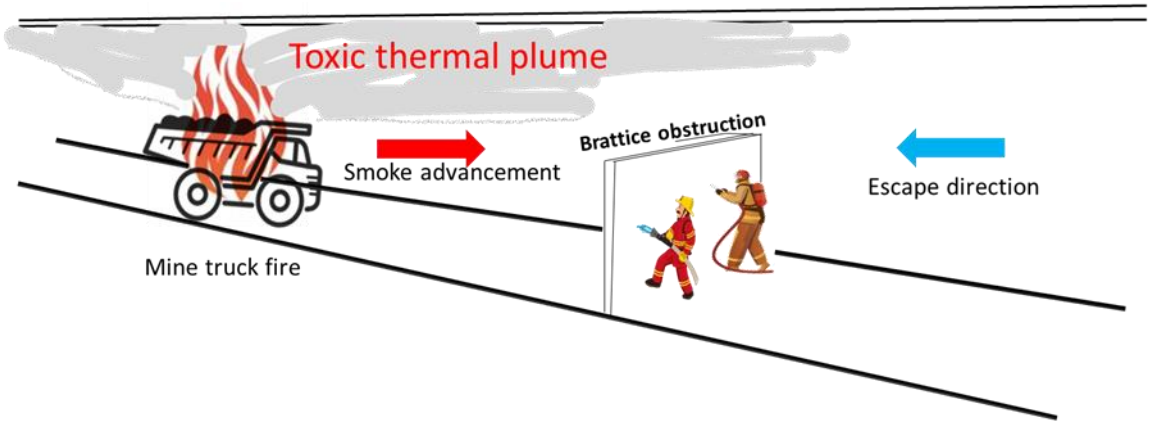

Figure 6. Miners using brattice obstruction for self-escape from fires.

Figure 6 shows a truck fire along an underground mine roadway and two miners approaching the fire with a brattice barrier in the escape direction. The movable brattice could be deployed to redirect the thermal plume toward the mine ceiling thus improving the escape chance. Some CFD studies have proven that using this technique could also reduce CO concentration and impede smoke arrival rate in underground spaces during an evacuation process. In one study, an obstruction in the form of a brattice barrier which occupies 70.0 % of a mine roadway reduced the CO concentration by up to 43.0 % and

increased the airway visibility by up to 30.0 % (Adjiski et al., 2016). Likewise, numerical results show that smoke arrival time significantly increased when obstruction existed in the tunnel. In the investigation, an obstacle occupying about 31.0 % of the tunnel cross-section placed at a different distance from the tunnel floor in a 12.0 m long tunnel effectively reduced back-layering length (Gannouni & Maad, 2015).

Similarly, Yu et al. (Yu et al., 2016) and Luo et al. (Luo et al., 2013) have demonstrated that obstructions like air curtains could help in the confinement of smoke by conducting CFD simulation and experimental studies of fire and smoke flow fields in a wind tunnel. In their study, Yu et al. (Yu et al., 2016) analyzed the performance of air curtains in blocking fire-induced smoke by using a momentum ratio parameter “R” to evaluate the sealing effectiveness “E” of the air curtains. For low values of R, it was discovered that the E increased as R increased. On the other hand, higher values of R result in reduced effectiveness since the smoke is pushed downstream by the downward impinging airflow. Similarly, experiments and simulation results showed that air curtains assisted in controlling the discharge and diffusion of smoke (Luo et al., 2013). This was revealed from the observation that the CO concentration at the entrance significantly decreases whenever the curtain is used. Therefore, we can conclude that an optimal evacuation plan could be improved when obstructions are properly utilized in specified locations in the underground operations (Adjiski & Despodov, 2020b).

5.2.2. Mesh Size. The mesh or grid size used for a CFD simulation may range from millimeters to a few centimeters depending on the size of the geometry, the desired modeling accuracy, and the level of detail to be obtained. It is the principal factor that determines the resolution of the CFD simulation and could impact properties like fire

smoke temperature measured at the airway ceiling. For this reason, appropriate grid sensitivity should be done to obtain mesh independence. In FDS, the grid size can be derived by the fire characteristic diameter given in Eq (8) (Weng et al., 2015):

$$D^* = \left(\frac{\dot{Q}}{\rho_\infty c_p T_\infty \sqrt{g}}\right)^{2/5} \quad (8)$$

where ρ_∞ designates the ambient air density kg/m^3, δx denotes the nominal size of the mesh cell, $\dot{Q}$ represents the total heat release rate of the fire (kW), C_p is the specific heat capacity of air (KJ/kg/k), T_∞ is the temperature (K) of the surrounding air, and g is the acceleration due to gravity (usually taken as 9.81 m/s^2) (McGrattan et al., 2016; Overholt, 2014).

The ratio of fire characteristic size to grid size ($D^*/\delta x$) known as the plume resolution (PR) index is normally used to describe the quality of the calculation grid (Gannouni & Maad, 2015). The higher this value is, the finer the meshes are. This value is recommended to be in the range of 4 to 16 based on mesh sensitivity studies from the literature (McGrattan et al., 2016; McGrattan et al., 2014). Although some studies have used values outside of this range, for example, the FM panels test used a value between 12 to19, the NIST-RSE test used a value of 12 to 32, the National Research Council of Canada (NRCC) façade test used values of 18 to 24, while the Sandia Plume fire test used values of 20 to 118. PR index of 10 or a grid size of 23-92 cm has been widely validated to produce reliable results for tunnel fire modeling (Chen et al., 2019).

Increasing the PR index generally increases the computational time of the FDS calculations and may not necessarily lead to improved accuracy of the prediction. For example, in one of the studies that evaluated mesh sensitivity, increasing PR from 12 to 24 increased the computational time by a factor of up to 5 with a minimal improvement in

simulation accuracy (Lin & Chuah, 2008). For this reason, a multi-grid system can be used to minimize computational resources while maintaining accuracy for large domains. In a study that investigated the effectiveness of tunnel entrance sealing ratio on the fire behavior inside a tunnel, a 200.0 m tunnel with a 10.0 m by 3.0 m fire source in the middle was simulated. It used a PR value of 10 for the middle 60.0 m section with the fire source, and a value of 5 for the rest of the model. The longitudinal decay and ceiling temperatures predicted by the model agreed well with earlier experimental findings (Huang et al., 2018). In a simulation study for a 13.0 km long tunnel fire (Chen et al., 2019), δx was set to 25.0 cm for the domain in the fire region while for the other regions, a value between 50.0 – 100.0 cm was adopted while maintaining a sufficient resolution.

5.2.3. Turbulence Model. The Reynolds Averaged Navier-Stokes (RANS) and the Large Eddy Simulation (LES) are the major turbulent models widely used in mine fire simulation. The RANS and LES are CFD techniques that also solve the Navier-Stokes equations but are appropriate for modeling low-speed, thermally-driven flow with a focus on the transport phenomenon of heat and smoke from fires (McGrattan et al., 2012).

LES resolves the fire characteristics according to the grid size, whereas the RANS averages the values over significantly larger spatial and temporal scales other than the characteristic given by the numerical grid (Van Maele & Merci, 2008). While some researchers have presented arguments that scenarios like fire plumes, ceiling points, and other low-speed thermally driven flow are best represented by LES techniques, the accuracy of the LES results strongly depends on the quality of the mesh, and it leads to more turbulent thermal diffusion when compared to RANS (Van Maele & Merci, 2008). Generally, LES is more accurate than the RANS approach because the large eddies contain

most of the turbulent energy, and account for most of the momentum transfer and energy turbulent mixing (Zhiyin, 2015). This is one of the reasons why most of the available fire simulation packages such as FDS and Pyrosim are based on LES (McGRATTAN, 2005; McGrattan et al., 2012). However, the computation time for LES has been observed to be usually higher than that of the RANS models (Zhai et al., 2007; Zhang et al., 2007).

Moreso, there is a possibility that different RANS sub-models give different results (Vasanth et al., 2013). Whereas, for LES, the dynamics of the pool fires from laminar to turbulent transition could be captured without needing to tune or adjust the turbulence model parameters (Maragkos & Merci, 2020). The default settings i.e., the constant Smagorinsky model (where P_{rt}=0.5, S_{ct}=0.5, and C_s=0.17), is adopted in most studies for the LES. Although, it can sometimes be modified by adopting the dynamic Smagorinsky model where the turbulent parameters such as the turbulent Prandtl number (P_{rt}), turbulent Schmidt number (S_{ct}), and sub-grid scale dynamic viscosity (C_s), are changed.

5.2.4. Selection of Fire Chemistry. The critical ventilation velocity of the fire is barely impacted by the fire chemistry selection made for the CFD simulation. To assess the impact of fuel on critical ventilation velocity, methane, and propane were employed as fuel in one simulation study for small tunnels and propane and methane for large tunnels (C. Hwang & J. Edwards, 2005). However, no significant difference was observed for the critical velocity. Instead, it was discovered that the critical velocity was strongly influenced by the HRR and the tunnel dimension. Even though most of the CFD fire simulations used propane as the fire source, Yi et al. (Yi et al., 2013) used methanol as fuel in one study to simulate the fire source. Nevertheless, the choice of fuel is expected to influence the heat release rate of the fire. This is because different fuels have different heats of combustion.

Additionally, lighter fuels such as methanol are expected to burn faster and have a corresponding higher mass loss rate compared to more dense fuel like diesel thus influencing the heat release rate.

5.3. FDS VS OTHER CFD

FDS is an LES-based CFD solver widely used for fire simulation studies. There are two main advantages of FDS compared to other CFD solvers. One is that the solver is designed to solve low-speed thermally driven flow, which is a good approximation for fire in confined spaces. This is because it primarily solves a form of the Navier-Stokes equations appropriate for low-speed flows with an emphasis on smoke and heat transport from fires (Kerber & Milke, 2007). For this reason, FDS has been popularly deployed to model fires with low Mach numbers (Ma< 0.3) such as atrium fire configurations, fires in tunnels, and building fires since all these situations represent confined spaces. In a study, verification of FDS accuracy was conducted for low-speed flow in a small-scale tunnel and atrium fire configuration (Tilley et al., 2011). The numerical simulation results of the atrium height and back-layering distance show very promising agreement with the experiments even though further work is required to verify this. Another study used low Mach characteristics of FDS to conduct a performance-based assessment of a proposed ventilation strategy for a residential block atrium and from the analysis, an effective smoke extraction strategy was developed (Al-Waked et al., 2021).

The other advantage of FDS is that it can provide transient solutions with enough temporal and spatial resolutions using less computational time. This is achieved by using the EDC (Eddy Dissipation Concept) non-premixed combustion model which requires

significantly lower CPU times. It could be further enhanced by utilizing the MPI parallel processing capabilities in FDS to decrease the simulations' processing time (Weisenpacher et al., 2011). For example, in some studies to analyze heat and smoke propagation in a large-scale compartment fire, Fluent requires twice or more CPU times than FDS when standard settings are used (Weisenpacher et al., 2011; Zanzi et al., 2019). In another study, Verda et al. (Verda et al., 2021) used less computational time in a tunnel with a cross-section of 4.8 m and 600.0 m long by incorporating a Whitesmoke code into FDS through direct coupling and still obtained acceptable accuracy. Also, FDS only took about 0.9 hours for a CFD simulation that requires 3.9 hours in FLEUNT while it still maintained higher accuracy (Gu et al., 2020).

FDS generally performs better when compared to other fire CFD fire solvers. A study evaluated its performance based on hydrocarbon pool fire experiments with pool sizes ranging from 1.5 m to 6.0 m. The fractional bias of ± 30% and the normalized mean square error ≤0.5 were used as performance criteria to evaluate the level of agreement with experimental measurements. On all the evaluated variables, including flame temperature, burning rate, heat flux, flame height, flame surface, and surface emissive power, it was discovered that FDS performed better than other CFD algorithms. Similar findings were observed in a study comparing FDS and FLUENT when studying ceiling temperature and smoke layer thickness in tunnels (Binbin, 2011; Chiew, 2013). In the subway platform fire study (Binbin, 2011), it was found that the FLUENT prediction was much higher than the measured values and has greater fluctuations in the temperature curve when compared with FDS. Even though the FDS predicted a lower temperature compared to measured values, the results were found to be within ± 20%. The study indicated that Fluent over-predicted

the temperature for points 1.0 m high and above in a room that is 3.0 m high. On the contrary, FDS and Fluent show reasonable agreement in the investigation conducted by Zanzi et al. (Zanzi et al., 2019), despite the observed proximity in temperature results for a large compartment fire in an underground transportation hub, FDS still showed superiority in simulating the mass flow rates of cold air coming through natural vents and the mass flow rates of CO2 through the west vent and forced ventilation grilles.

Furthermore, many other studies have evaluated the accuracy of FDS modeling against full-scale fire experiments in mining scenarios. FDS was used to unravel the behavior of self-heating coal and its combustion characteristics in the gob area thereby, providing useful information about the potential environmental threats in an underground coal mine (Fernández-Alaiz, Castañón, Gómez-Fernández, Bernardo-Sánchez, et al., 2020; Fernánez-Alaiz et al., 2020). In the paper, an experimental procedure was established to investigate potential collapse situations in an underground coal mine using a sub-level method. The setup was reproduced in the laboratory scale and FDS was used to assess the behavior of a possible fire and the results were validated with experimental data. In another study, FDS was used to simulate mining vehicle (a loader and a drill rig) fires in an underground mine drift based on full-scale experiments (Hansen, 2020). Although the FDS predicted a much higher temperature compared to the full-scale test, the prediction values were still within ± 30%. The higher prediction values were attributed to the choice of radiative fraction values adopted and studies have shown that radiative fraction should be analyzed based on fire time and size before modeling fire. A value of 35 % is generally acceptable for the radiative fraction from the literature. However, reducing the radiative fraction from 0.35 to 0.00 brought the predicted peak temperature of FDS from 225 ^{o} C

down to 100 ^{o} C in an investigation. This implies that the radiative fraction parameter has a significant effect on the FDS simulation output (Jahn et al., 2008).

The major limitations of the FDS are in its meshing capabilities. FDS is not very efficient in modeling complex geometry and regular building blocks are mostly used for mesh generation (Binbin, 2011). Other CFD solvers for fire simulation such as FireFOAM and FLUENT could incorporate general structured or unstructured polyhedral meshes thereby improving the accuracy of the simulation results (Trouvé & Wang, 2010). The FDS can only use rectilinear meshes in fire simulation, so the mesh geometry is restricted to multi-block rectangular cartesian coordinates. Therefore, a very fine mesh must be created by increasing the number of cell sizes to represent a smooth curvature that impacts the simulation time.

6. EXISTING EMERGENCY EVACUATION PLANNING STRATEGIES FROM UNDERGROUND FIRES

Studies to assess, quantify, and model fire emergency evacuations can be classified into two main categories. They are the optimization approach, and the risk assessment and evaluation methods (see Figure 7). The optimization method focuses primarily on developing an improved algorithm for identifying the shortest distance between any two points while the risk assessment approach involves risk evaluation using simulation tools. The optimization algorithm mainly tries to find the shortest path to safety from any location without considering the dynamics of the fire. Moreover, the shortest path might not be the safest path. The risk evaluation method, on the other hand, involves computer simulation of different combinations of fire properties at different locations underground to determine

the worst possible scenario in an event of a fire outbreak. This method is further divided into two main sub-categories which are: fire numerical simulation and personnel evacuation simulation. Regardless of the methods, different techniques aim to solve a single objective problem- to minimize casualties during a fire disaster and safely evacuate occupants in an underground structure.

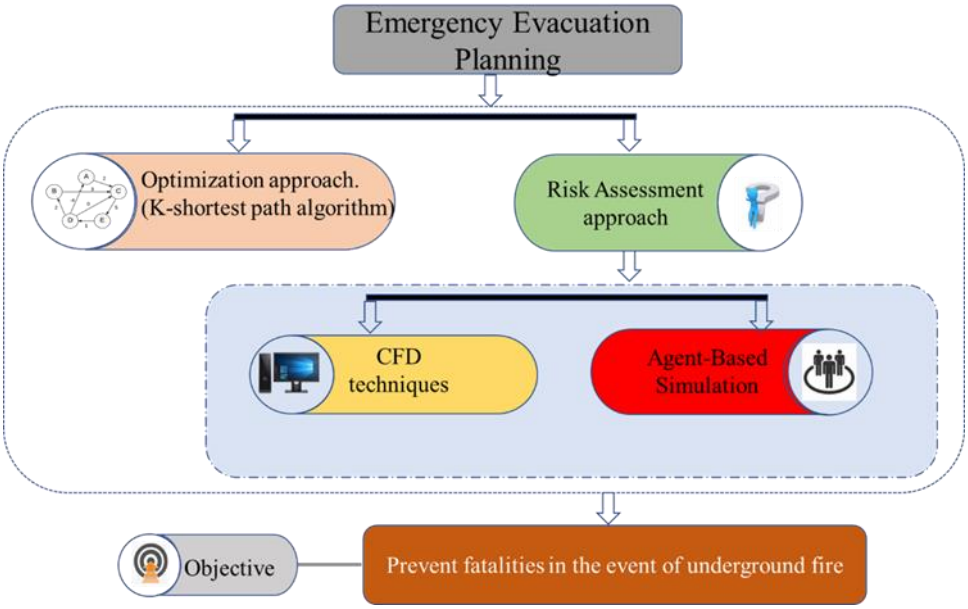

Figure 7. Summary of existing mine fire evacuation planning methods.

A more recent technology that has been deployed mostly for Australian and Swedish mines for mine emergency evacuation assessment and planning is the Mobilaris Emergency Support (MES) developed by Epiroc. The system provides a highly versatile and connected communication system that has the capability of sending messages to miners during an emergency and keeping track of miners who are aware of the emergency and those that are not while visualizing the whole process in real-time. From the virtual interface, all movement of personnel can be monitored, and miners could be guided to

refuge chambers and evacuated as quickly as possible according to defined procedures. The EMS has been adopted as a standard emergency device in Swedish UG mines and it has proven to reduce the evacuation time by 25-50 % (Epiroc, 2023).

6.1. OPTIMIZATION APPROACH

The optimization approach for underground evacuation planning is primarily based on the Network Path Planning Strategy (NPPS) which uses the k-shortest path algorithm. Numerous optimization algorithms have been developed so far to improve the safe egress of occupants from a confined environment (Adjiski & Despodov, 2020b; Eppstein, 1998; Hong et al., 2018; Hong, Li, Wu, & Xu, 2019; Jalali & Noroozi, 2009; Jin, Chen, & Jiang, 2013; Zheng & Liu, 2019). The optimum solution could either be applied to maximize exit usage efficiency or minimize the egress time depending on the optimization procedure adopted. For instance, the path planning method was used to develop a 3D constrained space model to establish a priority route for evacuation in constrained space scenarios (Hong, Li, Wu, & Xu, 2019). In the study, the confined space was modeled as a 3D connected graph, and a priority-oriented network planning algorithm was constructed to maximize evacuation exit utilization efficiency and minimize the whole evacuation delay. In a similar study, multi-objective dynamic route network planning was introduced to solve emergency evacuation problems in restricted spaces such as the underground (Hong et al., 2018). The study evaluated a multisource to multi-destination evacuation model in confined spaces with the objectives of minimizing the whole evacuation delay and maximizing evacuation efficiency. Furthermore, two different optimization techniques were adopted to develop safe egress for emergency evacuation in an underground space.

To discover the quickest pathways between the accident site and safe locations in a network of underground mines, the Floyd-Warshall and Pi optimization algorithms, which are based on the K-shortest path, were implemented in the first study (Jalali & Noroozi, 2009) while in the other paper, deep reinforcement learning was employed to develop a multi-agent deep deterministic policy gradient algorithm that could search for optimal evacuation route during a disaster (Zheng & Liu, 2019). A proper evaluation of the methodologies indicated that although both methods have a common goal, they achieved their objective using different approaches. For instance, the Floyd-Warshall and Pi algorithms formulate the problem on a directed and weighted graph. In the first approach, the shortest escape time between every two given points is determined and assigned as the access route while the latter approach employs four main steps which include modeling the crowd and the environment, grouping the crowd and selecting a leader, hierarchical path planning, and finally followed by the analysis of the evacuation results. As computing ability continues to grow, more improved optimization algorithms could be developed and sometimes an ensemble of different algorithms using machine learning could be adapted to improve fire safety in underground environments (Guo & Zhang, 2022).

6.2. RISK ASSESSMENT METHODS

Risk assessments for fire evacuation can be done by various means which range from simple hand calculations involving egress time concept, numerical fire simulation using CFD, or more robust simulation modeling methods involving personnel evacuation using Agent-Based models (ABMs).

6.2.1. Empirical Calculations. Some empirical formulae have been proposed to evaluate fire and evacuation risk in confined spaces. For instance, available safe-egress time (ASET) and required safe-egress time (RSET) was proposed to determine the evacuation risk from underground fires (N. Wang et al., 2021; Zhang et al., 2016). The ASET is defined as the time duration from which the fire starts to the point where occupants could no longer be evacuated while RSET is required time to evacuate occupants to a safe zone once a fire occurs. The ASET could be represented as a function of the minimal time for the CO concentration to reach the threshold limit as follow.

$$ASET = \min\left(T_{co}, T_{temp}\right) \tag{9}$$

where T_{co} indicates the time for CO to reach a threshold value of 5×10^{-4} mol/mol, while T_{temp} represents the time taken for the smoke temperature to reach a critical value of 60 ^{o} C. On the other hand, the required safe egress time could be further decomposed as follow.

$$RSET = T_r + T_{pre} + T_m \tag{10}$$

where T_r is the recognition time (that is the time from when the fire occurs to when the occupants get the fire alarm notification), T_{pre} denotes preparation time for evacuation upon receiving alarm notification, and T_m indicates the duration from when evacuation begins to the end of the evacuation process. By determining the ASET and RSET for designing fire scenarios in an underground structure, one can evaluate the risk level and make recommendations as to how safe egress could be improved for each scenario. On the other hand, some researchers introduced a novel four-dimension parameter system that incorporates Average Evacuation Time (AET), Average Waiting Time (AWT), and Average Moving Distance (AMD) in addition to the Required Safety Egress Time (RSET) to quantitatively describe the evacuation from four aspects (Chen et al., 2021). The study

proposed a dimensionless parameter, Risk Index (RI) for the risk evaluation and comparison, and the findings show that the RI for AWT is distinctly higher than other Risk Indexes based on twelve designed scenarios and over 600 simulation runs.

Another risk assessment technique is to determine the route of minimal CO emission since most fatalities from mine fires can be attributed to CO and smoke inhalation (Yuan et al., 2016; Zhou, 2009a). Evacuation planning was successfully carried out by simulating different fire scenarios and locating the optimal evacuation routes based on minimal exposure to carbon monoxide CO during the evacuation process. In one of the papers, the optimal evacuation route was established by estimating the CO concentration over time in different routes based on different fire simulation scenarios. Additionally, in other to account for the cumulative effects of CO inhalation, the CO concentration was presented in a weighted format using a fractional effective dose (FED) (Adjiski & Despodov, 2020b). The study showed that knowing the minimal CO exposure route could help enhance emergency planning and save miners' life during an underground fire.

6.2.2. Fire Numerical Simulation using CFD. CFD has been successfully used to simulate tunnel fires and has accurately predicted the temperature in the mine airways and tunnels thus improving tunnels and underground fire safety practices (Adjiski et al., 2016; Cheng et al., 2016; Guo & Zhang, 2014; C. Hwang & J. Edwards, 2005; Yuan & Smith, 2009, 2015). In one study two full-scale fire tests were conducted in the Colli Berici tunnel and the gas temperature was measured at a different location for the different tests and similar results were also obtained from the CFD simulation (Cafaro & Bertola, 2010). Similarly, Rahmani et al.(Rahmani et al., 2004), applied CFD using large eddy simulation to study fire in tunnels and examined the temperature profile in a model tunnel (25.0 m

long by 2.0 m wide by 1.0 m height) to verify the reliability of the CFD model while a combination of experimental analysis and CFD simulation was used to study fire propagation in a sublevel coal mine by (Fernández-Alaiz, Castañón, Gómez-Fernández, Bernardo-Sánchez, et al., 2020; Fernánez-Alaiz et al., 2020). The various studies indicated that CFD analysis is a reliable way of understanding the fire risk and thus emergency evacuation strategies could be developed based on the simulations results. For example, in one of the studies, three different scenarios were examined and CFD successfully modeled the evolution of fire in the mine (Fernández-Alaiz, Castañón, Gómez-Fernández, Bernardo-Sánchez, et al., 2020; Fernánez-Alaiz et al., 2020). Furthermore, (P. Woodburn & R. Britter, 1996) used CFD to simulate tunnel fire and (Yuan & Smith, 2009) modeled spontaneous heating in a large coal chamber using CFD and the studies showed that CFD demonstrated good predictive performance for fire and heat simulation.

Unlike the optimization approach which primarily focuses on the shortest path, CFD has superiority in that it can be applied to analyze smoke spread and reverse flow conditions in addition to temperature evolution (C. Hwang & J. Edwards, 2005; McGrattan et al., 1998; Zhou et al., 2018) which is the major cause of casualties in the underground. For example, a major question that often comes to mind is how to apply the optimization algorithm if the fire occurs along the shortest path and the shortest path is smoke-filled which could lead to the death of the miners. With CFD however, ventilation conditions and back-layering phenomenon can be understood, and appropriate emergency response can be developed. CFD was used to predict CO spread in an underground mine and the experimental results validate that FDS could efficiently and accurately predict the spread of smoke in the underground (Yuan et al., 2016). A similar result was also obtained from

the CFD simulation of back-layering during a tunnel fire test (Cafaro & Bertola, 2010). Several other studies have employed CFD to develop an emergency evacuation plan during a fire disaster. For example, a CFD model was created to predict the suppression of a conveyor belt fire with water spray (Yuan & Smith, 2015). The model was validated using extensive experimental data that combined the suppression action of water spray with the spread of flames. From the findings, it can be concluded that CFD successfully predicted emergency strategies such as the location of the sprinkler and their activation temperature. More so, the work of Adjiski et al. (Adjiski et al., 2016) further demonstrated that CFD could be a very versatile tool for underground mine fire modeling by employing it to investigate the effectiveness of brattice barriers for underground firefighting and hazard mitigation.

6.2.3. Agent-Based Modelling Approach. Over the past ten years, interest in a novel modeling technique known as agent-based modeling and simulation (ABMS), or simply agent-based models (ABMs), which models a system as a collection of autonomous decision-making agents, has increased (Bonabeau, 2002; Dong et al., 2022; Macal & North, 2009). Such models have a symbiotic relationship with computing technology and more sophisticated models have now become feasible since more complex algorithms, toolkits, and libraries have been developed (Gilbert & Bankes, 2002). A schematic workflow interaction of miners as agents in a typical agent-based evacuation model for underground confined space is presented in Figure 8.

From the illustration depicted in Figure 8, the miners are the agents. Each miner has a set of attributes, rules, behaviors, and memory unique to them. Also, each miner can freely communicate with every other miner due to agent-agent interactions. One significant

advantage of this novel method is that it encompasses the fire field data (which include temperature, heat, smoke, and fire gas) obtained from full-scale experiments or validated CFD modeling alongside their interactions with the geometrical properties associated with the confined space in question. The simulation is conducted in a virtual 3D viewer platform such as pathfinder. The 3D viewer platform is a virtual reality platform and could help us further analyze how agents interact in an event of a fire and prepare for subsequent evacuation. By simulating personnel evacuation with ABMs, we can have a better understanding of the interactions of the agent with their environment during a fire emergency, thereby improving fire safety preparedness in the undergrounds.

Just like CFD application in scenario analysis to determine the risk level for different fire situations, ABMs can be used to visualize how the implementation of various emergency plans influences safe egress during an emergency through comparative analysis. An agent-based model study on the comparative analysis of different evacuation strategies using the GAMA simulation platform and the results indicated that following the evacuation signs is the best strategy in the case that was considered (Nguyen et al., 2013). For this case study, following emergency signs yielded a survival chance of 82.48 %, following the crowd yielded a 70.97 % survival rate, and following own's paths yielded a much lower survival chance of 58.55 %. Similarly, a risk assessment study for evacuees using three blind evacuation strategies was conducted to determine the most suitable escape plan in smoke-filled confinement, and the survival chance from the simulation was analyzed in the research (Nguyen et al., 2013).

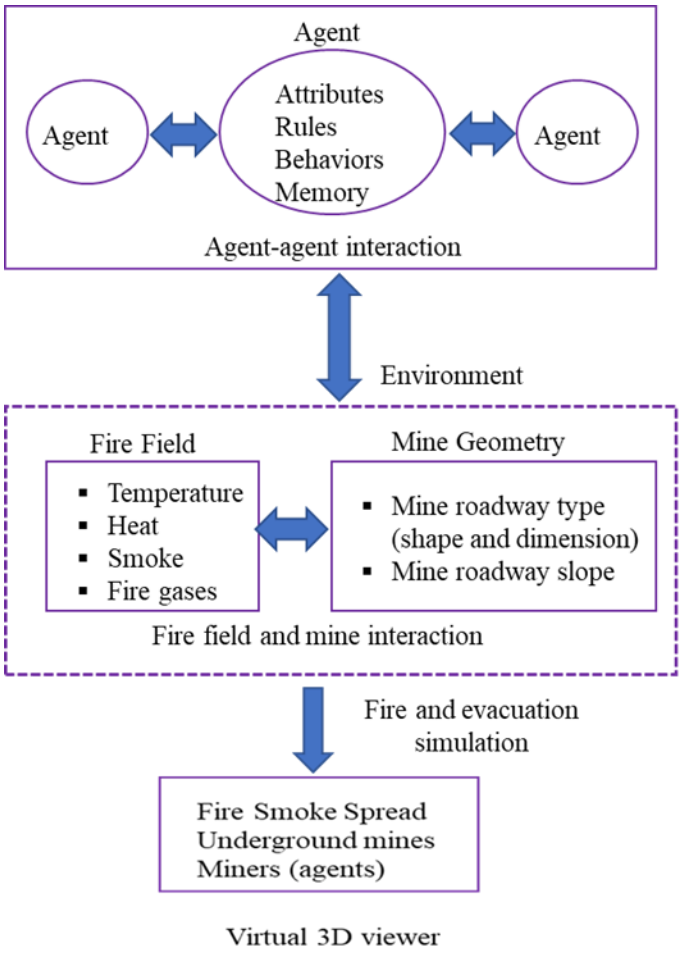

Figure 8. A schematic of agent-based evacuation strategies for underground confined spaces.

The three blind evaluation strategies were (1) wall tracking by evacuees (2) evacuees going straight, and (3) random motion of evacuees. The wall-tracking technique was observed to produce a higher rate of survival based on the different risk assessment (RA) parameters considered.

The proportion of survivors, the level of toxicity, and the duration of escape are the RA factors that are assessed, and in the instance of a blind evacuation due to smoke spread, the wall tracking technique results in a higher percentage of survivors, a lower level of toxicity, and a shorter escape time.

Additionally, ABMs can model individual evacuee behaviors with varying levels of knowledge about the confinement's internal structure and simulate predictable spatial accessibility that is altered by activated fire safety facilities, which would also enhance fire safety (Tan et al., 2015). In one study, a prototype model was developed to evaluate the influence of spatial change on evacuation performance during a fire emergency. The advantage of this model is that it offers the flexibility of examining the influence of changes that occur in the connectivity of the structure and the evacuee's knowledge of the spatial environment. Each evacuee will be able to select their escape route based on the assumed spatial accessibility. Sometimes, ABMs can be coupled with simplified egress modeling such as a 1D smoke propagation model to further improve fire safety assessment (Ronchi et al., 2019). In this scenario, one-dimensional smoke spread calculations are performed to estimate the visibility conditions, as well as the level of toxic gas concentration produced from the fire and the outputs, which are used as inputs for advanced egress modeling such as the ABMs.

ABMs have been successfully deployed to model fire and smoke spread in underground mines. Li et al. (Li et al., 2015) conducted a study to visualize underground mine fire based on an established cellular automata model. The study sought to investigate fire source combustion and fire fume spread. The temperature was monitored at specific locations in the mine while ABMs successfully measured the subsurface quantities of gases, primarily CO and CO_2, in real-time. The findings indicated that this simulation pathway might be used to predict disasters caused by underground mine fires because the measured values and estimated values agreed very well. Additionally, by visualizing the temporal and spatial changes in temperature and the concentration of hazardous gases, it is

possible to determine the hazard area and the extent of the hazard in the event of a fire disaster. In another study, Salarian et al. (Salarian et al., 2020), employed ABMs to simulate defined scenarios and calculate the evacuation times of passengers in a subway. The study focused on reducing evacuation times in the event of a fire by using a safe zone approach in the "Pathfinder" simulation software. Eighteen different scenarios were examined, and the best evacuation strategy was found by increasing the number of exit doors from 2 to 4 while simultaneously considering the safe zone. On the other hand, Edrisi et al., (Edrisi et al., 2021) demonstrated that ABMs could be used to simulate underground metro station evacuation. Three different exit choice models were developed and compared in the study. The models include the multinomial logit model, the modified multinomial logit model with revising decisions, and the shortest path exit option. The egress times for each model were obtained and compared and the results indicate that the modified exit choice model gives the best result because it has a more realistic representation of human behavior.

Another advantage of ABMs over-optimization and CFD evacuation strategy is that it allows the disaggregation of systems into individual components. These are governed by their own set of rules and individual characteristics thus enhancing better performance and superiority in modeling complex systems (Crooks & Heppenstall, 2012). It also can incorporate fire field data and mine geometry to simulate miners' responses during evacuation (Tang & Ren, 2008; Tang & Ren, 2012). The current underground evacuation model does not consider the evacuee's awareness of the predictable change that could occur in the spatial accessibility of evacuation routes. These shortcomings can be resolved with ABMs. The existing ventilation network models and CFD simulations also neglect the

occupants' behavior and evacuees' dynamism in confined spaces like the underground. Again, these limitations can be overcome with ABMs and agent-based simulations have been successfully used to simulate human behavior with predictable spatial accessibility in a fire emergency (Tan et al., 2015). More so, unlike traditional models, ABMs try to represent how individuals and the environmental variables that affect them vary in the space-time continuum and other dimensions. They usually involve processes that we know to be important but that is somewhat complex to be included in simpler models (Steven F. Railsback & Volker Grimm, 2019). Because of the growing popularity and flexibility of ABMs, many researchers have since considered using agent-based models to plan emergency evacuation from buildings during a disaster although only a few studies have attempted to use ABMs for evacuation in underground mines.

6.3. STATE-OF-THE-ART PRACTICAL MEASURES AND LESSONS LEARNED

The Moura No. 2 disaster that occurred in Queensland in 1994 led to the implementation and enforcement of annual level 1 emergency exercises done by UG coal mines in the State of Queensland, Australia since 1998 (Dent, 2002; Halim & Brune, 2019; Hopkins, 2020; Queensland-Government, 2022; Roxborough, 1997). Years later, many other countries including Canada, Chile, China, India, Indonesia, Mexico, New Zealand, South Africa, and the United States have also adopted this type of legislation to mitigate disasters in their mines. The exercises are typically held every year or every two years depending on the country's legislation. In the US, MSHA has mandated that this exercise should be done yearly and the adoption of this of the Queensland model is a testament to the effectiveness of this model. These exercises have helped to improve mine safety in

Queensland and around the world. The key lessons learned could be summarized as follows (Queensland-Government, 2022):

- Communication and coordination: In an emergency, everyone involved must be able to communicate effectively with each other. This includes mine workers, mine management, emergency services, and government agencies. Clear and concise communication plans and procedures are essential, as well as regular training and drills to ensure that everyone knows their role in an emergency.
- Emergency kits: A well-stocked emergency kit is essential for any mine. This should include first aid supplies, fire extinguishers, and breathing apparatus. In the event of an emergency, these supplies can be used to save lives.
- Equipment and infrastructure: Regular inspections and maintenance of mine equipment and infrastructure are essential to identify and correct potential hazards. This includes things like ventilation systems, electrical systems, and machinery. By taking steps to mitigate risks, mines can help to prevent accidents and fatalities.
- Culture of safety: A culture of safety is essential for any mine. This means that workers feel comfortable reporting hazards and taking steps to mitigate risks. By creating a culture of safety, mines can help to create a safer working environment for everyone.

7. CONCLUSIONS AND FUTURE OUTLOOK

Due to the depletion of shallow ore reserves, underground mines are becoming deeper to access higher-grade mineral resources. The occurrence of fires in deeper underground confined spaces will pose severe hazards. Similarly, the number of tunnels

and subways in cities is increasing rapidly. This is due to the growing popularity of public transportation, as well as the need for more efficient transportation networks. However, the increase in the number of tunnels and subways also poses a new fire safety challenge. To address the fire safety challenges, it is important to understand fire characteristics and implement appropriate fire safety measures and emergency evacuation plans.

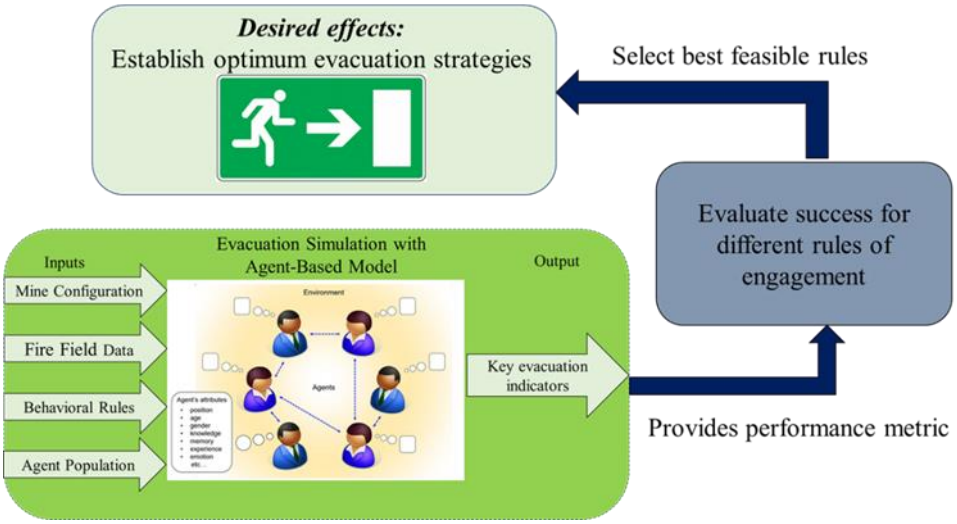

Figure 9. Proposed structure of Underground Mines evacuation model using ABMs.

First, in this study, we analyzed the current advancement in underground mine fire studies by identifying the critical factors such as ventilation conditions, nature of the fuel, geometrical constraints, and simulation methods that could impact fire safety, thus optimizing emergency evacuation plans. Furthermore, the advantages and the defects of the existing mine fire simulation and evacuation planning are presented in which a novel approach to the underground emergency evacuation management system (see Figure 9) is proposed to help miners self-escape during a fire hazard.

The proposed evacuation model will take into consideration the mine configuration (that is, the geometrical parameters), fire field data (mainly the heat release rate, smoke

spread behavior, flame characteristics, and nature of fuel), behavioral rules governing miners' evacuation such as miners' age, sex, education, and experience (which could be obtained from emergency drills like the level 1 emergency drills conducted annually in the State of Queensland) (Halim & Brune, 2019; Queensland-Government, 2022), and finally, the agent population which in this case is the number of miners expected to be underground. This can be achieved by direct coupling of fire dynamics simulation with agent-based evacuation models to form an integrated emergency response system like the Mobilaris Emergency Support.

Current evacuation strategies are based on static evacuation plans. This evacuation method only offers a rigid evacuation path and does not consider changes in the topology of the evacuation network or changes in the evacuation path caused by hazard dynamics. More problematically, just a few locations in the underground mines have evacuation plans, making it difficult for evacuees to access the information from the static evacuation routes.

To develop reliable self-escape methods for miners during a fire accident, it is imperative to investigate evacuation models by computing the risk factor and the chances of safe escape during an underground fire. This type of model needs to present a complete, comprehensive conceptual model of human behavior in fire evacuations. Agent-based modeling is one reliable way to go, and it has continued to gain worldwide attention and application because of its ability to reliably model numerous complex situations which might be impossible using other conventional modeling tools (Macal & North, 2009).

Although some evident progress has been made in developing safe evacuation models and strategies for buildings, tunnels, and underground facilities, the search for an

optimal evacuation procedure for different fire scenarios still presents a challenging task to fire researchers. This is primarily due to the stochastic nature of the input data used for mine fire modeling. For instance, methods for quantification of the efficacy of a model used in another slightly different geometry should be devised. The determination of the probability of safe evacuation for each person in an underground mine based on the selected evacuation strategy must be researched. The method to safely evacuate the miners from the underground immediately after a fire outbreak without first conducting firefighting operations is another proposed research topic. Also, given different evacuation routes from the underground, the best measures used to determine the best evacuation route should be studied.

These are some of the drawbacks faced with much of the existing literature trying to model underground mine fire using data obtained from building scaled model tunnels in the laboratory. These issues and many other defects in underground mine fire studies have been addressed in this work thus improving our understanding of fire risk and the required preparedness for emergency evacuation in underground mines and other similar underground confined spaces.

REFERENCES

Adjiski, V., & Despodov, Z. (2020). Methodology for Optimal Fire Evacuations in Underground Mines Based on Simulated Scenarios. In Fire Safety and Management Awareness. IntechOpen.

Adjiski, V., Mirakovski, D., Despodov, Z., & Mijalkovski, S. (2015). Simulation and optimization of evacuation routes in case of fire in underground mines. Journal of Sustainable Mining, 14(3), 133, 143.https://doi.org/https://doi.org/10.1016/j.jsm.2015.10.001

Adjiski, V., Mirakovski, D., Despodov, Z., & Mijalkovski, S. (2016). CFD simulation of the brattice barrier method for approaching underground mine fires. Mining Science, 23, 161-172.

Al-Waked, R., Nasif, M., Groenhout, N., & Partridge, L. (2021). Natural ventilation of residential building Atrium under fire scenario. Case Studies in Thermal Engineering, 26, 101041. https://doi.org/https://doi.org/10.1016/j.csite.2021.101041

Babrauskas, V. (1983). Estimating large pool fire burning rates. Fire Technology, 19, 251-261.

Beard, A. N., Jowitt, P., & Carvel, R. (1999). The effect of forced longitudinal ventilation on a pool fire in a tunnel. 8th Int Conf Interflam'99-Fire Science and Engineering,

Binbin, W. (2011). Comparative Research on FLUENT and FDS's Numerical Simulation of Smoke Spread in Subway Platform Fire. Procedia Engineering, 26, 1065-1075. https://doi.org/https://doi.org/10.1016/j.proeng.2011.11.2275

Bonabeau, E. (2002). Agent-based modeling: Methods and techniques for simulating human systems. Proceedings of the national academy of sciences, 99(suppl_3), 7280-7287.

Brakea, R., Hattbc, A., & Sanid, R. (2015). Modeling and Simulation of Multiple Underground Mine Fire Scenarios at Freeport Indonesia.

Brnich, M., Kowalski-Trakofler, K. M., & Brune, J. (2010). Underground coal mine disasters 1900-2010: Events, responses, and a look to the future. Extracting the science: a century of mining research, 363-372.

Brohez, S., Delvosalle, C., Marlair, G., & Tewarson, A. (2000). The measurement of heat release from oxygen consumption in sooty fires. Journal of fire sciences, 18(5), 327-353.

Bubbico, R., Dusserre, G., & Mazzarotta, B. (2016). Calculation of the flame size from burning liquid pools. Chemical Engineering Transactions, 53, 67-72.

Cafaro, E., & Bertola, V. (2010). Fires in tunnels: Experiments and modelling. The Open Thermodynamics Journal, 4(1).

Carvel, R., Beard, A. N., Jowitt, P., & Drysdale, D. (2001). Variation of heat release rate with forced longitudinal ventilation for vehicle fires in tunnels. Fire Safety Journal, 36(6), 569-596.

Carvel, R. O., Beard, A. N., & Jowitt, P. (2001). The influence of longitudinal ventilation systems on fires in tunnels. Tunnelling and Underground Space Technology, 16(1), 3-21.

Chang, X., Laage, L. W., & Greuer, R. E. (1990). A User's Manual for MFIRE: A Computer Simulation Program for Mine Ventilation and Fire Modeling (Vol. 9245). US Department of the Interior, Bureau of Mines.

Chasko, L. L., Conti, R. S., Lazzara, C. P., & Wiehagen, W. J. (2005). Fire response preparedness for underground mines. In. Pittsburgh, PA: Pittsburgh Research Laboratory (National Institute for Occupational Safety and Health).

Chen, J., Liu, C., Meng, Y., & Zhong, M. (2021). Multi-Dimensional evacuation risk evaluation in standard subway station. Safety Science, 142, 105392. https://doi.org/https://doi.org/10.1016/j.ssci.2021.105392

Chen, L. F., Hu, L. H., Zhang, X. L., Zhang, X. Z., Zhang, X. C., & Yang, L. Z. (2015). Thermal buoyant smoke back-layering flow length in a longitudinal ventilated tunnel with ceiling extraction at difference distance from heat source. Applied Thermal Engineering, 78, 129-135. https://doi.org/https://doi.org/10.1016/j.applthermaleng.2014.12.034

Chen, Y.-J., Shu, C.-M., Ho, S.-P., Kung, H.-C., Chien, S.-W., Ho, H.-H., & Hsu, W.-S. (2019). Analysis of smoke movement in the Hsuehshan tunnel fire. Tunnelling and Underground Space Technology, 84, 142-150. https://doi.org/https://doi.org/10.1016/j.tust.2018.11.007

Cheng, J., Li, S., Zhang, F., Zhao, C., Yang, S., & Ghosh, A. (2016). CFD modelling of ventilation optimization for improving mine safety in longwall working faces. Journal of Loss Prevention in the Process Industries, 40, 285-297.

Cheng, L. H., Ueng, T. H., & Liu, C. W. (2001). Simulation of ventilation and fire in the underground facilities. Fire Safety Journal, 36(6), 597-619. https://doi.org/https://doi.org/10.1016/S0379-7112(01)00013-3

Chiew, H. Z. (2013). Fire dynamics simulation (FDS) study of fire in structures with curved geometry [Bachelor thesis, Universiti Tunku Abdul Rahman]. http://eprints.utar.edu.my/818/1/ME-2013-0908547-1.pdf

Chow, W. K., Han, S., & Chow, C. (2008). Estimation of heat release rate for gasoline pool fires. International Conference on Building Energy and Environment, The Hong Kong Polytechnic University.

Chow, W. K., Wong, K. Y., & Chung, W. Y. (2010). Longitudinal ventilation for smoke control in a tilted tunnel by scale modeling. Tunnelling and Underground Space Technology, 25(2), 122-128. https://doi.org/https://doi.org/10.1016/j.tust.2009.10.001

Conti, R. S. (2005). Fire Response Preparedness for Underground Mines. U.S. Department of Health and Human Services, Public Health Service, Centers for Disease Control and Prevention, National Institute for Occupational Safety and Health, Pittsburgh Research Laboratory. https://books.google.com/books?id=5-zgAAAAMAAJ

Crooks, A. T., & Heppenstall, A. J. (2012). Introduction to Agent-Based Modelling. In A. J. Heppenstall, A. T. Crooks, L. M. See, & M. Batty (Eds.), Agent-Based Models of Geographical Systems (pp. 85-105). Springer Netherlands. https://doi.org/10.1007/978-90-481-8927-4_5

Deckers, X., Haga, S., Tilley, N., & Merci, B. (2013). Smoke control in case of fire in a large car park: CFD simulations of full-scale configurations. Fire Safety Journal, 57, 22-34. https://doi.org/https://doi.org/10.1016/j.firesaf.2012.02.005

Dent, P. (2002). Developments in mine safety in Queensland, post Moura No. 2 underground coal mine disaster. Queensland Government Mining Journal, 102.

Dong, B.-X., Shan, M., & Hwang, B.-G. (2022). Simulation of transportation infrastructures resilience: a comprehensive review. Environmental Science and Pollution Research, 29(9), 12965-12983. https://doi.org/10.1007/s11356-021-18033-w

Duy Huy, N., Cao Khai, N., Van Thinh, N., Van Quang, N., Minh Chien, N., & Khac Duy, N. (2022). Simulating and Predicting Escape Routes for Ventilation Network of Duong Huy Coal Company using Ventsim DESIGN Software. Inżynieria Mineralna.

Edrisi, A., Lahoorpoor, B., & Lovreglio, R. (2021). Simulating metro station evacuation using three agent-based exit choice models. Case Studies on Transport Policy, 9(3), 1261-1272. https://doi.org/https://doi.org/10.1016/j.cstp.2021.06.011

Epiroc. (2023). Retrieved Accessed May 22, 2023. from https://www.epiroc.com/en-us/products/digital-solutions/sustainable-and-safe-operations/mobilaris-emergency-support

Eppstein, D. (1998). Finding the k shortest paths. SIAM J. Comput., 28. https://doi.org/10.1137/S0097539795290477

Fan, C., Zhang, L., Jiao, S., Yang, Z., Li, M., & Liu, X. (2018). Smoke spread characteristics inside a tunnel with natural ventilation under a strong environmental wind. Tunnelling and Underground Space Technology, 82, 99-110. https://doi.org/https://doi.org/10.1016/j.tust.2018.08.004

Fernández-Alaiz, F., Castañón, A. M., Gómez-Fernández, F., & Bascompta, M. (2020). Mine fire behavior under different ventilation conditions: Real-scale tests and CFD modeling. Applied Sciences, 10(10), 3380.

Fernández-Alaiz, F., Castañón, A. M., Gómez-Fernández, F., Bernardo-Sánchez, A., & Bascompta, M. (2020). Determination and fire analysis of gob characteristics using CFD. Energies, 13(20), 5274.

Fernánez-Alaiz, F., Castañón, A. M., Gómez-Fernández, F., Bernardo-Sánchez, A., & Bascompta, M. (2020). Analysis of the fire propagation in a sublevel coal mine. Energies, 13(14), 3754.

Gannouni, S., & Maad, R. B. (2015). Numerical study of the effect of blockage on critical velocity and backlayering length in longitudinally ventilated tunnel fires. Tunnelling and Underground Space Technology, 48, 147-155. https://doi.org/https://doi.org/10.1016/j.tust.2015.03.003

Gilbert, N., & Bankes, S. (2002). Platforms and methods for agent-based modeling. Proceedings of the national academy of sciences, 99(suppl_3), 7197-7198.

Greuer, R. E. (1977). Study of mine fires and mine ventilation: pt. 1, Computer simulation of ventilation systems under the influence of mine fires.

Gu, D., Zheng, Z., Zhao, P., Xie, L., Xu, Z., & Lu, X. (2020). High-efficiency simulation framework to analyze the impact of exhaust air from covid-19 temporary hospitals and its typical applications. Applied Sciences, 10(11), 3949.

Guo, K., & Zhang, L. (2022). Adaptive multi-objective optimization for emergency evacuation at metro stations. Reliability Engineering & System Safety, 219, 108210. https://doi.org/https://doi.org/10.1016/j.ress.2021.108210

Guo, X., & Zhang, Q. (2014). Analytical solution, experimental data and CFD simulation for longitudinal tunnel fire ventilation. Tunnelling and Underground Space Technology, 42, 307-313. https://doi.org/https://doi.org/10.1016/j.tust.2014.03.011

Haack, A. (1998). Fire protection in traffic tunnels: General aspects and results of the EUREKA project. Tunnelling and Underground Space Technology, 13(4), 377-381. https://doi.org/https://doi.org/10.1016/S0886-7798(98)00080-7

Haghighat, A. (2017). Fire Simulation Cost Reduction for Improved Safety and Response for Underground Spaces [Doctoral dissertation, Virginia Tech]. https://vtechworks.lib.vt.edu/handle/10919/79672

Haghighat, A., & Gillies, S. (2015). Fire Behavior Analysis of a Mine Future Plan. 15th North American Mine Ventilation Symposium, Department of Mining and Minerals Engineering, Virginia Tech , USA.

Haghighat, A., Luxbacher, K., & Lattimer, B. Y. (2018). Development of a Methodology for Interface Boundary Selection in the Multiscale Road Tunnel Fire Simulations. Fire Technology, 54(4), 1029-1066. https://doi.org/10.1007/s10694-018-0724-0

Halim, A., & Brune, J. (2019). Do refuge chambers represent a good strategy to manage emergencies in underground coal mines? Mining, Metallurgy & Exploration, 36, 1191-1199.

Han, J., Wang, Z., Geng, P., Wang, F., Wen, J., & Liu, F. (2021). The effect of blockage and tunnel slope on smoke spread and ceiling temperature distribution in a natural-ventilated metro depot. Energy and Buildings, 253, 111540. https://doi.org/https://doi.org/10.1016/j.enbuild.2021.111540

Hansen, R. (2018). Fire statistics from the mining industry in New South Wales, Queensland and Western Australia. Brisbane: The University of Queensland.

Hansen, R. (2019). Fire behaviour of multiple fires in a mine drift with longitudinal ventilation. International Journal of Mining Science and Technology, 29(2), 245-254.

Hansen, R. (2020). Modelling temperature distributions and flow conditions of fires in an underground mine drift. Geosystem Engineering, 23(6), 299-314.

Hansen, R., & Ingason, H. (2013a). Full-scale fire experiments with mining vehicles in an underground mine (978-91-7485-115-1 (ISBN)). (Studies in Sustainable Technology / Forskningsrapport, Issue. http://urn.kb.se/resolve?urn=urn:nbn:se:mdh:diva-20912

Hansen, R., & Ingason, H. (2013b). Heat release rate measurements of burning mining vehicles in an underground mine. Fire Safety Journal, 61, 12-25.

Hardy, R. J., & Heasley, K. A. (2006, 2006). Ventilation simulation programs Mine Vent and MFIRE: Updates to advance the technology of simulation programming. 11th US/North American Mine Ventilation Symposium, Pennsylvania, USA.

Hong, Y., Li, D., Wu, Q., & Xu, H. (2018). Dynamic Route Network Planning Problem for Emergency Evacuation in Restricted-Space Scenarios. Journal of Advanced Transportation, 2018, 4295419. https://doi.org/10.1155/2018/4295419

Hong, Y., Li, D., Wu, Q., & Xu, H. (2019). Priority-oriented route network planning for evacuation in constrained space scenarios. Journal of Optimization Theory and Applications, 181, 279-297.

Hopkins, A. (2020). Managing major hazards: The lessons of the Moura mine disaster. United Kingdom :Taylor & Francis. https://www.google.com/books/edition/Managing_Major_Hazards/UMzxDwAAQBAJ?hl=en&gbpv=1

Hu, Y., Liu, X., Wang, F., & Cheng, C. (2012). An overview of agent-based evacuation models for building fires. International Conference on Networking, Sensing and Control. IEEE, Beijing, China.

Hu, Y., Wang, F., & Liu, X. (2014). A CPSS Approach for Emergency Evacuation in Building Fires. IEEE Intelligent Systems, 29(3), 48-52. https://doi.org/10.1109/MIS.2014.38

Huang, Y., Li, Y., Dong, B., Li, J., & Liang, Q. (2018). Numerical investigation on the maximum ceiling temperature and longitudinal decay in a sealing tunnel fire. Tunnelling and Underground Space Technology, 72, 120-130.

Huggett, C. (1980). Estimation of rate of heat release by means of oxygen consumption measurements. Fire and Materials, 4(2), 61-65.

Hwang, C., & Edwards, J. (2005). The critical ventilation velocity in tunnel fires—a computer simulation. Fire Safety Journal, 40(3), 213-244.

Ingason, H., & Li, Y. Z. (2010a). Model scale tunnel fire tests with longitudinal ventilation. Fire Safety Journal, 45(6-8), 371-384.

Ingason, H., & Li, Y. Z. (2010b). Model scale tunnel fire tests with longitudinal ventilation. Fire Safety Journal, 45(6), 371-384. https://doi.org/https://doi.org/10.1016/j.firesaf.2010.07.004

Ingason, H., Li, Y. Z., & Lönnermark, A. (2015). Runehamar tunnel fire tests. Fire Safety Journal, 71, 134-149. https://doi.org/https://doi.org/10.1016/j.firesaf.2014.11.015

Ingason, H., & Wickström, U. (2007). Measuring incident radiant heat flux using the plate thermometer. Fire Safety Journal, 42(2), 161-166. https://doi.org/https://doi.org/10.1016/j.firesaf.2006.08.008

Jahn, W., Rein, G., & Torero, J. L. (2008). The effect of model parameters on the simulation of fire dynamics. Fire Safety Science, 9, 1341-1352. https://doi.org/doi:10.3801/IAFSS.FSS.9-1341

Jalali, S. E., & Noroozi, M. (2009). Determination of the optimal escape routes of underground mine networks in emergency cases. Saf. Sci., 47. https://doi.org/10.1016/j.ssci.2009.01.001

Jin, W., Chen, S., & Jiang, H. (2013). Finding the K shortest paths in a time-schedule network with constraints on arcs. Computers & operations research, 40(12), 2975-2982.

Jinzhang, J., & Fengxiao, W. (2022). Study on emergency escape route planning under fire accidents in the Burtai coal mine. Scientific reports, 12(1), 13074. https://doi.org/10.1038/s41598-022-15437-7

Kerber, S., & Milke, J. A. (2007). Using FDS to Simulate Smoke Layer Interface Height in a Simple Atrium. Fire Technology, 43(1), 45-75. https://doi.org/10.1007/s10694-007-0007-7

Khan, M. M., Tewarson, A., & Chaos, M. (2016). Combustion characteristics of materials and generation of fire products. In SFPE handbook of fire protection engineering (pp. 1143-1232). Springer.

Kong, J., Xu, Z., You, W., Wang, B., Liang, Y., & Chen, T. (2021). Study of smoke back-layering length with different longitudinal fire locations in inclined tunnels under natural ventilation. Tunnelling and Underground Space Technology, 107, 103663.

Kong, J., You, W., Xu, Z., Liu, H., & Li, H. (2022). A numerical study on smoke behaviors in inclined tunnel fires under natural ventilation. Journal of Safety Science and Resilience, 3(2), 169-178.

KSL.com. (2022, Sept. 23). Retrieved Accesssed May 22, 2023. from https://www.ksl.com/article/50482277/lila-canyon-mine-fire-still-burning-in-carbon-county

Kuligowski, E. D. (2008). Modeling human behavior during building fires (NIST Technical Note 1619 Issue. https://citeseerx.ist.psu.edu/document?repid=rep1&type=pdf&doi=91d98730af8730f525c678ba12a1fc66121c1993

Laage, L. W., & Yang, H. (1991). Mine fire experiments at the Waldo Mine: heat flow. Proceedings of the US Mine Ventilation Symposium, West Virginia University, Morgantown, WV, USA.

Laage, L. W., & Yang, H. (1995, 5-7 Jun). Mine fire experiments and simulation with MFIRE. U.S. mine ventilation symposium, Lexington, KY (United States).

Lam, C. S., & Weckman, E. J. (2015). Wind-blown pool fire, Part II: Comparison of measured flame geometry with semi-empirical correlations. Fire Safety Journal, 78, 130-141.

Lee, Y.-P., & Tsai, K.-C. (2012). Effect of vehicular blockage on critical ventilation velocity and tunnel fire behavior in longitudinally ventilated tunnels. Fire Safety Journal, 53, 35-42. https://doi.org/https://doi.org/10.1016/j.firesaf.2012.06.013

Lemaire, T., & Kenyon, Y. (2006). Large Scale Fire Tests in the Second Benelux Tunnel. Fire Technology, 42(4), 329-350. https://doi.org/10.1007/s10694-006-8434-4

Li, C., Li, J., Hu, L., & Hou, D. (2015). Visualization and simulation model of underground mine fire disaster based on Cellular Automata. Applied Mathematical Modelling, 39(15), 4351-4364. https://doi.org/https://doi.org/10.1016/j.apm.2014.12.051

Li, Y. Z., Lei, B., & Ingason, H. (2010). Study of critical velocity and backlayering length in longitudinally ventilated tunnel fires. Fire Safety Journal, 45(6-8), 361-370.

Li, Y. Z., Lei, B., & Ingason, H. (2011). The maximum temperature of buoyancy-driven smoke flow beneath the ceiling in tunnel fires. Fire Safety Journal, 46(4), 204-210. https://doi.org/https://doi.org/10.1016/j.firesaf.2011.02.002

Liang, Y., Zhang, J., Ren, T., Wang, Z., & Song, S. (2018). Application of ventilation simulation to spontaneous combustion control in underground coal mine: A case study from Bulianta colliery. International Journal of Mining Science and Technology, 28(2), 231-242. https://doi.org/https://doi.org/10.1016/j.ijmst.2017.12.005

Lin, C.-J., & Chuah, Y. K. (2008). A study on long tunnel smoke extraction strategies by numerical simulation. Tunnelling and Underground Space Technology, 23(5), 522-530. https://doi.org/https://doi.org/10.1016/j.tust.2007.09.003

Lönnermark, A., Claesson, A., Lindström, J., Li, Y. Z., Kumm, M., & Ingason, H. (2012). Full-scale fire tests with a commuter train in a tunnel. S. T. R. I. o. Sweden. https://www.diva-portal.org/smash/get/diva2:962670/FULLTEXT01.pdf

Luo, N., Li, A., Gao, R., Zhang, W., & Tian, Z. (2013). An experiment and simulation of smoke confinement utilizing an air curtain. Safety Science, 59, 10-18. https://doi.org/https://doi.org/10.1016/j.ssci.2013.04.009

Macal, C. M., & North, M. J. (2009, 13-16 Dec. 2009). Agent-based modeling and simulation. Proceedings of the 2009 Winter Simulation Conference (WSC), Austin, TX, USA.

Maragkos, G., & Merci, B. (2020). On the use of dynamic turbulence modelling in fire applications. Combustion and Flame, 216, 9-23. https://doi.org/https://doi.org/10.1016/j.combustflame.2020.02.012

Marková, I., Lauko, J., Makovická Osvaldová, L., Mózer, V., Svetlík, J., Monoši, M., & Orinčák, M. (2020). Fire size of gasoline pool fires. International journal of environmental research and public health, 17(2), 411.

McGRATTAN, K. (2005). Fire modeling: where are we? where are we going? Fire Safety Science, 8, 53-68.

McGrattan, K., McDermott, R., Floyd, J., Hostikka, S., Forney, G., & Baum, H. (2012). Computational fluid dynamics modelling of fire. International Journal of Computational Fluid Dynamics, 26(6-8), 349-361.

McGrattan, K., Peacock, R., & Overholt, K. (2016). Validation of fire models applied to nuclear power plant safety. Fire Technology, 52, 5-24.

McGrattan, K. B., Baum, H. R., & Rehm, R. G. (1998). Large eddy simulations of smoke movement. Fire Safety Journal, 30(2), 161-178.

McGrattan, K. B., Peacock, R. D., & Overholt, K. J. (2014). Verification and validation of selected fire models for nuclear power plant applications supplement 1. U. S. N. R. C. NUREG-1824. https://www.nist.gov/publications/verification-and-validation-selected-fire-models-nuclear-power-plant-applications-1

Meng, N., Liu, B., Li, X., Jin, X., Huang, Y., & Wang, Q. (2018). Effect of blockage-induced near wake flow on fire properties in a longitudinally ventilated tunnel. International Journal of Thermal Sciences, 134, 1-12. https://doi.org/https://doi.org/10.1016/j.ijthermalsci.2018.07.037

Miao, Z., Wenhua, S., Ji, W., & Zhen, C. (2014). Accident consequence simulation analysis of pool fire in fire dike. Procedia Engineering, 84, 565-577.

Mossberg, A., Nilsson, D., & Wahlqvist, J. (2021). Evacuation elevators in an underground metro station: A Virtual Reality evacuation experiment. Fire Safety Journal, 120, 103091.

Nematollahi Sarvestani, A., Oreste, P., & Gennaro, S. (2023). Fire Scenarios Inside a Room-and-Pillar Underground Quarry Using Numerical Modeling to Define Emergency Plans. Applied Sciences, 13(7), 4607.

Newman, J. S. (1984). Experimental evaluation of fire-induced stratification. Combustion and flame, 57(1), 33-39.

Nguyen, M. H., Ho, T. V., & Zucker, J.-D. (2013). Integration of smoke effect and blind evacuation strategy (SEBES) within fire evacuation simulation. Simulation Modelling Practice and Theory, 36, 44-59.

NIOSH. (2021). Mine Disasters by Accident Type, 1839-2021 Retrieved Accessed May 22, 2023 from https://wwwn.cdc.gov/NIOSH-Mining/MMWC/MineDisasters/AccidentType

Oka, Y., & Atkinson, G. T. (1995). Control of smoke flow in tunnel fires. Fire Safety Journal, 25(4), 305-322. https://doi.org/https://doi.org/10.1016/0379-7112(96)00007-0

Oka, Y., Kakae, N., Imazeki, O., & Inagaki, K. (2013). Temperature property of ceiling jet in an inclined tunnel. Procedia Engineering, 62, 234-241.

Onifade, M. (2021). Towards an emergency preparedness for self-rescue from underground coal mines. Process Safety and Environmental Protection, 149, 946-957. https://doi.org/https://doi.org/10.1016/j.psep.2021.03.049

Onifade, M., Genc, B., Said, K., Fourie, M., & Akinseye, P. (2022). Overview of mine rescue approaches for underground coal fires: A South African perspective. Journal of the Southern African Institute of Mining and Metallurgy, 122(5), 213-226.

Overholt, K. J. (2014). Verification and validation of commonly used empirical correlations for fire scenarios. US Department of Commerce, National Institute of Standards and Technology.

Palacios, A., Rengel, B., Casal, J., Pastor, E., & Planas, E. (2020). Computational fluid dynamics modelling of hydrocarbon fires in open environments: Literature review. The Canadian Journal of Chemical Engineering, 98(11), 2381-2396.

Poulsen, A., & Jomaas, G. (2012). Experimental study on the burning behavior of pool fires in rooms with different wall linings. Fire Technology, 48, 419-439.

Queensland-Government. (2022). Queensland level 1 mine emergency exercise reports Retrieved Accessed May 22, 2023. from https://www.publications.qld.gov.au/dataset/queensland-level-1-mine-emergency-exercise-reports

Rahmani, A., Carlotti, P., Gay, B., & Buffat, M. (2004). Simulating fires in tunnels using large eddy simulation. International Conference Tunnel Safety and Ventilation, Graz Conference Proceedings, Graz, Austria.

Railsback, S. F., & Grimm, V. (2019). Agent-based and individual-based modeling: a practical introduction. Princeton university press. https://www.google.com/books/edition/Agent_Based_and_Individual_Based_Modelin/Zrh2DwAAQBAJ?hl=en&gbpv=0

Rew, C., & Deaves, D. (1999). Fire spread and flame length in ventilated tunnels-a model used in Channel tunnel assessments. Proceedings of the international conference on tunnel fires and escape from tunnels., Lyon, France.

Ronchi, E., Arias, S., La Mendola, S., & Johansson, N. (2019). A fire safety assessment approach for evacuation analysis in underground physics research facilities. Fire Safety Journal, 108, 102839.

Roxborough, F. (1997). Anatomy of a disaster-the explosion at Moura No 2 coal mine, Australia. Mining Technology, 79(906), pp. 37-43. https://www.osti.gov/etdeweb/biblio/453622

Salarian, A. H., Mashhadizadeh, A., & Bagheri, M. (2020). Simulating Passenger Evacuation in Railway Station under Fire Emergency using Safe Zone Approach. Transportation Research Record, 2674(11), 806-812. https://doi.org/10.1177/0361198120950316

Salvagni, R. G., Centeno, F. R., & Indrusiak, M. L. S. (2019). Burning rate, flame geometry and temperature of convection-controlled circular diesel oil pool fire under air crossflow conditions. Journal of hazardous materials, 368, 560-568.

Salvagni, R. G., Indrusiak, M. L. S., & Centeno, F. R. (2020). Biodiesel oil pool fire under air crossflow conditions: burning rate, flame geometric parameters and temperatures. International Journal of Heat and Mass Transfer, 149, 119164.

Shafee, S., & Yozgatligil, A. (2018). An analysis of tunnel fire characteristics under the effects of vehicular blockage and tunnel inclination. Tunnelling and Underground Space Technology, 79, 274-285. https://doi.org/https://doi.org/10.1016/j.tust.2018.05.019

Shen, T.-S. (2005). ESM: a building evacuation simulation model. Building and Environment, 40(5), 671-680. https://doi.org/https://doi.org/10.1016/j.buildenv.2004.08.029

Singh, C. S., Bhattacharjee, R., & Agrawal, H. (2021). An investigation on emergency response system during Anjan hill coal mine disaster using control task analysis–a cognitive approach. Journal of Mines, Metals and Fuels, 445-454.

Smith, A. C., & Thimons, E. D. (2009). A summary of US mine fire research. SME annual meeting and exhibit, Denver, Colorado.

Steinhaus, T., Welch, S., Carvel, R. O., & Torero, J. L. (2007). Large-scale pool fires. Thermal Science, 11(2), 101-118.

Stewart, C. (2021). Challenges and solutions in the development of the VentFIRE mine network fire simulator. In Mine Ventilation (pp. 300-308). CRC Press.

Stewart, C., Aminossadati, S., & Kizil, M. (2015). Underground fire rollback simulation in large scale ventilation models. 15th North American Mine Ventilation Symposium,

Tan, L., Hu, M., & Lin, H. (2015). Agent-based simulation of building evacuation: Combining human behavior with predictable spatial accessibility in a fire emergency. Information Sciences, 295, 53-66.

Tang, F., & Ren, A. (2008). Agent-based evacuation model incorporating fire scene and building geometry. Tsinghua Science and Technology, 13(5), 708-714. https://doi.org/10.1016/S1007-0214(08)70115-9

Tang, F. Q., & Ren, A. (2012). GIS-based 3D evacuation simulation for indoor fire. Build. Environ., 49. https://doi.org/10.1016/j.buildenv.2011.09.021

Tang, W., Yuan, L., Bahrami, D., & Rowland, J. (2021). Water spray suppression of leaked oil fires: A numerical study. In Mine Ventilation (pp. 309-316). CRC Press.

Tewarson, A. (1980). Heat release rate in fires. Fire and Materials, 4(4), 185-191.

Thomas, P. H. (1963). The size of flames from natural fires. Symposium (International) on Combustion, Elsevier.

Tilley, N., Rauwoens, P., & Merci, B. (2011). Verification of the accuracy of CFD simulations in small-scale tunnel and atrium fire configurations. Fire Safety Journal, 46(4), 186-193. https://doi.org/https://doi.org/10.1016/j.firesaf.2011.01.007

Trevits, M. A., Yuan, L., Teacoach, K., Valoski, M., & Urosek, J. (2009). Understanding mine fires by determining the characteristics of deep-seated fires. SME Annual Meeting, Denver, Colorado.

Trouvé, A., & Wang, Y. (2010). Large eddy simulation of compartment fires. International Journal of Computational Fluid Dynamics, 24(10), 449-466.

Tsai, K.-C., Chen, H.-H., & Lee, S.-K. (2010). Critical ventilation velocity for multi-source tunnel fires. Journal of Wind Engineering and Industrial Aerodynamics, 98(10), 650-660. https://doi.org/https://doi.org/10.1016/j.jweia.2010.06.006

Van Maele, K., & Merci, B. (2008). Application of RANS and LES field simulations to predict the critical ventilation velocity in longitudinally ventilated horizontal tunnels. Fire Safety Journal, 43(8), 598-609. https://doi.org/https://doi.org/10.1016/j.firesaf.2008.02.002

Vasanth, S., Tauseef, S. M., Abbasi, T., & Abbasi, S. A. (2013). Assessment of four turbulence models in simulation of large-scale pool fires in the presence of wind using computational fluid dynamics (CFD). Journal of Loss Prevention in the Process Industries, 26(6), 1071-1084. https://doi.org/https://doi.org/10.1016/j.jlp.2013.04.001

Verda, V., Borchiellini, R., Cosentino, S., Guelpa, E., & Tuni, J. M. (2021). Expanding the FDS Simulation Capabilities to Fire Tunnel Scenarios Through a Novel Multi-scale Model. Fire Technology, 57(5), 2491-2514. https://doi.org/10.1007/s10694-020-01081-y

Vermesi, I., Rein, G., Colella, F., Valkvist, M., & Jomaas, G. (2017). Reducing the computational requirements for simulating tunnel fires by combining multiscale modelling and multiple processor calculation. Tunnelling and Underground Space Technology,64, 146-153. https://doi.org/https://doi.org/10.1016/j.tust.2016.12.016

Wan, H., Gao, Z., Han, J., Ji, J., Ye, M., & Zhang, Y. (2019). A numerical study on smoke back-layering length and inlet air velocity of fires in an inclined tunnel under natural ventilation with a vertical shaft. International Journal of Thermal Sciences, 138, 293-303.

Wang, J., Yuan, J., Fang, Z., Tang, Z., Qian, P., & Ye, J. (2018). A model for predicting smoke back-layering length in tunnel fires with the combination of longitudinal ventilation and point extraction ventilation in the roof. Tunnelling and Underground Space Technology, 80, 16-25.

Wang, N., Gao, Y., Li, C.-y., & Gai, W.-m. (2021). Integrated agent-based simulation and evacuation risk-assessment model for underground building fire: A case study. Journal of Building Engineering, 40, 102609.

Wei, F., Fangping, Z., & Huiqing, L. (2011). The Use of 3D Simulation System in Mine Ventilation Management. Procedia Engineering, 26, 1370-1379. https://doi.org/https://doi.org/10.1016/j.proeng.2011.11.2313

Weisenpacher, P., Halada, L., & Glasa, J. (September 11-15). Computer simulation of fire in a tunnel using parallel version of FDS. MCS7 Conference Proceedings, Chia Laguna, Cagliari, Sardinia, Italy.

Weng, M.-c., Lu, X.-l., Liu, F., Shi, X.-p., & Yu, L.-x. (2015). Prediction of backlayering length and critical velocity in metro tunnel fires. Tunnelling and Underground Space Technology, 47, 64-72. https://doi.org/https://doi.org/10.1016/j.tust.2014.12.010

Woodburn, P., & Britter, R. (1996). CFD simulations of a tunnel fire—Part II. Fire Safety Journal, 26(1), 63-90.

Wu, F., Zhou, R., Shen, G., Jiang, J., & Li, K. (2018). Effects of ambient pressure on smoke back-layering in subway tunnel fires. Tunnelling and Underground Space Technology, 79, 134-142. https://doi.org/https://doi.org/10.1016/j.tust.2018.05.011

Xiang, Z., Si, G., Wang, Y., Belle, B., & Webb, D. (2021). Goaf gas drainage and its impact on coal oxidation behaviour: A conceptual model. International Journal of Coal Geology, 248, 103878. https://doi.org/https://doi.org/10.1016/j.coal.2021.103878

Yi, L., Niu, J. L., Xu, Z. S., & Wu, D. X. (2013). Experimental studies on smoke movement in a model tunnel with longitudinal ventilation. Tunnelling and Underground Space Technology, 35, 135-141. https://doi.org/https://doi.org/10.1016/j.tust.2013.01.005

Yu, L.-X., Beji, T., Zadeh, S. E., Liu, F., & Merci, B. (2016). Simulations of Smoke Flow Fields in a Wind Tunnel Under the Effect of an Air Curtain for Smoke Confinement. Fire Technology, 52(6), 2007-2026. https://doi.org/10.1007/s10694-016-0598-y

Yuan, J.-P., Fang, Z., Yin, Z.-C., & Lo, S.-M. (2009). Combined network model for occupant evacuation in building fires [22_Publication in policy or professional journal]. Tumu Jianzhu yu Huanjing Gongcheng/Journal of Civil, Architectural and Environmental Engineering, 31(2). http://www.scopus.com/inward/record.url?scp=66149096626&partnerID=8YFLogxK

https://www.scopus.com/record/pubmetrics.uri?eid=2-s2.0-66149096626&origin=recordpage

Yuan, L., & Smith, A. C. (2009). CFD modeling of spontaneous heating in a large-scale coal chamber. Journal of Loss Prevention in the Process Industries, 22(4), 426-433. https://doi.org/https://doi.org/10.1016/j.jlp.2009.02.016

Yuan, L., & Smith, A. C. (2015). Numerical modeling of water spray suppression of conveyor belt fires in a large-scale tunnel. Process Safety and Environmental Protection, 95, 93-101. https://doi.org/https://doi.org/10.1016/j.psep.2015.02.018

Yuan, L., Zhou, L., & Smith, A. C. (2016). Modeling carbon monoxide spread in underground mine fires. Applied Thermal Engineering, 100, 1319-1326. https://doi.org/https://doi.org/10.1016/j.applthermaleng.2016.03.007

Zanzi, C., Gómez, P., López, J., & Hernández, J. (2019). Analysis of Heat and Smoke Propagation and Oscillatory Flow through Ceiling Vents in a Large-Scale Compartment Fire. Applied Sciences, 9(16).

Zhai, Z. J., Zhang, Z., Zhang, W., & Chen, Q. Y. (2007). Evaluation of Various Turbulence Models in Predicting Airflow and Turbulence in Enclosed Environments by CFD: Part 1—Summary of Prevalent Turbulence Models. HVAC&R Research, 13(6), 853-870. https://doi.org/10.1080/10789669.2007.10391459

Zhang, G., Zhu, G., Yuan, G., & Wang, Y. (2016). Quantitative risk assessment methods of evacuation safety for collapse of large steel structure gymnasium caused by localized fire. Safety Science, 87, 234-242. https://doi.org/https://doi.org/10.1016/j.ssci.2016.04.013

Zhang, X. (2012). Underground mine fire simulation using multiscale modeling approach [Doctoral dissertation, Missouri University of Science and Technology.]. https://www.proquest.com/docview/1322967711?pq-origsite=gscholar&fromopenview=true

Zhang, X., Lin, Y., Shi, C., & Zhang, J. (2021). Numerical simulation on the maximum temperature and smoke back-layering length in a tilted tunnel under natural ventilation. Tunnelling and Underground Space Technology, 107, 103661. https://doi.org/https://doi.org/10.1016/j.tust.2020.103661

Zhang, Z., Zhang, W., Zhai, Z. J., & Chen, Q. Y. (2007). Evaluation of Various Turbulence Models in Predicting Airflow and Turbulence in Enclosed Environments by CFD: Part 2—Comparison with Experimental Data from Literature. HVAC&R Research, 13(6), 871-886. https://doi.org/10.1080/10789669.2007.10391460

Zhen, C., & Xiaolin, W. (2014). Analysis for Combustion Properties of Crude Oil Pool Fire. Procedia Engineering, 84, 514-523. https://doi.org/https://doi.org/10.1016/j.proeng.2014.10.463

Zheng, S., & Liu, H. (2019). Improved Multi-Agent Deep Deterministic Policy Gradient for Path Planning-Based Crowd Simulation. IEEE Access, 7, 147755-147770. https://doi.org/10.1109/ACCESS.2019.2946659

Zhiyin, Y. (2015). Large-eddy simulation: Past, present and the future. Chinese Journal of Aeronautics, 28(1), 11-24. https://doi.org/https://doi.org/10.1016/j.cja.2014.12.007

Zhou, L. (2009). Improvement of the mine fire simulation program MFIRE [Doctoral dissertation West Virginia University]. https://researchrepository.wvu.edu/etd/2937/

Zhou, L., Smith, A., & Yuan, L. (2016). New improvements to MFIRE to enhance fire modeling capabilities. Mining engineering, 68(6), 45.

Zhou, L., & Smith, A. C. (2012). Improvement of a mine fire simulation program—incorporation of smoke rollback into MFIRE 3.0. Journal of fire sciences, 30(1), 29-39.

Zhou, L., Yuan, L., Bahrami, D., Thomas, R. A., & Rowland, J. H. (2018). Numerical and experimental investigation of carbon monoxide spread in underground mine fires. Journal of Fire Sciences, 36(5), 406-418. https://doi.org/10.1177/0734904118793891

Zhou, L., Yuan, L., Thomas, R., Bahrami, D., & Rowland, J. (2020). An Improved Method to Calculate the Heat Release Rate of a Mine Fire in Underground Mines. Mining, Metallurgy & Exploration, 37(6), 1941-1949.

Zhu, Y., Wang, D., Shao, Z., Xu, C., Zhu, X., Qi, X., & Liu, F. (2019). A statistical analysis of coalmine fires and explosions in China. Process Safety and Environmental Protection, 121, 357-366. https://doi.org/https://doi.org/10.1016/j.psep.2018.11.013

II. ENHANCING FIRE SAFETY IN UNDERGROUND MINES: AN EXPERIMENTAL AND NUMERICAL STUDY ON TEMPERATURE ATTENUATION, GAS EVOLUTION, AND BIFURCATION INFLUENCE FOR IMPROVED EMERGENCY RESPONSE

Salami O.B[a], Ashish Ranjan Kumar[b], Iqbal Aamir[a], Robert Ilango Pushparaj[a] Guang Xu[a]*

[a] Department of Mining and Explosives Engineering, Missouri University of Science and Technology, Rolla, Missouri, 65401, USA

[b] Department of Energy and Mineral Engineering, Penn State University Park, PA 16802, USA

ABSTRACT

The occurrence of underground mine fires remains a significant and persistent safety challenge in the mining industry, posing imminent risks to both miners' lives and the operational integrity of mining facilities. Current underground mine fire studies lack scale accuracy due to lab experiments and fail to consider bifurcation effects on smoke gas temperature. This study performed full-scale experiments and built validated CFD models to explore the interactive impact of ventilation and fire size on temperature attenuation, gas behavior, and CO generation in underground mines. A new empirical correlation for temperature decay in the mine drift was developed and its accuracy was compared with established models in the literature. In addition, the influence of bifurcation on maximum smoke temperature was analyzed. This research combines full-scale experiments and validated CFD modeling to address major gaps in underground mine fire studies. Unlike previous methods, our approach explores the interactive effects of ventilation, fire size, temperature attenuation, and toxic gas spread, offering unprecedented insights. This

innovation enables the development of tailored fire safety standards for mines, ensuring safer designs, rapid fire suppression, and improved evacuation strategies. By bridging theory and practice, our work transforms fundamental knowledge, empowering the mining industry to enhance safety measures, protect lives, and mitigate the impact of underground mine fires.

Keywords: Full-scale fire, temperature attenuation, buoyancy-driven flow, underground space bifurcation, emergency evacuation.

1. INTRODUCTION

Fires in underground confined spaces are extremely dangerous and remains one of the most catastrophic environmental hazards that may occur in mines (Chen et al., 2023; Fernández-Alaiz, Castañón, et al., 2020a; Huang et al., 2022; Kamran et al., 2023; Khan & Abbasi, 1999; Lei et al., 2021; Mavhura, 2019; O. B. Salami et al., 2023; Oluwafemi Babatunde Salami, G. Xu, et al., 2023; Yuan et al., 2018). Studies have shown that mine fires produce high levels of toxic gases and smoke which could be dispersed quickly through the ventilation network to various parts of the underground workings (Düzgün & Leveson, 2018; Kamran et al., 2023; O. B. Salami et al., 2023). The toxic smoke released during fires further reduce visibility and escape chances of trapped occupants during fires (Chen et al., 2023; Kirytopoulos et al., 2014; Lee & Ghazali, 2018; Lei et al., 2021). Most fatalities due to underground fires could be attributed to the inhalation of noxious smoke gases mainly carbon monoxide (Bahrami et al., 2021; Chen et al., 2023; Zhou, 2009b; Zhou et al., 2018).

Quantifying fire development is critical to developing improved industrial fire safety measures such as predicting the fire development trends, evaluating the severity of the accidents, assessing the losses due to fires in real-time and informing the fire fighting and emergency response tactics (Huang et al., 2022; Oluwafemi Babatunde Salami, Guang Xu, et al., 2023; Yuan et al., 2018). Currently, underground mine fire hazard quantification, fire risk assessment, and risk mitigation studies have employed a wide range of approaches ranging from small scale experimental, full-scale tests, and numerical methods such as computational fluid dynamics (CFD)(Hansen & Ingason, 2013a; Ingason & Li, 2010; Li et al., 2011; Lu, Weng, Liu, Wang, Han, & Cheung, 2022; Oka & Atkinson, 1995; Yuan et al., 2016).

Several studies have been conducted using experimental and numerical techniques on mine fire detection, suppression, and firefighting (Hansen; Lei et al., 2021; Yuan et al., 2018). Liu et al (Liu et al., 2017) establishes a new temperature decay model due to fire-induced smoke in node are of an underground mine but neglected the influence of bifurcation on maximum smoke gas temperature. Hong et al (Hong et al., 2022) used a combination of different machine models to predict the spread of smoke of fire smoke in mine tunnels. The study demonstrated that ML models such as random forest (RF), support vector machine (SVM), and artificial neural network could predict whether back flow of fire smoke will occur or not. Dong et al (Dong et al., 2017) investigated the effectiveness of aqueous form for fire-fighting in underground and discovered that foam could block the cracks in coal goaf thus preventing the supply of air to the goaf and subsequent oxidation which may lead to fire. In another study, Chen et al (Chen et al., 2023) conducted studies that allow the design of a fire protection system for tunnel fires. The effect of centralized

ceiling smoke exhaust system with air curtains were examined with plug-holing phenomenon during a tunnel fire and a new predictive model that could predict the smoke efficiency for the coupled system with a fire size of up to 20 MW was developed.

In addition, some studies have also investigated the heat release of mining vehicles in a full-scale fire test by burning mining trucks in an underground mine (Hansen, 2019a; Hansen & Ingason, 2013b, 2013c). Whereas, many other researchers have employed numerical approaches such as CFD and ventilation network analysis models to complement full-scale fire experiments (Gannouni & Maad, 2015; Haghighat et al., 2018; Yuan & Smith, 2015; Yuan et al., 2016; Zhu et al., 2016). This is due to the high cost of conducting full-scale tests, and sometimes to examine fires that are too dangerous or expensive to effectuate in real-world settings (O. B. Salami et al., 2023).

CFD has been successfully applied to evaluate fires hazards, fire suppression performances, and smoke and gases dispersion in mining related problems (Chang et al., 2019; Fernández-Alaiz, Castañón, et al., 2020a; O. B. Salami et al., 2023; Xu et al., 2016; Yuan & Smith, 2015). In a series of studies, full-scale tests and analogous CFD simulations were deployed to examine the ventilation influence on mine fire evolution (Fernández-Alaiz, Castañón, et al., 2020a; Fernández-Alaiz, Castañón, Gómez-Fernández, Bernardo-Sánchez, et al., 2020; Fernánez-Alaiz et al., 2020). Findings from the CFD simulations were extended to examine the hazards of potential fire occurrence and the effectiveness of available emergency response in the mine (Fernández-Alaiz, Castañón, et al., 2020a). The study highlighted important trends of the fire based on the ventilation-fuel load ratio, thus successfully predicting the potential impact of fires within the underground space. In another research, a CFD model was developed to evaluate the effect of sprinkler activation

temperature, water flow rate, and the location of the sprinkler on the suppression of conveyor belts fires in mines (Yuan & Smith, 2015).

Presently, our understanding about fires and toxic gases spread in underground mines are inadequate to develop appropriate fire risk assessment framework for underground mining environments. First, most of the existing fire risk management studies were conducted using a model-scale tunnel apparatus in the laboratory which makes it impossible to preserve all the dimensionless terms derived by the scaling theory (Li & Ingason, 2012; O. B. Salami et al., 2023). Second, findings from existing literature are failed to account for the influence of bifurcations on the maximum smoke gas temperature beneath the ceiling in an underground mine, as compared to transport tunnels. The generation of carbon monoxide (CO)-a chief cause of miners' fatalities in the underground - has been neglected in most mine/tunnel fire studies (Han et al., 2021; Huang et al., 2018; Li & Ingason, 2012; Li et al., 2011; Tang et al., 2018; Zhang et al., 2021).

Another major concern is that accidents continue to occur despite the tremendous progress that has been made regarding the risk assessment frameworks and the owing to the complex nature of underground environments (Gehandler, 2015). Therefore, it remains unclear whether just applying risk assessment method can ensure sufficient preparedness against a fire occurrence (Ntzeremes & Kirytopoulos, 2019). To address this shortcoming, it important to employ a combination of full-scale experimental and numerical techniques that will enable further understanding of the fire and smoke spread mechanism, and the influence of bifurcation on maximum smoke gas temperature induced by fire in an underground mine.

The objective of this study was to investigate the interactive influence of ventilation and fire size on temperature attenuation, maximum excess gas temperature, and toxic gas spread using full-scale experiments. Furthermore, a CFD model was built and validated based on the experimental scenario, and the model was extended to investigate the influence of bifurcations on maximum excess smoke gas temperature due to fire-induced smoke flow in the underground mine. A new empirical correlation for temperature decay in the mine drift was developed and the accuracy analyzed by comparing the new model with some of the existing models. The influence of fire size and ventilation conditions on the generation of carbon monoxide (CO) in the mine was also analyzed using the peak value of CO emitted during each fire test. The importance of this study is to aid the development of new fire safety standards and suppression techniques. This research would serve a reliable guide for estimating the fire intensity and assessing the risk of fires in deep underground environments and would aid a safe, and environmentally friendly fire risk management in the future design of subsurface environments. The data obtained from this study will be very useful to validate existing mine fire CFD models, thus improving the safe application of emergency evacuation strategies and escape plans in case of underground fires.

2. EXPERIMENTAL METHODS

2.1. TEST LOCATION

The Missouri S&T experimental mine was used as the test site for this investigation. The layout of the mine is presented in Figure 1. The mine airways are approximately

rectangular in shape with an average width of 2.6 m and height of 3.2 m. The mine is a typical room-and-pillar underground mine with four pillars and a main drift about 54 m long. Air entered the mine from the entrance at the lower part of the map in Figure 1 and was exhausted through a main fan on the surface.

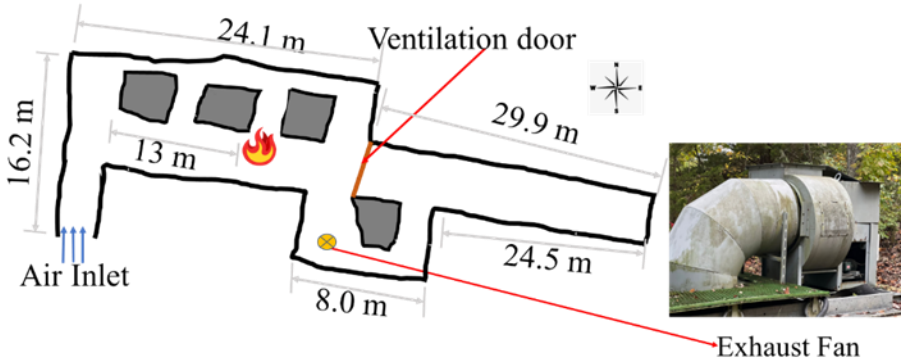

Figure 1. Plan view of the study location and the exhaust fan.

2.2. FULL SCALE FIRE

The weighing scale was first set up and the fire pan was then placed on a 30 cm by 30 cm frame to avoid direct contact with the scale since the elevated temperature may destroy the scale. Secondly, the scale was tarred to zero before the diesel was poured into the pan to get precise weight of the fuel. The monitors and sensors were then synchronized to log the data from a remote computer before the fire pool was ignited.

Longitudinal ventilation velocity in the mine was determined 3 m downstream of the fire location using the point transverse method before each fire pool test. The fire pool was placed at 13 m from the in-by portal along the main drift (indicated by a fire ion in Figure 1). The points traverse measurements were conducted using a rotating vane electrical anemometer. The measurement was done by dividing the cross section into nine

equal rectangle area and measuring the velocity at center points for 30 s before taking the average reading of the anemometer. The measuring point along the cross-section is denoted as P1 to P9 as shown in Figure 2.

Two factors: The fire pool size and ventilation rate were used for the experimental design: each factor had three levels and a total of nine experimental runs were conducted using a 3k factorial design. The factors and the measured ambient temperature are presented in Table 1.

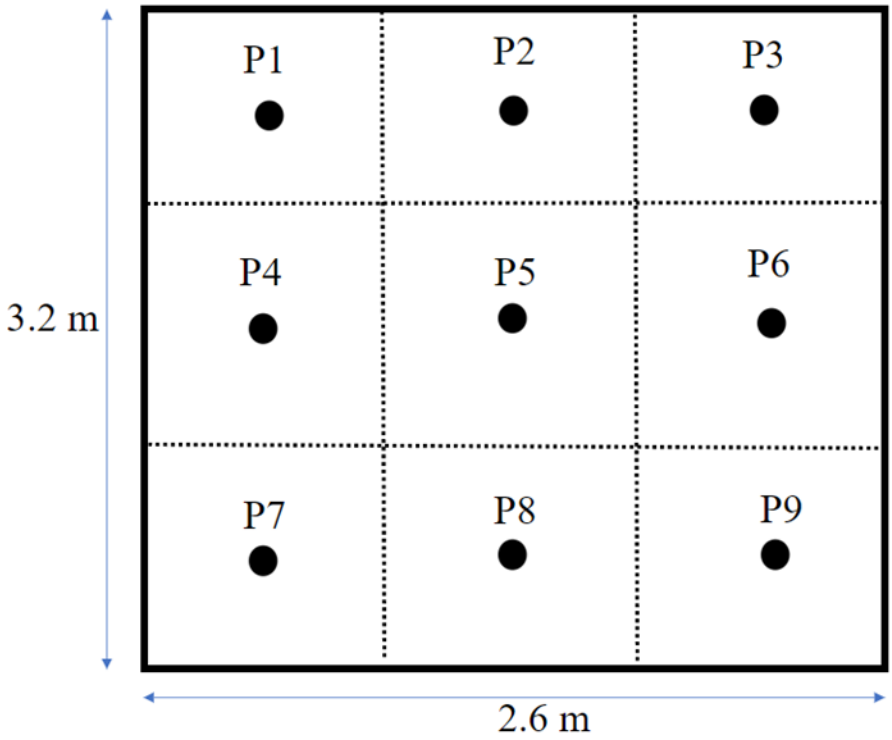

Figure 2. Velocity measuring points at the station's cross section 3m downstream of fire.

Pool containers of diameter 0.3 m, 0.5 m, and 0.7 m, as shown in Figure 3(a), were used for this investigation, while longitudinal ventilation conditions were varied by adjusting the ceiling smoke extraction rate between 0-100 %. 0% ventilation implies the

exhaust fan was put off; the 50 % ventilation is achieved by turning the fan on but blocking half of the fan duct cross-section area using a circular wooden board as shown in Figure 3 (b) while 100 % ventilation is achieved when the fan duct is completely opened as depicted in Figure 3(c).

Table 1. Randomized experimental test cases.

Experiment	1	2	3	4	5	6	7	8	9
Ventilation rate (%)	100	50	0	0	50	50	100	100	0
Exhaust Air Volume (m^3/s)	5.42	2.97	0.24	0.24	2.97	2.97	5.42	5.42	0.24
Fire Size (m)	0.7	0.5	0.5	0.7	0.7	0.3	0.3	0.5	0.3
Ambient Temperature (^oC)	27.5	22.5	22.5	22.5	19.5	19.5	19.5	19.5	19.5

For each of the fire test, 0.5 gal of diesel was used. After each test, 10 mins were allowed with the fan fully operational to exhaust the smoke and allow the underground temperature to reset to near ambient conditions for the subsequent experimentation. The mine had a ventilation door located at approximately 12 m from the fire pool downstream which separated the testing region from the blind heading of the main drift in the underground. Thus, the fire could be considered axisymmetric within the test region. CO monitors (EasyLog CO monitors), denoted as “G” in Figure 4, were placed 4 m upstream and downstream of the fire and 1.5 m above the floor to measure the carbon monoxide concentration. Smoke temperature was measured beneath the mine ceiling, and at position 1 m below the roof of the mine using K-type thermocouples.

(a)Fire Pans (b)Fan at 50% (c)Fan at 100%

Figure 3. Fire pans and the fan opening.

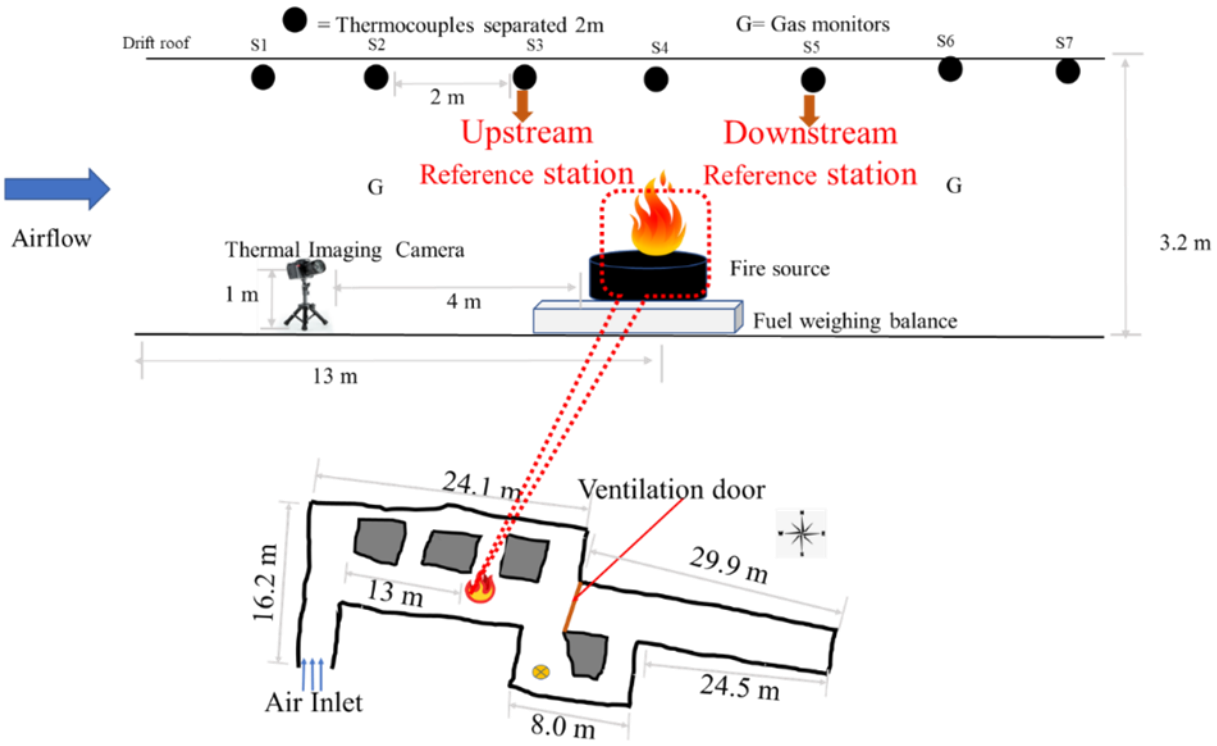

Figure 4. Complete experimental instrumentation.

At the roof of the mine, thermocouples were installed at all seven locations (S1-S7), as depicted in Figure 4, whereas thermocouples could only be installed at stations S1, S2, S3, S5, S6, and S7 1m below the roof of the mine. No thermocouple was installed at S6 because it was too close to the fire surface and could be destroyed quickly by the fire.

Additionally, a thermal imaging camera (TIC) was mounted 4m upstream of fire during the tests. The TIC was utilized to capture the surface temperature of the fire for the post fire analysis of the fire flame properties. A sample of the image from the TIC taken during the experiment is shown in Figure 5.

Figure 5. Sample image from TIC.

2.2.1. Heat Release Rate (HRR) Determination. The heat release rate is the most important fire parameter. It is also a very critical input for CFD simulations of fire. The HRR was used to estimate the fire intensity. It can be determined by measuring the changes in the mass of the fuel to the burning time, as given in Equation (1) (Yuan et al., 2016; Zhou et al., 2018):

$$Q = m''\Delta H_c \quad (1)$$

where m"is the burning rate or mass loss rate (kgs^{-1}), and ΔH_c is the heat of combustion ($kJ.kg^{-1}$).

2.2.2. Thermal Image and Flame Analysis. The flame analysis was done using the FLIR E 86 Thermal Imagining Camera (TIC). The FLIR E 86 was embedded with high performance features required for quick and accurate detection of hot spots. The TIC has a 464 ×348 pixel and an expanded temperature range for accurate temperature detection. However, the temperature range of 0-650 ^{o} C was selected for this study. The purpose of analyzing the flame was to identify high-risk zones to fire rescuers and emergency responders for a given fire scenario, thereby improving fire safety. The TIC images were analyzed using the image segmentation toolbox in MATLAB, which was achieved by following the basics steps: (1) identifying elevated temperature spots (2) extracting the temperature values at the marked spot (3) plotting temperature values at the marked spot (4) obtaining maximum temperature values for the marked regions.

3. NUMERICAL SIMULATIONS

3.1. COMPUTATIONAL DOMAIN

The grid size used for a CFD- fire dynamic simulation (FDS) is the principal factor that determines the resolution of the FDS simulation. It could impact properties like fire smoke temperature measured at the underground ceiling. For this reason, appropriate grid sensitivity should be done to obtain mesh independence. In FDS, the grid size can be derived by the fire characteristic diameter given in Equation (2) (McGrattan et al., 2013; Weng et al., 2015):

$$D^* = \left(\frac{\dot{Q}}{\rho_\infty c_p T_\infty \sqrt{g}}\right)^{2/5} \tag{2}$$

where δx denotes the nominal size of the mesh cell, $\dot{Q}$ represents the total heat release rate of the fire (kW), ρ_∞ designates the ambient air density kg/m^3, C_p is the specific heat capacity of air (KJ/kg/k), T_∞ is the ambient temperature (K), and g is the acceleration due to gravity (usually taken as 9.81 m/s^2) (McGrattan et al., 2013; McGrattan et al., 2016; Overholt, 2014).

The ratio of the fire characteristic size to grid size ($D^*/\delta x$), known as the plume resolution (PR) index, is normally used to describe the quality of the calculation grid (Gannouni & Maad, 2015). The higher this value is, the finer the meshes are and the more computational time is required for the CFD simulation. However, sensitivity studies from the literature have recommended that values between 4 to 16 are sufficient to obtain an appropriate resolution with minimal computational requirements (McGrattan et al., 2013; McGrattan et al., 2014). The mesh size for this simulation is also determined by this rule. For this study, the computational domain was obtained by setting the x, x', y, y', z, and z' to 0, 54, 0, 12.5, and 0, 3.2 where x, y, and z represent the minimum values and x', y', and z' denote the maximum values for the coordinates x, y, and z, respectively.

The mesh size for this simulation was determined based on the experimental case considered before the model was validated. The experimental case examined was 0.7 m diameter pool fire with a 100 % smoke ceiling extraction. The maximum HRR of the fire obtained from the experiment was 425.0 KW. The computed characteristics fire diameter, D*, was 4.91. Based on the calculated fire characteristics diameter, a mesh size of 0.2 m was selected to obtain fine mesh for the grid calculations.

3.2. SIMULATION PARAMETERS AND BOUNDARY CONDITIONS

For this study, the default setting for the dynamic turbulence modeling was retained. The default settings adopted the constant Smagorinsky model (where P_{rt}=0.5, S_{ct}=0.5, and C_s=0.17). Furthermore, the environmental conditions were set to the experimental conditions during the fire test. The HRRPUA for the FDS simulation was set based on 425 KW fire and the calculated pool area. The reaction type was set as "HEPTANE'', "CO_YIELD =0.1", and the "SOOT_YIELD =0.1". The main inlet to the mine was modeled as "OPEN" surface. Similarly, the exhaust fan was modeled as "EXHASUT" with a specified volume flow of 5.42 m^3/s. Furthermore, the pillars were modeled as a slab obstruction, the materials for the walls were set as "CONCRETE", and the surfaces of the wall were assigned "INERT" for the FDS simulation. Concrete was used as the material for the mine walls and ceiling. The properties of the concrete were set as follows: density (2100 kg/m^3), specific heat (879J/kg K), and thermal conductivity were 1.10 W/m K according to Seike et al. (Seike et al., 2017).

Furthermore, to ensure that the numerical results were reliable and computationally correct, the time step was constrained such that the Courant-Friedrichs-Lewy (CFL) condition given in Equation (3) was satisfied (Cheong et al., 2009; Gannouni & Maad, 2015):

$$\delta t \, max \left(\frac{u}{\delta x}, \frac{v}{\delta y}, \frac{w}{\delta z}\right) \leq 1 \tag{3}$$

The initial time step was specified automatically in FDS by dividing the grid size by the characteristic velocity of the flow. The value of the time step could be determined by Equation (4):

$$\frac{5(\delta x \delta y \delta z)^{1/3}}{\sqrt{gH}} \quad (4)$$

For each time step during the calculations, the velocities u, v, and w were tested to ensure that the CFL condition was met. In a situation where CFL is greater than 1.0, the time step is set to 0.8 of its allowed peak value, and the velocities are recalculated and tested again. This is because the solutions to the equations cannot be updated with a time step greater than 1.0 which implies a parcel of fluid crossing the grid cell (Cheong et al., 2009). The time step was set between 0.8-1.0 for this study.

The fire was simulated utilizing a high-performance computer with FDS 6.7.6 using the large eddy simulation (LES) turbulence model. The whole domain was divided into four continuous domains and each domain was assigned to a processor to minimize the computational time. The ambient temperature for the simulation was set based on the measured value during the experiment., the set pressure was 101325.0 Pa, and simulation time was set to 600.0 s.

3.3. TEMPERATURE DISTRIBUTION

The temperature distribution in the underground environment is critical for the fire safety design and proactive measures such as the selection of appropriate tunnel lining materials, deployment of proper smoke control strategies, fire suppression systems, and emergency evacuation planning. To better enhance our understanding about the temperature evolution in mines, two main temperature indicators were considered for this investigation: temperature attenuation and maximum excess gas temperature beneath the tunnel ceiling.

Temperature attenuation may either be longitudinal or transverse (Li & Ingason, 2018). Longitudinal temperature attenuation indicates the temperature decay along the underground drift while the transverse temperature attenuation measures the temperature decay between the walls of the tunnel/drift. However, the longitudinal temperature variation along the mine airways is more important than the transverse temperature evolution as occupants tend to evacuate along the airways instead of moving zigzag between the walls of the mine airways. Thus, only the longitudinal temperature attenuation and maximum excess smoke temperature beneath the ceiling were considered for analysis in this study. A theoretical background of the two main temperature distribution indicators is presented below.

3.3.1. Longitudinal Temperature Attenuation. In an earlier study, an empirical model for temperature distribution beneath a tunnel ceiling was developed for fires that are centrally located in beamed channels as follow (Delichatsios, 1981):

$$\frac{\overline{\Delta T}}{\overline{\Delta T_0}}\left(\frac{l_b}{H}\right)^{1/3} = 0.49e^{\left\{-6.67tS_t\left(\frac{l_b}{H}\right)^{1/3}\right\}} \quad (5)$$

where ΔT_0 is the average temperature rise near the ceiling over the fire source , $\overline{\Delta T}$ is the average instantaneous temperature rise at a specified location from the fire axis, l_b represents the beam depth, H is the separation between the fire surface and the ceiling, and S_t is the Stanton number which was estimated to be 0.03 from the correlation of experimental data obtained from the study. The temperature attenuation conformed with exponential decay laws and subsequent investigations corroborated this finding. A later study by Hu et al (Hu et al., 2013; L. H. Hu et al., 2008), involving series of full-scale tests in large tunnels and vehicular tunnels, showed that temperature beneath the ceiling in a

longitudinally ventilated tunnel can be expressed as an exponential decay given by Equation (6):

$$\frac{\Delta T_x}{\Delta T_r} = e^{-\beta(x-x_r)} \tag{6}$$

where ΔT_x is the maximum increase in temperature x m away from a reference point, ΔT_r is the maximum increase in temperature at the reference point, x is the distance from the coordinate origin, x_r denotes the distance of separation between the fire and the coordinate origin, and β is the temperature attenuation factor.

Zhao et al (Zhao et al., 2019) investigated the ceiling temperature distribution in a 1:20 reduced-scaled model tunnel and estimated the attenuation factor to be 0.536 for a tunnel fire with a two-point extraction ventilation system. Thus, using their attenuation factor, a modified Hu's equation was obtained as given by eq. (7):

$$\frac{\Delta T_x}{\Delta T_r} = e^{-0.536(x-x_r)} \tag{7}$$

Another study involving a total of twelve tests in a model tunnel (with similarity of 1:23), Ingason and Li (Ingason & Li, 2010) demonstrated that the distribution of excess gas temperature beneath ceiling without ceiling mechanical smoke extraction can be expressed as a sum of two attenuation given by Equation (8):

$$\frac{\Delta T_x}{\Delta T_r} = 0.57e^{-0.13(\frac{x-x_r}{H})} + 0.43e^{-0.048(\frac{x-x_r}{H})} \tag{8}$$

Therefore, the generalized temperature decay model beneath tunnel/drift ceiling can be modified using exponential model as presented in Equation (9):

$$\frac{\Delta T_x}{\Delta T_r} = Ae^{-F1(\frac{x-x_r}{H})} + Be^{-F2(\frac{x-x_r}{H})} \tag{9}$$

where A, B, F1, and F2 are coefficients.

Although Hu's model with the assumption of zero entrainment of air from counter flow remains the most widely used model for tunnel ceiling temperature attenuation, most of the existing models were developed based on one-dimensional spreading phase (see Figure 6) downstream of the fire (Zhao et al., 2018).

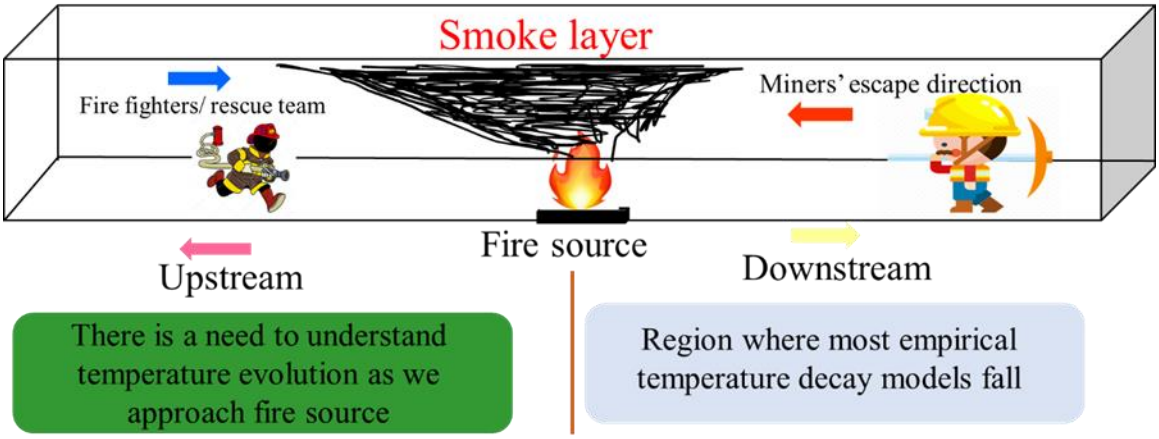

Figure 6 Illustration of region of applicability of existing temperature attenuation models.

However, as seen from Figure 6, it is also important to understand how the temperature evolves along the airway from a reference point upstream. This could help fire fighters and rescue teams to have an insight into the fire situation in the underground based on the observed temperature upstream of the fire. In this study, the temperature distribution upstream of the fire source was also examined and analyzed. Figure 6 illustrates an emergency scenario where miners tried to escape from the fire and the fire-fighters/rescue team were advancing from the upstream position to put out the fire to evacuate the trapped occupants.

3.3.2. Maximum Excess Smoke Temperature. The maximum temperature beneath the ceiling to which an underground structure or tunnel is exposed during a fire must be determined to identify the required fire protection needed for the tunnel structure

(Han et al., 2021; Hu et al., 2013; Li & Ingason, 2012; Li et al., 2011; Tang et al., 2018; Zhang et al., 2021). The activation of fire suppression systems depends on the preset activation temperature, and the potential temperature rise expected during a fire outbreak (Li & Ingason, 2018; Tang et al., 2021; Yuan & Smith, 2015). To know the possible excess rise in temperature that may occur for these types of structures, several predictive models were developed to foretell maximum temperature of thermal plume in an underground environment (Chen et al., 2020; Hu et al., 2013; Hu et al., 2006; Kurioka et al., 2003; Li & Ingason, 2012; Li et al., 2011).

(Kurioka et al., 2003) conducted an extensive experimental investigation into fire properties in the near field region and developed an empirical formula for the maximum temperature. Likewise, Li et al (Li & Ingason, 2012; Li et al., 2011) applied the thermal plume theory to examine the maximum gas temperature beneath the tunnel ceiling and observed that the maximum gas temperature observed could be categorized into two regions for situations when the flame region is lower than the ceiling height. They showed that the relationship between the maximum gas temperature and the dimensionless heat release rate could be a linear or polynomial expression depending on the calculated values for the dimensionless ventilation velocity. Hu et al's group (Hu et al., 2013) studied the effect of tunnel slope on the maximum temperature of fire-induced hot gases and discovered that the gas temperature decay faster as the tunnel slope increases. Their investigation yielded a new empirical model that incorporated the effect of tunnel slope on temperature decay beneath tunnel ceiling.

In another study, the influence of tunnel sealing ratio on maximum temperature beneath ceiling was examined and a new empirical model was developed (Chen et al.,

2020). The study introduced the concept of critical sealing ratio which was observed to decrease as the heat release rate increased.

Despite the numerous predictive models developed, many of these models could be derived by slight modifications from the Kurioka's (Kurioka et al., 2003) and Li's (Li et al., 2011) models. Thus, the two fundamental models were presented for further analysis in this study.

(Kurioka et al., 2003) model relates the maximum change in thermal plume temperature to a dimensionless HRR and Froude number as follows.

$$\frac{\Delta T_{max}}{T_a} = \gamma \left(\frac{Q'^{2/3}}{Fr^{1/3}}\right)^{\varepsilon}, \tag{10}$$

where Q' is the dimensionless heat release rate of the fire expressed as:

$$Q' = \frac{Q}{(\rho_a C_p T_a g^{1/2} H_d^{5/2})}$$

Fr represents the Froude number and it is expressed as:

$$Fr = \frac{U^2}{gH_d},$$

where ρ_a, T_a, H_d, and u denote density, temperature of the ambient air, effective height of tunnel (that is, height from the surface of the fire source to the tunnel ceiling), and the longitudinal air velocity in the tunnel, respectively. The value of the constant parameters depends on the ratio of $\left(\frac{Q'^{2/3}}{Fr^{1/3}}\right)$ as follow:

$$\left(\frac{Q'^{2/3}}{Fr^{1/3}}\right) < 1.35, \qquad \gamma = 1.77, \varepsilon$$

$$\left(\frac{Q'^{2/3}}{Fr^{1/3}}\right) \geq 1.35, \qquad \gamma = 2.54, \varepsilon$$

Conversely, Li et al (Li et al., 2011) expressed the maximum change in temperature rise as a function of the HRR and effective tunnel height based on the value of a dimensionless ventilation velocity as follows:

$$f(x) = \begin{cases} 17.5\dfrac{Q^{2/3}}{H_{ef}^{5/3}}, & V' \leq 0.19 \\ \dfrac{Q}{V b_{fo}^{1/3} H_{ef}^{5/3}}, & V' > 0.19 \end{cases} \quad (11)$$

where Q, H_{ef}, V, V', and b_{fo}, represent the heat release rate, effective tunnel height, ventilation velocity, dimensionless ventilation velocity, and radius of the fire pool, respectively. The dimensionless ventilation velocity is given by:

$$V' = \frac{V}{\left(\dfrac{gQ}{b_{fo}\rho_a c_p T_a}\right)^{1/3}}$$

4. RESULTS AND DISCUSSION

4.1. AIR FLOW/ LONGITUDINAL VENTILATION VELOCITY

The results of the longitudinal velocity obtained from the point traverse anemometer reading are presented in Table 2. The calculated airflow at the fan exhaust was 0.24 m^3/s, 2.97 m^3/s, and 5.42 m^3/s for ventilation conditions of 0 %, 50 %, and 100 %, respectively. The corresponding longitudinal ventilation velocity obtained was 0.220 m/s, 0.093 m/s, and 0.012 m/s for 100 % and 50 % smoke extraction rate, and natural ventilation conditions, respectively. From Table 2, the virtually all the transverse points recorded "0.00" for Exp 3, Exp 4, and Exp 5. This implies that there is not airflow along the traverse

point. This is because the fan was put off for those experiments. As you can see in Table 1, the ventilation rate is 0 % for these experiments.

Table 2. Point traverse airflow 3 m downstream of fire.

S/N	P1	P2	P3	P4	P5	P6	P7	P8	P9
Exp 1	0.47	0.33	0.27	0.32	0.12	0.00	0.33	0.16	0.04
Exp 2	0.16	0.16	0.21	0.00	0.00	0.07	0.07	0.11	0.06
Exp 3	0.00	0.00	0.00	0.00	0.00	0.00	0.07	0.00	0.04
Exp 4	0.00	0.00	0.00	0.00	0.00	0.00	0.07	0.00	0.04
Exp 5	0.16	0.16	0.21	0.00	0.00	0.07	0.07	0.11	0.06
Exp 6	0.16	0.16	0.21	0.00	0.00	0.07	0.07	0.11	0.06
Exp 7	0.47	0.33	0.27	0.32	0.12	0.00	0.33	0.16	0.04
Exp 8	0.47	0.33	0.27	0.32	0.12	0.00	0.33	0.16	0.04
Exp 9	0.00	0.00	0.00	0.00	0.00	0.00	0.07	0.00	0.04

4.2. HEAT RELEASE RATE (HRR) CALCULATIONS

The HRR results in the order of decreasing maximum temperature are presented in Table 3. Based on Table 3, the fire size had a profound effect on the burning rate while longitudinal ventilation had a negligible effect on the burning rate due to the very low ventilation velocity observed in the mine during the fire tests. For instance, considering test experimental cases 5 and 6, a decrease of fire size to about a half may cause the burning time to increase with a factor of up to 4.5 if the ventilation is kept constant.

4.3. TEMPERATURE ATTENUATION FACTOR

A typical temperature evolution curves observed during the test is shown in Figure 7. The case presented was for Test No 2 (i.e., 0.7 D, 50 % Vent). This pattern was the same

for all other test cases. The details of temperature evolution for other cases are not presented since our primary focus was the maximum smoke temperature at each measuring station. Hence, for the purpose of this analysis, only the maximum smoke temperature was considered.

Table 3. Heat release rate values obtained for the experimental cases.

S/N	Test Case	Pool diameter (m)	Ventilation Opening (%)	HRR (KW)
1	Exp 4	0.7	0	425
2	Exp 5	0.7	50	425
3	Exp 1	0.7	100	425
4	Exp 3	0.5	0	212.5
5	Exp 2	0.5	50	212.5
6	Exp 8	0.5	100	212.5
7	Exp 9	0.3	0	85
8	Exp 6	0.3	50	85
9	Exp 7	0.3	100	85

The results of the observed maximum smoke temperature are presented in Figure 8 and Figure 9. Figure 8 shows the temperature distribution at the mine ceiling, while Figure 9 shows that temperature evolution 1 m below the mine roof. The negative x-axis represents upstream locations, and the positive distance signs represent downstream positions of fire.

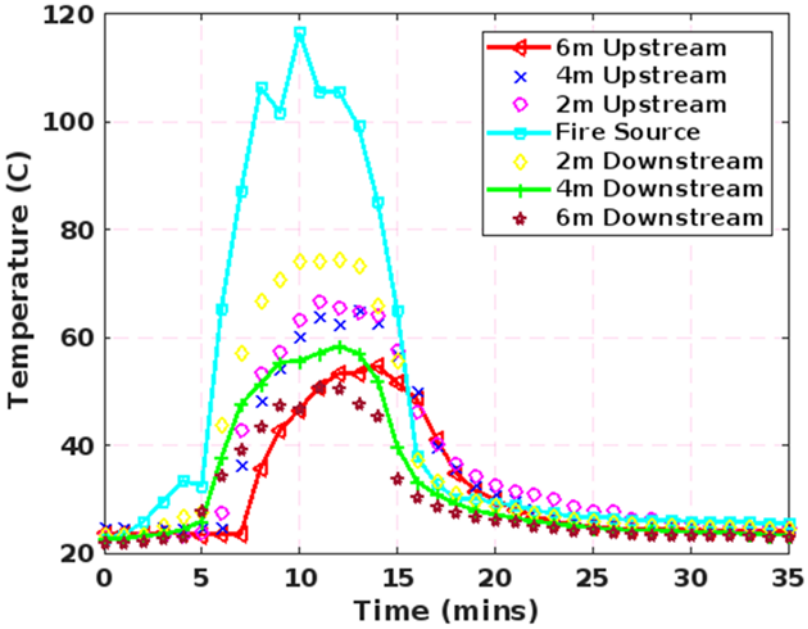

Figure 7. Temperature curves measured at different distances for Test 2.

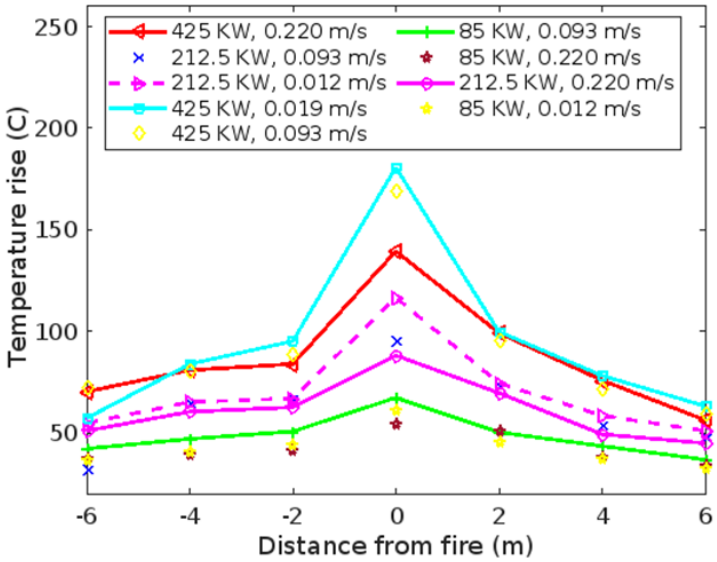

Figure 8. Maximum rise in smoke temperature at the mine roof for the different.

Generally, the maximum temperature is observed to decrease as the distance from the fire source increases. The maximum rise in smoke temperature beneath the mine roof

(presented in Figure 8) within the quasi-steady stage at the different measuring stations were employed for subsequent calculations of temperature decay. The analysis of temperature decay in Figure 10 showed the overall temperature attenuation was greater in the downstream (attenuation factor of 0.17) than in the upstream (attenuation factor of 0.12).

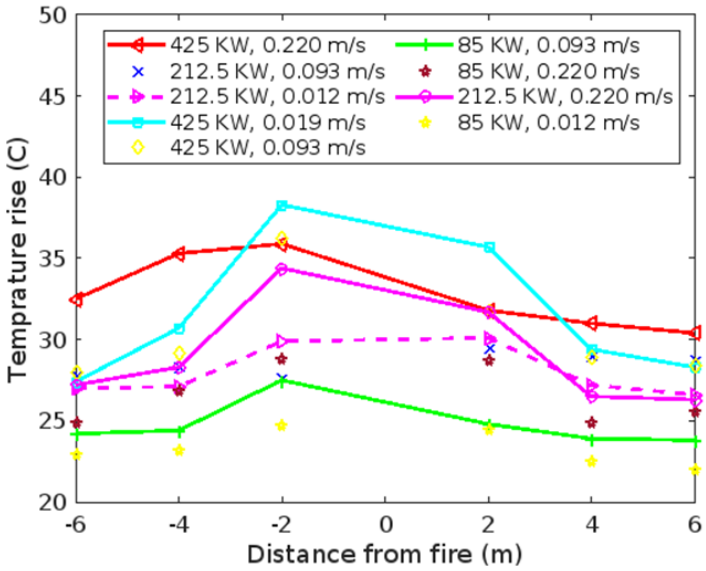

Figure 9. Maximum rise in smoke temperature 1 m below the mine roof for the different ventilation conditions.

This may be due to smoke roll-back in the upstream. Also, this could be due the smoke mixes with fresh air faster as the smoke travel downstream towards the ventilation exhaust.

For the derivation of the attenuation models of both upstream and downstream of the fire, an improved technique (Tao & Zeng, 2022), which incorporating a two-dimensional spreading phase for the temperature distribution was introduced instead of the conventional one-dimensional temperature decay model. Firstly, we normalized the smoke temperature T_x, measured by the thermocouples from a distance x from the fire to a

dimensionless temperature $\Delta T_{ND,x}$ by a reference value T_r and the ambient air temperature T_a is as follow:

$$\Delta T_{ND,x} = \frac{T_x - T_a}{T_r - T_a}. \quad (12)$$

The reference temperatures T_r for the upstream and downstream positions were taken at stations S3 and station S5 (as shown in Figure 4), 2m upstream and downstream of the fire source, respectively. The dimensionless normalized temperatures were plotted against the distance of separation of the thermocouples measuring stations to the fire source as seen in Figure 10. The experimental data from each test was fitted to an exponential function using the following equations:

$$\Delta T_{ND,x} = a.e^{b(x-x_r)}. \quad (13)$$

The dimensionless normalized temperatures can be properly fitted using the exponential function (Zhao et al., 2019). The average value of the attenuation factors was determined and used for developing the empirical model in this study. Finally, a two-dimensional spreading phase empirical model that could predict the temperature distribution for an axisymmetric fire in a mine drift was developed. Based on the results in Figure 10, the semi-empirical calculation model is summarized as follows:

$$f(x) = \begin{cases} 0.98e^{-0.12(x-x_r)} & upstream\ of\ fire\ source \\ 0.98e^{-0.17(x-x_r)} & downstream\ of\ fire\ source \end{cases} \quad (14)$$

A comparison of the new predictive model with existing models was done to validate our new model Ingason and Li's model (Ingason & Li, 2010) developed a model using a reduced-scale tunnel with no mechanical smoke extraction.

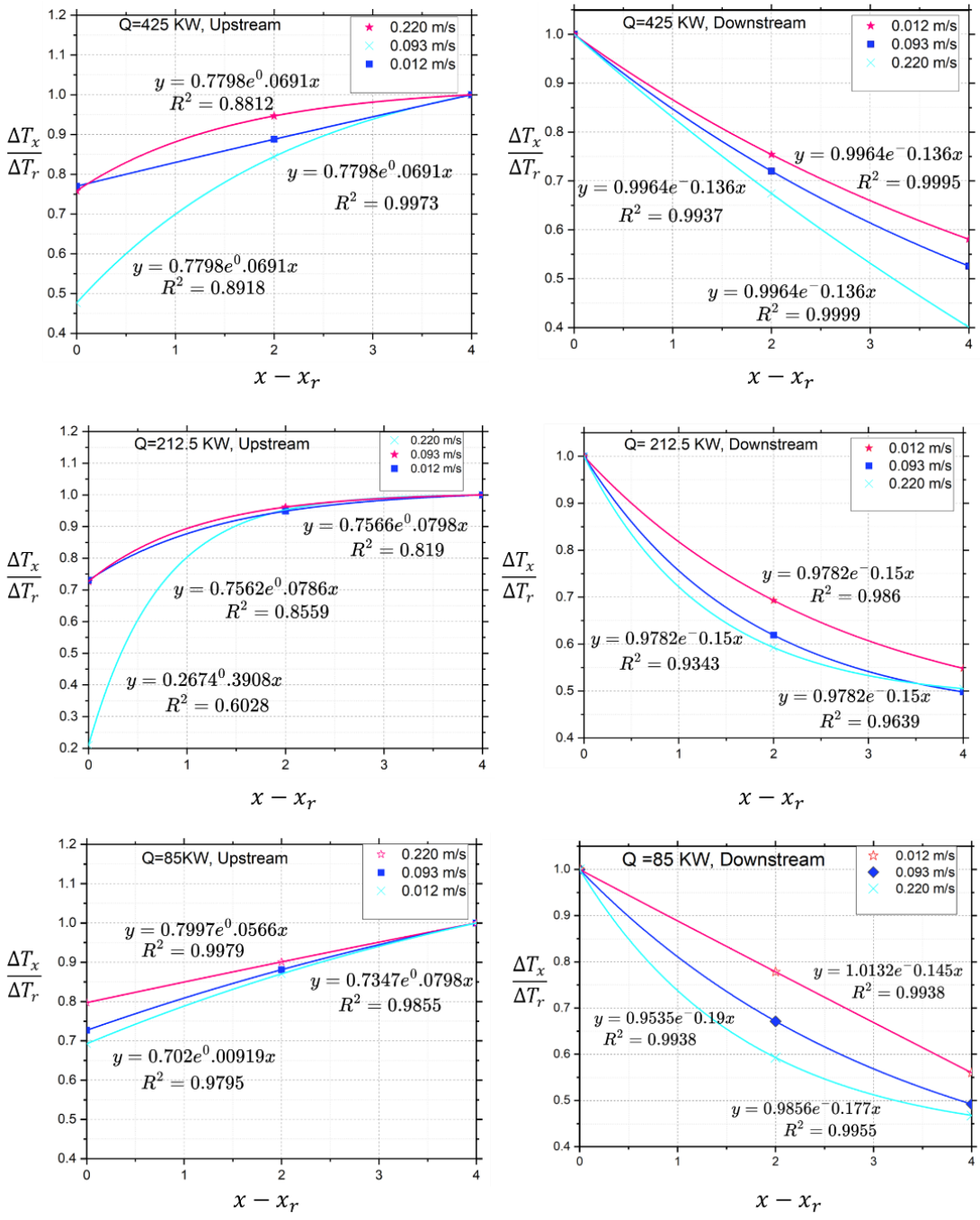

Figure 10. Correlation of temperature attenuation in the mine drift for different fire sizes and longitudinal ventilation conditions.

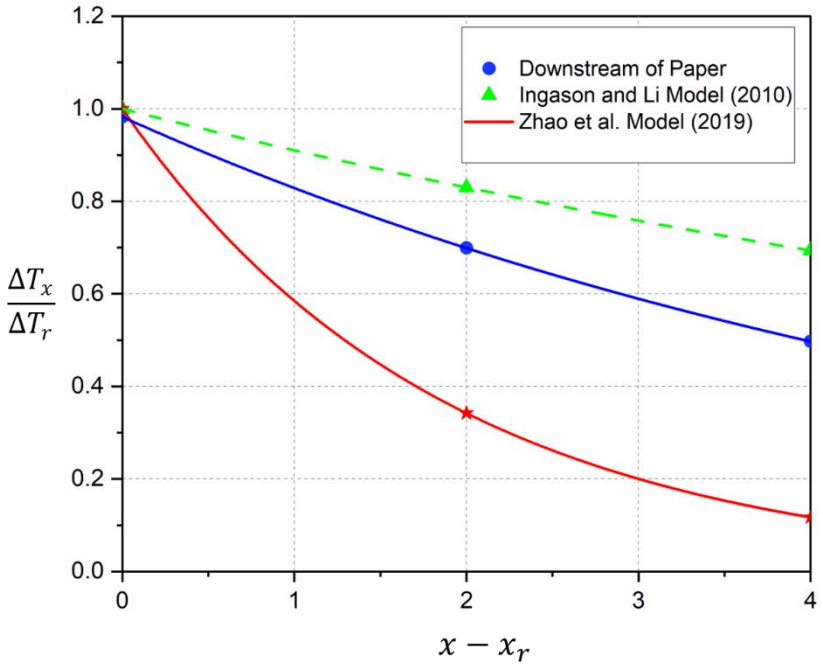

Figure 11. Comparison of between temperature attenuation model developed and existing typical temperature attenuation models.

Zhao et al.'s model (Zhao et al., 2019) also developed a temperature attenuation model using a reduced scale model tunnel but with a two-point mechanical smoke extraction point. However, the attenuation model developed in this study was based on a single-point smoke extraction system. As deduced from Figure 11, that the temperature decay rate increased as more smoke extraction point was added compared to the case with no mechanical smoke extraction.

4.4. MAXIMUM EXCESS SMOKE TEMPERATURE

Similarly, the maximum smoke temperature during the experiment was measured and compared to two commonly used empirical models for predicting the maximum temperature rise beneath the tunnel ceiling as analyzed in Section 3.3.2. The results are presented in Figure 12. The predicted maximum smoke temperature rise was plotted

against the measured values. It is observed that Li et al.'s model demonstrated better predictive capability than the Kurioka's et al. model. Kurioka et al's model predicted a constant smoke temperature for the nine experimental cases which implies that the accuracy of Kurioka et al.'s model may be greatly affected for large values of $\left(\frac{Q'^{2/3}}{Fr^{1/3}}\right)$ since $\left(\frac{Q'^{2/3}}{Fr^{1/3}}\right)$ was found to be greater than 1.35 for all the experimental cases considered in this investigation. This finding corroborates previous study by confirming that a value of $\left(\frac{Q'^{2/3}}{Fr^{1/3}}\right)$>1.35 leads to a constant $\Delta T_{max}/T_a$ regardless of the HRR (Ji et al., 2012). Analysis of the Kurioka et al.'s model indicates that the maximum gas temperature becomes infinitely large when the ventilation velocity tends to zero (Ji et al., 2012; Li & Ingason, 2012; Li et al., 2011). This implies that the model cannot predict the maximum temperature accurately for low ventilation velocity.

The results from this study showed that Li et al.'s model has a better performance in predicting the maximum gas temperature for a very small ventilation velocity which further validate the results from the study by Li and Ingason (Li & Ingason, 2012). Therefore, for a low ventilation velocity (i.e V' ≤ 0.19), the maximum temperature beneath ceiling in a mine drift was mainly influenced by the HRR. Thus, for a longitudinal ventilation velocity, V', ≤ 0.19, the maximum excess temperature in a mine drift could be determined by Equation (15):

$$T_{max} = \begin{cases} 17.5\dfrac{Q^{2/3}}{H_{ef}^{5/3}} \\ Constant \end{cases} \tag{15}$$

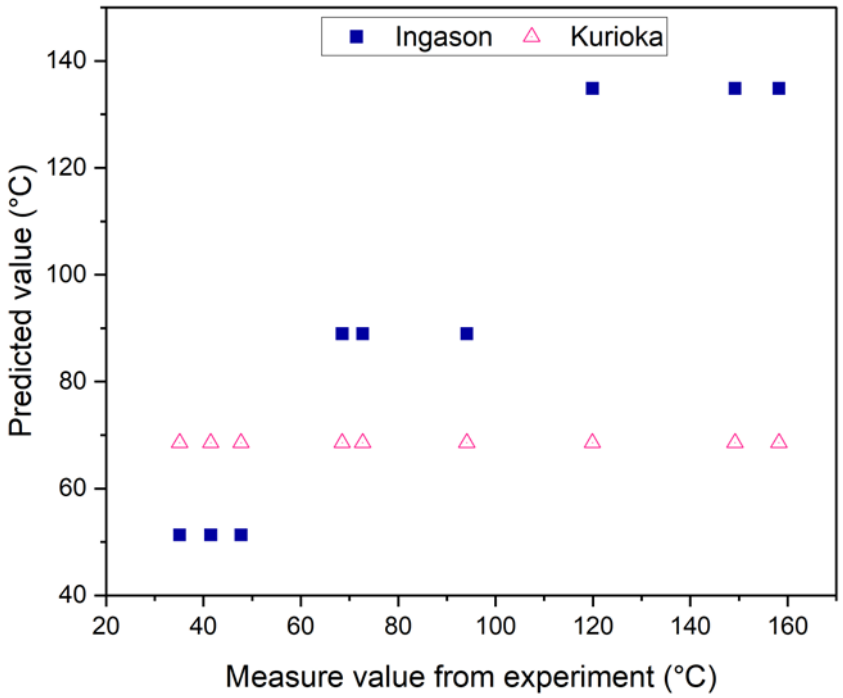

Figure 12. Comparison of empirical models measured values of the smoke temperature rise beneath the ceiling.

4.5. THERMAL IMAGE AND FLAME ANALYSIS

Figure 13 shows the flame evolution for a 212.5 KW fire. Figure 13 (a), (b), (c), and (d) depict the flame shape for the fire growth stage, flashover stage, burning stage, and decay stage, respectively. D denotes the pool fire diameter while D_c is the diameter of the flame. This is a typical evolution for different fire sizes. Figure 13 displays that D_c becomes greater than D once the fire reaches the flashover stage and the value starts to decrease through the decay stage to the complete burnout.

The flame height was measured for the different burning stages and the maximum flame height was recorded. The maximum flame height observed was 1.2 m for a pool fire with diameter of 0.5 m. This corresponds to $\frac{H}{D}$ =2.4. The comparison of the observed experimental data with some exiting empirical model is presented in Table 4. By

computing the error from the different empirical models, Miao et al.'s model (Miao et al., 2014), which represents the simplest approach for computing the flame height, based on the diameter of the pool gives the closet approximation of $\frac{H}{D}$.

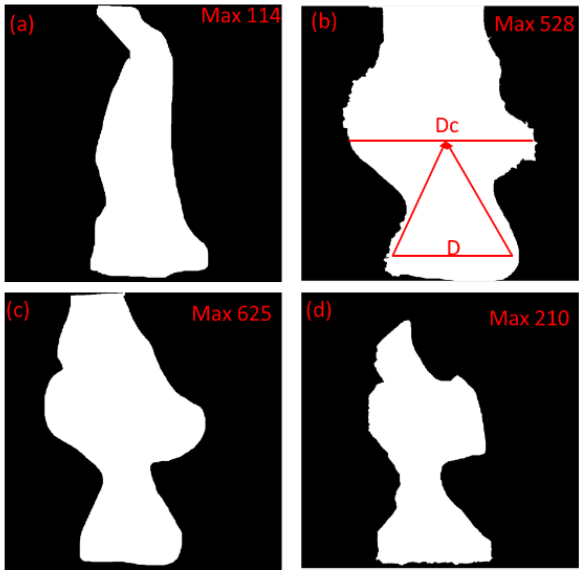

Figure 13. Evolution of the flame shape for 212.5 KW fire.

Table 4. Comparison of empirical models for flame height calculations.

Reference	Formulae	Calculated (m)	Measured (m)	Error (%)
Thomas et al., (P. Thomas, 1963)	$\frac{H}{D} = 42\left(\frac{m''}{\rho_a\sqrt{gD}}\right)^{0.61}$	3.7	2.4	-57%
Heskestad's model (Heskestad, 1995)	$\frac{H}{D} = \frac{0.235Q^{2/5}}{D} - 1.02$	2.9	2.4	-24%
Miao et al's (Miao et al., 2014)	$\frac{H}{D} = 1.73 + 0.33D^{-1.43}$	2.6	2.4	-9%

Heskestad's model (Heskestad, 1995) computed a value within an ± 30%. However, Thomas' model (P. Thomas, 1963) over predicted $\frac{H}{D}$ for this scenario. One reason that may account for this discrepancy may be due to the level of details required to accurately compute the value of $\frac{H}{D}$ using Thomas' formulae.

4.6. CO EVOLUTION IN THE TUNNEL

The CO profile for each of the test cases upstream of the fire is presented in Figure 14 (a) to (c). Generally, the CO concentration is observed to be greatly influenced by ventilation conditions. From Figure 14 (a) & (b), it can be observed that increasing the ventilation rate from 0 % to 100 % reduced the maximum CO by up to about 40 %. Even though a slight deviation is seen in Figure 14 (c), the spike in CO level when the ventilation rate was 50 % could probably be attributed to an instrumental error. Analysis of the peak CO concentration upstream and downstream of the fire presented in Figure 14 (b) shows some competing trends. For tests 1 to 4 and test 9, the peak CO concentration was found to be higher downstream than in the upstream. However, this trend can be seen to take a swing for tests 5 to 8, where the peak CO concentration upstream was higher than the measured value downstream of the mine. Additionally, the inconsistency in the CO concentration trend may result from the leakages in the tunnel because of the presence of multiple bifurcation in the underground test area. The prior study by Yuan et al. (Yuan et al., 2016) illustrated that airflow leakages could cause a reduction in the concentration of CO in an underground entries.

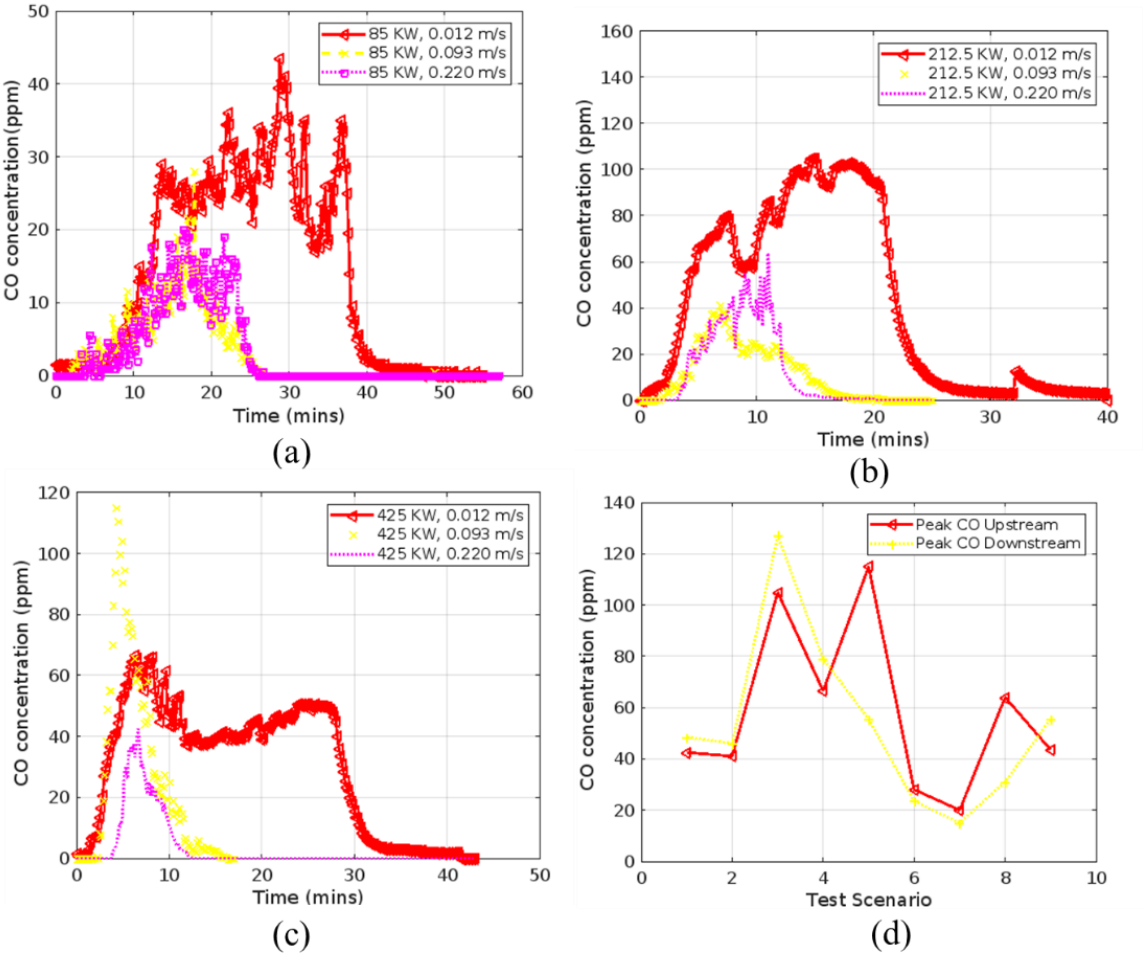

Figure 14. Typical CO evolution curve and comparison of peak CO concentration for upstream and downstream positions.

4.7. INFLUENCE OF BIFURCATION

Prior to conducting the FDS simulation to investigate the influence of bifurcation, the HRR of the experimental and simulation was compared to check for consistency. The results of the HRR histories for both FDS and experiment are presented in Figure 15. The peak HRR measured during the experiment was 425.0 KW while that obtained from the simulation approximately 400.0 KW which was acceptable because the deviation was only about 5.9 %. In addition, the primary objective of the simulation was not to evaluate FDS

accuracy but to extend FDS capability to investigate how bifurcations present in real underground mines may influence the maximum smoke gas temperature compared to their tunnel fires counterparts. A schematic of the dichotomy between bifurcated and non-bifurcated scenario is shown in Figure 15. The first scenario showing bifurcation in Figure 15 (a) is common in mines because of the several development faces that may be present in the mines while the second scenario represented the ubiquitous cases mostly found in road tunnels.

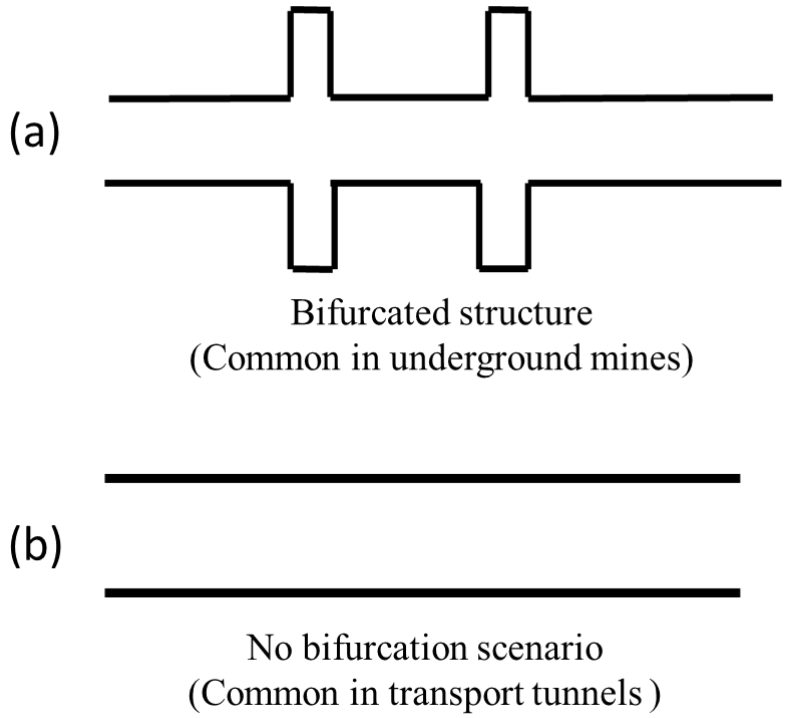

Figure 15. Schematic of bifurcated and non-bifurcated underground space.

For this study, the no-bifurcation condition was developed by simply blocking off the rooms within the room-and-pillar mine with a concrete obstruction in the FDS model. Maximum smoke temperature measured upstream and downstream for the bifurcated and non-bifurcated scenario from the FDS simulation is presented in Figure 17. Based on

Figure 17, the maximum ceiling jet temperature increased when there was no bifurcation in the drift. However, the temperature evolution for both scenarios followed a similar trend. For both bifurcated and non-bifurcated scenarios, the ceiling jet temperature decreased as we moved away from the fire source both in the upstream and downstream directions.

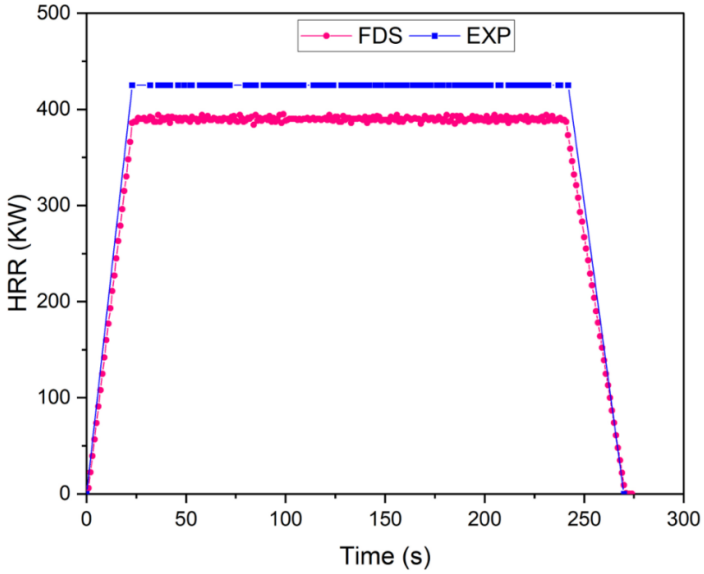

Figure 16. Comparison of the HRR curve for the experiment and simulation.

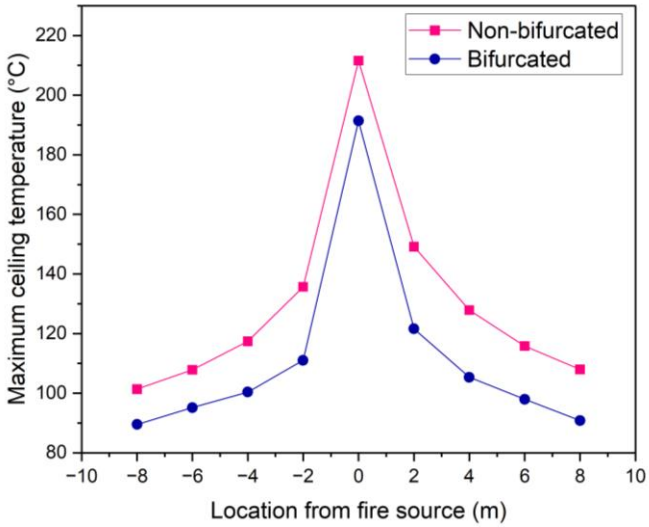

Figure 17. Comparison of the maximum excess smoke temperature for the bifurcated and non-bifurcated scenario.

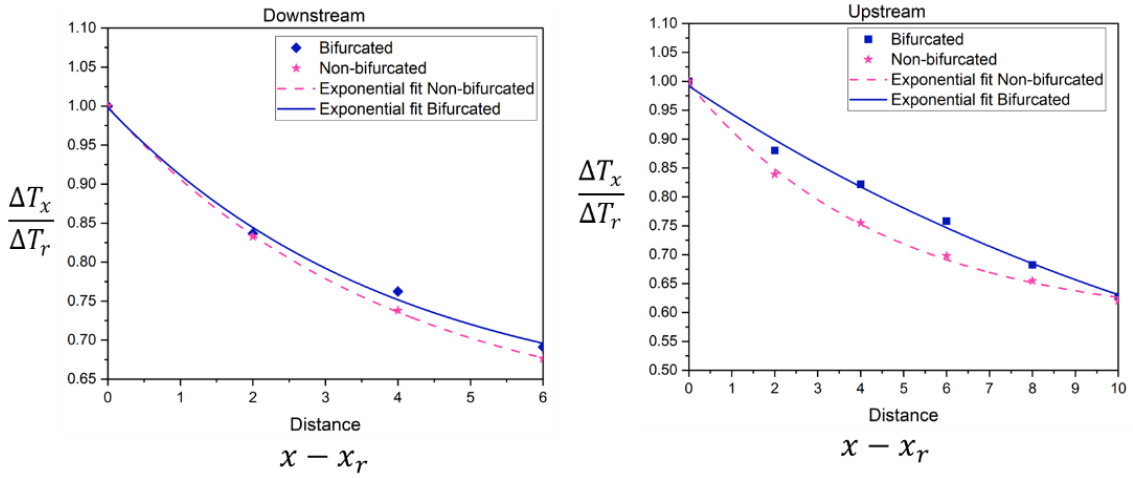

Figure 18. Comparison of temperature attenuation for bifurcated and non-bifurcated scenarios.

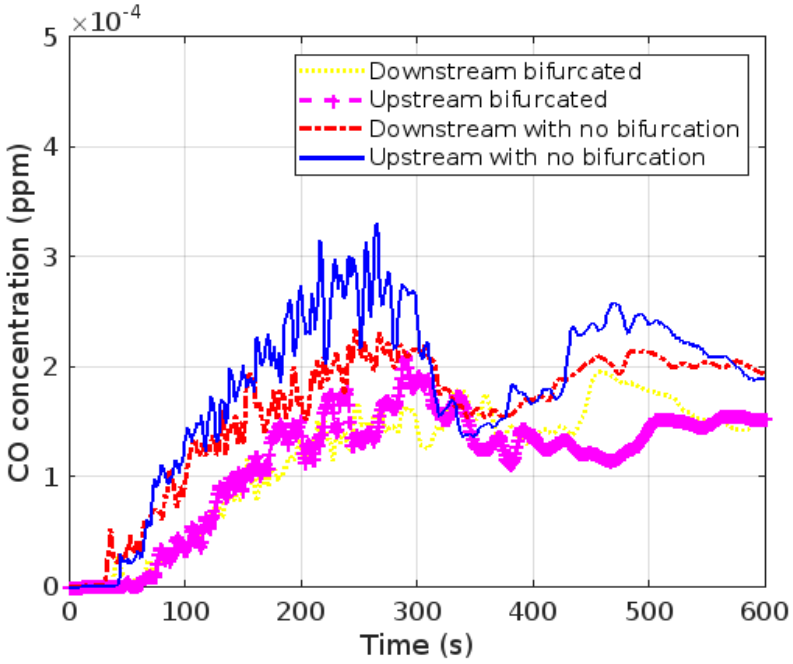

Figure 19. Comparison of the CO concentration for bifurcated and non-bifurcated scenarios.

Additionally, it can be observed the curve of the exponential fitting does not completely overlap for the bifurcated and non-bifurcated scenarios which indicates that the rate of temperature decay for the two cases differ, as depicted in Figure 18. Based on the

results in Figure 18, the empirical model for the bifurcated and non-bifurcated scenario can be summarized as follow:

$$f(x) = \begin{cases} 0.9807e^{-0.052(x-x_r)}, & Bifurcated \\ 0.9510e^{-0.056(x-x_r)}, & Non-bifurcated \end{cases} \quad (16)$$

Likewise, the temperature distribution for the bifurcated and non-bifurcated scenario, and the spread of toxic carbon monoxide were examined to investigate how bifurcation affects the toxicity concentration. This is the main cause of fatality in the underground mine fires. Two gas detectors placed 2.0 m upstream and downstream of the fire in the FDS model were used to measure the CO concentration during the simulation. The result of the CO concentration is presented in Figure 19. The findings depicted that tunnel bifurcation had a strong influence on the CO concentration in an underground space. As can be seen in the upstream and downstream positions, the CO concentration was higher for non-bifurcated cases, which indicate that bifurcation could serve as a cross-passage for toxic gases to diffuse quickly to other portions of the confined space thus reducing the overall peak value of the toxic gas concentration.

5. CONCLUSION

Full-scale fire tests were conducted in an underground mine drift and the analysis of temperature attenuation and the maximum excess gas temperature beneath a mine drift was presented in this study using an experimental and theoretical approach. In addition, a CFD model was developed and validated using the experimental data and the model was extended to study the influence of bifurcation on the temperature and toxic gases spread in

an underground. The temperature evolution upstream and downstream of the mine drift were fitted using an exponential correlation and a new empirical model of temperature attenuation given by Equation (14) was proposed. The attenuation model upstream of fire could predict the temperature rise as we moved towards the fire from any upstream location. This correlation is valid for HRR value between 85-425 KW and maximum excess gas temperature of up to 160 ^{o} C. This type of prognosticative attenuation model will further improve firefighting and suppression strategy as responders move towards the fire zone during an emergency.

Temperature attenuation, maximum excess gas temperature, and CO evolution were observed to be strongly influenced by ventilation conditions. Furthermore, experimental data were used to verify the existing formulae for the maximum excess gas temperature beneath a tunnel/ mine drift. Tests results showed a good agreement with Li et al.'s model compared to Kurioka et al.'s model. Also, the fire pool diameter was observed to be sufficient for determining flame height characteristics based on Miao's empirical model. Test results showed a good correlation between the measured flame height from experimental and calculated values from the empirical formulae. The influence of different fire locations, such as fires in the blind heading and effective tunnel height (i.e., the separation between the bottom of the fire source and the tunnel ceiling) was not considered in this paper, therefore, it may influence the temperature and smoke propagation and will be investigated in future research.

Furthermore, bifurcation had a strong influence on the temperature evolution and product of combustion spread in underground environments. The magnitude of the influence of bifurcation was not considered in this study and shall be investigated in future

work. Additionally, there are several combustible materials that could lead to fires in the underground mines. These materials include wood, coal, rubber, belt, equipment etc. Future studies should evaluate the combustibility of these materials as only diesel pool combustion was investigated in this study. Finally, the findings from this study could serve as the fire field data in building and optimizing emergency evacuation plans, in addition to validating existing CFD models for underground mines and other confined space environments.

REFERENCES

Bahrami, D., Zhou, L., & Yuan, L. (2021). Field Verification of an Improved Mine Fire Location Model. Mining, Metallurgy & Exploration, 38(1), 559-566. https://doi.org/10.1007/s42461-020-00314-6

Chang, P., Xu, G., Zhou, F., Mullins, B., & Abishek, S. (2019). Comparison of underground mine DPM simulation using discrete phase and continuous phase models. Process Safety and Environmental Protection, 127, 45-55. https://doi.org/https://doi.org/10.1016/j.psep.2019.04.027

Chen, C., Zhang, Y., Lei, P., & Jiao, W. (2020). A study for predicting the maximum gas temperature beneath ceiling in sealing tactics against tunnel fire. Tunnelling and Underground Space Technology, 98, 103275. https://doi.org/https://doi.org/10.1016/j.tust.2019.103275

Chen, Z., Liu, Z., Huang, L., Niu, G., Yan, J., & Wang, J. (2023). Research on the effect of ceiling centralized smoke exhaust system with air curtains on heat confinement and plug-holing phenomenon in tunnel fires. Process Safety and Environmental Protection, 169, 646-659. https://doi.org/https://doi.org/10.1016/j.psep.2022.11.054

Cheong, M., Spearpoint, M., & Fleischmann, C. (2009). Calibrating an FDS simulation of goods-vehicle fire growth in a tunnel using the runehamar experiment. Journal of fire protection engineering, 19(3), 177-196.

Delichatsios, M. A. (1981). The flow of fire gases under a beamed ceiling. Combustion and flame, 43, 1-10.

Dong, S., Lu, X., Wang, D., Wang, H., Zheng, K., Shi, Q., & Chen, M. (2017). Experimental investigation of the fire-fighting characteristics of aqueous foam in underground goaf. Process Safety and Environmental Protection, 106, 239-245. https://doi.org/https://doi.org/10.1016/j.psep.2016.12.009

Düzgün, H. S., & Leveson, N. (2018). Analysis of soma mine disaster using causal analysis based on systems theory (CAST). Safety Science, 110, 37-57. https://doi.org/https://doi.org/10.1016/j.ssci.2018.07.028

Fernández-Alaiz, F., Castañón, A. M., Gómez-Fernández, F., & Bascompta, M. (2020). Mine fire behavior under different ventilation conditions: Real-scale tests and CFD modeling. Applied Sciences, 10(10), 3380.

Fernández-Alaiz, F., Castañón, A. M., Gómez-Fernández, F., Bernardo-Sánchez, A., & Bascompta, M. (2020). Determination and fire analysis of gob characteristics using CFD. Energies, 13(20), 5274.

Fernánez-Alaiz, F., Castañón, A. M., Gómez-Fernández, F., Bernardo-Sánchez, A., & Bascompta, M. (2020). Analysis of the fire propagation in a sublevel coal mine. Energies, 13(14), 3754.

Gannouni, S., & Maad, R. B. (2015). Numerical study of the effect of blockage on critical velocity and backlayering length in longitudinally ventilated tunnel fires. Tunnelling and Underground Space Technology, 48, 147-155. https://doi.org/https://doi.org/10.1016/j.tust.2015.03.003

Gehandler, J. (2015). Road tunnel fire safety and risk: a review. Fire Science Reviews, 4(1), 2. https://doi.org/10.1186/s40038-015-0006-6

Haghighat, A., Luxbacher, K., & Lattimer, B. Y. (2018). Development of a Methodology for Interface Boundary Selection in the Multiscale Road Tunnel Fire Simulations. Fire Technology, 54(4), 1029-1066. https://doi.org/10.1007/s10694-018-0724-0

Han, J., Wang, Z., Geng, P., Wang, F., Wen, J., & Liu, F. (2021). The effect of blockage and tunnel slope on smoke spread and ceiling temperature distribution in a natural-ventilated metro depot. Energy and Buildings, 253, 111540. https://doi.org/https://doi.org/10.1016/j.enbuild.2021.111540

Hansen, R. (2010). Overview of fire and smoke spread in underground mines.

Hansen, R. (2019). Design of fire scenarios for Australian underground hard rock mines–Applying data from full-scale fire experiments. Journal of Sustainable Mining, 18(4), 163-173.

Hansen, R., & Ingason, H. (2013a). Full-scale fire experiments with mining vehicles in an underground mine (978-91-7485-115-1 (ISBN)). (Studies in Sustainable Technology / Forskningsrapport, Issue. http://urn.kb.se/resolve?urn=urn:nbn:se:mdh:diva-20912

Hansen, R., & Ingason, H. (2013b). Full-scale fire experiments with mining vehicles in an underground mine.

Hansen, R., & Ingason, H. (2013c). Heat release rate measurements of burning mining vehicles in an underground mine. Fire Safety Journal, 61, 12-25. https://doi.org/https://doi.org/10.1016/j.firesaf.2013.08.009

Heskestad, G. (1995). Fire plumes, SFPE handbook of fire protection engineering. Nation Fire Protection Association, Quincy, Massachusetts.

Hong, Y., Kang, J., & Fu, C. (2022). Rapid prediction of mine tunnel fire smoke movement with machine learning and supercomputing techniques. Fire Safety Journal, 127, 103492. https://doi.org/https://doi.org/10.1016/j.firesaf.2021.103492

Hu, L., Chen, L., Wu, L., Li, Y., Zhang, J., & Meng, N. (2013). An experimental investigation and correlation on buoyant gas temperature below ceiling in a slopping tunnel fire. Applied Thermal Engineering, 51(1-2), 246-254.

Hu, L. H., Huo, R., Peng, W., Chow, W. K., & Yang, R. X. (2006). On the maximum smoke temperature under the ceiling in tunnel fires. Tunnelling and Underground Space Technology, 21(6), 650-655. https://doi.org/https://doi.org/10.1016/j.tust.2005.10.003

Hu, L. H., Zhou, J. W., Huo, R., Peng, W., & Wang, H. B. (2008). Confinement of fire-induced smoke and carbon monoxide transportation by air curtain in channels. Journal of Hazardous Materials, 156(1), 327-334. https://doi.org/https://doi.org/10.1016/j.jhazmat.2007.12.041

Huang, P., Chen, M., Chen, K., Zhang, H., Yu, L., & Liu, C. (2022). A combined real-time intelligent fire detection and forecasting approach through cameras based on computer vision method. Process Safety and Environmental Protection, 164, 629-638. https://doi.org/https://doi.org/10.1016/j.psep.2022.06.037

Huang, Y., Li, Y., Dong, B., Li, J., & Liang, Q. (2018). Numerical investigation on the maximum ceiling temperature and longitudinal decay in a sealing tunnel fire. Tunnelling and Underground Space Technology, 72, 120-130.

Ingason, H., & Li, Y. Z. (2010). Model scale tunnel fire tests with longitudinal ventilation. Fire Safety Journal, 45(6-8), 371-384.

Ji, J., Fan, C., Zhong, W., Shen, X., & Sun, J. (2012). Experimental investigation on influence of different transverse fire locations on maximum smoke temperature under the tunnel ceiling. International Journal of Heat and Mass Transfer, 55(17-18), 4817-4826.

Kamran, M., Wattimena, R. K., Armaghani, D. J., Asteris, P. G., Jiskani, I. M., & Mohamad, E. T. (2023). Intelligent based decision-making strategy to predict fire intensity in subsurface engineering environments. Process Safety and Environmental Protection, 171, 374-384. https://doi.org/https://doi.org/10.1016/j.psep.2022.12.096

Khan, F. I., & Abbasi, S. A. (1999). Major accidents in process industries and an analysis of causes and consequences. Journal of Loss Prevention in the Process Industries, 12(5), 361-378. https://doi.org/https://doi.org/10.1016/S0950-4230(98)00062-X

Kirytopoulos, K., Konstandinidou, M., Nivolianitou, Z., & Kazaras, K. (2014). Embedding the human factor in road tunnel risk analysis. Process Safety and Environmental Protection, 92(4), 329-337. https://doi.org/https://doi.org/10.1016/j.psep.2014.03.006

Kurioka, H., Oka, Y., Satoh, H., & Sugawa, O. (2003). Fire properties in near field of square fire source with longitudinal ventilation in tunnels. Fire Safety Journal, 38(4), 319-340.

Lee, Y. S., & Ghazali, F. E. M. (2018). Major Functional Risks for Operation and Maintenance of Tunnelling Projects. ESTEEM, 14.

Lei, B., He, B., Zhao, Z., Xu, G., & Wu, B. (2021). A method for identifying the fire status through ventilation systems using tracer gas for improved rescue effectiveness in roadway drivage of coal mines. Process Safety and Environmental Protection, 151, 151-157. https://doi.org/https://doi.org/10.1016/j.psep.2021.05.010

Li, Y. Z., & Ingason, H. (2012). The maximum ceiling gas temperature in a large tunnel fire. Fire Safety Journal, 48, 38-48.

Li, Y. Z., & Ingason, H. (2018). Overview of research on fire safety in underground road and railway tunnels. Tunnelling and Underground Space Technology, 81, 568-589.

Li, Y. Z., Lei, B., & Ingason, H. (2011). The maximum temperature of buoyancy-driven smoke flow beneath the ceiling in tunnel fires. Fire Safety Journal, 46(4), 204-210.

Liu, C., Zhong, M., Shi, C., Zhang, P., & Tian, X. (2017). Temperature profile of fire-induced smoke in node area of a full-scale mine shaft tunnel under natural ventilation. Applied Thermal Engineering, 110, 382-389. https://doi.org/https://doi.org/10.1016/j.applthermaleng.2016.08.147

Lu, X., Weng, M., Liu, F., Wang, F., Han, J., & Cheung, S. C. (2022). Study on smoke temperature profile in bifurcated tunnel fires with various bifurcation angles under natural ventilation. Journal of Wind Engineering and Industrial Aerodynamics, 225, 105001. https://doi.org/https://doi.org/10.1016/j.jweia.2022.105001

Mavhura, E. (2019). A systems approach for assessing emergency preparedness in underground mines of Zimbabwe. Resources Policy, 62, 1-8. https://doi.org/https://doi.org/10.1016/j.resourpol.2019.03.005

McGrattan, K., Hostikka, S., McDermott, R., Floyd, J., Weinschenk, C., & Overholt, K. (2013). Fire dynamics simulator technical reference guide volume 1: mathematical model. NIST special publication, 1018(1), 175.

McGrattan, K., Peacock, R., & Overholt, K. (2016). Validation of fire models applied to nuclear power plant safety. Fire Technology, 52, 5-24.

McGrattan, K. B., Peacock, R. D., & Overholt, K. J. (2014). Verification and validation of selected fire models for nuclear power plant applications supplement 1. U. S. N. R. C. NUREG-1824. https://www.nist.gov/publications/verification-and-validation-selected-fire-models-nuclear-power-plant-applications-1

Miao, Z., Wenhua, S., Ji, W., & Zhen, C. (2014). Accident consequence simulation analysis of pool fire in fire dike. Procedia Engineering, 84, 565-577.

Ntzeremes, P., & Kirytopoulos, K. (2019). Evaluating the role of risk assessment for road tunnel fire safety: A comparative review within the EU. Journal of traffic and transportation engineering (English edition), 6(3), 282-296.

Oka, Y., & Atkinson, G. T. (1995). Control of smoke flow in tunnel fires. Fire Safety Journal, 25(4), 305-322. https://doi.org/https://doi.org/10.1016/0379-7112(96)00007-0

Overholt, K. J. (2014). Verification and validation of commonly used empirical correlations for fire scenarios. US Department of Commerce, National Institute of Standards and Technology.

Salami, O. B., Xu, G., Kumar, A. R., & Pushparaj, R. I. (2023). Underground Mining Fire Hazards and optimization of Emergency Evacuation strategies: The issues, existing methodology and limitations, and way forward. Process Safety and Environmental Protection. https://doi.org/https://doi.org/10.1016/j.psep.2023.07.012

Salami , O. B., Xu, G., Kumar, A. R., & Pushparaj, R. I. (2023). Underground mining fire hazards and the optimization of emergency evacuation strategies (EES): The issues, existing methodology and limitations, and way forward. Process Safety and Environmental Protection, 177, 617-634. https://doi.org/https://doi.org/10.1016/j.psep.2023.07.012

Salami, O. B., Xu, G., Kumar, A. R., Pushparaj, R. I., & Iqbal, A. (2023). Fire-induced temperature attenuation under the influence of a single ceiling smoke extraction point in a bifurcated drift. In Underground Ventilation (pp. 399-410). CRC Press.

Seike, M., Kawabata, N., & Hasegawa, M. (2017). Quantitative assessment method for road tunnel fire safety: Development of an evacuation simulation method using CFD-derived smoke behavior. Safety Science, 94, 116-127. https://doi.org/https://doi.org/10.1016/j.ssci.2017.01.005

Tang, F., Cao, Z., Palacios, A., & Wang, Q. (2018). A study on the maximum temperature of ceiling jet induced by rectangular-source fires in a tunnel using ceiling smoke extraction. International Journal of Thermal Sciences, 127, 329-334. https://doi.org/https://doi.org/10.1016/j.ijthermalsci.2018.02.001

Tang, W., Yuan, L., Bahrami, D., & Rowland, J. (2021). Water spray suppression of leaked oil fires: A numerical study. In Mine Ventilation (pp. 309-316). CRC Press.

Tao, L., & Zeng, Y. (2022). Effect of single-side centralized exhaust on smoke control and temperature distribution in longitudinal ventilation tunnel fires. Tunnelling and Underground Space Technology, 119, 104241.

Thomas, P. (1963). The size of flames from natural fires. Symposium (International) on Combustion,

Weng, M.-c., Lu, X.-l., Liu, F., Shi, X.-p., & Yu, L.-x. (2015). Prediction of backlayering length and critical velocity in metro tunnel fires. Tunnelling and Underground Space Technology, 47, 64-72. https://doi.org/https://doi.org/10.1016/j.tust.2014.12.010

Xu, G., Jong, E. C., Luxbacher, K. D., & McNair, H. M. (2016). Effective utilization of tracer gas in characterization of underground mine ventilation networks. Process Safety and Environmental Protection, 99, 1-10. https://doi.org/https://doi.org/10.1016/j.psep.2015.10.001

Yuan, L., & Smith, A. C. (2015). Numerical modeling of water spray suppression of conveyor belt fires in a large-scale tunnel. Process Safety and Environmental Protection, 95, 93-101. https://doi.org/https://doi.org/10.1016/j.psep.2015.02.018

Yuan, L., Thomas, R. A., Rowland, J. H., & Zhou, L. (2018). Early fire detection for underground diesel fuel storage areas. Process Safety and Environmental Protection, 119, 69-74. https://doi.org/https://doi.org/10.1016/j.psep.2018.07.022

Yuan, L., Zhou, L., & Smith, A. C. (2016). Modeling carbon monoxide spread in underground mine fires. Applied Thermal Engineering, 100, 1319-1326. https://doi.org/https://doi.org/10.1016/j.applthermaleng.2016.03.007

Zhang, X., Lin, Y., Shi, C., & Zhang, J. (2021). Numerical simulation on the maximum temperature and smoke back-layering length in a tilted tunnel under natural ventilation. Tunnelling and Underground Space Technology, 107, 103661.

Zhao, P., Yuan, Z., Yuan, Y., Yu, N., & Yu, T. (2019). A study on ceiling temperature distribution and critical exhaust volumetric flow rate in a long-distance subway tunnel fire with a two-point extraction ventilation system. Energies, 12(8), 1411.

Zhao, S., Liu, F., Wang, F., & Weng, M. (2018). Experimental studies on fire-induced temperature distribution below ceiling in a longitudinal ventilated metro tunnel. Tunnelling and Underground Space Technology, 72, 281-293.

Zhou, L. (2009). Improvement of the mine fire simulation program MFIRE.

Zhou, L., Yuan, L., Bahrami, D., Thomas, R. A., & Rowland, J. H. (2018). Numerical and experimental investigation of carbon monoxide spread in underground mine fires. Journal of fire sciences, 36(5), 406-418.

Zhu, H., Shen, Y., Yan, Z., Guo, Q., & Guo, Q. (2016). A numerical study on the feasibility and efficiency of point smoke extraction strategies in large cross-section shield tunnel fires using CFD modeling. Journal of Loss Prevention in the Process Industries, 44, 158-170.

III. NUMERICAL INVESTIGATION OF FIRE-INDUCED BUOYANCY-DRIVEN FLOWS DUE TO KEY MINING ACTIVITIES IN AN UNDERGROUND DEVELOPMENT HEADING

Salami O.B[a], Jurgen F. Brune [b], Guang Xu[a]*

[a] Department of Mining and Explosives Engineering, Missouri University of Science and Technology, Rolla, Missouri, 65401, USA.

[b] Department of Mining Engineering, Colorado School of Mines Golden, CO 80401 USA.

ABSTRACT

This study investigates the intricacies of equipment fires in blind heading of an underground development blind heading using CFD modeling. A series of fire dynamic simulations was conducted for various longitudinal ventilation velocities (L_v= 2, 3, and 4 m/s) and distances of the auxiliary ventilation duct (D_f = 10, 15, and 20 m) to the face of the blind heading to gain insights on temperature distribution and smoke spread mechanism in the underground blind heading. The findings indicated that the distance of the auxiliary ventilation duct from the blind face of an underground development heading has a strong impact on the smoke stratification of the fire-induced ceiling jet. The high-velocity flow from the auxiliary duct and leads to turbulent eddies characterized by high levels of fluctuating vorticity in the blind heading, and the extent of the turbulent region increases as the distance between the blind face and the auxiliary ventilation duct increases. On the other hand, the longitudinal ventilation velocity was observed to have a negligible influence on fire smoke gas temperature in the blind heading. The significance of this research extends to the realm of fire safety engineering, where computational fluid

dynamics (CFD) modeling plays a pivotal role in the design and evaluation of fire protection systems. Through this study, we enrich the literature on equipment fire dynamics in underground environment, thus enabling the development of more effective safety protocols for emergency preparedness in underground mining environment.

Keywords: Underground fire safety, Computational fluid dynamics, large eddy simulation, buoyancy-driven flow, auxiliary ventilation.

1. INTRODUCTION

The blind heading of an underground development face poses a significant risk of fires during key mining activities and accidents in underground mines can often lead to catastrophic consequences. In room-and-pillar coal mines for instance, they are the major source of methane and coal dust with a high potential of ignition and explosion (Feroze & Genc, 2017; Hansen, 2017, 2019a; Hansen & Ingason, 2013a). Additionally, mobile equipment such as the drilling rig, jumbo drill, continuous miner, etc engage in long hours of operation in the bling heading of a development face and possess threats of equipment fires which are extremely hazardous to the safety of miners (Conti, 2001; De Rosa, 2004; Hansen, 2009, 2017, 2019a, 2019b, 2023; Hansen & Ingason, 2013a). It is noteworthy that, unlike fires occurring mid-tunnel, where smoke movement can be influenced by critical ventilation velocities, fires in blind headings restrict smoke flow to a unidirectional path, thus forcing miners to escape through the smoke-filled blind heading. Since 2000, the United States has experienced over 150 underground mine fires, including instances of methane explosions, resulting in fatalities and numerous reports of face ignitions and

spontaneous combustion fires have been reported to the Mine Safety and Health Administration (MSHA) annually (NIOSH, 2021b).

The upshot of an underground mine fire is primarily voluminous smoke that could be dispersed to other areas of the subsurface environment through the ventilation network, and this may result to severe fatalities due to the aspiration of CO (Bahrami et al., 2021; Conti, 2001; Zhou, 2009b; Zhou et al., 2018). Smoke produced from fires in confined spaces such as channels, tunnels, and underground mines has accounted for more than 85% of the fatality in confined space environments (Gao et al., 2016). The smoke contains noxious gases that could suffocate personnel after descending to a certain height (Long et al., 2022). Furthermore, the smoke reduces visibility thereby seriously hindering emergency evacuation (Oluwafemi Babatunde Salami, Guang Xu, et al., 2023; Oluwafemi Babatunde Salami, G. Xu, et al., 2023). Furthermore, the increased implementation of subsurface transportation systems has led to the proliferation of subways and tunnels in urban areas, which in turn has heightened the potential risks associated with fires in these confined spaces (Barbato et al., 2014; Gehandler, 2015; Haghighat & Luxbacher, 2019; Li & Ingason, 2018; Zhang & Huang, 2022). Consequently, the dangers of fires in subways and tunnels have become a significant concern in contemporary urban planning and public safety initiatives.

Because of the high cost and difficulty of repeating full-scale tests, numerical methods such as computational fluid dynamics (CFD) have been widely adopted for fire risk assessment and simulation of fire scenarios. Several researchers have applied CFD to model fire and smoke spread in mines and tunnels (Adjiski, 2014; Adjiski et al., 2016; Fernández-Alaiz, Castañón, et al., 2020a; Gannouni & Maad, 2015; L. Hu et al., 2008; P.

J. Woodburn & R. E. Britter, 1996; Yuan et al., 2016; Zhu et al., 2016), and in the development of management strategies for thermal conditions in underground mines (Sasmito et al., 2015), or for the purpose of evacuation planning (Vancho Adjiski et al., 2015). Adjiski (Adjiski, 2014) developed a 3D model tunnel (50 m long, 4 m wide, and 3 m high) and studied the influence of ventilation on fire with a heat release rate of 500 kw/m2. In another study, (Adjiski et al., 2016) used CFD simulation to evaluate the effectiveness of a brattice obstruction to improve safe evacuation and firefighting conditions for underground miners. They analyzed two scenarios of tunnel fires with and without a brattice obstruction and the findings showed that using a brattice obstruction could enhance firefighting and safe evacuation.

CFD modeling has also been applied to enhance other fire safety measures such as the efficiency of water suppression for conveyor belt fires (Yuan & Smith, 2015), carbon monoxide spread during mine fires (Yuan et al., 2016), methane dispersion and methane management in underground mines (Kurnia et al., 2014), and the effect of tunnel bifurcation angle on the product of combustion spread in the underground space (Lu, Weng, Liu, Wang, Han, & Cheung, 2022; Lu, Weng, Liu, Wang, Han, & Chipok Cheung, 2022).

More closely connected to this study is the application of CFD in the development face of an underground heading and many works have been done on the control of the thermal environment in mine development heading/drift using CFD (Adjiski, 2014; Adjiski & Despodov, 2020b; Vancho Adjiski et al., 2015; Adjiski et al., 2016; Ding et al., 2017; Feroze & Genc, 2017; Li et al., 2022; Xin et al., 2021). (Xin et al., 2021) investigated the performance of auxiliary overlap ventilation systems including the far-forcing-near-

exhausting (FFNE) and the near-forcing-far-exhausting (NFFE) configurations that are widely used in underground mines. The study found that the NFFE has a superior cooling performance by comparing air velocity, temperature, and relative humidity values in the development heading. (Feroze & Genc, 2017) analyzed the effect of line brattice ventilation system variables on the airflow near a blind heading. Three factors including the heading dimension, the settings of the line brattice, and the velocity of air from the last through road into the heading were evaluated to estimate the optimum ventilation to the face of the heading. (Li et al., 2022) employed CFD to explore the appropriate oxygen supply duct type for optimum ventilation strategy in the blind heading of a plateau mine. The results from the study demonstrated that using a slit oxygen outlet has a better oxygen-enrichment effect in the blind heading when compared to traditional oxygen supply method. (Ding et al., 2017) utilized CFD to examine the airflow distribution in a three-center arch-section tunnel to examine the influence of air velocity and tunnel cross-section on airflow distribution. For the different cases examined, they discovered the airflow distribution showed circular pattern and the average velocity points was observed to be close to the tunnel wall under different airflow velocity.

Nevertheless, despite the enormous literature on underground mine fires, our understanding of equipment fire dynamics in the development face of underground is limited, and current studies are insufficient to predict smoke backflow in underground drift due to a fire in the blind heading. Classical models on smoke gas temperatures and smoke back layering in previous studies is limited to straight tunnels (Chow et al., 2010; Gannouni & Maad, 2015; Haghighat & Luxbacher, 2019; Ingason & Li, 2010; Li et al., 2021; Wu et al., 2018). In addition, the fire locations are also assumed to be mostly in the main drift of

the mine or at the middle of the tunnel (Gannouni & Maad, 2015; Li et al., 2021; Wu et al., 2018; Zhao et al., 2018). However, in real mining situations, there are cross-passages in the underground and most of the equipment fires are likely to occur in the blind heading of the drift where the machines are constantly operating. Existing studies about the evolution of fire in the blind heading are still limited and no previous study has attempted to evaluate the potential hazard of an equipment fire in the blind heading of an underground development face. Similarly, the smoke spread mechanism would be influenced by the existence of a blind heading along a drift. Previous studies have not taken this into account. This study aims to fill this gap by investigating a realistic equipment fire in the blind heading of an underground development.

The objective of this study is to investigate the dynamics of an equipment fire in the blind heading of an underground development blind heading under different ventilation conditions. The key factors including the longitudinal ventilation velocity in the mine drift and the location of the auxiliary ventilation to the face of the blind heading are examined to analyze the fire risk of the equipment fire. A series of fire dynamic simulations with longitudinal ventilation, L_v = 2, 3, and 4 m/s were conducted for various distances to face, D_f from the auxiliary ventilation. D_f = 10, 15, and 20 m were examined in this paper. This study provides a novel contribution to the existing literature on subsurface fire dynamics and will improve our risk assessment framework and emergency preparedness for underground mine fire accidents. The implications of these findings extend to the broader field of fire safety engineering, where the use of CFD modeling has become increasingly prevalent in designing and assessing fire protection systems.

2. MODEL SETUP

The fire was assumed to occur during a drilling operation in an underground development face as depicted in Figure 1. The main drift of the mine is 200 m and blind heading has been developed up to 50 m when the fire occurred. The mine is assumed to be a typical underground development in the US and has a regular dimension of width 4 m and height 5 m. The heat release rate (HRR) value is the most important parameter for fire hazard analysis (Gannouni & Maad, 2015; Haghighat & Luxbacher, 2019; Hansen, 2017; Hansen & Ingason, 2013a; Oluwafemi Babatunde Salami, Guang Xu, et al., 2023). To make our simulation very realistic and practically significant, HRR data from a full-scale experiment was used in this study. Previous study of a full-scale fire test involving a drilling rig found that the maximum heat release rate of a drilling rig (Atlas Copco Boomer) on fire could be up to 29.4 MW (Hansen, 2017; Hansen & Ingason, 2013a). This value was assumed as the HRR for the equipment fire in this study and the fire source was modeled as a 2 m by 2 m burner for ther CFD simulation. From the equipment specification data sheet, the Atlas Copco Boomer WE3 C has a total installed electrical power rating of 237 KW (Atlas-Copco, 2008). Therefore, by applying the basic ventilation dilution criteria of 0.06 m^3/s per kw for diesel equipment (Halim, 2017; Rawlins, 2006), the required airflow to the development was calculated to be 14.2 m^3/s. This value was used as the input parameter for the flow in the auxiliary ventilation duct to the face in this study. The duct was designed to extend 5 m from the blind heading junction into the main drift and the diameter of the duct was set to 0.6 m for the CFD simulation. Finally, thermocouples were installed below the roof of the blind heading to measure the temperature distribution in the

mine during the fire. The complete instrumentation of the blind heading is presented in Figure 2. The thermocouples were installed 0.5 m below the roof of the blind heading and 2 m apart in the horizontal direction as depicted in Figure 2.

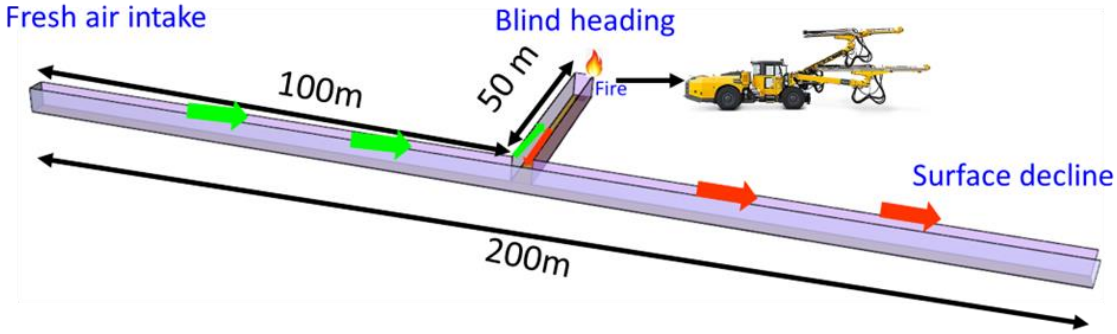

3D view

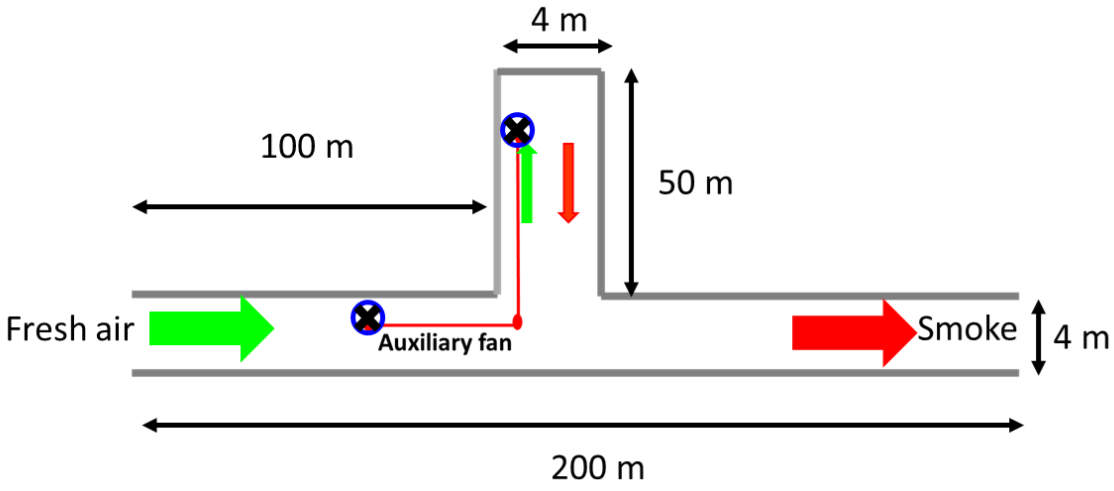

Top view

Figure 1. Schematic of numerical model.

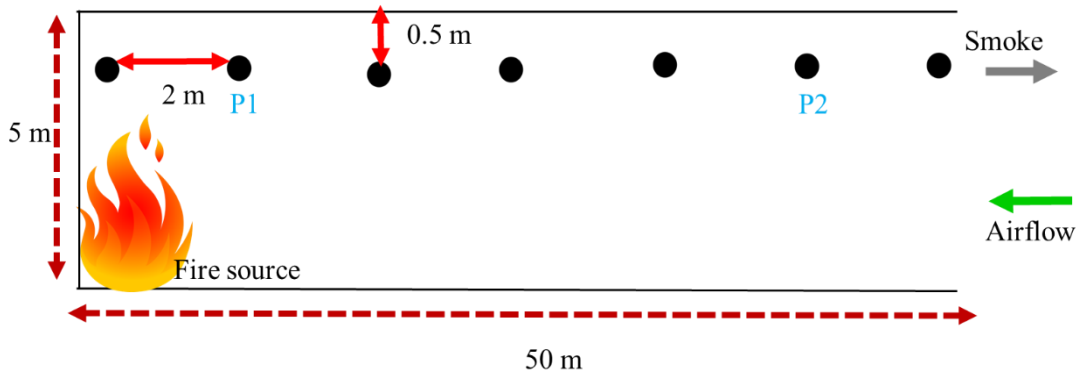

Figure 2. Thermocouples arrangement in the blind heading.

3. NUMERICAL SIMULATION

3.1. THE SOLVER

One of the most popular CFD tools used for mine fire simulation is the Fire Dynamic Simulator (FDS) developed by NIST (McGrattan et al., 2013; Oluwafemi Babatunde Salami, Guang Xu, et al., 2023; Trouvé & Wang, 2010). The FDS is an open-source CFD software freely available to researchers from the National Institute of Standards and Technology U.S. Department of Commerce website (FDS-SMV (nist.gov)). They primarily solve the Navier-Stokes equations (Equations (1) & (2)) for fluid flow with low Mach number (Ma < 0.3) (Gaitonde, 2006; McGrattan et al., 2013; McGrattan et al., 2012; McGrattan et al., 1998; Oluwafemi Babatunde Salami, Guang Xu, et al., 2023; Trouvé & Wang, 2010). FDS can efficiently model low-speed thermally driven flow such as heat and smoke transport phenomenon. Several researchers have applied CFD techniques to solve fire-related problems in mining engineering (Cheng et al., 2016; Fernández-Alaiz, Castañón, et al., 2020a; C. C. Hwang & J. C. Edwards, 2005; Trouvé & Wang, 2010). Most of the studies demonstrated that FDS generally performs better when

compared to other fire CFD solvers. This is because the solver was primarily designed to solve low-speed thermally driven flow. In addition to that, FDS provides more detailed spatial resolutions using less computational time compared to other CFD models (McGrattan et al., 1998; Oluwafemi Babatunde Salami, Guang Xu, et al., 2023; Trouvé & Wang, 2010).

$$\nabla . \mathrm{U} = 0 \tag{1}$$

$$\frac{\partial \mathrm{U}}{\partial t} + (\mathrm{U}\nabla).\mathrm{U} = -\frac{1}{\rho}\nabla p + v\nabla^2 U \tag{2}$$

where U is the fluid velocity at a point in the flow domain, p is the pressure of the fluid. ρ represents the fluid density and v denotes the kinematic viscosity (Gaitonde, 2006).

3.2. FDS SIMULATION

In this study, the effect of two key factors, the longitudinal ventilation, and the distance between the auxiliary fan to the blind heading on temperature distribution and smoke backflow from the blind heading to the main drift were examined. Longitudinal ventilation velocities of 2 m/s, 3 m/s, and 4 m/s were investigated while the auxiliary fan was placed 10 m, 15 m, and 20 m from the blind heading. A total of nine simulations were conducted. The detailed numerical simulation cases are presented in Table 1.

3.2.1. Simulation Parameters and Boundary Conditions. For this study, the default setting for dynamic turbulence modeling was retained. The default settings adopt the constant Smagorinsky model (where P_{rt}=0.5, S_{ct}=0.5, and C_s=0.17). Furthermore, the environmental conditions in the model were set to the experimental conditions during the fire test to mimic the exact environmental situation during the experiment. The measured

HRR from the experiment field tests was set as the heat release rate per unit area (HRRPUA) in the FDS simulations.

Table 1. Simulation cases for this study.

Distance of auxiliary fan development from blind heading (m)	Longitudinal velocity(m/s)	Simulation case [Distance (m), velocity (m/s)]
10	2	[10, 2]
	3	[10, 3]
	4	[10, 4]
15	2	[15, 2]
	3	[15, 3]
	4	[15, 4]
20	2	[20, 2]
	3	[20, 3]
	4	[20, 4]

The reaction type was set as “HEPTANE’’, and the “SOOT_YIELD =0.1”. The surface decline to the mine was modeled as “OPEN” surface. Similarly, the main drift that receives fresh air from the ventilation shaft was modeled as “SUPPLY” to provide ventilation to the blind heading. The different airflow rate was assigned to the supply based on the set simulation scenario. The mine walls were set as “CONCRETE”, and the surfaces of the wall were assigned “INERT” for the FDS simulation. Concrete was used as the material for the mine walls and ceiling. It possessed a density of 2100 kg/m^3, specific heat of 879J/kg K, and thermal conductivity of 1.10 W/m K (Seike et al., 2017), while the thickness of the wall was set to 0.2 m. However, because FDS threats the wall as a thin obstruction which results in a computational error when the mesh size is increased from 0.2 m to 0.5m for sensitivity studied, “Thicken” was applied to the obstruction properties of the wall for the FDS simulation of mesh sizes 0.4m and 0.5m. This however has no significant effect on the results of the FDS simulation as the major purpose of this is to

prevent a “VENT” in the computational domain from hanging in the air which leads to error in the computation.

To ensure that the numerical results are reliable and computationally correct, the time step is constrained such that the Courant-Friedrichs-Lewy (CFL) condition is satisfied (Cheong et al., 2009; Gannouni & Maad, 2015):

$$\delta t \, max \left(\frac{u}{\delta x}, \frac{v}{\delta y}, \frac{w}{\delta z}\right) \leq 1 \tag{3}$$

The initial time step is specified automatically in FDS by dividing the grid size by the characteristic velocity of the flow. The value of the time step is given as

$$\frac{5(\delta x \delta y \delta z)^{1/3}}{\sqrt{gH}} \tag{4}$$

For each time step during the calculations, the velocities u, v, w are tested to ensure that the CFL condition is met. In a situation where CFL is greater than 1.0, the time step is set to 0.8 of its allowed peak value, and the velocities are recalculated and tested again since the solutions to the equations cannot be updated with a time step greater than 1.0 which implies a parcel of fluid crossing the grid cell (Cheong et al., 2009). The CFL number and time steps obtained for the different mesh sizes during the simulation are presented in Figure 3. The CFL number was between 0.8 to 1.0 for all the cases. All three cases satisfy the stability criterion and indicates that our model is computationally correct.

The fire was simulated using a high-performance laboratory computer with the latest version of FDS, FDS 6.7.7 at the time of this simulation. The main drift and the development face blind heading domain were divided into four continuous meshes each and the entire mine domain has eight meshes. Each mesh was assigned to an MPI, and the number of Open MP processes was set to 2.

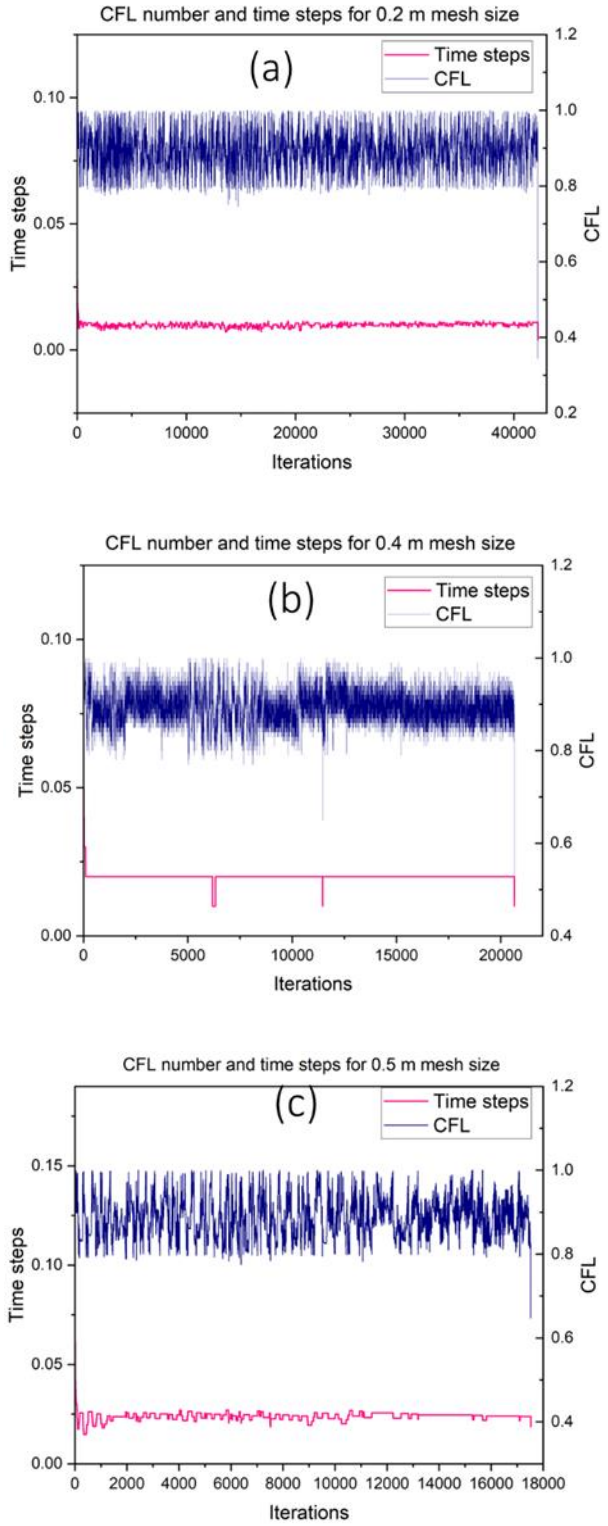

Figure 3. CFL number and time steps for different mesh sizes.

This will enable the calculations in each computational mesh to be done in parallel to speed up the processing time. The ambient temperature inside and outside the mine was set to the default value of 20 ^{o} C in the FDS while the pressure was set to 101325.0 Pa. The simulation time was set to 420.0 s (which implies that the drilling rig fire was assumed to burn ten times faster compared to the real scale experimental time of 70.0 mins (4200.0 s). The reason for this is to reduce the computational resources of simulating for days since the major fire evolution could be captured within the current simulation framework. Large eddy simulation (LES) was adopted as the turbulent model for this study.

3.3. TURBULENCE MODEL

LES adopts the closure model used in describing unresolved convective transport for fire in confined spaces (Trouvé & Wang, 2010). The steps given below explain how to set up the LES simulation for fire in a confined space such as an underground mine (McGrattan et al., 2013b; McGrattan, 2005; Rodi et al., 1997):

First, an evolution equation is formulated for the kinetic energy of the gas by taking the dot product of the momentum equation and the velocity vector u:

$$\rho \frac{D\boldsymbol{u}}{Dt} . \boldsymbol{u} \equiv \rho \frac{D\left(\frac{|\boldsymbol{u}|^2}{2}\right)}{Dt} = \cdots - \emptyset \qquad (5)$$

The sink term, $\emptyset$, known as the dissipation function can be obtained from the viscous stress tensor τ, and the velocity vector as given by equation (6).

$$\emptyset = \tau . \nabla \boldsymbol{u} = \mu \left[2 \left(\frac{\partial u}{\partial x} \right)^2 + \cdots \right] \qquad (6)$$

The sink term also shows up in the energy equation with the extra terms hidden for the sake of clarity and simplicity. The expression is merely explaining in mathematical terms how the kinetic energy of the flow is converted into thermal energy due to viscosity.

$$\frac{D}{Dt}(\rho h) = \cdots + \emptyset \tag{7}$$

The dissipative effect of the viscosity can thus be represented as a large-scale flow simulation by the expression:

$$\mu_{LES} = \rho(C_s\Delta)^2 \left[2\left(\frac{\delta\bar{u}}{\delta x}\right)^2 + \cdots\right]^{1/2} \tag{8}$$

Where:

C_s is an empirical constant generally taken to be equal to 0.2 (Rahmani et al., 2004),

Δ is the grid size of the cell, and the term in bracket has the same functional form as the dissipation function.

The thermal conductivity and material diffusivity are related to the LES viscosity by:

$$k_{LES} = \frac{\mu_{LES}c_p}{P_r} \quad ; \quad D_{LES} = \frac{\mu_{LES}}{\rho S_c} \tag{9}$$

Where P_r, is the turbulent Prandtl number and S_c is the Schmidt number.

3.4. MESH SENSITIVITY STUDY

The grid size is the principal factor that determines the resolution of the CFD simulation and could impact properties like fire smoke temperature measured at the airway ceiling. For this reason, appropriate grid sensitivity should be done to obtain mesh independence. In FDS, the grid size could be derived by the fire characteristic diameter given in Equation (10) (McGrattan et al., 2013; Weng et al., 2015):

$$D^* = \left(\frac{\dot{Q}}{\rho_\infty c_p T_\infty \sqrt{g}}\right)^{2/5} \quad (10)$$

where δx denotes the nominal size of the mesh cell, $\dot{Q}$ represents the total heat release rate of the fire (kW), ρ_∞ designates the ambient air density kg/m^3, C_p is the specific heat capacity of air (KJ/kg/k), T_∞ is the ambient temperature (K), and g is the acceleration due to gravity (usually taken as 9.81 m/s^2) (McGrattan et al., 2013; McGrattan et al., 2016; Overholt, 2014).

The ratio of fire characteristic size to grid size (D*/δx) known as the plume resolution (PR) index is normally used to describe the quality of the calculation grid (Gannouni & Maad, 2015). The higher this value is, the finer the meshes are and the more computational time is required for the CFD simulation. However, sensitivity studies from the literature have recommended that values between 4 to 16 are sufficient to obtain an appropriate resolution with minimal computational requirements (McGrattan et al., 2013; McGrattan et al., 2014). The mesh size for this simulation is also determined by this rule. For this study, the computational domain is obtained by setting the x, x', y, y', z, and z' to -1.0, 201.0, -1.0, 5.0, -1.0, 6.0 for the main underground drift and 99.0, 105.0, 5.0, 55.0, -1.0, 6.0 for the development face blind heading. Here, where x, y, z represents the minimum values and x', y', z' represents the maximum values for the coordinates x, y, z respectively.

According to Hasen, the calculated maximum HRR for the drilling rig is 29.4MW (Hansen, 2017, 2019b). The mesh sensitivity study is conducted based on this HRR value by using different mesh sizes to determine the suitable mesh for the desired accuracy before further computation. The characteristics fire diameter D* computed is 3.67. From the calculated fire characteristics diameter, difference mesh sizes are computed as presented

in Table 2. A comparison of the HRR and temperature history plots is presented in Figure 4 and Figure 5 respectively. As seen in Figure 5, the temperature measured at points P1 and P2 (see Figure 2) shows that the mesh sizes have very close history plots and that reducing the mesh size does not significantly influence the temperature value, however, it could significantly increase the computational resources. Station P1 and P2 are 2 m and 10 m from the blind heading respectively. By comparing Figure 5 (a) and (b), the values in Figure 5 (b) match better compared to Figure 5 (a). This may be due to the high turbulence near the fire and usually, studies have shown that smaller mesh sizes around the fire zone could improve the temporal resolution of the computational domain. Hence, a mesh size of 0.4 m was chosen as adequate for this study and applied for subsequent calculations. The summary of the mesh parameter is presented in Table 3.

Table 2. Computed mesh size for sensitivity studies based on D^*.

Mesh type	Ratio	Computed mesh size (m)
Coarse	$D^*/5$	~ 0.7
Medium	$D^*/10$	~0.4
Fine	$D^*/16$	~0.2

Table 3. Mesh parameters.

Case scenario	Mesh size $\Delta x \times \Delta y \times \Delta z$	The total number of cells in the model	Simulation time (hr.)
Model 1	0.2×0.2×0.2	1,323,000	32.84
Model 2	0.4×0.4×0.4	170,100	7.39
Model 3	0.5×0.5×0.5	84,672	3.71

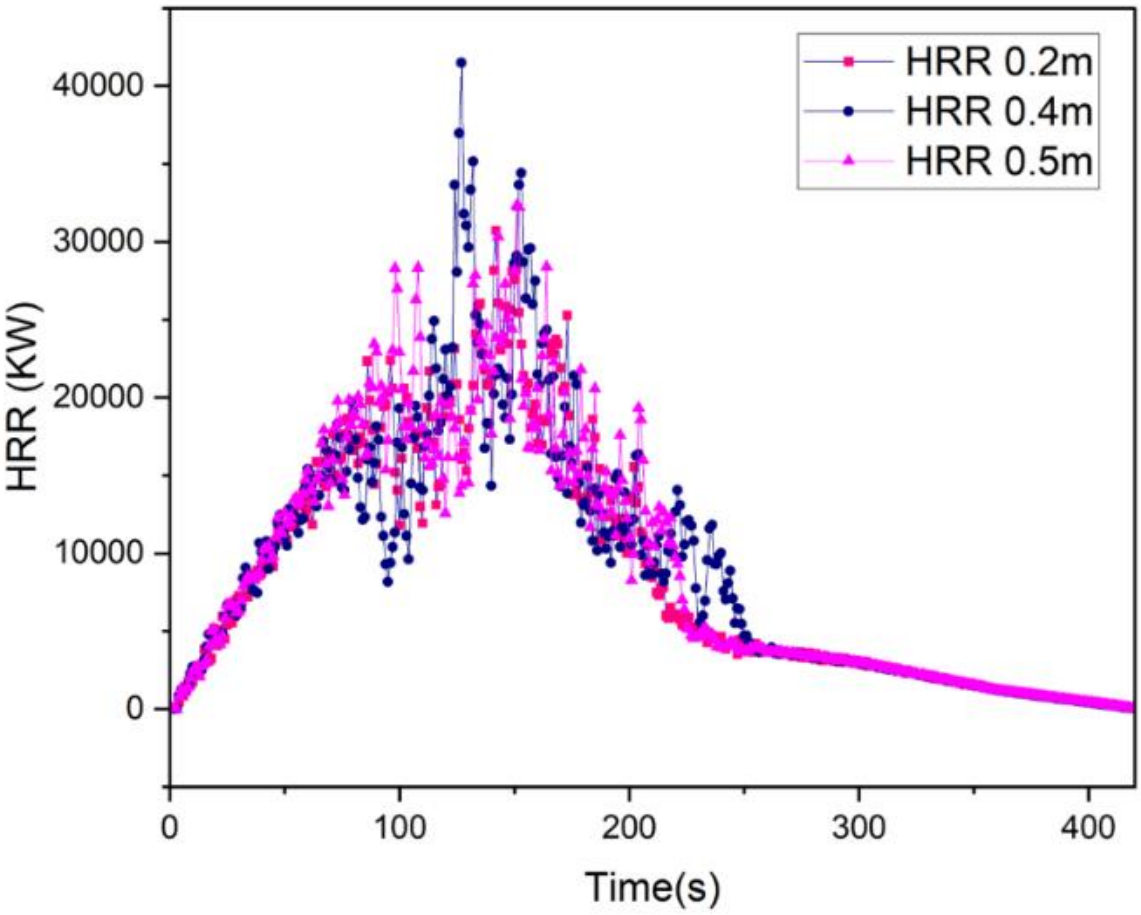

Figure 4. Comparison HRR time history for different mesh sizes.

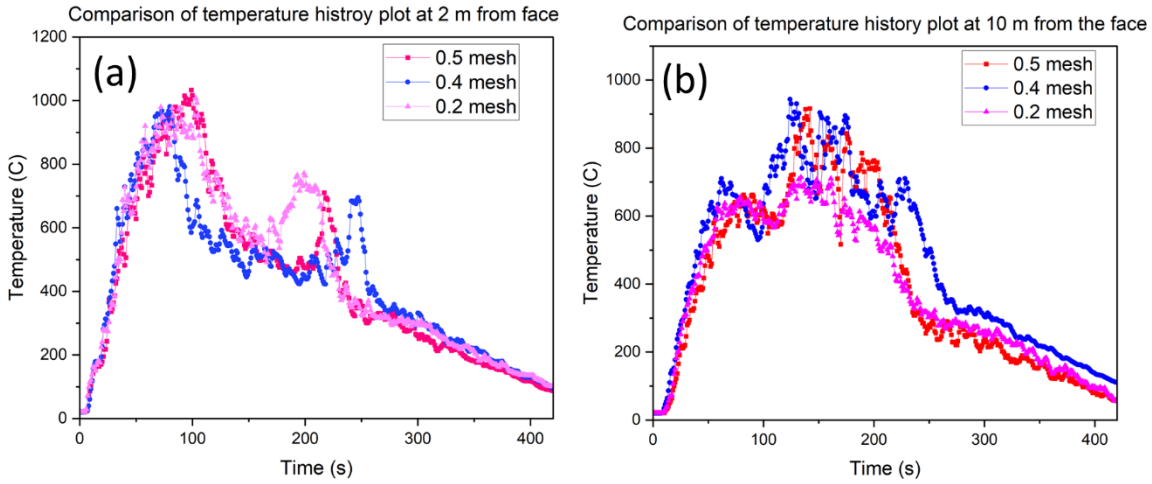

Figure 5. Comparison of temperature history plots at stations P1 and P2 along the blind heading.

4. RESULTS AND DISCUSSION

4.1. EFFECT OF LONGITUDINAL VELOCITY

Figure 6 shows the maximum ceiling temperature distribution along the blind heading of the underground development heading for various intake airway velocities.

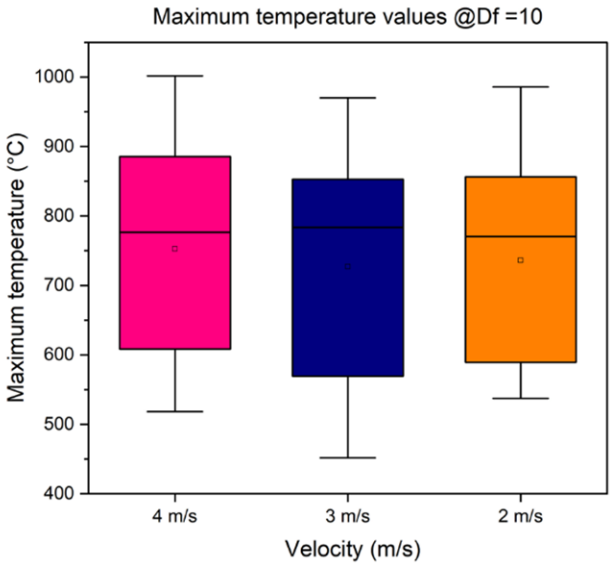

Figure 6. Temperature variance @D_f =10 m from face.

The maximum, minimum, and mean temperature values for the different ventilation conditions are very similar and the intake airway ventilation in the main drift does not have a significant impact on the measured temperature values beneath the ceiling of the blind heading.

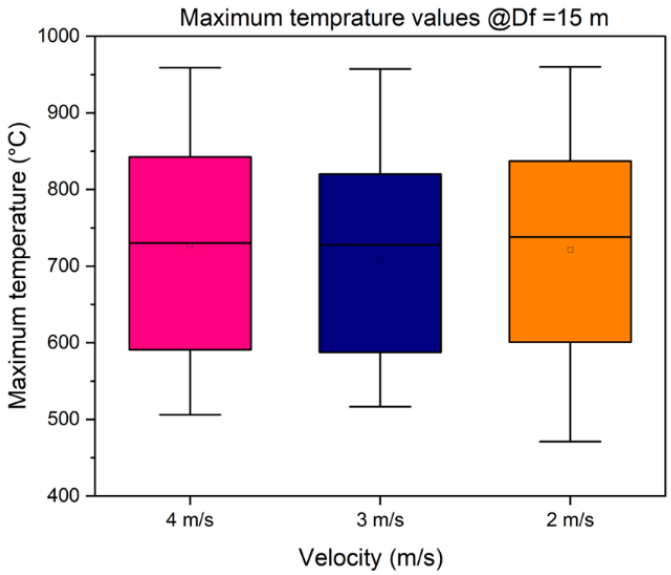

Figure 7. Temperature variance @D_f =15 m from face.

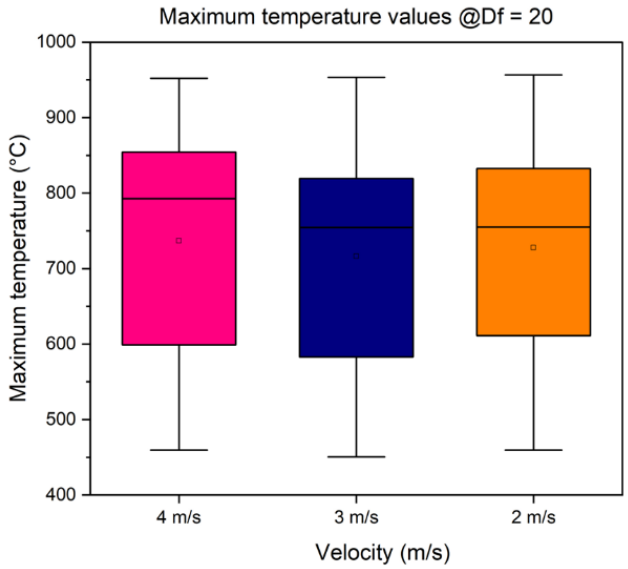

Figure 8. Temperature variance @D_f = 20 m from face.

Similar results are observed in Figure 7 and Figure 8. In Figure 6, the maximum and minimum temperature was about 1000 ^{o} C and 500 ^{o} C respectively for intake velocities of 4 m/s and 2 m/s. There was a slight difference in the simulated maximum and minimum temperature for velocity of 3 m/s which may be due to turbulence fluctuations, and this is not very significant. In Figure 7 and Figure 8, the maximum and minimum temperatures for the different velocities are approximately 950 ^{o} C and 500 ^{o} C. It could be seen that the temperature values are relatively the same for the same value of D_f. However, the maximum temperature values decrease slightly as D_f is increased. Although previous studies have shown that ventilation have an impact on temperature in straight tunnels, this study examines the impact on temperature along a blind heading which mainly depends on auxiliary ventilation rather than longitudinal ventilation. Blind heading mainly depends on auxiliary ventilation for the supply of fresh air to keep a conducive working environment in the development heading.

4.2. EFFECT OF D_f ON TEMPERATURE STRATIFICATION

Figure 9 to Figure 11 depicts that the position of the auxiliary ventilation duct has a strong impact on the temperature stratification beneath the roof of the blind heading. For instance, in Figure 9, the presence of the ventilation duct divides the blind heading into two regions: (1) a region of high turbulence and, (2) a region of stable stratification. A high turbulence region is observed between the face and the location of duct outlet. It can be observed that there is poor smoke layer stratification from the outlet of the ventilation duct to the face of the blind heading due to the high-speed flow from the ventilation duct. The high-velocity flow opposes the natural upward movement of the fire smoke along the

tunnel ceiling. This disruption could lead to the ceiling jet becoming unstable, causing fluctuations in temperature (as depicted in the region of high turbulence from Figure 9 to Figure 11), velocity, and direction.

Similarly, in Figure 10 and Figure 11, the high flow velocity creates turbulence in the airflow beneath the blind heading. The interaction between the high-velocity flow and the ceiling jet leads to turbulent eddies characterized by high levels of fluctuating vorticity. Beyond the auxiliary ventilation outlet, there is a relatively stable layer of smoke along the blind heading ceiling. A comparison between Figure 9, Figure 10, and Figure 11 indicates that the extent of the turbulent region increases as the distance between the blind face and the auxiliary ventilation duct increases. When the distance between the auxiliary ventilation duct and the blind was 10 m, the turbulent region was about 14 m from the face. This increased to about 19 m when D_f=15 m, and to about 24 m when D_f was increased to 20 m.

4.3. VELOCITY AND SMOKE BACKFLOW BLIND HEADING

The velocity profile measured 160 s (40 s after fire peak) during the fire is present in Figure 12. The time was selected because the smoke backflow was observed to be maximum at this time. The velocity in the smoke region has higher average values due to ceiling jet mix which leads to complex interaction between different air layers. The distance of the auxiliary ventilation does not impact the airflow in the blind heading and the main airway.

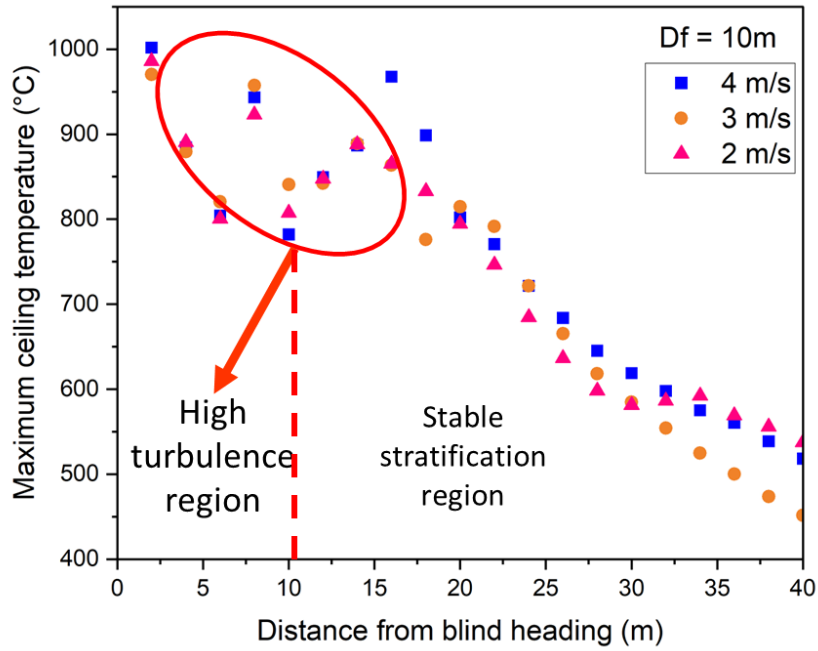

Figure 9 Maximum ceiling temperature for different longitudinal velocities at D_f =10 m.

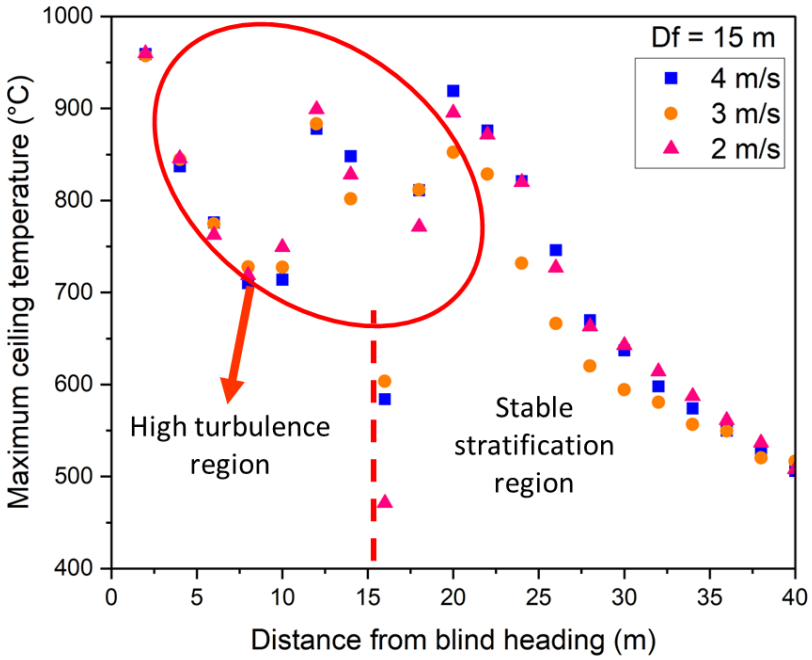

Figure 10. Maximum ceiling temperature for different longitudinal velocities at D_f =15 m.

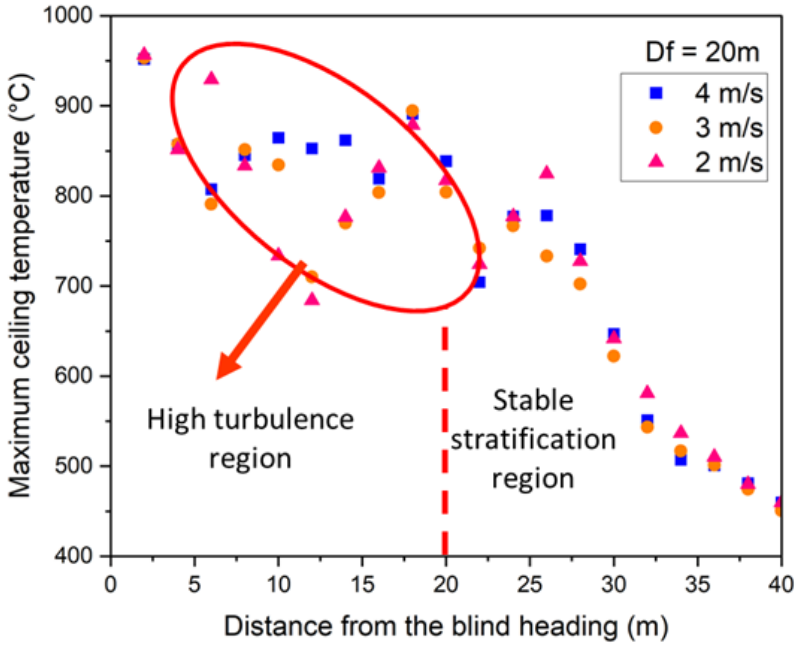

Figure 11. Maximum ceiling temperature for different longitudinal velocities at D_f = 20 m.

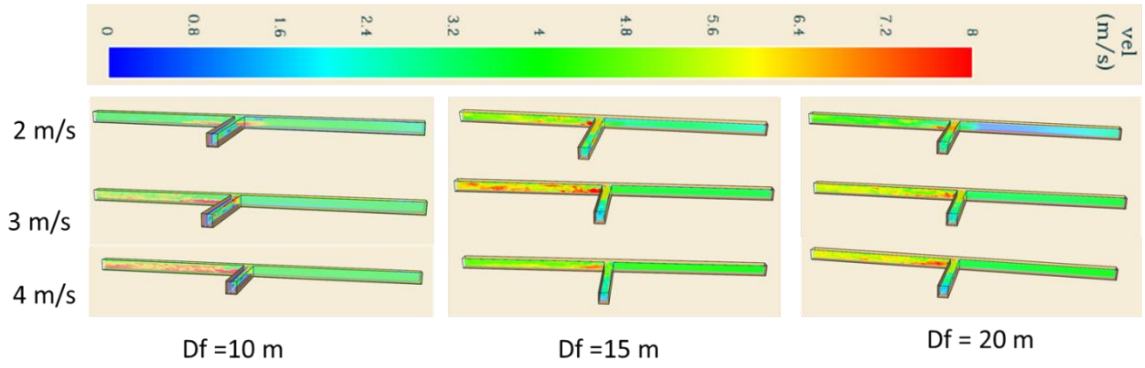

Figure 12. Velocity at 160 s (40 s after fire peak).

Figure 13 illustrates the smoke dispersion patterns in the underground environment based on various ventilation rates and the position of auxiliary ventilation outlets to the development face. Notably, Figure 12 shows the substantial impact of intake airway ventilation conditions within the primary airflow pathway on smoke reversal occurring at the blind heading junction. Specifically, at a longitudinal ventilation velocity of 2 m/s, the

smoke exhibited a backflow phenomenon from the blind heading junction, extending approximately 15 meters. Conversely, when the longitudinal ventilation rate was increased to 3 m/s, the entirety of the smoke was effectively directed toward the exhaust decline. The impact of smoke spread on visibility condition is presented in Figure 14. It shows that the visibility is directly impacted by the fire smoke. The region filled with smoke tends to have poor visibility compared to the smoke-free region. The visibility was observed to reduce from 30 m to about 5 m during the peak of the fire.

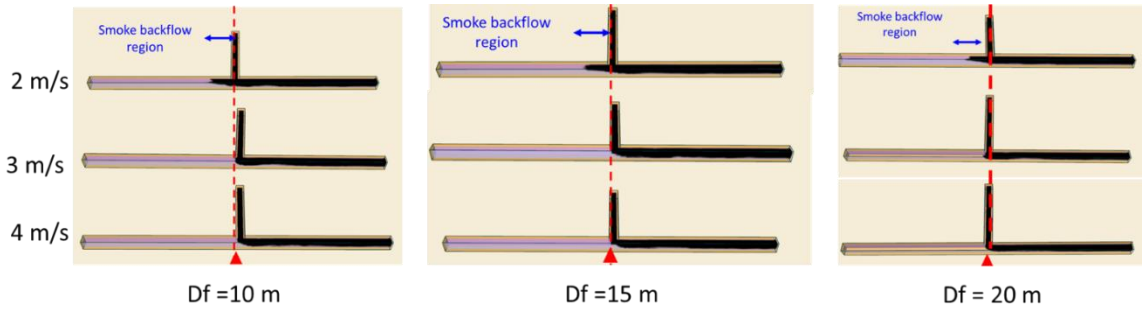

Figure 13. Smoke backflow at 160 s.

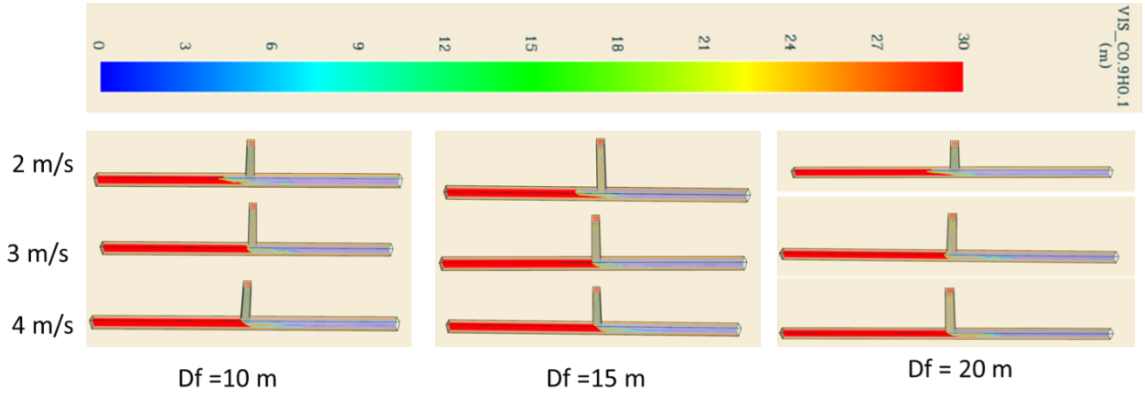

Figure 14. Visibility at 160 s.

Figure 13 shows that the calculated back layering length and critical ventilation velocity observed from the blind heading junction could be predicted to a reasonable

accuracy by exiting empirical models found in literature which were developed using straight tunnels (Ingason & Li, 2010; Li et al., 2010a). However, when the smoke backflow from the blind face was taken into account, exiting empirical model such as (Ingason & Li, 2010) and (Li et al., 2010a) underestimated the back layering length. Moreso, according to Figure 15, it is possible that the length of the blind heading, and changes in the heat release rate, and the auxiliary ventilation could impact the critical velocity and smoke backflow phenomenon. This was not investigated in this study and would be examined in subsequent research.

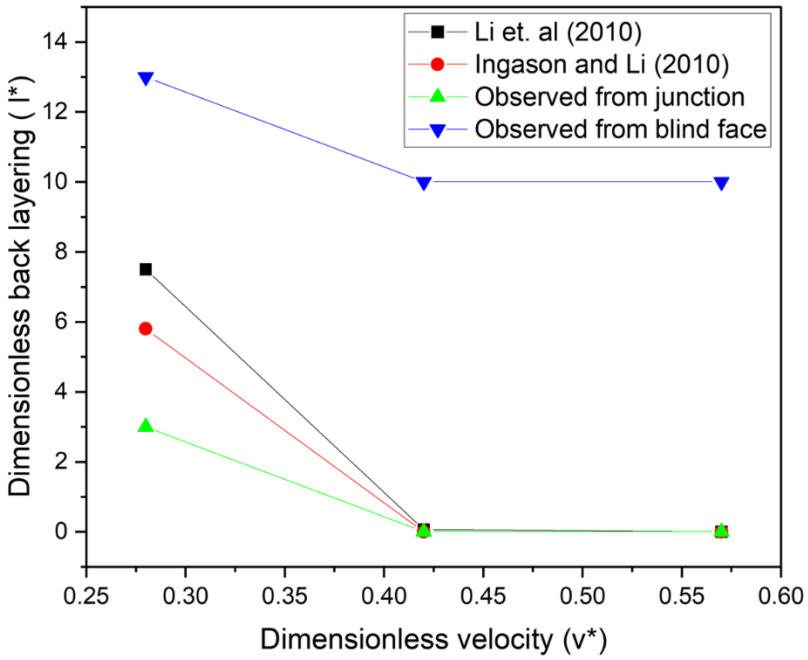

Figure 15. Dimensionless back layering vs dimensionless velocity.

4.4. MODEL VALIDATION

Model validation is important to ensure credibility and reliability. To ensure credibility of our results, our model was evaluated against full scale experimental data

involving a drilling fire in an underground mine by Hansen (Hansen, 2017, 2020; Hansen & Ingason, 2013a). The measured HRR from the experiment is depicted in Figure 16. This HRR history plot was used as the input for the simulation to mimic the experimental condition by invoking a "Fire_RAMP" function in the FDS code.

The simulation boundary conditions were set based on the experimental conditions (See APPENDIX for FDS validation code). The drift dimension was roughly 6 m by 8 m. The length of the drift where the experiment took place was approximately 100 m. The drilling rig was located at approximately 54 m from the exhaust drift. The exhaust drift was approximately 40 m. Before the fire experiment, a tempest fan was placed as the beginning of the drift (about 46 m from the drilling rig) to push the smoke to the exhaust. The fan's capacity was 217 000 m^3/hr., and this was modeled as a "SUPPLY" inlet with a volume flow rate of 60.27 m^3/s for the FDS simulation. All other properties such as reaction type, wall properties, and HRR are set as described in Section 3.2.1.

During the experiment, a thermocouple was installed at the top of the boom of the drilling rig to measure the temperature on top of the boom. The length of the Rocket Boomer drilling rig with boom was 12.4 m. In the simulation, a thermocouple was installed at 12 m from the center of the fire to depict the boom of the drilling rig. A comparison between the experimental values and the predicted value from the simulation is presented in Figure 17. The results from the CFD modeling were found to fit the experimental data very well. Most importantly, our model predicted the maximum ceiling temperature to a high degree of accuracy which indicates that out model is reliable. A comparison of our model prediction performance with similar studies conducted in literature such as the Yuan et al's model (Yuan & Smith, 2015; Yuan et al., 2016), Fernandez et al's model

(Fernández-Alaiz, Castañón, et al., 2020a), and Hansen's model (Hansen, 2020) also show that our model validation is acceptable by looking at the experimental and predicted data trends. Similarly, a comparison of the velocity probe measurement that was installed approximately 4.4 m below the roof at the exhaust drift is presented in Figure 18. The results of the CFD modeling were found to fit the experimental values very well during the initial and extinction phase of the fire but overestimated the fire gas velocities in the combustion phase. This has been earlier reported by Hansen (Hansen, 2020), and the increased differences was observed to coincide with the initiation of a higher fire growth rate and higher heat release rates during the drilling rig experiment which the CFD model does not seem to properly account for.

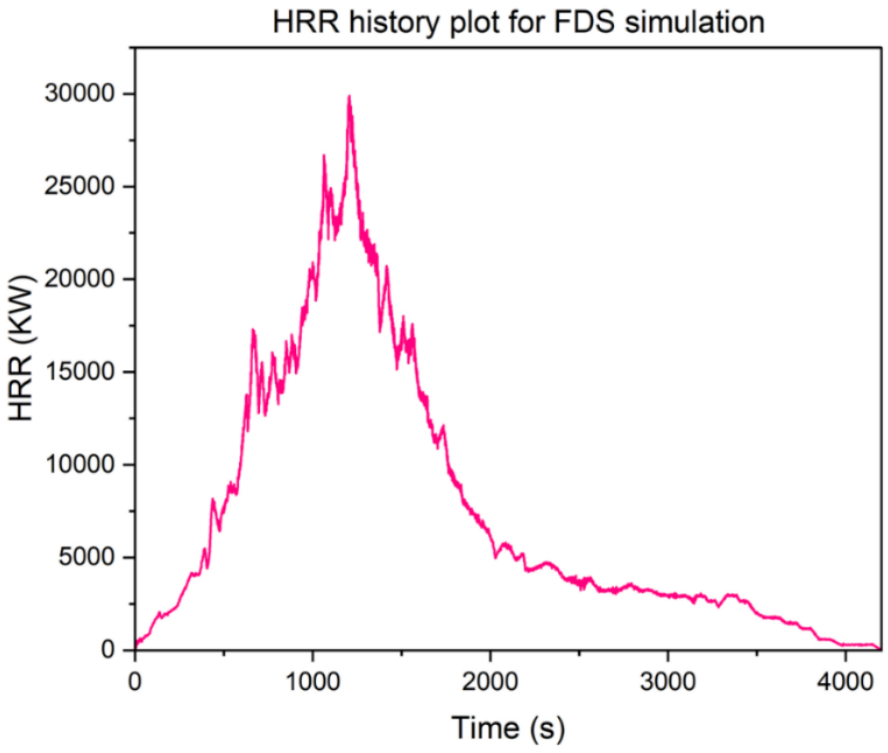

Figure 16. HRR time history plot from Hansen full-scale experiment (Hansen, 2017, 2020; Hansen & Ingason, 2013a).

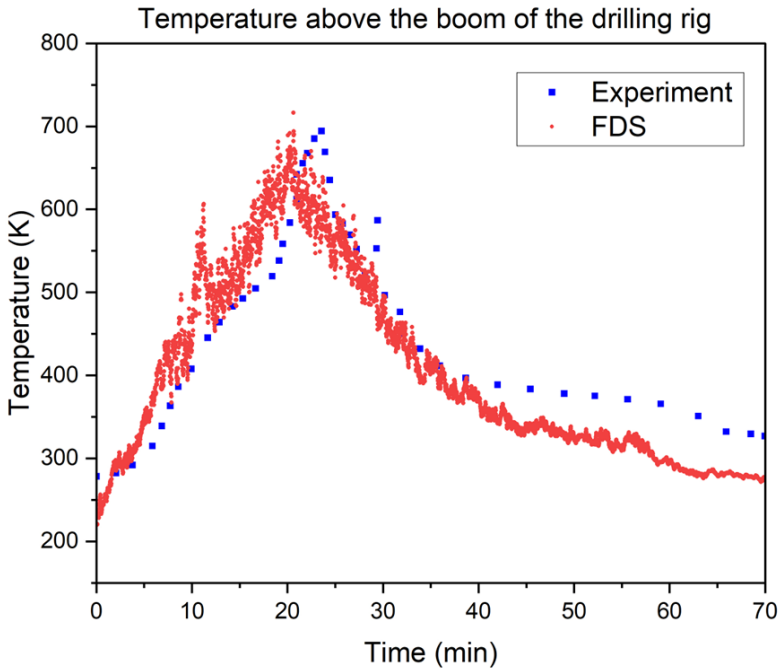

Figure 17. Comparison of fire gas temperature at thermocouple Tc35 for the drilling rig fire test.

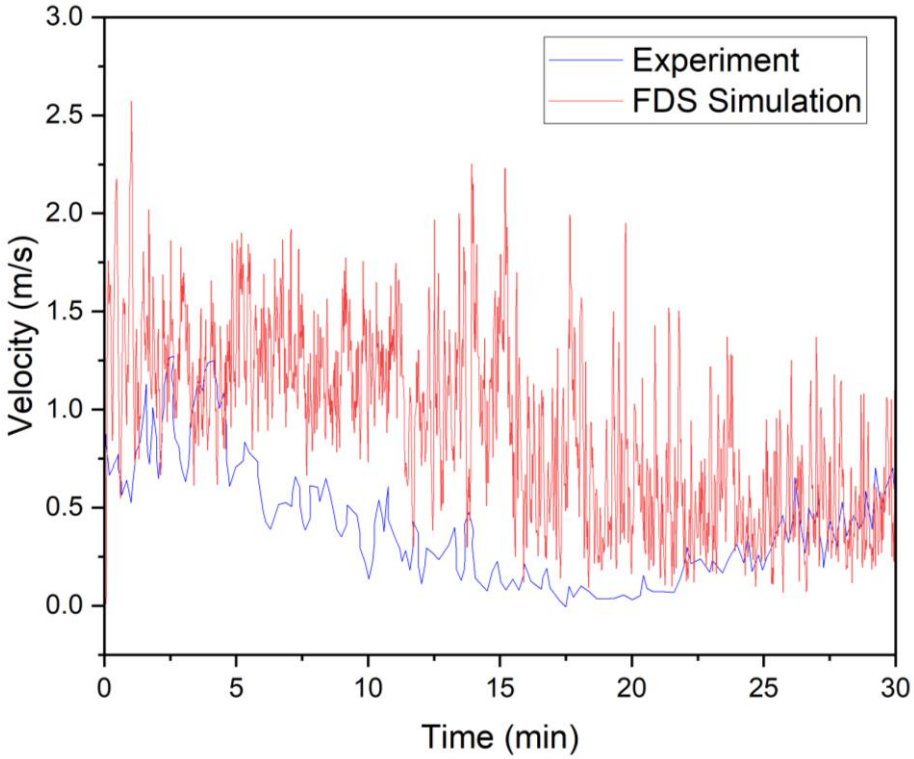

Figure 18. Comparison of velocity 4.4 m below the ceiling at the middle of the exhaust.

5. CONCLUSIONS

In this study, a numerical investigation using FDS 6.7.6 was conducted to examine the evolution of an equipment fire in the blind heading of an underground development during key mining activities. The maximum temperature beneath a ceiling of fire-induced ceiling jets flows with various distances D_f between the auxiliary ventilation duct and the blind face of an underground blind heading under different longitudinal ventilation was analyzed for improved fire safety practices in an underground mining environment. The findings indicated that the distance of the auxiliary ventilation duct from the blind face of an underground development heading has a strong impact on the flow and stratification of the fire-induced ceiling jet. The ceiling jet, which is a relatively stable layer of air along the tunnel ceiling, gets disrupted due to the high-speed flow in the opposite direction. The opposing flows could lead to increased energy dissipation due to the turbulence generated. This energy dissipation affects the overall airflow patterns and can impact the ventilation efficiency within the blind heading and similar subsurface structures such as tunnels. Additionally, smoke backflow from the blind heading junction was investigated and the critical ventilation velocity was found to be approximately 3.0 m/s for this scenario. Furthermore, a constant flow (14.2 m^3/s) based on the ventilation dilution requirement of the operating equipment was investigated and the influence of changing flow from the ventilation duct was not examined and would be considered in our future work. The findings from this study could aid in the new design of tunnels and other underground spaces to improve ventilation planning and life safety in confined spaces.

APPENDIX

&HEAD CHID='modelv8', TITLE='MODEL_VALIDATION'/

&TIME T_END=4200.0/

&DUMP DT_PL3D=10.0, DT_SLCF=1.0, DT_SL3D=1.0, NFRAMES=4200, WRITE_XYZ=.TRUE., PLOT3D_QUANTITY='MASS FRACTION','MASS FRACTION','MASS FRACTION','VISIBILITY','VISIBILITY', PLOT3D_SPEC_ID (1:4)='CARBON DIOXIDE','CARBON MONOXIDE','OXYGEN','SOOT', CFL_FILE =.TRUE./

&MISC SIMULATION_MODE='LES'/

&MESH ID='Mesh02-01', IJK=25,50,20, XB=99.0,109.0,9.0,29.0,-1.0,7.0/

&MESH ID='Mesh02-02', IJK=25,50,20, XB=99.0,109.0,29.0,49.0,-1.0,7.0/

&MESH ID='Mesh01-01-merged-01', IJK=51,25,20, XB=-1.0,19.4,-1.0,9.0,-1.0,7.0/

&MESH ID='Mesh01-01-merged-02', IJK=51,25,20, XB=19.4,39.8,-1.0,9.0,-1.0,7.0/

&MESH ID='Mesh01-01-merged-03', IJK=51,25,20, XB=39.8,60.2,-1.0,9.0,-1.0,7.0/

&MESH ID='Mesh01-01-merged-04', IJK=50,25,20, XB=60.2,80.2,-1.0,9.0,-1.0,7.0/

&MESH ID='Mesh01-01-merged-05', IJK=51,25,20, XB=80.2,100.6,-1.0,9.0,-1.0,7.0/

```
&MESH ID='Mesh01-01-merged-06', IJK=51,25,20, XB=100.6,121.0,-1.0,9.0,-
1.0,7.0/
&REAC ID='HEPTANE',
    FYI='NIST NRC FDS5 Validation',
    FUEL='REAC_FUEL',
    FORMULA='C7H16',
    CO_YIELD=0.01,
    SOOT_YIELD=0.1/
&DEVC ID='Tc36', QUANTITY='THERMOCOUPLE', XYZ=47.0,4.0,5.7/
&DEVC ID='Tc35', QUANTITY='THERMOCOUPLE', XYZ=52.0,4.0,5.7/
&DEVC ID='Tc2', QUANTITY='THERMOCOUPLE', XYZ=103.0,45.0,5.2/
&DEVC ID='Tc1', QUANTITY='THERMOCOUPLE', XYZ=105.0,45.0,5.2/
&DEVC ID='Tc4', QUANTITY='THERMOCOUPLE', XYZ=101.0,45.0,5.2/
&DEVC ID='Tc5', QUANTITY='THERMOCOUPLE', XYZ=103.0,45.0,4.0/
&DEVC ID='Tc7', QUANTITY='THERMOCOUPLE', XYZ=103.0,45.0,2.8/
&DEVC ID='Tc9', QUANTITY='THERMOCOUPLE', XYZ=103.0,45.0,1.6/
&DEVC ID='Tc06', QUANTITY='THERMOCOUPLE', XYZ=47.0,4.0,5.3/
&DEVC ID='Tc07', QUANTITY='THERMOCOUPLE', XYZ=48.0,4.0,5.3/
&DEVC ID='Tc08', QUANTITY='THERMOCOUPLE', XYZ=49.0,4.0,5.3/
&DEVC ID='Tc09', QUANTITY='THERMOCOUPLE', XYZ=50.0,4.0,5.3/
&DEVC ID='Tc10', QUANTITY='THERMOCOUPLE', XYZ=51.0,4.0,5.3/
&DEVC ID='Tc11', QUANTITY='THERMOCOUPLE', XYZ=52.0,4.0,5.3/
&DEVC ID='Diff3', QUANTITY='VELOCITY', XYZ=103.0,45.0,5.2/
```

```
&DEVC ID='Diff6', QUANTITY='VELOCITY', XYZ=103.0,45.0,4.0/
&DEVC ID='Diff8', QUANTITY='VELOCITY', XYZ=103.0,45.0,2.8/
&DEVC ID='Diff10', QUANTITY='VELOCITY', XYZ=103.0,45.0,1.6/
&MATL ID='CONCRETE',
    FYI='NBSIR 88-3752 - ATF NIST Multi-Floor Validation',
    SPECIFIC_HEAT=1.04,
    CONDUCTIVITY=1.8,
    DENSITY=2280.0/
&SURF ID='Wall',
    RGB=146,202,166,
    BACKING='VOID',
    MATL_ID(1,1)='CONCRETE',
    MATL_MASS_FRACTION(1,1)=1.0,
    THICKNESS(1)=0.2/
&SURF ID='Fire',
    COLOR='RED',
    HRRPUA=7350.0,
    RAMP_Q='Fire_RAMP_Q',
    TMP_FRONT=300.0/
&RAMP ID='Fire_RAMP_Q', T=0.0, F=0.01/
&RAMP ID='Fire_RAMP_Q', T=78.45, F=0.03/
&RAMP ID='Fire_RAMP_Q', T=102.59, F=0.05/
&RAMP ID='Fire_RAMP_Q', T=138.79, F=0.07/
```

&RAMP ID='Fire_RAMP_Q', T=144.83, F=0.06/

&RAMP ID='Fire_RAMP_Q', T=193.1, F=0.07/

&RAMP ID='Fire_RAMP_Q', T=235.34, F=0.08/

&RAMP ID='Fire_RAMP_Q', T=259.48, F=0.1/

&RAMP ID='Fire_RAMP_Q', T=289.66, F=0.12/

&RAMP ID='Fire_RAMP_Q', T=313.79, F=0.14/

&RAMP ID='Fire_RAMP_Q', T=362.07, F=0.14/

&RAMP ID='Fire_RAMP_Q', T=380.17, F=0.17/

&RAMP ID='Fire_RAMP_Q', T=392.24, F=0.19/

&RAMP ID='Fire_RAMP_Q', T=398.28, F=0.17/

&RAMP ID='Fire_RAMP_Q', T=404.31, F=0.15/

&RAMP ID='Fire_RAMP_Q', T=416.38, F=0.17/

&RAMP ID='Fire_RAMP_Q', T=428.45, F=0.25/

&RAMP ID='Fire_RAMP_Q', T=434.48, F=0.28/

&RAMP ID='Fire_RAMP_Q', T=476.72, F=0.22/

&RAMP ID='Fire_RAMP_Q', T=482.76, F=0.25/

&RAMP ID='Fire_RAMP_Q', T=506.9, F=0.27/

&RAMP ID='Fire_RAMP_Q', T=531.03, F=0.3/

&RAMP ID='Fire_RAMP_Q', T=549.14, F=0.3/

&RAMP ID='Fire_RAMP_Q', T=573.28, F=0.29/

&RAMP ID='Fire_RAMP_Q', T=579.31, F=0.32/

&RAMP ID='Fire_RAMP_Q', T=591.38, F=0.34/

&RAMP ID='Fire_RAMP_Q', T=627.59, F=0.47/

&RAMP ID='Fire_RAMP_Q', T=633.62, F=0.41/

&RAMP ID='Fire_RAMP_Q', T=651.72, F=0.5/

&RAMP ID='Fire_RAMP_Q', T=657.76, F=0.56/

&RAMP ID='Fire_RAMP_Q', T=663.79, F=0.58/

&RAMP ID='Fire_RAMP_Q', T=669.83, F=0.58/

&RAMP ID='Fire_RAMP_Q', T=675.86, F=0.56/

&RAMP ID='Fire_RAMP_Q', T=687.93, F=0.5/

&RAMP ID='Fire_RAMP_Q', T=693.97, F=0.44/

&RAMP ID='Fire_RAMP_Q', T=700.0, F=0.47/

&RAMP ID='Fire_RAMP_Q', T=712.07, F=0.53/

&RAMP ID='Fire_RAMP_Q', T=718.1, F=0.5/

&RAMP ID='Fire_RAMP_Q', T=730.17, F=0.43/

&RAMP ID='Fire_RAMP_Q', T=742.24, F=0.46/

&RAMP ID='Fire_RAMP_Q', T=754.31, F=0.48/

&RAMP ID='Fire_RAMP_Q', T=766.38, F=0.51/

&RAMP ID='Fire_RAMP_Q', T=772.41, F=0.54/

&RAMP ID='Fire_RAMP_Q', T=778.45, F=0.54/

&RAMP ID='Fire_RAMP_Q', T=790.52, F=0.51/

&RAMP ID='Fire_RAMP_Q', T=802.59, F=0.46/

&RAMP ID='Fire_RAMP_Q', T=808.62, F=0.49/

&RAMP ID='Fire_RAMP_Q', T=832.76, F=0.48/

&RAMP ID='Fire_RAMP_Q', T=844.83, F=0.53/

&RAMP ID='Fire_RAMP_Q', T=850.86, F=0.56/

&RAMP ID='Fire_RAMP_Q', T=868.97, F=0.52/

&RAMP ID='Fire_RAMP_Q', T=881.03, F=0.57/

&RAMP ID='Fire_RAMP_Q', T=911.21, F=0.52/

&RAMP ID='Fire_RAMP_Q', T=923.28, F=0.55/

&RAMP ID='Fire_RAMP_Q', T=929.31, F=0.58/

&RAMP ID='Fire_RAMP_Q', T=935.34, F=0.61/

&RAMP ID='Fire_RAMP_Q', T=965.52, F=0.63/

&RAMP ID='Fire_RAMP_Q', T=977.59, F=0.68/

&RAMP ID='Fire_RAMP_Q', T=1001.72, F=0.7/

&RAMP ID='Fire_RAMP_Q', T=1019.83, F=0.65/

&RAMP ID='Fire_RAMP_Q', T=1037.93, F=0.76/

&RAMP ID='Fire_RAMP_Q', T=1043.97, F=0.76/

&RAMP ID='Fire_RAMP_Q', T=1050.0, F=0.79/

&RAMP ID='Fire_RAMP_Q', T=1056.03, F=0.81/

&RAMP ID='Fire_RAMP_Q', T=1062.07, F=0.9/

&RAMP ID='Fire_RAMP_Q', T=1068.1, F=0.87/

&RAMP ID='Fire_RAMP_Q', T=1086.21, F=0.78/

&RAMP ID='Fire_RAMP_Q', T=1098.28, F=0.85/

&RAMP ID='Fire_RAMP_Q', T=1122.41, F=0.77/

&RAMP ID='Fire_RAMP_Q', T=1152.59, F=0.8/

&RAMP ID='Fire_RAMP_Q', T=1176.72, F=0.85/

&RAMP ID='Fire_RAMP_Q', T=1188.79, F=0.88/

&RAMP ID='Fire_RAMP_Q', T=1194.83, F=0.94/

&RAMP ID='Fire_RAMP_Q', T=1200.86, F=1.0/

&RAMP ID='Fire_RAMP_Q', T=1206.9, F=1.0/

&RAMP ID='Fire_RAMP_Q', T=1212.93, F=0.97/

&RAMP ID='Fire_RAMP_Q', T=1249.14, F=0.85/

&RAMP ID='Fire_RAMP_Q', T=1255.17, F=0.8/

&RAMP ID='Fire_RAMP_Q', T=1261.21, F=0.82/

&RAMP ID='Fire_RAMP_Q', T=1267.24, F=0.76/

&RAMP ID='Fire_RAMP_Q', T=1273.28, F=0.79/

&RAMP ID='Fire_RAMP_Q', T=1279.31, F=0.77/

&RAMP ID='Fire_RAMP_Q', T=1297.41, F=0.75/

&RAMP ID='Fire_RAMP_Q', T=1333.62, F=0.73/

&RAMP ID='Fire_RAMP_Q', T=1363.79, F=0.71/

&RAMP ID='Fire_RAMP_Q', T=1369.83, F=0.65/

&RAMP ID='Fire_RAMP_Q', T=1375.86, F=0.59/

&RAMP ID='Fire_RAMP_Q', T=1418.1, F=0.7/

&RAMP ID='Fire_RAMP_Q', T=1424.14, F=0.67/

&RAMP ID='Fire_RAMP_Q', T=1430.17, F=0.64/

&RAMP ID='Fire_RAMP_Q', T=1442.24, F=0.61/

&RAMP ID='Fire_RAMP_Q', T=1472.41, F=0.53/

&RAMP ID='Fire_RAMP_Q', T=1490.52, F=0.56/

&RAMP ID='Fire_RAMP_Q', T=1502.59, F=0.58/

&RAMP ID='Fire_RAMP_Q', T=1508.62, F=0.61/

&RAMP ID='Fire_RAMP_Q', T=1520.69, F=0.56/

&RAMP ID='Fire_RAMP_Q', T=1550.86, F=0.56/

&RAMP ID='Fire_RAMP_Q', T=1556.9, F=0.59/

&RAMP ID='Fire_RAMP_Q', T=1599.14, F=0.47/

&RAMP ID='Fire_RAMP_Q', T=1641.38, F=0.46/

&RAMP ID='Fire_RAMP_Q', T=1647.41, F=0.43/

&RAMP ID='Fire_RAMP_Q', T=1671.55, F=0.41/

&RAMP ID='Fire_RAMP_Q', T=1677.59, F=0.39/

&RAMP ID='Fire_RAMP_Q', T=1707.76, F=0.39/

&RAMP ID='Fire_RAMP_Q', T=1731.9, F=0.41/

&RAMP ID='Fire_RAMP_Q', T=1743.97, F=0.39/

&RAMP ID='Fire_RAMP_Q', T=1750.0, F=0.37/

&RAMP ID='Fire_RAMP_Q', T=1762.07, F=0.34/

&RAMP ID='Fire_RAMP_Q', T=1786.21, F=0.32/

&RAMP ID='Fire_RAMP_Q', T=1834.48, F=0.3/

&RAMP ID='Fire_RAMP_Q', T=1840.52, F=0.28/

&RAMP ID='Fire_RAMP_Q', T=1991.38, F=0.22/

&RAMP ID='Fire_RAMP_Q', T=2015.52, F=0.2/

&RAMP ID='Fire_RAMP_Q', T=2027.59, F=0.17/

&RAMP ID='Fire_RAMP_Q', T=2075.86, F=0.2/

&RAMP ID='Fire_RAMP_Q', T=2112.07, F=0.19/

&RAMP ID='Fire_RAMP_Q', T=2142.24, F=0.17/

&RAMP ID='Fire_RAMP_Q', T=2184.48, F=0.18/

&RAMP ID='Fire_RAMP_Q', T=2196.55, F=0.15/

&RAMP ID='Fire_RAMP_Q', T=2256.9, F=0.15/

&RAMP ID='Fire_RAMP_Q', T=2317.24, F=0.16/

&RAMP ID='Fire_RAMP_Q', T=2377.59, F=0.15/

&RAMP ID='Fire_RAMP_Q', T=2413.79, F=0.13/

&RAMP ID='Fire_RAMP_Q', T=2462.07, F=0.13/

&RAMP ID='Fire_RAMP_Q', T=2510.34, F=0.12/

&RAMP ID='Fire_RAMP_Q', T=2564.66, F=0.13/

&RAMP ID='Fire_RAMP_Q', T=2606.9, F=0.11/

&RAMP ID='Fire_RAMP_Q', T=2661.21, F=0.11/

&RAMP ID='Fire_RAMP_Q', T=2721.55, F=0.11/

&RAMP ID='Fire_RAMP_Q', T=2781.9, F=0.12/

&RAMP ID='Fire_RAMP_Q', T=2842.24, F=0.11/

&RAMP ID='Fire_RAMP_Q', T=2902.59, F=0.11/

&RAMP ID='Fire_RAMP_Q', T=2962.93, F=0.1/

&RAMP ID='Fire_RAMP_Q', T=3023.28, F=0.1/

&RAMP ID='Fire_RAMP_Q', T=3083.62, F=0.1/

&RAMP ID='Fire_RAMP_Q', T=3101.72, F=0.1/

&RAMP ID='Fire_RAMP_Q', T=3143.97, F=0.09/

&RAMP ID='Fire_RAMP_Q', T=3162.07, F=0.1/

&RAMP ID='Fire_RAMP_Q', T=3204.31, F=0.1/

&RAMP ID='Fire_RAMP_Q', T=3222.41, F=0.09/

&RAMP ID='Fire_RAMP_Q', T=3264.66, F=0.09/

&RAMP ID='Fire_RAMP_Q', T=3282.76, F=0.08/

```
&RAMP ID='Fire_RAMP_Q', T=3325.0, F=0.1/
&RAMP ID='Fire_RAMP_Q', T=3385.34, F=0.1/
&RAMP ID='Fire_RAMP_Q', T=3403.45, F=0.09/
&RAMP ID='Fire_RAMP_Q', T=3445.69, F=0.09/
&RAMP ID='Fire_RAMP_Q', T=3487.93, F=0.07/
&RAMP ID='Fire_RAMP_Q', T=3536.21, F=0.06/
&RAMP ID='Fire_RAMP_Q', T=3578.45, F=0.06/
&RAMP ID='Fire_RAMP_Q', T=3620.69, F=0.06/
&RAMP ID='Fire_RAMP_Q', T=3662.93, F=0.05/
&RAMP ID='Fire_RAMP_Q', T=3717.24, F=0.05/
&RAMP ID='Fire_RAMP_Q', T=3753.45, F=0.04/
&RAMP ID='Fire_RAMP_Q', T=3801.72, F=0.04/
&RAMP ID='Fire_RAMP_Q', T=3850.0, F=0.02/
&RAMP ID='Fire_RAMP_Q', T=3910.34, F=0.02/
&RAMP ID='Fire_RAMP_Q', T=3970.69, F=0.01/
&RAMP ID='Fire_RAMP_Q', T=4031.03, F=0.01/
&RAMP ID='Fire_RAMP_Q', T=4091.38, F=0.01/
&RAMP ID='Fire_RAMP_Q', T=4151.72, F=0.01/
&RAMP ID='Fire_RAMP_Q', T=4200.0, F=0.0/
&SURF ID='Supply',
    RGB=0,51,255,
    VOLUME_FLOW=-60.27/
```

&OBST ID='Main drift floor', XB=0.0,120.0,0.0,8.0,-0.2,0.0,
PERMIT_HOLE=.FALSE., THICKEN=.TRUE., SURF_ID='Wall'/

&OBST ID='Exhaust floor', XB=100.0,108.0,8.0,48.0,-0.2,0.0,
PERMIT_HOLE=.FALSE., THICKEN=.TRUE., SURF_ID='Wall'/

&OBST ID='Wall_1', XB=0.0,120.0,-0.1,0.1,0.0,6.0, RGB=203,203,255,
TRANSPARENCY=0.396078, PERMIT_HOLE=.FALSE., THICKEN=.TRUE.,
SURF_ID='Wall'/

&OBST ID='Main drift roof', XB=0.0,120.0,0.0,8.0,5.8,6.0,
COLOR='INVISIBLE', SURF_ID='Wall'/

&OBST ID='Exhaust roof', XB=100.0,108.0,8.0,48.0,5.8,6.0,
COLOR='INVISIBLE', SURF_ID='Wall'/

&OBST ID='inlet wall', XB=0.0,0.2,0.0,8.0,0.0,6.0, PERMIT_HOLE=.FALSE.,
THICKEN=.TRUE., SURF_ID='INERT'/

&OBST ID='Wall_2', XB=99.8,100.2,9.0,29.0,-0.2,5.8,
PERMIT_HOLE=.FALSE., THICKEN=.TRUE., SURF_ID='Wall'/

&OBST ID='Wall_2', XB=99.8,100.2,29.0,47.8,-0.2,5.8,
PERMIT_HOLE=.FALSE., THICKEN=.TRUE., SURF_ID='Wall'/

&OBST ID='Wall_2', XB=-0.2,19.4,7.8,8.2,-0.2,5.8, PERMIT_HOLE=.FALSE.,
THICKEN=.TRUE., SURF_ID='Wall'/

&OBST ID='Wall_2', XB=19.4,39.8,7.8,8.2,-0.2,5.8, PERMIT_HOLE=.FALSE.,
THICKEN=.TRUE., SURF_ID='Wall'/

&OBST ID='Wall_2', XB=39.8,60.2,7.8,8.2,-0.2,5.8, PERMIT_HOLE=.FALSE.,
THICKEN=.TRUE., SURF_ID='Wall'/

&OBST ID='Wall_2', XB=60.2,80.2,7.8,8.2,-0.2,5.8, PERMIT_HOLE=.FALSE., THICKEN=.TRUE., SURF_ID='Wall'/

&OBST ID='Wall_2', XB=80.2,100.2,7.8,8.2,-0.2,5.8, PERMIT_HOLE=.FALSE., THICKEN=.TRUE., SURF_ID='Wall'/

&OBST ID='Wall_2', XB=99.8,100.2,8.2,9.0,-0.2,5.8, PERMIT_HOLE=.FALSE., THICKEN=.TRUE., SURF_ID='Wall'/

&OBST ID='Wall_3', XB=107.8,108.2,9.0,29.0,-0.2,5.8, PERMIT_HOLE=.FALSE., THICKEN=.TRUE., SURF_ID='Wall'/

&OBST ID='Wall_3', XB=107.8,108.2,29.0,47.8,-0.2,5.8, PERMIT_HOLE=.FALSE., THICKEN=.TRUE., SURF_ID='Wall'/

&OBST ID='Wall_3', XB=107.8,108.2,8.2,9.0,-0.2,5.8, PERMIT_HOLE=.FALSE., THICKEN=.TRUE., SURF_ID='Wall'/

&OBST ID='Wall_3', XB=107.8,120.2,7.8,8.2,-0.2,5.8, PERMIT_HOLE=.FALSE., THICKEN=.TRUE., SURF_ID='Wall'/

&OBST ID='Wall_3', XB=119.8,120.2,-0.2,7.8,-0.2,5.8, PERMIT_HOLE=.FALSE., THICKEN=.TRUE., SURF_ID='Wall'/

&VENT ID='Mesh Vent: Mesh02 [YMAX]', SURF_ID='OPEN', XB=99.0,109.0,49.0,49.0,-1.0,7.0/

&VENT ID='Vent fire', SURF_ID='Fire', XB=46.0,48.0,3.0,5.0,0.0,0.0, RGB=255,51,51/

&VENT ID='inlet airflow', SURF_ID='Supply', XB=0.0,0.0,0.0,8.0,0.0,6.0/

&SLCF QUANTITY='TEMPERATURE', VECTOR=.TRUE., PBY=4.0/

```
&SLCF QUANTITY='VELOCITY', VECTOR=.TRUE., PBY=4.0/

&SLCF QUANTITY='VISIBILITY', VECTOR=.TRUE., PBY=4.0/

&SLCF QUANTITY='TEMPERATURE', VECTOR=.TRUE.,

XB=0.0,120.0,0.0,8.0,0.0,6.0, FYI='Temp'/

&SLCF QUANTITY='VELOCITY', VECTOR=.TRUE.,

XB=0.0,120.0,0.0,8.0,0.0,6.0, FYI='Vel'/

&SLCF QUANTITY='VISIBILITY', VECTOR=.TRUE.,

XB=0.0,120.0,0.0,8.0,0.0,6.0, FYI='viz'/

&SLCF QUANTITY='TEMPERATURE', VECTOR=.TRUE.,

XB=100.0,107.9,8.0,48.0,0.0,6.0, FYI='Temp'/

&SLCF QUANTITY='VISIBILITY', VECTOR=.TRUE.,

XB=100.0,107.9,8.0,48.0,0.0,6.0, FYI='viz'/

&SLCF QUANTITY='VELOCITY', VECTOR=.TRUE.,

XB=100.0,107.9,8.0,48.0,0.0,6.0, FYI='vel'/

&TAIL /
```

REFERENCES

Adjiski, V. (2014). Possibilities for simulating the smoke rollback effect in underground mines using CFD software. GeoScience Engineering, 60(2).

Adjiski, V., & Despodov, Z. (2020). Methodology for Optimal Fire Evacuations in Underground Mines Based on Simulated Scenarios. In Fire Safety and Management Awareness. IntechOpen.

Adjiski, V., Mirakovski, D., Despodov, Z., & Mijalkovski, S. (2015). Simulation and optimization of evacuation routes in case of fire in underground mines. Journal of Sustainable Mining, 14(3), 133-143. https://doi.org/https://doi.org/10.1016/j.jsm.2015.10.001

Adjiski, V., Mirakovski, D., Despodov, Z., & Mijalkovski, S. (2016). CFD simulation of the brattice barrier method for approaching underground mine fires. Mining Science, 23, 161-172.

Atlas-Copco. (2008). Atlas Copco Face drilling rigs http://www.rockdrilltech.com/download/Rocket%20Boomer%20WE3C.pdf

Bahrami, D., Zhou, L., & Yuan, L. (2021). Field Verification of an Improved Mine Fire Location Model. Mining, Metallurgy & Exploration, 38(1), 559-566. https://doi.org/10.1007/s42461-020-00314-6

Barbato, L., Cascetta, F., Musto, M., & Rotondo, G. (2014). Fire safety investigation for road tunnel ventilation systems–an overview. Tunnelling and Underground Space Technology, 43, 253-265.

Cheng, J., Li, S., Zhang, F., Zhao, C., Yang, S., & Ghosh, A. (2016). CFD modelling of ventilation optimization for improving mine safety in longwall working faces. Journal of Loss Prevention in the Process Industries, 40, 285-297.

Cheong, M., Spearpoint, M., & Fleischmann, C. (2009). Calibrating an FDS simulation of goods-vehicle fire growth in a tunnel using the runehamar experiment. Journal of fire protection engineering, 19(3), 177-196.

Chow, W. K., Wong, K. Y., & Chung, W. Y. (2010). Longitudinal ventilation for smoke control in a tilted tunnel by scale modeling. Tunnelling and Underground Space Technology, 25(2), 122-128. https://doi.org/https://doi.org/10.1016/j.tust.2009.10.001

Conti, R. S. (2001). Responders To Underground Mine Fires. Proceedings of the 32nd Annual Institute on Mining Health, Safety and Research, Salt Lake City, Utah, August 5-7, 2001. Jenkins FM, Langton J, McCarter MK, Rowe B, eds. Salt Lake City, UT: University of Utah, 2001 Aug; :111-121, Salt Lake City, UT.

De Rosa, M. I. (2004). Analyses of mobile equipment fires for all U.S. surface and underground coal and metal/nonmetal mining categories, 1990-1999 [Report]. https://stacks.cdc.gov/view/cdc/8339 (Information circular (National Institute for Occupational Safety and Health) ; 9467)

Ding, C., He, X., & Nie, B. (2017). Numerical simulation of airflow distribution in mine tunnels. International Journal of Mining Science and Technology, 27(4), 663-667. https://doi.org/https://doi.org/10.1016/j.ijmst.2017.05.017

Fernández-Alaiz, F., Castañón, A. M., Gómez-Fernández, F., & Bascompta, M. (2020). Mine fire behavior under different ventilation conditions: Real-scale tests and CFD modeling. Applied Sciences, 10(10), 3380.

Fernández-Alaiz, F., Castañón, A. M., Gómez-Fernández, F., Bernardo-Sánchez, A., & Bascompta, M. (2020). Determination and fire analysis of gob characteristics using CFD. Energies, 13(20), 5274.

Feroze, T., & Genc, B. (2017). A CFD model to evaluate variables of the line brattice ventilation system in an empty heading. Journal of the Southern African Institute of Mining and Metallurgy, 117, 97-108. http://www.scielo.org.za/scielo.php?script=sci_arttext&pid=S2225-62532017000200003&nrm=iso

Gaitonde, U. (2006). Quality Criteria for Large Eddy Simulation. University of Manchester.

Gannouni, S., & Maad, R. B. (2015). Numerical study of the effect of blockage on critical velocity and backlayering length in longitudinally ventilated tunnel fires. Tunnelling and Underground Space Technology, 48, 147-155. https://doi.org/https://doi.org/10.1016/j.tust.2015.03.003

Gao, Z. H., Ji, J., Fan, C. G., Li, L. J., & Sun, J. H. (2016). Determination of smoke layer interface height of medium scale tunnel fire scenarios. Tunnelling and Underground Space Technology, 56, 118-124. https://doi.org/https://doi.org/10.1016/j.tust.2016.02.009

Gehandler, J. (2015). Road tunnel fire safety and risk: a review. Fire Science Reviews, 4(1), 2. https://doi.org/10.1186/s40038-015-0006-6

Haghighat, A., & Luxbacher, K. (2019). Determination of critical parameters in the analysis of road tunnel fires. International Journal of Mining Science and Technology, 29(2), 187-198. https://doi.org/https://doi.org/10.1016/j.ijmst.2018.05.003

Halim, A. (2017, 2017). Ventilation requirements for diesel equipment in underground mines–Are we using the correct values.

Hansen, R. (2009). Literature survey–fire and smoke spread in underground mines.

Hansen, R. (2017). Fire behavior of mining vehicles in underground hard rock mines. International Journal of Mining Science and Technology, 27(4), 627-634. https://doi.org/https://doi.org/10.1016/j.ijmst.2017.05.010

Hansen, R. (2019a). Design of fire scenarios for Australian underground hard rock mines–Applying data from full-scale fire experiments. Journal of Sustainable Mining, 18(4), 163-173.

Hansen, R. (2019b). Design of fire scenarios for Australian underground hard rock mines – Applying data from full-scale fire experiments. Journal of Sustainable Mining, 18(4), 163-173. https://doi.org/https://doi.org/10.1016/j.jsm.2019.07.003

Hansen, R. (2019c). Fire behaviour of multiple fires in a mine drift with longitudinal ventilation. International Journal of Mining Science and Technology, 29(2), 245-254. https://doi.org/https://doi.org/10.1016/j.ijmst.2018.05.005

Hansen, R. (2020). Modelling temperature distributions and flow conditions of fires in an underground mine drift. Geosystem Engineering, 23(6), 299-314.

Hansen, R. (2023). Fire Prevention and Fire Mitigation in Underground Hard Rock Mines.

Hansen, R., & Ingason, H. (2013). Full-scale fire experiments with mining vehicles in an underground mine (978-91-7485-115-1 (ISBN)). (Studies in Sustainable Technology / Forskningsrapport, Issue. http://urn.kb.se/resolve?urn=urn:nbn:se:mdh:diva-20912

Hu, L., Huo, R., & Chow, W. K. (2008). Studies on buoyancy-driven back-layering flow in tunnel fires. Experimental Thermal and Fluid Science, 32(8), 1468-1483.

Hwang, C. C., & Edwards, J. C. (2005). The critical ventilation velocity in tunnel fires—a computer simulation. Fire Safety Journal, 40(3), 213-244. https://doi.org/https://doi.org/10.1016/j.firesaf.2004.11.001

Ingason, H., & Li, Y. Z. (2010). Model scale tunnel fire tests with longitudinal ventilation. Fire Safety Journal, 45(6-8), 371-384.

Juganda, A., Strebinger, C., Brune, J. F., & Bogin, G. E. (2020). Discrete modeling of a longwall coal mine gob for CFD simulation. International Journal of Mining Science and Technology, 30(4), 463-469.

Kurnia, J. C., Sasmito, A. P., & Mujumdar, A. S. (2014). CFD simulation of methane dispersion and innovative methane management in underground mining faces. Applied Mathematical Modelling, 38(14), 3467-3484. https://doi.org/https://doi.org/10.1016/j.apm.2013.11.067

Li, Y., Zhang, X., Sun, X., & Zhu, N. (2021). Maximum temperature of ceiling jet flow in longitudinal ventilated tunnel fires with various distances between fire source and cross-passage. Tunnelling and Underground Space Technology, 113, 103953. https://doi.org/https://doi.org/10.1016/j.tust.2021.103953

Li, Y. Z., & Ingason, H. (2018). Overview of research on fire safety in underground road and railway tunnels. Tunnelling and Underground Space Technology, 81, 568-589.

Li, Z., Li, R., Xu, Y., & Xu, Y. (2022). Study on the Optimization and Oxygen-Enrichment Effect of Ventilation Scheme in a Blind Heading of Plateau Mine. International journal of environmental research and public health, 19(14).

Long, Z., Chen, J., Qiu, P., & Zhong, M. (2022). Study on the smoke layer height in subway platform fire under natural ventilation. Journal of Building Engineering, 56, 104758. https://doi.org/https://doi.org/10.1016/j.jobe.2022.104758

Lu, X., Weng, M., Liu, F., Wang, F., Han, J., & Cheung, S. C. (2022). Study on smoke temperature profile in bifurcated tunnel fires with various bifurcation angles under natural ventilation. Journal of Wind Engineering and Industrial Aerodynamics, 225, 105001. https://doi.org/https://doi.org/10.1016/j.jweia.2022.105001

Lu, X., Weng, M., Liu, F., Wang, F., Han, J., & Chipok Cheung, S. (2022). Effect of bifurcation angle and fire location on smoke temperature profile in longitudinal ventilated bifurcated tunnel fires. Tunnelling and Underground Space Technology, 127, 104610. https://doi.org/https://doi.org/10.1016/j.tust.2022.104610

McGrattan, K., Hostikka, S., McDermott, R., Floyd, J., Weinschenk, C., & Overholt, K. (2013a). Fire dynamics simulator technical reference guide volume 1: mathematical model. NIST special publication, 1018(1), 175.

McGrattan, K., Hostikka, S., McDermott, R., Floyd, J., Weinschenk, C., & Overholt, K. J. N. s. p. (2013b). Fire dynamics simulator user's guide. 1019(6), 1-339.

McGrattan, K., McDermott, R., Floyd, J., Hostikka, S., Forney, G., & Baum, H. (2012). Computational fluid dynamics modelling of fire. International Journal of Computational Fluid Dynamics, 26(6-8), 349-361.

McGrattan, K., Peacock, R., & Overholt, K. (2016). Validation of fire models applied to nuclear power plant safety. Fire Technology, 52, 5-24.

McGrattan, K. B., Baum, H. R., & Rehm, R. G. (1998). Large eddy simulations of smoke movement. Fire Safety Journal, 30(2), 161-178.

McGrattan, K. B., Peacock, R. D., & Overholt, K. J. (2014). Verification and validation of selected fire models for nuclear power plant applications supplement 1. U. S. N. R. C. NUREG-1824. https://www.nist.gov/publications/verification-and-validation-selected-fire-models-nuclear-power-plant-applications-1

McGrattan, K. B. J. F. S. S. (2005). Fire Modeling: Where Are We? Where Are We Going? , 8, 53-68.

NIOSH. (2021). Mining Topic: Fire Fighting https://www.cdc.gov/niosh/mining/topics/FireFighting.html

Overholt, K. J. (2014). Verification and validation of commonly used empirical correlations for fire scenarios. US Department of Commerce, National Institute of Standards and Technology.

Rahmani, A., Carlotti, P., Gay, B., & Buffat, M. (2004). Simulating fires in tunnels using large eddy simulation. International Conference Tunnel Safety and Ventilation, Graz Conference Proceedings,

Rawlins, C. A. (2006, 2006). Underground mine ventilation planning, heat loads, and diesel equipment.

Rodi, W., Ferziger, J., Breuer, M., & Pourquie, M. J. T.-A. S. o. M. E. J. o. F. E. (1997). Status of large eddy simulation: results of a workshop. 119, 248-262.

Salami , O. B., Xu, G., Kumar, A. R., & Pushparaj, R. I. (2023). Underground mining fire hazards and the optimization of emergency evacuation strategies (EES): The issues, existing methodology and limitations, and way forward. Process Safety and Environmental Protection, 177, 617-634. https://doi.org/https://doi.org/10.1016/j.psep.2023.07.012

Salami, O. B., Xu, G., Kumar, A. R., Pushparaj, R. I., & Iqbal, A. (2023). Fire-induced temperature attenuation under the influence of a single ceiling smoke extraction point in a bifurcated drift. In Underground Ventilation (pp. 399-410). CRC Press.

Sasmito, A. P., Kurnia, J. C., Birgersson, E., & Mujumdar, A. S. (2015). Computational evaluation of thermal management strategies in an underground mine. Applied Thermal Engineering, 90, 1144-1150. https://doi.org/https://doi.org/10.1016/j.applthermaleng.2015.01.062

Seike, M., Kawabata, N., & Hasegawa, M. (2017). Quantitative assessment method for road tunnel fire safety: Development of an evacuation simulation method using CFD-derived smoke behavior. Safety Science, 94, 116-127. https://doi.org/https://doi.org/10.1016/j.ssci.2017.01.005

Trouvé, A., & Wang, Y. (2010). Large eddy simulation of compartment fires. International Journal of Computational Fluid Dynamics, 24(10), 449-466.

Weng, M.-c., Lu, X.-l., Liu, F., Shi, X.-p., & Yu, L.-x. (2015). Prediction of backlayering length and critical velocity in metro tunnel fires. Tunnelling and Underground Space Technology, 47, 64-72. https://doi.org/https://doi.org/10.1016/j.tust.2014.12.010

Woodburn, P. J., & Britter, R. E. (1996). CFD simulations of a tunnel fire—Part II. Fire Safety Journal, 26(1), 63-90. https://doi.org/https://doi.org/10.1016/0379-7112(96)00019-7

Wu, F., Zhou, R., Shen, G., Jiang, J., & Li, K. (2018). Effects of ambient pressure on smoke back-layering in subway tunnel fires. Tunnelling and Underground Space Technology, 79, 134-142. https://doi.org/https://doi.org/10.1016/j.tust.2018.05.011

Xin, S., Wang, W., Zhang, N., Zhang, C., Yuan, S., Li, H., & Yang, W. (2021). Comparative studies on control of thermal environment in development headings using force/exhaust overlap ventilation systems. Journal of Building Engineering, 38, 102227. https://doi.org/https://doi.org/10.1016/j.jobe.2021.102227

Yuan, L., & Smith, A. C. (2015). Numerical modeling of water spray suppression of conveyor belt fires in a large-scale tunnel. Process Safety and Environmental Protection, 95, 93-101. https://doi.org/https://doi.org/10.1016/j.psep.2015.02.018

Yuan, L., Zhou, L., & Smith, A. C. (2016). Modeling carbon monoxide spread in underground mine fires. Applied Thermal Engineering, 100, 1319-1326. https://doi.org/https://doi.org/10.1016/j.applthermaleng.2016.03.007

Zhang, Y., & Huang, X. (2022). A review of tunnel fire evacuation strategies and state-of-the-art research in China. Fire Technology, 1-34.

Zhao, S., Liu, F., Wang, F., & Weng, M. (2018). Experimental studies on fire-induced temperature distribution below ceiling in a longitudinal ventilated metro tunnel. Tunnelling and Underground Space Technology, 72, 281-293.

Zhou, L. (2009). Improvement of the mine fire simulation program MFIRE.

Zhou, L., Yuan, L., Bahrami, D., Thomas, R. A., & Rowland, J. H. (2018). Numerical and experimental investigation of carbon monoxide spread in underground mine fires. Journal of Fire Sciences, 36(5), 406-418. https://doi.org/10.1177/0734904118793891

Zhu, H., Shen, Y., Yan, Z., Guo, Q., & Guo, Q. (2016). A numerical study on the feasibility and efficiency of point smoke extraction strategies in large cross-section shield tunnel fires using CFD modeling. Journal of Loss Prevention in the Process Industries, 44, 158-170

IV. AN AGENT-BASED PARAMETRIC ANALYSIS OF MINERS' EVACUATION TIME FROM AN UNDERGROUND FIRE FOR IMPROVED EMERGENCY PLANNING

Oluwafemi Salami[a], Guang Xu[a], Samuel Frimpong[a]

[a]Department of Mining and Explosives Engineering, Missouri University of Science and Technology Rolla, USA

ABSTRACT

This study investigates the critical importance of efficient crew evacuation during hazardous situations in underground mining environments. Focusing on a drilling rig (29.4 MW) fire scenario, the research examines the evacuation duration for a 25-member crew through model-based evaluations of designated escape routes. The findings emphasize the significant impact of fire-induced smoke on evacuation times, challenging assumptions about the shortest path being the safest or fastest. The study underscores the necessity of optimizing evacuation efficiency by selecting appropriate routes in an emergency in the underground. While specifically addressing fire-related risks, it acknowledges the potential applicability of the evacuation modeling approach to other hazards in underground mines, albeit without accounting for their direct influence on evacuation procedures. The insights gleaned from this study serve as a crucial resource for enhancing safety protocols within mining operations, highlighting the need for further exploration into comprehensive evacuation strategies considering various hazards present underground.

1. INTRODUCTION

Evacuation of personnel during an emergency is very challenging because of the uncertainty of accidents and the complex nature of individual characteristics an remains a key aspect of fire performance-based design (Anastasios et al., 2022; Huang et al., 2010; Pan et al., 2019; Ronchi et al., 2019; Oluwafemi Babatunde Salami, Guang Xu, et al., 2023; Oluwafemi Babatunde Salami, G. Xu, et al., 2023; D. Wang et al., 2021; H.-R. Wang et al., 2014). In an underground environment, the smoke and toxic gases build up rapidly (Huang et al., 2010; Osunmakinde, 2013; Pushparaj et al., 2023; Salami & Xu, 2022; Oluwafemi Babatunde Salami, G. Xu, et al., 2023), and personnel are required to evacuate quickly in a difficult walking environment such as tunnels or a manhole/viaduct with very low visibility (Liu et al., 2023; Pan et al., 2019). Poor response and preparedness for emergencies in such environment could lead to severe catastrophe and appropriate emergency plan must be put in place to minimize or completely avoid causalities (Oluwafemi Babatunde Salami, Guang Xu, et al., 2023).

Over the years, evacuation time during an underground emergency has been calculated using analytical methods (Kallianiotis et al., 2018; Ronchi et al., 2012; Zhong et al., 2008). This approach is primarily based on K-shortest path solution (Adjiski & Despodov, 2020a; Eppstein, 1998; Hong et al., 2018; Hong, Li, Wu, Xu, et al., 2019; Jalali & Noroozi, 2009; Jin, Chen, Jiang, et al., 2013; Zheng & Liu, 2019). In one study, path planning technique was applied to develop a 3D constrained space model in order to establish a safe evacuation route in constrained space scenarios (Hong, Li, Wu, Xu, et al., 2019). The confined space was modelled as a 3D connected graph and a priority-oriented

network planning algorithm was constructed to maximize evacuation exit utilization efficiency and minimize the whole evacuation delay. (Jalali & Noroozi, 2009) applied the path planning approach to determine the shortest escape time between place of accident and safe places as well as their corresponding routes in an underground mines network. (Zheng & Liu, 2019) employed deep reinforcement learning to establish an optimal evacuation route during a disaster and later used experimental results to validate the effectiveness of the model by multi-agent deep deterministic policy gradient algorithm. Nevertheless, recent investigation has shown that the evacuation times from determined by this method are usually highly underestimated and may jeopardize a successful evacuation mission (Tutak, 2020)

Some other researchers have also applied numerical method such as CFD to determine optimal evacuation routes based on minimal exposure to carbon monoxide (CO) during the evacuation process (Adjiski & Despodov, 2020a; V. Adjiski et al., 2015; Yuan et al., 2016). However, CFD stand alone is not sufficient to predict evacuation time and thus is not sufficient to development optimum evacuation strategy.

One way to optimize CFD is to integrate it with an agent-based evacuation model (ABM) platform to determine the impact of the fire on the evacuation time. ABM offers us an improved technique of determining evacuation time which incorporates fire field data and human behavior during an evacuation (Thornton et al., 2011; Tutak, 2020). In addition, ABMs approach is low cost, easily repeatable, and provides detailed information from a single run of the simulations (Bi & Gelenbe, 2019). ABMs have numerous merits over traditional fire evacuation models. For instance, ABMs allows the disaggregation of systems into individual components which are governed by their own set of rules and

individual characteristics (Crooks & Heppenstall, 2012). It also has the superior ability to incorporate fire field data and mine geometry to simulate miners response during evacuation (Tan et al., 2015; Tang & Ren, 2008; Tang & Ren, 2012). Unlike traditional emergency escape models, ABMs try to represent how individuals, and the environmental variables that affect them vary in space-time continuum and other dimensions. (Steven F Railsback & Volker Grimm, 2019). Because of the growing popularity and flexibility of ABMs, many researchers have since considered using agent-based models to plan emergency evacuation in confined spaces during a disaster although only a few studies have attempted to use ABMs for evacuation in underground mines.

(Tutak & Gvozdkova, 2020) and (Tutak, 2020) investigated the impact of the walking speed of crew on evacuation time from an underground heading using ABM. They found out that the movement speed of crew depends on the conditions in the heading such as the presence or absence of smoke. (Ronchi et al., 2019) and (Edrisi et al., 2021) demonstrated that ABM could be used for the assessment of evacuation procedure in underground facilities. (Ronchi et al., 2012) developed a simplified egress model that incorporated design fire scenarios, occupant behaviors and boundary conditions of the underground structure to develop an integrated evacuation model for improved emergency response. Additionally, Edrisi et al., (Edrisi et al., 2021) compared three different exist choice models' underground metro station to determine the optimum model that best replicate the physical scenario in the metro. (Jevtić, 2020) examined the influence of underground depth and miners speed on evacuation time using ABM. The findings indicate that deeper depth pose serious danger during an emergency evacuation process. (Liu et al., 2023) analyzed the evacuation time of occupants in an underground tunnel by using a

combined CFD and egress simulation model. The findings from the study showed that visibility is the major contributing factor that could hinder self-escape during an underground fire.

In another study (Li et al., 2015) successfully measured the underground concentrations of the gases majorly CO and CO2 in real time while the temperature was measured at specific locations in the mine using ABMs. The results showed that the measured values very well agree with the calculated values which is an indication that the simulation of underground mine fire disasters using ABMs is feasible. In addition, the hazard area and the and the extent of the hazard in the fire disaster can be determined by creating a visualization of the temporal and spatial changes in temperature and hazardous gases gas concentration. However, none of these studies have assessed the impact of smoke-induced speed reduction factor on the on the personnel during evacuation. The speed reduction factor could impact the evacuation time and overall efficiency of an evacuation process. For instance, due to smoke-induced speed reduction factor on the walking speed of the crew, the shorter distance may not be the faster escape route because evacuee tends to slow down due to poor visibility. This paper plans to fill this gap by assessing the consequence of evacuee slowing down due to fire-induced smoke and poor visibility on evacuation time. The findings from this study will lead to new frontiers in emergency management in underground confined spaces and fire safety engineering. The schematic of the study approach is presented in Figure 1. First a design fire scenario based on full-scale experiment of a drilling rig fire in an underground development heading was examined. A computational fluid dynamics model was developed based on the experiment

and the results incorporated into the Pathfinder egress model to analyze the evacuation time.

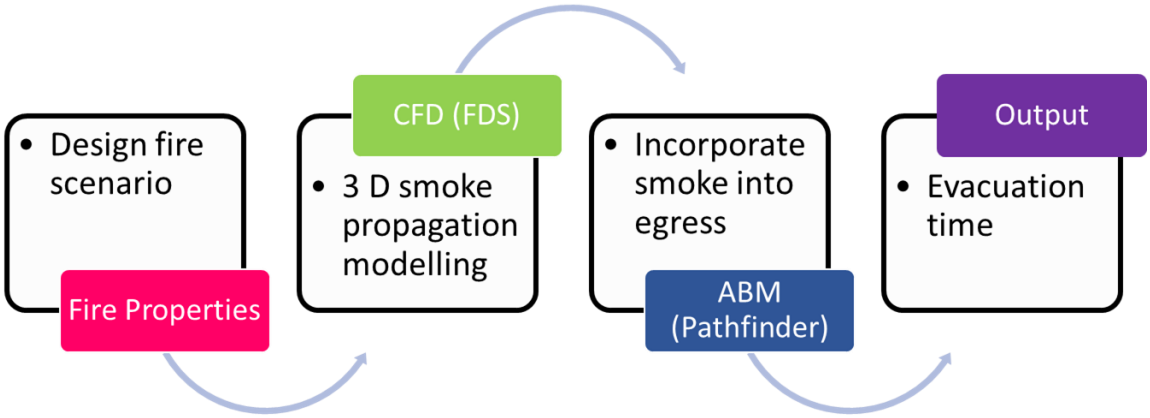

Figure 1. Flow chart of the study approach.

2. SIMULATION METHOD AND MODEL FORMALISM

2.1. MODEL FORMALISM

The fire was assumed to occur during a drilling operation in an underground development face as depicted in Figure 2. The access drift of the mine is 200 m and blind heading has been developed up to 50 m when the fire occurred. The mine is assumed to be a typical underground development in the US and has a regular dimension of width 4 m and height 5 m. The most important fire simulation parameter is the HRR. To capture the fire properties and smoke gas temperature, results from a full-scale experimental study conducted by Hansen (Hansen, 2020; Hansen & Ingason, 2013a) was used. From the study, the peak heat release rate of a drilling fire is 29.4 MW. During the experiment, the fire lasted for approximately 4200 s (70 mins). The fire was simulated using the fire dynamics

simulator (FDS). During the FDS fire simulation, it was assumed that the fire lasted for 420 s (that is, the fire burnt ten times faster).

$$FED = \sum_{t1}^{t2} \frac{X_{CO} v_{CO2}}{35000 \times 60} \Delta t + \sum_{t1}^{t2} \frac{exp\left(\frac{X_{HCN} v_{CO2}}{43}\right)}{220 \times 60} \Delta t \quad (1)$$

$$V_{CO2} = \begin{cases} 1,, & X_{CO2} < 2\ \% \\ e^{\frac{X_{CO2}}{5}}, & X_{CO2} > 2\ \% \end{cases} \quad (2)$$

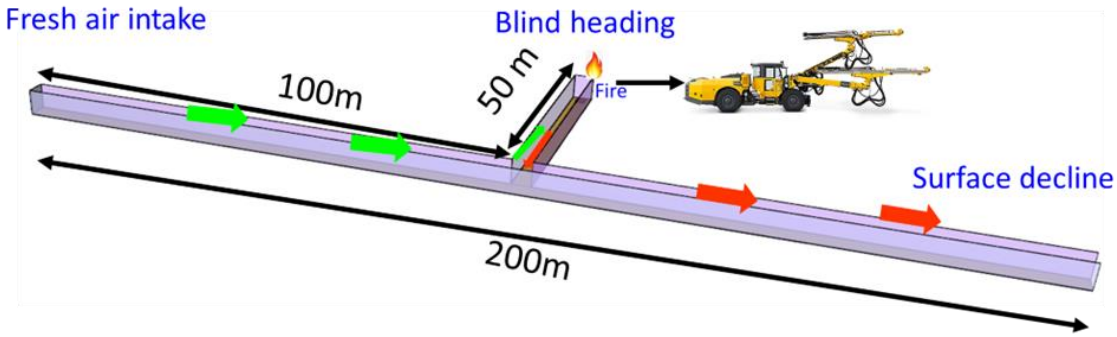

3D model of the underground

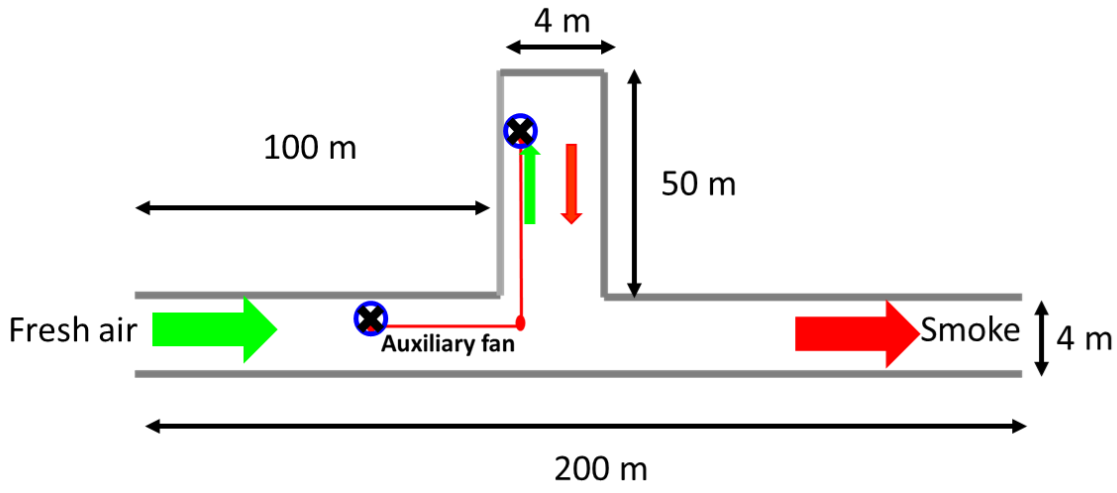

Top view of the underground structure

Figure 2. Schematic of model setup

This reduces the computational requirement of the CFD simulation as longer simulation time may take several hours or days (See Figure 3 for modified fire HRR curve). Miners are assumed to be working at the face when the fire began. The noxious species produced from the fire are calculated with the FDS model using appropriate mesh size and boundary conditions (See APPENDIX for the FDS fire simulation code). The results were then incorporated into the egress model to calculate the impact of the toxic gases are on personnel using the Purser's Fractional Effective Dose (FED) concept (Kim et al., 2013; Purser, 1992; Purser, 2000; Purser, 2003; Ronchi et al., 2019). The FED is determined from the ratio of the accumulated dose of inhaled toxic gases and the accumulated dose which leads to asphyxiation. The FED could be calculated using the equation below (Purser, 1992; Ronchi et al., 2019).

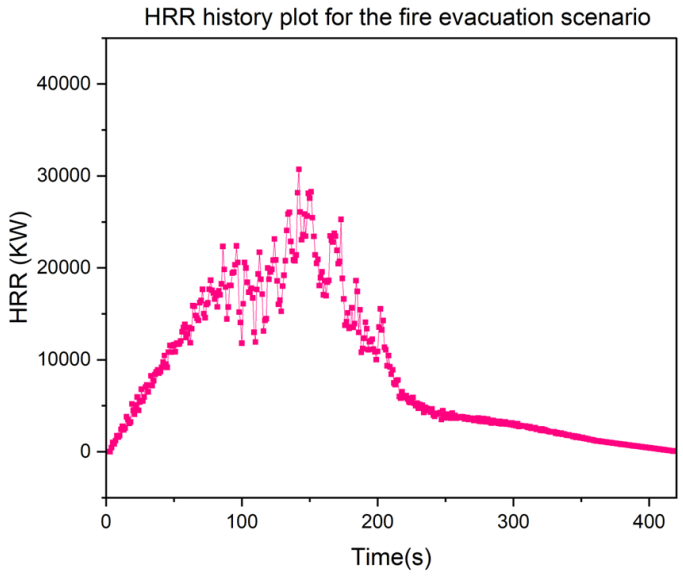

Figure 3. Heat release rate of the fire incident for the evacuation scenario.

The parameters for the model calculation are summarized in Table 1.

2.2. SIMULATION APPROACH

The pathfinder agent-based egress simulator was used for this study (Thunderhead-Engineering, 2021). The simulator was developed by Thunderhead Engineering and has two modes of describing the occupant's movement; mainly Society of Fire Protection Engineering (SFPE) model and the steering model (Mu et al., 2014; Pan et al., 2019; Qin et al., 2020; Ronchi et al., 2019; Ronchi et al., 2012; Thornton et al., 2011; Thunderhead-Engineering, 2021). The SFPE model takes the evacuation route length as the main reference model and occupants pick the evacuation exit according to nearby principle and neglects the bottleneck of human behavior such as queue (Qin et al., 2020; Ronchi et al., 2019). The steering model on the other hand employs the Reynold's steering behavioral model (Pan et al., 2019).

Table 1. Parameters for model calculation.

Parameter	Value
Length of development heading	50 m
Length of access drift	200 m
Location of heading from shaft	100 m
Location of development heading from surface decline	96 m
Dimension of the drift and heading	4 m by 5 m
Longitudinal ventilation in the main access drift	4.0 m/s
Auxiliary ventilation to blind heading	14.2 m3/s

In this model, the evacuation strategy is formulated by combining the evacuation route with possible occupant collision, and the safe path is determined based on the evacuation distance and the separation between the occupants (Qin et al., 2020). The steering mode uses a combination of steering and collision handling mechanism to control

how the miners achieve their goal in an emergency. This type of mechanism enables the miners to move along their path, avoid obstructions, and interact with other miners while heading towards a safe exit (Pan et al., 2019).Several studies on Pathfinder verification and validation have been established and literature have shown that pathfinder could provide a good representation of people's movement in real emergency situations (Kuligowski et al., 2005; Mu et al., 2014; Pan et al., 2019; Qin et al., 2020; Ronchi et al., 2019; Ronchi et al., 2012; Tutak & Gvozdkova, 2020). The simulator has a unique advantage in that every single occupant could have a predefined attribute that could impact their movement, speed, and decision during the evacuation (Thornton et al., 2011; Tutak, 2020; Tutak & Gvozdkova, 2020; H. R. Wang et al., 2014). Considering the scenario at hand, it was assumed that the miners must evacuate safely due to a drilling rig fire in an underground development heading.

A constant speed of 1.19 m/s based on the default values in pathfinder was most studies related underground/subsurface environment have used a speed of between 0.7 m/s -1.2 m/s for miners' evacuation during emergencies. This generally conform with the evacuation speed of crew under smoke conditions (Kuligowski et al., 2005; Qin et al., 2020; Ronchi et al., 2019; Tutak, 2020).

2.2.1. Incorporation of Smoke Effect on Miner's Speed. Previous researchers have demonstrated that fire smoke greatly impact visibility and the evacuee's performance during the escape process (Akizuki et al., 2007; Fridolf et al., 2014; Ronchi et al., 2018; Salami & Xu, 2022; Oluwafemi Babatunde Salami, Guang Xu, et al., 2023; Seike et al., 2016). When a serious fire breaks out causing smoke in large area, deterioration of visibility is expected (Akizuki et al., 2007). According to Fridolf et al (Fridolf et al., 2018),

the walking speed, w (m/s) can be correlated with the visibility, v (m) using equation (3) and Figure 4.

$$w = min\,[1; ma\,x\big(0.2; 1 - 0.34 * (3 - v)\big)] \quad (3)$$

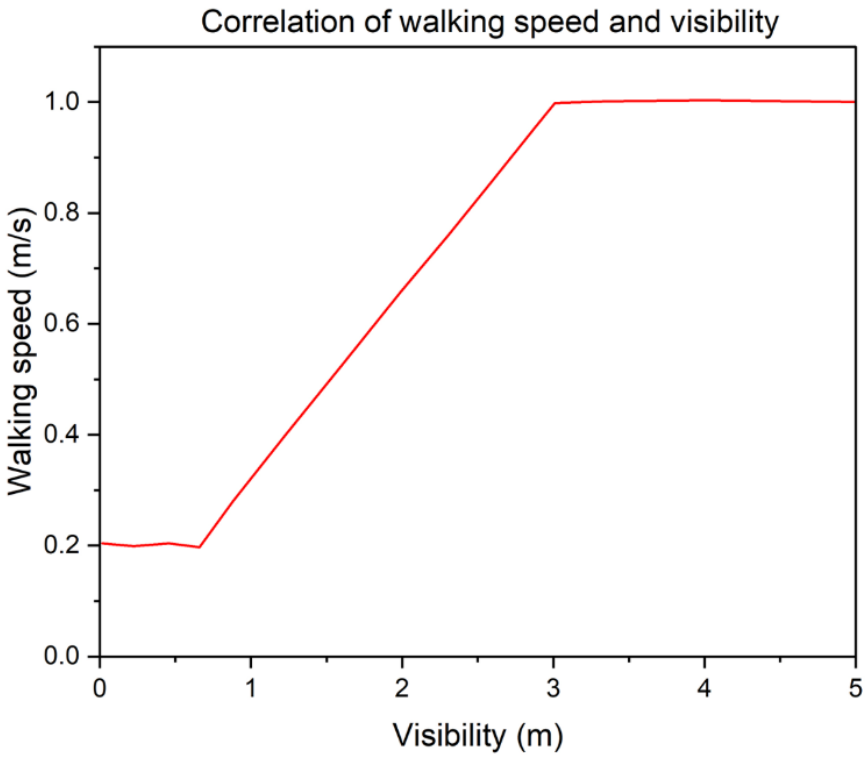

Figure 4. Correlation of walking speed and visibility in smoke filled condition (Fridolf et al., 2018).

In this study, the speed reduction factor was determined by measuring the visibility at 20 m interval along the access drift and at 10 m interval along the blind heading. The measurement was taken at a height of 2 m above the mine floor to represent the miners breathing zone. Previous studies have demonstrated that a measurement a height of 1.5 m to 2 m conforms with the tenability limit in confined spaces according to the National Fire

Protection Association (NFPA) 130 code (Kallianiotis et al., 2022; Lemaire & Kenyon, 2006; Rosberg et al., 2018; Seike et al., 2016; N. Wang et al., 2021).

3. RESULTS AND ANALYSIS

3.1. VISIBILITY

Miners in the model began to evacuate simultaneously for all the scenarios analyzed. That is, pre-movement time was assumed to be zero and miners began evacuation immediately the was noticed. However, the smoke density impacts the visibility of the miners as the fire spreads and miners slow down when walking through the smoke-filled tunnel.

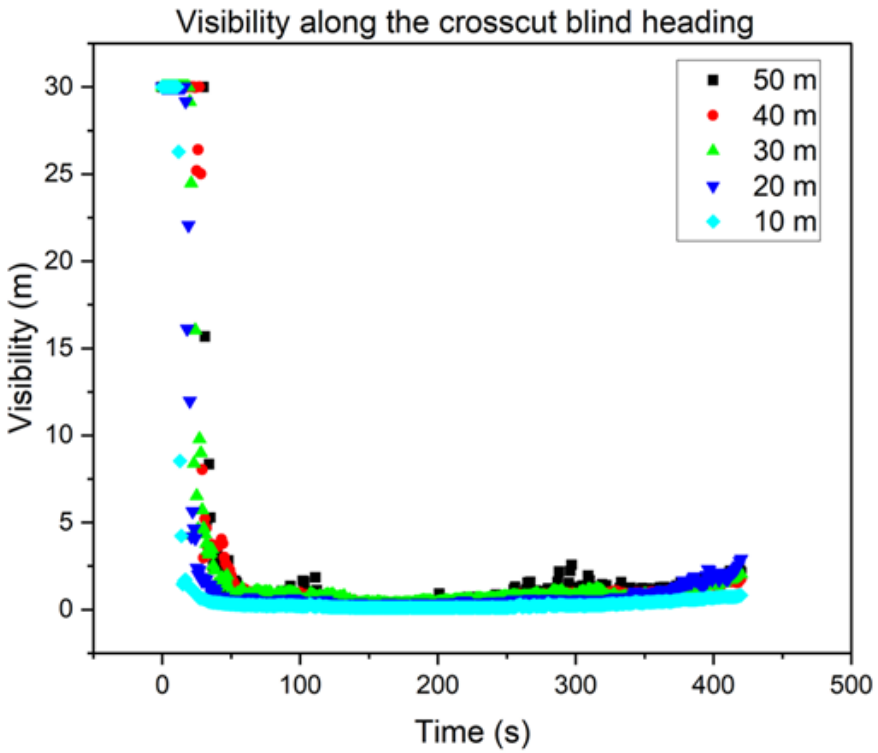

Figure 5. Smoke visibility along the blind heading.

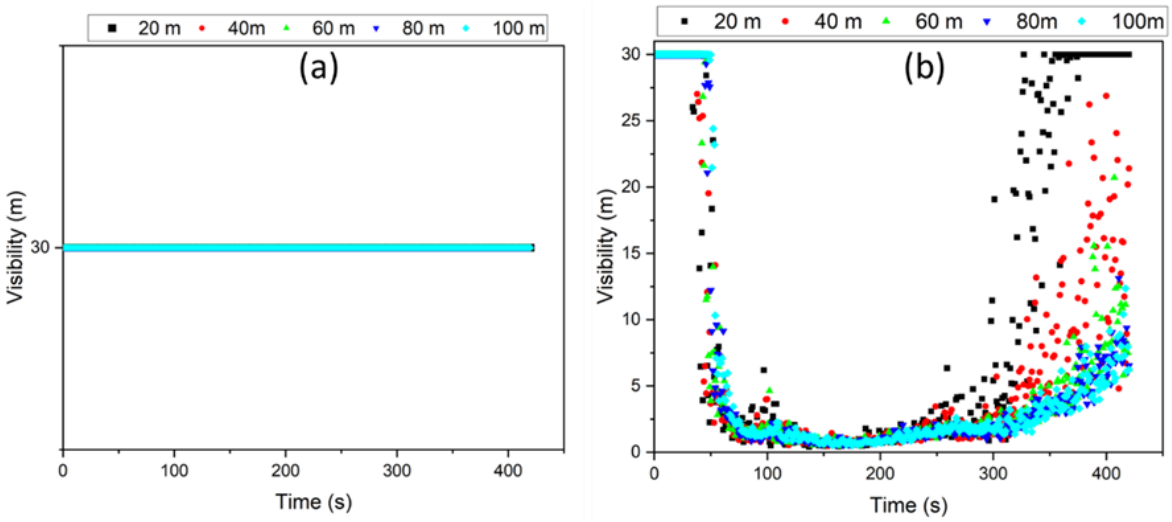

Figure 6. (a) Smoke visibility towards the shaft (b) Smoke visibility towards the surface decline.

The speed reduction factor varies depending on the smoke density in a particular location with the underground space. This enables our model to capture a more realistic accident scenario. From Figure 5, the fire smoke significantly impacts the visibility in the blind heading. The visibility reduced to almost 0 m in about 50 s which indicates that miners may be trapped in the blind heading if the there is a prolonged emergency response time. A contrasting trend is observed as miners escape from the blind heading to the access drift which connect the surface decline and the shaft. Figure 6 (a) & (b) shows the visibility conditions towards the shaft and surface decline respectively. From Figure 6 (a), the visibility conditions remain undisturbed along the shaft exit. This is expected as the FDS simulation shows that the airflow in the drift completely prevent a smoke rollback from the blind heading junction. Hence, the initially visibility situation was maintained during the entire fire. Figure 6 (b) however indicated that the visibility towards the surface decline decreases significantly during the fire growth stage. This is because the longitudinal

ventilation in the drift could not suppress the fire at this stage. Large volume of smoke is continually exhausted through the surface decline and the visibility improved as the fire enters the decline stage.

3.2. SPEED REDUCTION FACTOR

As the fire spreads and the subsurface environment becomes smoke-filled, the evacuation speed and agility of the miners reduces. The results of visibility depicted in Figure 5 and Figure 6 was applied to calculate the speed reduction factor on the miners due the smoke. The visibility remains undisturbed towards the exit shaft, the speed reduction factor will remain as the initial value (=1) for the entire simulation. However, since the visibility varies along the blind heading and towards the surface decline, the impact of smoke on miner's speed is calculated and presented as the speed reduction factor. The classification of the walking speed based on the speed reduction factor is depicted in Figure 7. The calculated speed reduction factor is presented in Figure 8. Figure 8 (a) & (b) shows the speed reduction factor along the blind heading and towards the surface decline respectively. The results indicates that the walking speed of the miners decreases as the visibility conditions get worse.

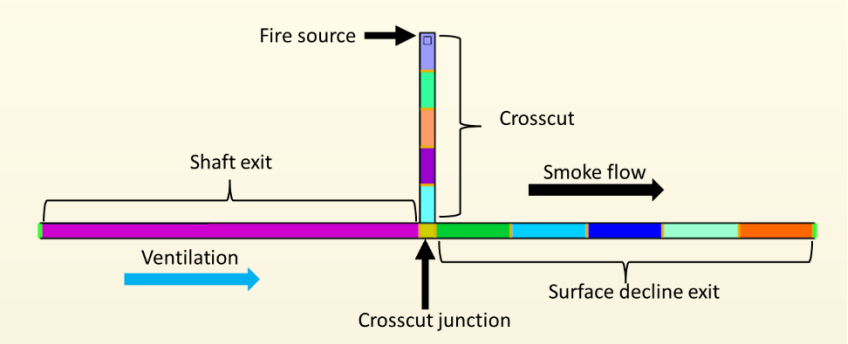

Figure 7. Speed reduction color code.

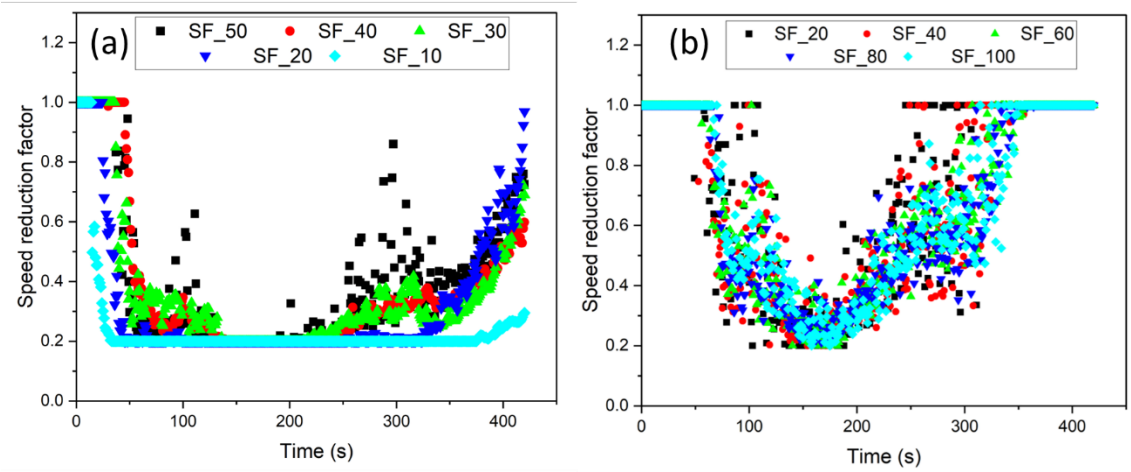

Figure 8. (a) Speed reduction factor due to smoke in the blind heading (b) Speed reduction factor towards the decline.

This happens primarily during the fire growth stage. The visibility condition could improve as the fire declines depending on the ventilation conditions in the subsurface environment. For instance, in the scenario at hand, the longitudinal ventilation velocity completely prevented the backflow of smoke from the blind heading junction towards the exit shaft. The smoke was pushed out of the underground through the surface decline and as the fire power reduces the visibility condition began to improve and the miners walking speed could increase.

3.3. BEHAVIORAL MODEL

Behavioral attributes could significantly impact any evacuation mission. The pathfinder platform consists of two behavioral model namely the SFPE and the Steering model as discussed in Section 2.2. The major difference between the models is that the miners avoid collision with one another however, they could collide with the walls in the SFPE mode while the steering model employs a no-collision rule. The effect of different

behavioral model was examined, and the result is presented in Figure 9. Figure 9 (a) depicts the overall evacuation time for model geometry (distance to surface decline = 96 m) while Figure 9 (b) the case for the modified geometry (See Section 3.4 for more information about the geometry).

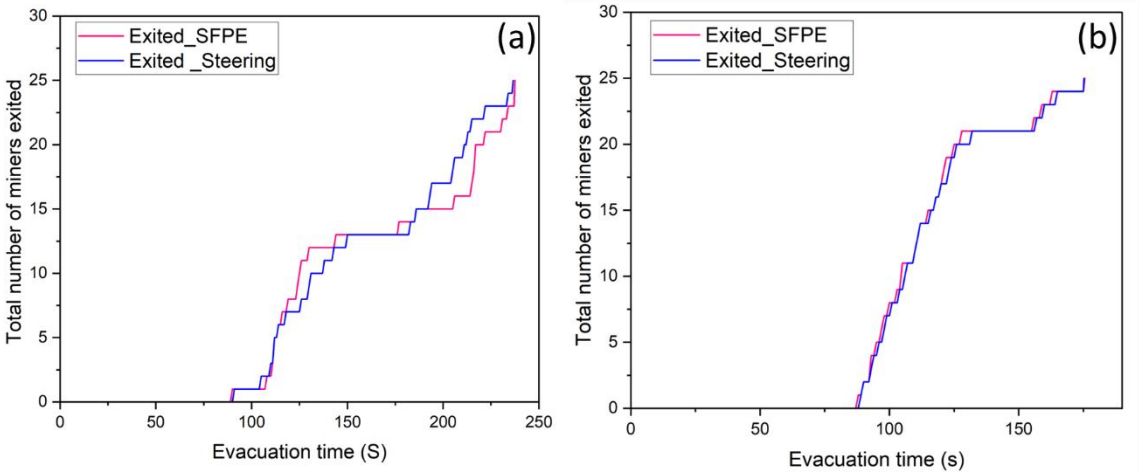

Figure 9. Comparison of different behavior model on overall evacuation time.

3.4. IMPACT OF GEOMETRY

During the evacuation simulation, it was observed that all the miners exited through the surface decline even though the path was filled with smoke gases. A careful analysis was conducted due to curiosity, and it was discovered that all the miners chose the exit with the shortest distance. A quick recall from Figure 2 shows that distance the shaft to the blind heading junction is 100 m. The blind heading is 4 m wide, and the entire length of the access drift is 200 m. This implies that the distance between the blind heading junction and the surface decline is 96 m (that is, the surface decline is 4 m shorter to the cross junction compared to the shaft location) and none of the miners exited through the shaft. Figure 10 depicts the evacuation time and exit usage for the original model configuration.

From Figure 10, the miners decided to use the shorter route (i.e., the surface decline) to evacuate from the fire.

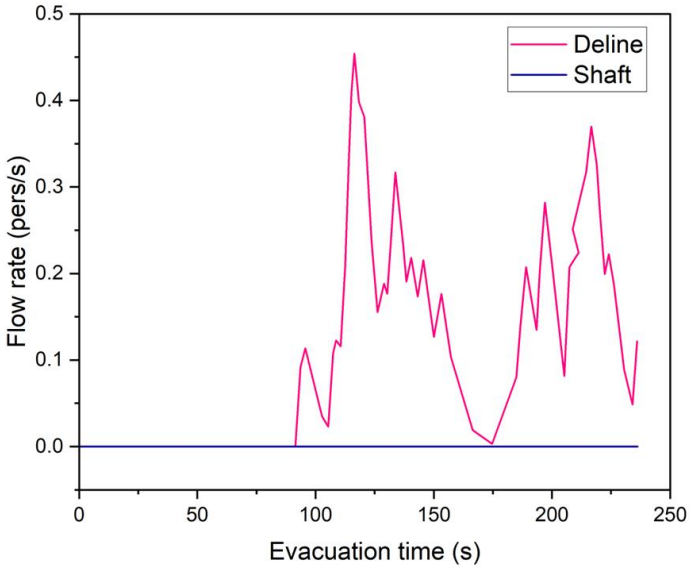

Figure 10. Exit usage for shorter distance to decline.

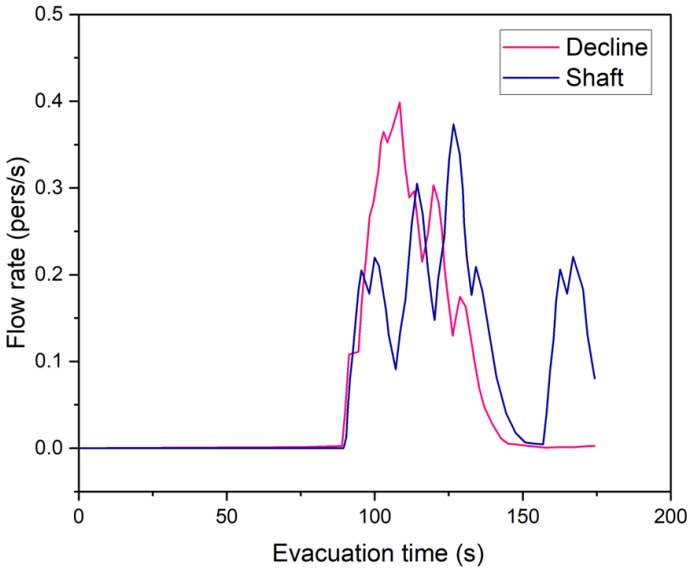

Figure 11. Exit usage for equal distance to both exits.

No miner exited through the shaft. To prove our assumption that the miners choose to exit through the shorter exit, our model was modified such that the shaft and surface decline are equidistant from the blind heading junction. The findings from the simulation are presented in Figure 11. From Figure 11, both exits were utilized by the miners during the evacuation. The miners decided to use both exits because both exits are equidistant from the hazard zone and thus same "distance weight".

3.5. IMPACT OF SMOKE SPEED REDUCTION FACTOR

In Section 3.4, we have seen that miners decided to choose evacuation exit based on the distance only. However, it is important to consider the other factors such as the smoke and other toxic gases that could impede safe escape during such incidents. Studies have shown that smoke is a critical factor that should be considered when planning for emergency evacuation in confined space like the underground mines. Thus, we further analyzed the impact of fire smoke on miner's speed to determine the optimum evacuation strategy for the case study. Figure 12 shows the required evacuation time based on different exit configuration for the no-smoke conditions.

The no-smoke conditions imply that the miners speed remains constant during the fire when there is no fire hazard. Findings indicate that there is no significant different in the evacuation time regardless of the exit the miners chose to evacuate from is fire smoke was not considered. This simulation case was achieved by the disintegration of the fire field data obtained from the FDS model from the ABM model. To examine the impact of smoke on the evacuation, the fire field data from the FDS model was integrated into the ABM model to replicate a more practical and realistic situation that the miners would be

subject to in real life. The speed reduction factor due to fire smoke was accounted for in the evacuation model and the results are presented in Figure 13. Figure 13 shows that the presence of fire smoke could significantly affect the evacuation time and the optimum

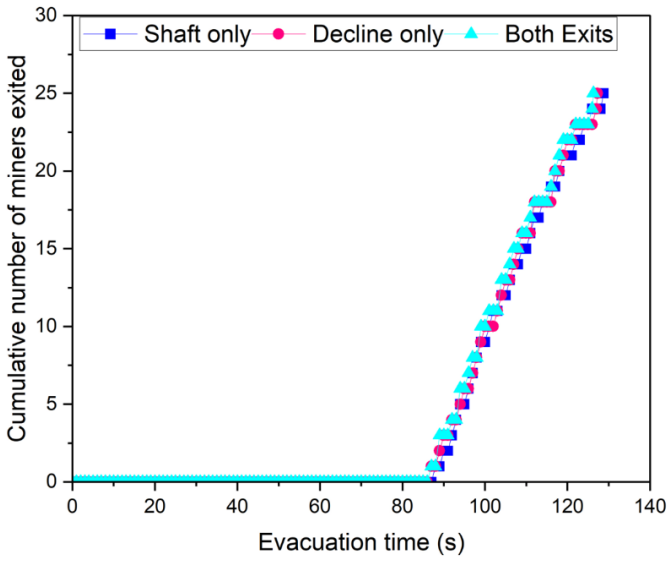

Figure 12. Evacuation time for different exit configuration without speed reduction factor.

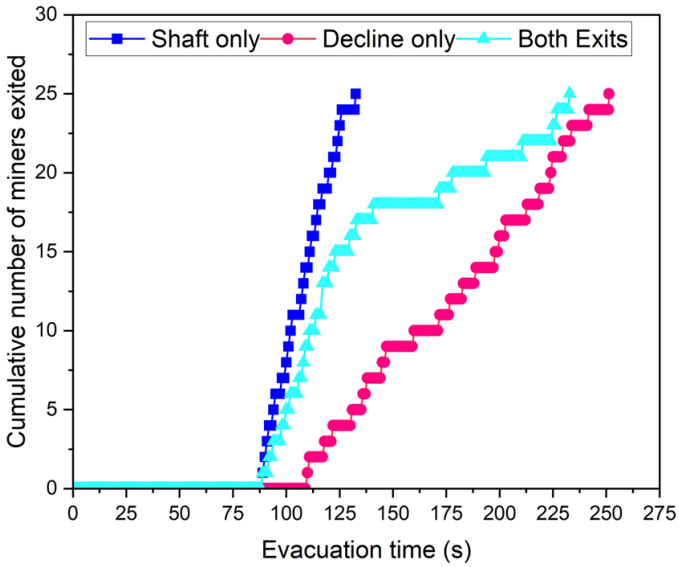

Figure 13. Evacuation time for different exit configuration with speed reduction factor.

escape route. It took the miners approximately 125 s to evacuate from the hazard if the shaft exit was used. However, the required evacuation time increased by 80 % when both exits were used, and by100 % when the miners evacuated through the surface decline.

The evaluation conducted for the evacuation time of the first evacuee and last evacuee is presented in Figure 14. The calculation performed indicates that the total time needed for the first and last miner to escape the fire hazard is the same regardless of the exit configuration for the no-smoke condition. The first and last miner were evacuated at approximately 88 s and 127 s respectively. However, the presence of smoke impacts the evacuation time of the first and last miner depending on the exit configuration. When the effect of smoke was considered in the model the first miner evacuated at approximately 132 s if the shaft exit was utilized.

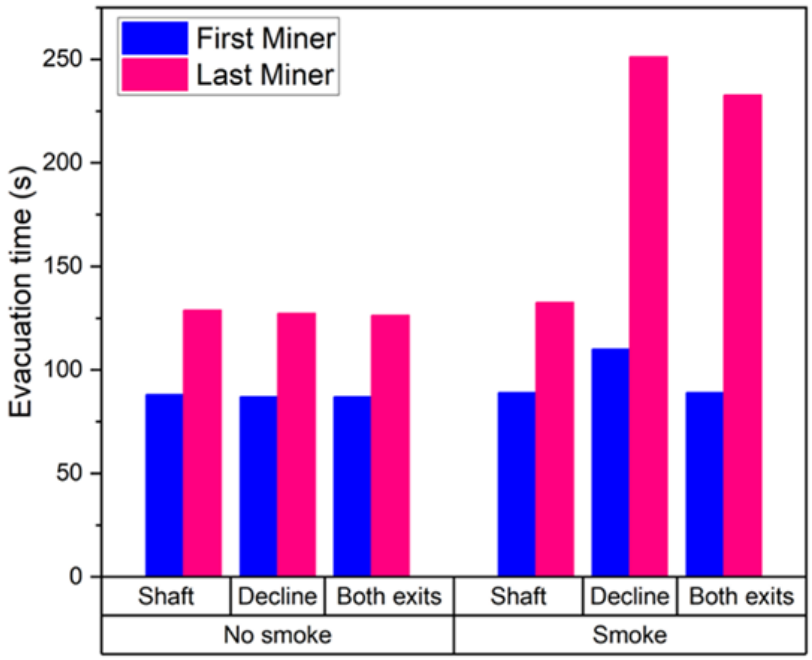

Figure 14. Comparison of evacuation time for different smoke-filled and no-smoke conditions.

The evacuation time increased to approximately 250 s (an increase of about 89 %) if the miner evacuated from through the surface decline. By contrast, the first miner evacuated at the earliest possible time (same value for using the shaft exit) if both exits are utilized. Nonetheless, the total evacuation time for the last evacuee increased significantly. This implies that increasing the number of exits in the smoke condition did not bring about a corresponding speed up in the evacuation process. Instead, the "evacuation efficiency" reduced by using both exits.

4. CONCLUSION

In the event of a hazardous situation, it is imperative for the crew to promptly vacate the danger area through pre-designated safe evacuation routes. To facilitate a seamless evacuation process, workers must be well-acquainted with the escape routes and the time required to traverse them. This aspect holds immense significance in the realm of occupational safety and places a substantial responsibility on mine safety teams. This study delves into this critical concern by presenting findings derived from model-based evaluations of crew evacuation procedures due to a drilling rig fire in an underground development heading. The objective of these tests was to ascertain the evacuation duration for a 25-member crew evacuating from a hazard zone within the underground.

The outcomes of the study revealed that incorporating speed reduction factor due to fire-induced smoke greatly impacts the total evacuation time for miners. This study shows that the shorter route may not necessarily be the quicker or safer route for self-escape. In addition, finding from this study demonstrates the need to optimize evacuation

efficiency by selecting the appropriate evacuation route during an underground danger. It is unequivocal that the insights garnered from this research should be harnessed to enhance safety protocols in the realm of mining operations. Finally, the current paper primarily concentrates on employing evacuation modeling to address fire-related risks in underground mining environment. However, underground mines may harbor various other hazards like combustible gases and high volume of fluids, this study does not account for their potential impact on evacuation procedures. However, the modeling approach presented here could be applied to such scenarios, provided there is no interaction between occupants and these additional hazards.

APPENDIX

```
&HEAD CHID='Fire_Simulation_Code', TITLE='Base_Model'/
&TIME T_END=420.0/
&DUMP DT_PL3D=10.0, DT_SLCF=1.0, DT_SL3D=1.0, NFRAMES=420,
WRITE_XYZ=.TRUE., PLOT3D_QUANTITY='VOLUME FRACTION','VOLUME
FRACTION','VOLUME FRACTION','TEMPERATURE','VISIBILITY',
PLOT3D_SPEC_ID(1:3)='CARBON DIOXIDE','CARBON MONOXIDE','OXYGEN'/
&MISC SIMULATION_MODE='LES'/
&MESH ID='Mesh01-01', IJK=126,15,18, XB=-1.0,49.4,-1.0,5.0,-1.0,6.0/
&MESH ID='Mesh01-02', IJK=126,15,18, XB=49.4,99.8,-1.0,5.0,-1.0,6.0/
&MESH ID='Mesh01-03', IJK=127,15,18, XB=99.8,150.6,-1.0,5.0,-1.0,6.0/
&MESH ID='Mesh01-04', IJK=126,15,18, XB=150.6,205.0,-1.0,5.0,-1.0,6.0/
```

```
&MESH ID='Mesh02-01', IJK=15,31,18, XB=99.0,105.0,5.0,17.4,-1.0,6.0/
&MESH ID='Mesh02-02', IJK=15,32,18, XB=99.0,105.0,17.4,30.2,-1.0,6.0/
&MESH ID='Mesh02-03', IJK=15,31,18, XB=99.0,105.0,30.2,42.6,-1.0,6.0/
&MESH ID='Mesh02-04', IJK=15,31,18, XB=99.0,105.0,42.6,55.0,-1.0,6.0/
&REAC ID='HEPTANE',
    FYI='NIST NRC FDS5 Validation',
    FUEL='REAC_FUEL',
    FORMULA='C7H16',
    CO_YIELD=0.01,
    SOOT_YIELD=0.1/
&DEVC ID='HVAC Velocity', QUANTITY='DUCT VELOCITY', DUCT_ID='D2'/
&DEVC ID='THCP', QUANTITY='THERMOCOUPLE', XYZ=102.0,54.0,4.9/
&DEVC ID='THCP01', QUANTITY='THERMOCOUPLE', XYZ=102.0,52.0,4.9/
&DEVC ID='THCP02', QUANTITY='THERMOCOUPLE', XYZ=102.0,50.0,4.9/
&DEVC ID='THCP03', QUANTITY='THERMOCOUPLE', XYZ=102.0,48.0,4.9/
&DEVC ID='THCP04', QUANTITY='THERMOCOUPLE', XYZ=102.0,46.0,4.9/
&DEVC ID='THCP05', QUANTITY='THERMOCOUPLE', XYZ=102.0,44.0,4.9/
&DEVC ID='THCP06', QUANTITY='THERMOCOUPLE', XYZ=102.0,42.0,4.9/
&DEVC ID='THCP07', QUANTITY='THERMOCOUPLE', XYZ=102.0,40.0,4.9/
&DEVC ID='THCP08', QUANTITY='THERMOCOUPLE', XYZ=102.0,38.0,4.9/
&DEVC ID='THCP09', QUANTITY='THERMOCOUPLE', XYZ=102.0,36.0,4.9/
&DEVC ID='THCP10', QUANTITY='THERMOCOUPLE', XYZ=102.0,34.0,4.9/
```

&DEVC ID='THCP11', QUANTITY='THERMOCOUPLE', XYZ=102.0,32.0,4.9/

&DEVC ID='THCP12', QUANTITY='THERMOCOUPLE', XYZ=102.0,30.0,4.9/

&DEVC ID='THCP13', QUANTITY='THERMOCOUPLE', XYZ=102.0,28.0,4.9/

&DEVC ID='THCP14', QUANTITY='THERMOCOUPLE', XYZ=102.0,26.0,4.9/

&DEVC ID='THCP15', QUANTITY='THERMOCOUPLE', XYZ=102.0,24.0,4.9/

&DEVC ID='THCP16', QUANTITY='THERMOCOUPLE', XYZ=102.0,22.0,4.9/

&DEVC ID='THCP17', QUANTITY='THERMOCOUPLE', XYZ=102.0,20.0,4.9/

&DEVC ID='THCP18', QUANTITY='THERMOCOUPLE', XYZ=102.0,18.0,4.9/

&DEVC ID='THCP19', QUANTITY='THERMOCOUPLE', XYZ=102.0,16.0,4.9/

&DEVC ID='THCP20', QUANTITY='THERMOCOUPLE', XYZ=102.0,14.0,4.9/

&DEVC ID='THCP21', QUANTITY='THERMOCOUPLE', XYZ=102.0,54.0,4.4/

&DEVC ID='THCP22', QUANTITY='THERMOCOUPLE', XYZ=102.0,52.0,4.4/

&DEVC ID='THCP23', QUANTITY='THERMOCOUPLE', XYZ=102.0,50.0,4.4/

&DEVC ID='THCP24', QUANTITY='THERMOCOUPLE', XYZ=102.0,48.0,4.4/

&DEVC ID='THCP25', QUANTITY='THERMOCOUPLE', XYZ=102.0,46.0,4.4/

&DEVC ID='THCP26', QUANTITY='THERMOCOUPLE', XYZ=102.0,44.0,4.4/

&DEVC ID='THCP27', QUANTITY='THERMOCOUPLE', XYZ=102.0,42.0,4.4/

&DEVC ID='THCP28', QUANTITY='THERMOCOUPLE', XYZ=102.0,40.0,4.4/

&DEVC ID='THCP29', QUANTITY='THERMOCOUPLE', XYZ=102.0,38.0,4.4/

&DEVC ID='THCP30', QUANTITY='THERMOCOUPLE', XYZ=102.0,36.0,4.4/

&DEVC ID='THCP31', QUANTITY='THERMOCOUPLE', XYZ=102.0,34.0,4.4/

&DEVC ID='THCP32', QUANTITY='THERMOCOUPLE', XYZ=102.0,32.0,4.4/

&DEVC ID='THCP33', QUANTITY='THERMOCOUPLE', XYZ=102.0,30.0,4.4/

&DEVC ID='THCP34', QUANTITY='THERMOCOUPLE', XYZ=102.0,28.0,4.4/

&DEVC ID='THCP35', QUANTITY='THERMOCOUPLE', XYZ=102.0,26.0,4.4/

&DEVC ID='THCP36', QUANTITY='THERMOCOUPLE', XYZ=102.0,24.0,4.4/

&DEVC ID='THCP37', QUANTITY='THERMOCOUPLE', XYZ=102.0,22.0,4.4/

&DEVC ID='THCP38', QUANTITY='THERMOCOUPLE', XYZ=102.0,20.0,4.4/

&DEVC ID='THCP39', QUANTITY='THERMOCOUPLE', XYZ=102.0,18.0,4.4/

&DEVC ID='THCP40', QUANTITY='THERMOCOUPLE', XYZ=102.0,16.0,4.4/

&DEVC ID='THCP41', QUANTITY='THERMOCOUPLE', XYZ=102.0,14.0,4.4/

&DEVC ID='THCP42', QUANTITY='THERMOCOUPLE', XYZ=102.0,54.0,3.9/

&DEVC ID='THCP43', QUANTITY='THERMOCOUPLE', XYZ=102.0,52.0,3.9/

&DEVC ID='THCP44', QUANTITY='THERMOCOUPLE', XYZ=102.0,50.0,3.9/

&DEVC ID='THCP45', QUANTITY='THERMOCOUPLE', XYZ=102.0,48.0,3.9/

&DEVC ID='THCP46', QUANTITY='THERMOCOUPLE', XYZ=102.0,46.0,3.9/

&DEVC ID='THCP47', QUANTITY='THERMOCOUPLE', XYZ=102.0,44.0,3.9/

&DEVC ID='THCP48', QUANTITY='THERMOCOUPLE', XYZ=102.0,42.0,3.9/

&DEVC ID='THCP49', QUANTITY='THERMOCOUPLE', XYZ=102.0,40.0,3.9/

&DEVC ID='THCP50', QUANTITY='THERMOCOUPLE', XYZ=102.0,38.0,3.9/

&DEVC ID='THCP51', QUANTITY='THERMOCOUPLE', XYZ=102.0,36.0,3.9/

&DEVC ID='THCP52', QUANTITY='THERMOCOUPLE', XYZ=102.0,34.0,3.9/

&DEVC ID='THCP53', QUANTITY='THERMOCOUPLE', XYZ=102.0,32.0,3.9/

&DEVC ID='THCP54', QUANTITY='THERMOCOUPLE', XYZ=102.0,30.0,3.9/

&DEVC ID='THCP55', QUANTITY='THERMOCOUPLE', XYZ=102.0,28.0,3.9/

&DEVC ID='THCP56', QUANTITY='THERMOCOUPLE', XYZ=102.0,26.0,3.9/

&DEVC ID='THCP57', QUANTITY='THERMOCOUPLE', XYZ=102.0,24.0,3.9/

&DEVC ID='THCP58', QUANTITY='THERMOCOUPLE', XYZ=102.0,22.0,3.9/

&DEVC ID='THCP59', QUANTITY='THERMOCOUPLE', XYZ=102.0,20.0,3.9/

&DEVC ID='THCP60', QUANTITY='THERMOCOUPLE', XYZ=102.0,18.0,3.9/

&DEVC ID='THCP61', QUANTITY='THERMOCOUPLE', XYZ=102.0,16.0,3.9/

&DEVC ID='THCP62', QUANTITY='THERMOCOUPLE', XYZ=102.0,14.0,3.9/

&DEVC ID='THCP63', QUANTITY='THERMOCOUPLE', XYZ=102.0,54.0,3.4/

&DEVC ID='THCP64', QUANTITY='THERMOCOUPLE', XYZ=102.0,52.0,3.4/

&DEVC ID='THCP65', QUANTITY='THERMOCOUPLE', XYZ=102.0,50.0,3.4/

&DEVC ID='THCP66', QUANTITY='THERMOCOUPLE', XYZ=102.0,48.0,3.4/

&DEVC ID='THCP67', QUANTITY='THERMOCOUPLE', XYZ=102.0,46.0,3.4/

&DEVC ID='THCP68', QUANTITY='THERMOCOUPLE', XYZ=102.0,44.0,3.4/

&DEVC ID='THCP69', QUANTITY='THERMOCOUPLE', XYZ=102.0,42.0,3.4/

&DEVC ID='THCP70', QUANTITY='THERMOCOUPLE', XYZ=102.0,40.0,3.4/

&DEVC ID='THCP71', QUANTITY='THERMOCOUPLE', XYZ=102.0,38.0,3.4/

&DEVC ID='THCP72', QUANTITY='THERMOCOUPLE', XYZ=102.0,36.0,3.4/

&DEVC ID='THCP73', QUANTITY='THERMOCOUPLE', XYZ=102.0,34.0,3.4/

&DEVC ID='THCP74', QUANTITY='THERMOCOUPLE', XYZ=102.0,32.0,3.4/

&DEVC ID='THCP75', QUANTITY='THERMOCOUPLE', XYZ=102.0,30.0,3.4/

&DEVC ID='THCP76', QUANTITY='THERMOCOUPLE', XYZ=102.0,28.0,3.4/

&DEVC ID='THCP77', QUANTITY='THERMOCOUPLE', XYZ=102.0,26.0,3.4/

&DEVC ID='THCP78', QUANTITY='THERMOCOUPLE', XYZ=102.0,24.0,3.4/

&DEVC ID='THCP79', QUANTITY='THERMOCOUPLE', XYZ=102.0,22.0,3.4/

```
&DEVC ID='THCP80', QUANTITY='THERMOCOUPLE', XYZ=102.0,20.0,3.4/
&DEVC ID='THCP81', QUANTITY='THERMOCOUPLE', XYZ=102.0,18.0,3.4/
&DEVC ID='THCP82', QUANTITY='THERMOCOUPLE', XYZ=102.0,16.0,3.4/
&DEVC ID='THCP83', QUANTITY='THERMOCOUPLE', XYZ=102.0,14.0,3.4/
&DEVC ID='THCP84', QUANTITY='THERMOCOUPLE', XYZ=102.0,54.0,2.9/
&DEVC ID='THCP85', QUANTITY='THERMOCOUPLE', XYZ=102.0,52.0,2.9/
&DEVC ID='THCP86', QUANTITY='THERMOCOUPLE', XYZ=102.0,50.0,2.9/
&DEVC ID='THCP87', QUANTITY='THERMOCOUPLE', XYZ=102.0,48.0,2.9/
&DEVC ID='THCP88', QUANTITY='THERMOCOUPLE', XYZ=102.0,46.0,2.9/
&DEVC ID='THCP89', QUANTITY='THERMOCOUPLE', XYZ=102.0,44.0,2.9/
&DEVC ID='THCP90', QUANTITY='THERMOCOUPLE', XYZ=102.0,42.0,2.9/
&DEVC ID='THCP91', QUANTITY='THERMOCOUPLE', XYZ=102.0,40.0,2.9/
&DEVC ID='THCP92', QUANTITY='THERMOCOUPLE', XYZ=102.0,38.0,2.9/
&DEVC ID='THCP93', QUANTITY='THERMOCOUPLE', XYZ=102.0,36.0,2.9/
&DEVC ID='THCP94', QUANTITY='THERMOCOUPLE', XYZ=102.0,34.0,2.9/
&DEVC ID='THCP95', QUANTITY='THERMOCOUPLE', XYZ=102.0,32.0,2.9/
&DEVC ID='THCP96', QUANTITY='THERMOCOUPLE', XYZ=102.0,30.0,2.9/
&DEVC ID='THCP97', QUANTITY='THERMOCOUPLE', XYZ=102.0,28.0,2.9/
&DEVC ID='THCP98', QUANTITY='THERMOCOUPLE', XYZ=102.0,26.0,2.9/
&DEVC ID='THCP99', QUANTITY='THERMOCOUPLE', XYZ=102.0,24.0,2.9/
&DEVC ID='THCP100', QUANTITY='THERMOCOUPLE',
XYZ=102.0,22.0,2.9/
```

```
&DEVC ID='THCP101', QUANTITY='THERMOCOUPLE',
XYZ=102.0,20.0,2.9/
&DEVC ID='THCP102', QUANTITY='THERMOCOUPLE',
XYZ=102.0,18.0,2.9/
&DEVC ID='THCP103', QUANTITY='THERMOCOUPLE',
XYZ=102.0,16.0,2.9/
&DEVC ID='THCP104', QUANTITY='THERMOCOUPLE',
XYZ=102.0,14.0,2.9/
&DEVC ID='THCP105', QUANTITY='THERMOCOUPLE',
XYZ=102.0,54.0,2.4/
&DEVC ID='THCP106', QUANTITY='THERMOCOUPLE',
XYZ=102.0,52.0,2.4/
&DEVC ID='THCP107', QUANTITY='THERMOCOUPLE',
XYZ=102.0,50.0,2.4/
&DEVC ID='THCP108', QUANTITY='THERMOCOUPLE',
XYZ=102.0,48.0,2.4/
&DEVC ID='THCP109', QUANTITY='THERMOCOUPLE',
XYZ=102.0,46.0,2.4/
&DEVC ID='THCP110', QUANTITY='THERMOCOUPLE',
XYZ=102.0,44.0,2.4/
&DEVC ID='THCP111', QUANTITY='THERMOCOUPLE',
XYZ=102.0,42.0,2.4/
```

```
&DEVC ID='THCP112', QUANTITY='THERMOCOUPLE',
XYZ=102.0,40.0,2.4/
&DEVC ID='THCP113', QUANTITY='THERMOCOUPLE',
XYZ=102.0,38.0,2.4/
&DEVC ID='THCP114', QUANTITY='THERMOCOUPLE',
XYZ=102.0,36.0,2.4/
&DEVC ID='THCP115', QUANTITY='THERMOCOUPLE',
XYZ=102.0,34.0,2.4/
&DEVC ID='THCP116', QUANTITY='THERMOCOUPLE',
XYZ=102.0,32.0,2.4/
&DEVC ID='THCP117', QUANTITY='THERMOCOUPLE',
XYZ=102.0,30.0,2.4/
&DEVC ID='THCP118', QUANTITY='THERMOCOUPLE',
XYZ=102.0,28.0,2.4/
&DEVC ID='THCP119', QUANTITY='THERMOCOUPLE',
XYZ=102.0,26.0,2.4/
&DEVC ID='THCP120', QUANTITY='THERMOCOUPLE',
XYZ=102.0,24.0,2.4/
&DEVC ID='THCP121', QUANTITY='THERMOCOUPLE',
XYZ=102.0,22.0,2.4/
&DEVC ID='THCP122', QUANTITY='THERMOCOUPLE',
XYZ=102.0,20.0,2.4/
```

```
&DEVC ID='THCP123', QUANTITY='THERMOCOUPLE',
XYZ=102.0,18.0,2.4/
&DEVC ID='THCP124', QUANTITY='THERMOCOUPLE',
XYZ=102.0,16.0,2.4/
&DEVC ID='THCP125', QUANTITY='THERMOCOUPLE',
XYZ=102.0,14.0,2.4/
&DEVC ID='THCP126', QUANTITY='THERMOCOUPLE',
XYZ=102.0,54.0,1.9/
&DEVC ID='THCP127', QUANTITY='THERMOCOUPLE',
XYZ=102.0,52.0,1.9/
&DEVC ID='THCP128', QUANTITY='THERMOCOUPLE',
XYZ=102.0,50.0,1.9/
&DEVC ID='THCP129', QUANTITY='THERMOCOUPLE',
XYZ=102.0,48.0,1.9/
&DEVC ID='THCP130', QUANTITY='THERMOCOUPLE',
XYZ=102.0,46.0,1.9/
&DEVC ID='THCP131', QUANTITY='THERMOCOUPLE',
XYZ=102.0,44.0,1.9/
&DEVC ID='THCP132', QUANTITY='THERMOCOUPLE',
XYZ=102.0,42.0,1.9/
&DEVC ID='THCP133', QUANTITY='THERMOCOUPLE',
XYZ=102.0,40.0,1.9/
```

```
&DEVC ID='THCP134', QUANTITY='THERMOCOUPLE',
XYZ=102.0,38.0,1.9/
&DEVC ID='THCP135', QUANTITY='THERMOCOUPLE',
XYZ=102.0,36.0,1.9/
&DEVC ID='THCP136', QUANTITY='THERMOCOUPLE',
XYZ=102.0,34.0,1.9/
&DEVC ID='THCP137', QUANTITY='THERMOCOUPLE',
XYZ=102.0,32.0,1.9/
&DEVC ID='THCP138', QUANTITY='THERMOCOUPLE',
XYZ=102.0,30.0,1.9/
&DEVC ID='THCP139', QUANTITY='THERMOCOUPLE',
XYZ=102.0,28.0,1.9/
&DEVC ID='THCP140', QUANTITY='THERMOCOUPLE',
XYZ=102.0,26.0,1.9/
&DEVC ID='THCP141', QUANTITY='THERMOCOUPLE',
XYZ=102.0,24.0,1.9/
&DEVC ID='THCP142', QUANTITY='THERMOCOUPLE',
XYZ=102.0,22.0,1.9/
&DEVC ID='THCP143', QUANTITY='THERMOCOUPLE',
XYZ=102.0,20.0,1.9/
&DEVC ID='THCP144', QUANTITY='THERMOCOUPLE',
XYZ=102.0,18.0,1.9/
```

```
&DEVC ID='THCP145', QUANTITY='THERMOCOUPLE',
XYZ=102.0,16.0,1.9/
&DEVC ID='THCP146', QUANTITY='THERMOCOUPLE',
XYZ=102.0,14.0,1.9/
&DEVC ID='Viz', QUANTITY='VISIBILITY', XYZ=102.0,4.0,2.0/
&DEVC ID='Viz01', QUANTITY='VISIBILITY', XYZ=102.0,2.0,2.0/
&DEVC ID='Viz02', QUANTITY='VISIBILITY', XYZ=112.0,2.0,2.0/
&DEVC ID='Viz03', QUANTITY='VISIBILITY', XYZ=122.0,2.0,2.0/
&DEVC ID='Viz04', QUANTITY='VISIBILITY', XYZ=132.0,2.0,2.0/
&DEVC ID='Viz05', QUANTITY='VISIBILITY', XYZ=142.0,2.0,2.0/
&DEVC ID='Viz06', QUANTITY='VISIBILITY', XYZ=152.0,2.0,2.0/
&DEVC ID='Viz07', QUANTITY='VISIBILITY', XYZ=162.0,2.0,2.0/
&DEVC ID='Viz08', QUANTITY='VISIBILITY', XYZ=172.0,2.0,2.0/
&DEVC ID='Viz09', QUANTITY='VISIBILITY', XYZ=182.0,2.0,2.0/
&DEVC ID='Viz10', QUANTITY='VISIBILITY', XYZ=192.0,2.0,2.0/
&DEVC ID='Viz11', QUANTITY='VISIBILITY', XYZ=202.0,2.0,2.0/
&DEVC ID='Viz12', QUANTITY='VISIBILITY', XYZ=92.0,2.0,2.0/
&DEVC ID='Viz13', QUANTITY='VISIBILITY', XYZ=82.0,2.0,2.0/
&DEVC ID='Viz14', QUANTITY='VISIBILITY', XYZ=72.0,2.0,2.0/
&DEVC ID='Viz15', QUANTITY='VISIBILITY', XYZ=62.0,2.0,2.0/
&DEVC ID='Viz16', QUANTITY='VISIBILITY', XYZ=52.0,2.0,2.0/
&DEVC ID='Viz17', QUANTITY='VISIBILITY', XYZ=42.0,2.0,2.0/
&DEVC ID='Viz18', QUANTITY='VISIBILITY', XYZ=32.0,2.0,2.0/
```

```
&DEVC ID='Viz19', QUANTITY='VISIBILITY', XYZ=22.0,2.0,2.0/
&DEVC ID='Viz20', QUANTITY='VISIBILITY', XYZ=12.0,2.0,2.0/
&DEVC ID='Viz21', QUANTITY='VISIBILITY', XYZ=2.0,2.0,2.0/
&DEVC ID='Viz22', QUANTITY='VISIBILITY', XYZ=102.0,14.0,2.0/
&DEVC ID='Viz23', QUANTITY='VISIBILITY', XYZ=102.0,24.0,2.0/
&DEVC ID='Viz24', QUANTITY='VISIBILITY', XYZ=102.0,34.0,2.0/
&DEVC ID='Viz25', QUANTITY='VISIBILITY', XYZ=102.0,44.0,2.0/
&DEVC ID='Viz26', QUANTITY='VISIBILITY', XYZ=102.0,54.0,2.0/
&DEVC ID='CO', QUANTITY='VOLUME FRACTION', SPEC_ID='CARBON
MONOXIDE', XYZ=102.0,2.0,2.0/
&DEVC ID='CO01', QUANTITY='VOLUME FRACTION',
SPEC_ID='CARBON MONOXIDE', XYZ=112.0,2.0,2.0/
&DEVC ID='CO02', QUANTITY='VOLUME FRACTION',
SPEC_ID='CARBON MONOXIDE', XYZ=122.0,2.0,2.0/
&DEVC ID='CO03', QUANTITY='VOLUME FRACTION',
SPEC_ID='CARBON MONOXIDE', XYZ=132.0,2.0,2.0/
&DEVC ID='CO04', QUANTITY='VOLUME FRACTION',
SPEC_ID='CARBON MONOXIDE', XYZ=142.0,2.0,2.0/
&DEVC ID='CO05', QUANTITY='VOLUME FRACTION',
SPEC_ID='CARBON MONOXIDE', XYZ=152.0,2.0,2.0/
&DEVC ID='CO06', QUANTITY='VOLUME FRACTION',
SPEC_ID='CARBON MONOXIDE', XYZ=162.0,2.0,2.0/
```

```
&DEVC ID='CO07', QUANTITY='VOLUME FRACTION',
SPEC_ID='CARBON MONOXIDE', XYZ=172.0,2.0,2.0/
&DEVC ID='CO08', QUANTITY='VOLUME FRACTION',
SPEC_ID='CARBON MONOXIDE', XYZ=182.0,2.0,2.0/
&DEVC ID='CO09', QUANTITY='VOLUME FRACTION',
SPEC_ID='CARBON MONOXIDE', XYZ=192.0,2.0,2.0/
&DEVC ID='CO10', QUANTITY='VOLUME FRACTION',
SPEC_ID='CARBON MONOXIDE', XYZ=202.0,2.0,2.0/
&DEVC ID='CO11', QUANTITY='VOLUME FRACTION',
SPEC_ID='CARBON MONOXIDE', XYZ=92.0,2.0,2.0/
&DEVC ID='CO12', QUANTITY='VOLUME FRACTION',
SPEC_ID='CARBON MONOXIDE', XYZ=82.0,2.0,2.0/
&DEVC ID='CO13', QUANTITY='VOLUME FRACTION',
SPEC_ID='CARBON MONOXIDE', XYZ=72.0,2.0,2.0/
&DEVC ID='CO14', QUANTITY='VOLUME FRACTION',
SPEC_ID='CARBON MONOXIDE', XYZ=62.0,2.0,2.0/
&DEVC ID='CO15', QUANTITY='VOLUME FRACTION',
SPEC_ID='CARBON MONOXIDE', XYZ=52.0,2.0,2.0/
&DEVC ID='CO16', QUANTITY='VOLUME FRACTION',
SPEC_ID='CARBON MONOXIDE', XYZ=42.0,2.0,2.0/
&DEVC ID='CO17', QUANTITY='VOLUME FRACTION',
SPEC_ID='CARBON MONOXIDE', XYZ=32.0,2.0,2.0/
```

```
&DEVC ID='CO18', QUANTITY='VOLUME FRACTION',
SPEC_ID='CARBON MONOXIDE', XYZ=22.0,2.0,2.0/
&DEVC ID='CO19', QUANTITY='VOLUME FRACTION',
SPEC_ID='CARBON MONOXIDE', XYZ=12.0,2.0,2.0/
&DEVC ID='CO20', QUANTITY='VOLUME FRACTION',
SPEC_ID='CARBON MONOXIDE', XYZ=2.0,2.0,2.0/
&DEVC ID='CO_exist of cc', QUANTITY='VOLUME FRACTION',
SPEC_ID='CARBON MONOXIDE', XYZ=102.0,4.0,2.0/
&DEVC ID='CO_exist of cc01', QUANTITY='VOLUME FRACTION',
SPEC_ID='CARBON MONOXIDE', XYZ=102.0,14.0,2.0/
&DEVC ID='CO_exist of cc02', QUANTITY='VOLUME FRACTION',
SPEC_ID='CARBON MONOXIDE', XYZ=102.0,24.0,2.0/
&DEVC ID='CO_exist of cc03', QUANTITY='VOLUME FRACTION',
SPEC_ID='CARBON MONOXIDE', XYZ=102.0,34.0,2.0/
&DEVC ID='CO_exist of cc04', QUANTITY='VOLUME FRACTION',
SPEC_ID='CARBON MONOXIDE', XYZ=102.0,44.0,2.0/
&DEVC ID='CO_exist of cc05', QUANTITY='VOLUME FRACTION',
SPEC_ID='CARBON MONOXIDE', XYZ=102.0,54.0,2.0/
&MATL ID='CONCRETE',
    FYI='NBSIR 88-3752 - ATF NIST Multi-Floor Validation',
    SPECIFIC_HEAT=1.04,
    CONDUCTIVITY=1.8,
    DENSITY=2280.0/
```

```
&SURF ID='Wall',
    RGB=146,202,166,
    BACKING='VOID',
    MATL_ID(1,1)='CONCRETE',
    MATL_MASS_FRACTION(1,1)=1.0,
    THICKNESS(1)=0.2/
&SURF ID='Fire',
    COLOR='RED',
    HRRPUA=7350.0,
    RAMP_Q='Fire_RAMP_Q',
    TMP_FRONT=300.0/
&RAMP ID='Fire_RAMP_Q', T=0.0, F=0.0/
&RAMP ID='Fire_RAMP_Q', T=60.0, F=0.5/
&RAMP ID='Fire_RAMP_Q', T=120.0, F=1.0/
&RAMP ID='Fire_RAMP_Q', T=180.0, F=0.3/
&RAMP ID='Fire_RAMP_Q', T=240.0, F=0.14/
&RAMP ID='Fire_RAMP_Q', T=300.0, F=0.1/
&RAMP ID='Fire_RAMP_Q', T=360.0, F=0.04/
&RAMP ID='Fire_RAMP_Q', T=420.0, F=0.0/
&SURF ID='Supply',
    RGB=0,51,255,
    VEL=-4.0/
&OBST ID='Main drift', XB=0.0,204.0,0.0,4.0,-0.2,0.0, SURF_ID='INERT'/
```

&OBST ID='Blind heading', XB=100.0,104.0,4.0,54.0,-0.2,0.0,
SURF_ID='INERT'/

&OBST ID='other wall', XB=0.0,204.0,-0.2,0.0,0.0,5.0, RGB=203,203,255,
TRANSPARENCY=0.396078, SURF_ID='Wall'/

&OBST ID='Main drift roof', XB=0.0,204.0,0.0,4.0,4.8,5.0,
COLOR='INVISIBLE', SURF_ID='INERT'/

&OBST ID='Blind heading roof', XB=100.0,104.0,4.0,54.0,4.8,5.0,
COLOR='INVISIBLE', SURF_ID='INERT'/

&OBST ID='Inlet', XB=-0.1,0.1,0.0,4.0,0.0,5.0, COLOR='GRAY 60',
SURF_ID='Supply'/

&OBST ID='Wall to Faces', XB=-0.2,49.4,3.8,4.2,0.166667,4.833333,
RGB=204,153,255, TRANSPARENCY=0.396078, SURF_ID='Wall'/

&OBST ID='Wall to Faces', XB=49.4,99.8,3.8,4.2,0.166667,4.833333,
RGB=204,153,255, TRANSPARENCY=0.396078, SURF_ID='Wall'/

&OBST ID='Wall to Faces', XB=99.8,100.2,3.8,5.0,0.166667,4.833333,
RGB=204,153,255, TRANSPARENCY=0.396078, SURF_ID='Wall'/

&OBST ID='Wall to Faces', XB=103.8,104.2,4.2,5.0,0.166667,4.833333,
RGB=204,153,255, TRANSPARENCY=0.396078, SURF_ID='Wall'/

&OBST ID='Wall to Faces', XB=103.8,150.6,3.8,4.2,0.166667,4.833333,
RGB=204,153,255, TRANSPARENCY=0.396078, SURF_ID='Wall'/

&OBST ID='Wall to Faces', XB=150.6,204.136508,3.8,4.2,0.166667,4.833333,
RGB=204,153,255, TRANSPARENCY=0.396078, SURF_ID='Wall'/

&OBST ID='Wall to Faces', XB=99.8,100.2,5.0,17.4,0.166667,4.833333, RGB=204,153,255, TRANSPARENCY=0.396078, SURF_ID='Wall'/

&OBST ID='Wall to Faces', XB=103.8,104.2,5.0,17.4,0.166667,4.833333, RGB=204,153,255, TRANSPARENCY=0.396078, SURF_ID='Wall'/

&OBST ID='Wall to Faces', XB=99.8,100.2,17.4,30.2,0.166667,4.833333, RGB=204,153,255, TRANSPARENCY=0.396078, SURF_ID='Wall'/

&OBST ID='Wall to Faces', XB=103.8,104.2,17.4,30.2,0.166667,4.833333, RGB=204,153,255, TRANSPARENCY=0.396078, SURF_ID='Wall'/

&OBST ID='Wall to Faces', XB=99.8,100.2,30.2,42.6,0.166667,4.833333, RGB=204,153,255, TRANSPARENCY=0.396078, SURF_ID='Wall'/

&OBST ID='Wall to Faces', XB=103.8,104.2,30.2,42.6,0.166667,4.833333, RGB=204,153,255, TRANSPARENCY=0.396078, SURF_ID='Wall'/

&OBST ID='Wall to Faces', XB=99.8,100.2,42.6,53.8,0.166667,4.833333, RGB=204,153,255, TRANSPARENCY=0.396078, SURF_ID='Wall'/

&OBST ID='Wall to Faces', XB=99.8,104.2,53.8,54.2,0.166667,4.833333, RGB=204,153,255, TRANSPARENCY=0.396078, SURF_ID='Wall'/

&OBST ID='Wall to Faces', XB=103.8,104.2,42.6,53.8,0.166667,4.833333, RGB=204,153,255, TRANSPARENCY=0.396078, SURF_ID='Wall'/

&VENT ID='Mesh Vent: Mesh01-04 [XMAX]', SURF_ID='OPEN', XB=205.0,205.0,-1.0,5.0,-1.0,6.0/

&VENT ID='Vent fire', SURF_ID='Fire', XB=101.0,103.0,51.0,53.0,0.0,0.0, RGB=255,51,51/

&VENT ID='Fan in', SURF_ID='HVAC', XB=94.0,96.0,4.0,4.0,3.0,5.0, COLOR='INVISIBLE'/

&VENT ID='Fan Out', SURF_ID='HVAC', XB=100.0,100.0,38.0,40.0,3.0,5.0, COLOR='INVISIBLE'/

&VENT ID='inlet airflow', SURF_ID='Supply', XB=-0.1,-0.1,0.0,4.0,0.0,5.0/

&HVAC ID='N1', TYPE_ID='NODE', DUCT_ID='D1', VENT_ID='Fan in'/

&HVAC ID='N2', TYPE_ID='NODE', DUCT_ID='D2', VENT_ID='Fan Out'/

&HVAC ID='IN', TYPE_ID='NODE', DUCT_ID='D1','D2', XYZ=100.0,4.0,4.0/

&HVAC ID='D1', TYPE_ID='DUCT', DIAMETER=0.6, NODE_ID='N1','IN', ROUGHNESS=1.0E-3, LENGTH=5.0/

&HVAC ID='D2', TYPE_ID='DUCT', DIAMETER=0.6, FAN_ID='F1', NODE_ID='IN','N2', ROUGHNESS=1.0E-3, LENGTH=35.0/

&HVAC ID='F1', TYPE_ID='FAN', VOLUME_FLOW=14.2/

&SLCF QUANTITY='TEMPERATURE', VECTOR=.TRUE., PBX=102.0/

&SLCF QUANTITY='VELOCITY', VECTOR=.TRUE., PBX=102.0/

&SLCF QUANTITY='VISIBILITY', VECTOR=.TRUE., PBX=102.0/

&SLCF QUANTITY='TEMPERATURE', VECTOR=.TRUE., PBY=2.0/

&SLCF QUANTITY='VELOCITY', VECTOR=.TRUE., PBY=2.0/

&SLCF QUANTITY='VISIBILITY', VECTOR=.TRUE., PBY=2.0/

&SLCF QUANTITY='VELOCITY', VECTOR=.TRUE., XB=0.0,200.0,0.0,4.0,0.0,5.0, FYI='Vel'/

&SLCF QUANTITY='VISIBILITY', VECTOR=.TRUE., XB=0.0,200.0,0.0,4.0,0.0,5.0, FYI='Viz'/

&SLCF QUANTITY='TEMPERATURE', VECTOR=.TRUE.,

XB=0.0,200.0,0.0,4.0,0.0,5.0, FYI='Tem'/

&SLCF QUANTITY='VELOCITY', VECTOR=.TRUE.,

XB=100.0,104.0,4.0,55.0,0.0,5.0, FYI='Vel'/

&SLCF QUANTITY='VISIBILITY', VECTOR=.TRUE.,

XB=100.0,104.0,4.0,55.0,0.0,5.0, FYI='Viz'/

&SLCF QUANTITY='TEMPERATURE', VECTOR=.TRUE.,

XB=100.0,104.0,4.0,55.0,0.0,5.0, FYI='Tem'/

&TAIL /

REFERENCES

Adjiski, V., & Despodov, Z. (2020). Methodology for Optimal Fire Evacuations in Underground Mines Based on Simulated Scenarios.

Adjiski, V., Mirakovski, D., Despodov, Z., & Mijalkovski, S. (2015). Simulation and optimization of evacuation routes in case of fire in underground mines. J. Sustain. Min., 14. https://doi.org/10.1016/j.jsm.2015.10.001

Akizuki, Y., Yamao, K., & Tanaka, T. (2007, 2007). Experimental study on walking speed in escape route considering luminous condition, smoke density and evacuee's visual acuity.

Anastasios, K., Despina, P., Nikolas, G., & Dimitrios, K. (2022). Evacuation in an Underground Space: A Real-Time Investigation of Occupants’ Travel Speed in Clear and Smoked Environments. Infrastructures, 7(4).

Bi, H., & Gelenbe, E. (2019). A survey of algorithms and systems for evacuating people in confined spaces. Electronics, 8(6), 711.

Crooks, A. T., & Heppenstall, A. J. (2012). Introduction to Agent-Based Modelling. In A. J. Heppenstall, A. T. Crooks, L. M. See, & M. Batty (Eds.), Agent-Based Models of Geographical Systems (pp. 85-105). Springer Netherlands. https://doi.org/10.1007/978-90-481-8927-4_5

Edrisi, A., Lahoorpoor, B., & Lovreglio, R. (2021). Simulating metro station evacuation using three agent-based exit choice models. Case studies on transport policy, 9(3), 1261-1272.

Eppstein, D. (1998). Finding the k shortest paths. SIAM J. Comput., 28. https://doi.org/10.1137/S0097539795290477

Fridolf, K., Andrée, K., Nilsson, D., & Frantzich, H. (2014). The impact of smoke on walking speed. Fire and Materials, 38(7), 744-759.

Fridolf, K., Nilsson, D., Frantzich, H., Ronchi, E., & Arias, S. (2018, 2018). Walking speed in smoke: Representation in life safety verifications.

Hansen, R. (2020). Modelling temperature distributions and flow conditions of fires in an underground mine drift. Geosystem Engineering, 23(6), 299-314.

Hansen, R., & Ingason, H. (2013). Full-scale fire experiments with mining vehicles in an underground mine (978-91-7485-115-1 (ISBN)). (Studies in Sustainable Technology / Forskningsrapport, Issue. http://urn.kb.se/resolve?urn=urn:nbn:se:mdh:diva-20912

Hong, Y., Li, D., Wu, Q., & Xu, H. (2018). Dynamic Route Network Planning Problem for Emergency Evacuation in Restricted-Space Scenarios. Journal of Advanced Transportation, 2018, 4295419. https://doi.org/10.1155/2018/4295419

Hong, Y., Li, D., Wu, Q., Xu, H. J. J. o. O. T., & Applications. (2019). Priority-oriented route network planning for evacuation in constrained space scenarios. 181(1), 279-297.

Huang, P., Kang, J., Kider, J. T., Sunshine-Hill, B., McCaffrey, J. B., Rios, D. V., & Badler, N. I. (2010). Real-time evacuation simulation in mine interior model of smoke and action.

Jalali, S. E., & Noroozi, M. (2009). Determination of the optimal escape routes of underground mine networks in emergency cases. Saf. Sci., 47. https://doi.org/10.1016/j.ssci.2009.01.001

Jevtić, R. B. (2020). Simulation of evacuation from mine as a safety measurement. Tehnika, 75(1), 110-119.

Jin, W., Chen, S., Jiang, H. J. C., & research, o. (2013). Finding the K shortest paths in a time-schedule network with constraints on arcs. 40(12), 2975-2982.

Kallianiotis, A., Papakonstantinou, D., Arvelaki, V., & Benardos, A. (2018). Evaluation of evacuation methods in underground metro stations. International journal of disaster risk reduction, 31, 526-534.

Kallianiotis, A., Papakonstantinou, D., Tolias, I. C., & Benardos, A. (2022). Evaluation of fire smoke control in underground space. Underground Space, 7(3), 295-310.

Kim, H. J., Bae, S.-Y., Choi, Y. K., Hong, K. B., & Ryou, H. S. (2013). Numerical analysis on the effect of improved fractional effective dose (FED) for evacuation by FDS_EVAC. Journal of the Korean Society of Safety, 28(1), 125-131.

Kuligowski, E. D., Peacock, R. D., & Hoskins, B. L. (2005). A review of building evacuation models. US Department of Commerce, National Institute of Standards and Technology ….

Lemaire, T., & Kenyon, Y. (2006). Large Scale Fire Tests in the Second Benelux Tunnel. Fire Technology, 42(4), 329-350. https://doi.org/10.1007/s10694-006-8434-4

Li, C., Li, J., Hu, L., & Hou, D. (2015). Visualization and simulation model of underground mine fire disaster based on Cellular Automata. Applied Mathematical Modelling, 39(15), 4351-4364. https://doi.org/https://doi.org/10.1016/j.apm.2014.12.051

Liu, Z., Gu, X., & Hong, R. (2023). Fire Protection and Evacuation Analysis in Underground Interchange Tunnels by Integrating BIM and Numerical Simulation. Fire, 6(4).

Mu, N., Song, W.-g., Qi, X.-x., Lu, W., & Cao, S.-c. (2014). Simulation of evacuation in a twin bore tunnel: analysis of evacuation time and egress selection. Procedia Engineering, 71, 333-342.

Osunmakinde, I. O. (2013). Towards safety from toxic gases in underground mines using wireless sensor networks and ambient intelligence. International Journal of Distributed Sensor Networks, 9(2), 159273.

Pan, Z., Wei, Q., Torp, O., & Lau, A. (2019). Influence of evacuation walkway design parameters on passenger evacuation time along elevated rail transit lines using a multi-agent simulation. Sustainability, 11(21), 6049.

Purser, D. A. (1992). The evolution of toxic effluents in fires and the assessment of toxic hazard. Toxicology Letters, 64-65, 247-255. https://doi.org/https://doi.org/10.1016/0378-4274(92)90196-Q

Purser, D. A. (2000). Toxic product yields and hazard assessment for fully enclosed design fires. Polymer International, 49(10), 1232-1255.

Purser, D. A. (2003). ASET and RSET: addressing some issues in relation to occupant behaviour and tenability. Fire Safety Science, 7, 91-102.

Pushparaj, R. I., Xu, G., Iqbal, A., & Salami, O. B. (2023). Characterization and preliminary assessment of diesel fire prior to setting up large size battery fire experiment. In Underground Ventilation (pp. 393-398). CRC Press.

Qin, J., Liu, C., & Huang, Q. (2020). Simulation on fire emergency evacuation in special subway station based on Pathfinder. Case Studies in Thermal Engineering, 21, 100677.

Railsback, S. F., & Grimm, V. (2019). Agent-based and individual-based modeling: a practical introduction. Princeton university press.

Ronchi, E., Arias, S., La Mendola, S., & Johansson, N. (2019). A fire safety assessment approach for evacuation analysis in underground physics research facilities. Fire safety journal, 108, 102839.

Ronchi, E., Colonna, P., Capote, J., Alvear, D., Berloco, N., & Cuesta, A. (2012). The evaluation of different evacuation models for assessing road tunnel safety analysis. Tunnelling and Underground Space Technology, 30, 74-84.

Ronchi, E., Fridolf, K., Frantzich, H., Nilsson, D., Walter, A. L., & Modig, H. (2018). A tunnel evacuation experiment on movement speed and exit choice in smoke. Fire safety journal, 97, 126-136.

Rosberg, D., Purchase, A., Fridolf, K., Brand, W. S. P., & Jungmansgatan, R. (2018, Oct 1-3). Acceptance criteria in fire safety engineering: a review and case study.

Salami, O., & Xu, G. (2022). EXPERIMENTAL INVESTIGATION OF FIRE AND PRODUCT OF COMBUSTION (POC) SPREAD IN UNDERGROUND MINES: A CASE STUDY. SME Annual Conference and Expo 2022,

Salami , O. B., Xu, G., Kumar, A. R., & Pushparaj, R. I. (2023). Underground mining fire hazards and the optimization of emergency evacuation strategies (EES): The issues, existing methodology and limitations, and way forward. Process Safety and Environmental Protection, 177, 617-634. https://doi.org/https://doi.org/10.1016/j.psep.2023.07.012

Salami, O. B., Xu, G., Kumar, A. R., Pushparaj, R. I., & Iqbal, A. (2023). Fire-induced temperature attenuation under the influence of a single ceiling smoke extraction point in a bifurcated drift. In Underground Ventilation (pp. 399-410). CRC Press.

Seike, M., Kawabata, N., & Hasegawa, M. (2016). Experiments of evacuation speed in smoke-filled tunnel. Tunnelling and Underground Space Technology, 53, 61-67. https://doi.org/https://doi.org/10.1016/j.tust.2016.01.003

Tan, L., Hu, M., & Lin, H. (2015). Agent-based simulation of building evacuation: Combining human behavior with predictable spatial accessibility in a fire emergency. Information Sciences, 295, 53-66.

Tang, F., & Ren, A. (2008). Agent-based evacuation model incorporating fire scene and building geometry. Tsinghua Science and Technology, 13(5), 708-714. https://doi.org/10.1016/S1007-0214(08)70115-9

Tang, F. Q., & Ren, A. (2012). GIS-based 3D evacuation simulation for indoor fire. Build. Environ., 49. https://doi.org/10.1016/j.buildenv.2011.09.021

Thornton, C., O'Konski, R., Hardeman, B., & Swenson, D. (2011). Pathfinder: an agent-based egress simulator. In Pedestrian and evacuation dynamics (pp. 889-892). Springer.

Thunderhead-Engineering. (2021). Pathfinder Technical Reference Manual https://support.thunderheadeng.com/docs/pathfinder/2021-2/technical-reference-manual/

Tutak, M. (2020). Analysis of the Time of Crew Evacuation from the Hazardous Area of Mining Exploitation Using Numerical Simulation. Multidisciplinary Aspects of Production Engineering, 3(1), 107-115. https://doi.org/doi:10.2478/mape-2020-0009

Tutak, M., & Gvozdkova, T. (2020). Model-based tests on the time of crew evacuation from the danger area in an excavated underground mine heading [10.1051/e3sconf/202017401053]. E3S Web Conf., 174. https://doi.org/10.1051/e3sconf/202017401053

Wang, D., Yang, Y., Zhou, T., & Yang, F. (2021). An investigation of fire evacuation performance in irregular underground commercial building affected by multiple parameters. Journal of Building Engineering, 37, 102146.

Wang, H.-R., Chen, Q.-G., Yan, J.-B., Yuan, Z., & Liang, D. (2014, 2014). Emergency guidance evacuation in fire scene based on pathfinder.

Wang, H. R., Chen, Q. G., Yan, J. B., Yuan, Z., & Liang, D. (2014, 25-26 Oct. 2014). Emergency Guidance Evacuation in Fire Scene Based on Pathfinder. 2014 7th International Conference on Intelligent Computation Technology and Automation,

Wang, N., Gao, Y., Li, C.-y., & Gai, W.-m. (2021). Integrated agent-based simulation and evacuation risk-assessment model for underground building fire: A case study. Journal of Building Engineering, 40, 102609.

Yuan, L., Zhou, L., & Smith, A. C. (2016). Modeling carbon monoxide spread in underground mine fires. Applied Thermal Engineering, 100, 1319-1326. https://doi.org/https://doi.org/10.1016/j.applthermaleng.2016.03.007

Zheng, S., & Liu, H. (2019). Improved Multi-Agent Deep Deterministic Policy Gradient for Path Planning-Based Crowd Simulation. IEEE Access, 7, 147755-147770. https://doi.org/10.1109/ACCESS.2019.2946659

Zhong, M., Shi, C., Tu, X., Fu, T., & He, L. (2008). Study of the human evacuation simulation of metro fire safety analysis in China. Journal of Loss Prevention in the Process Industries, 21(3), 287-298.

SECTION

2. CONCLUSIONS AND RECOMMENDATIONS

2.1. CONCLUSIONS

Fires occurring in deeper underground confined spaces pose significant hazards that must be addressed effectively. To tackle this challenge, it is crucial to comprehend the characteristics of fires and implement suitable safety measures and emergency evacuation plans.

In this study, we examined the current advancements in underground mine fire research, identifying critical factors such as ventilation conditions, fuel nature, geometrical constraints, and simulation methods influencing fire safety. This analysis optimizes emergency evacuation plans. The presentation outlines the advantages and shortcomings of existing mine fire simulation and evacuation planning, proposing a novel approach to underground emergency evacuation management. This approach empowers miners to self-escape during fire hazards.

The suggested evacuation method considers mine configuration (geometrical parameters), fire field data (heat release rate, smoke spread behavior, flame characteristics, and fuel nature), and the agent population (number of miners underground). This involves directly coupling fire dynamics simulation with agent-based evacuation models to create an integrated emergency response system.

Traditional evacuation strategies rely on static plans, providing a fixed evacuation path without considering changes in the evacuation network or path due to hazard

dynamics. Moreover, few locations in underground mines have evacuation plans, hindering evacuees' access to information about static evacuation routes.

To establish reliable self-escape methods for miners during a fire, it is essential to investigate evacuation models by computing risk factors and the likelihood of safe escape. This model should offer a comprehensive conceptualization of human behavior in fire evacuations. Agent-based modeling emerges as a reliable approach, gaining global attention due to its ability to model complex situations that may be challenging for conventional tools.

The study addresses drawbacks in existing literature attempting to model underground mine fires using data from scaled model tunnels in laboratories. By addressing these issues, the research enhances our understanding of fire risk and improves preparedness for emergency evacuation in underground mines and similar confined spaces.

2.2. LIMITATIONS AND RECOMMENDATIONS FOR FUTURE WORK

Although this work boost of immense progress in furthering our understanding of underground mine fire dynamics, developing effective risk assessment methodologies and mitigation strategies for underground mine fires requires a comprehensive understanding of the complex interactions between fire, ventilation systems, structural integrity, and human factors. Integrating these elements into practical, actionable measures remains a challenge. For example, conducting large-scale experiments involving large mining equipment to replicate underground mine fire scenarios is often impractical due to cost, safety concerns, and logistical challenges. As a result, this study relies on pool fire experiments and computational simulations, which may not fully capture the intricacies of

real-world scenarios. Additionally, addressing the multifaceted nature of underground mine fires often requires collaboration across disciplines such as fire science, mining engineering, geology, and environmental science. Encouraging and facilitating interdisciplinary research efforts can be challenging but is essential for advancing knowledge in this field.

Furthermore, the ABM model developed in this study is limited in that the model parameters were not derived from real underground miners' experience during a fire emergency. Hence, future work should focus on implementing the prototype model developed in this study in large underground mining environment with multiple development heading for verification and validation studies.

BIBLIOGRAPHY

Edrisi, A., Lahoorpoor, B., & Lovreglio, R. (2021). Simulating metro station evacuation using three agent-based exit choice models. Case studies on transport policy, 9(3), 1261-1272.

Edwards, J., & Hwang, C. (1999). CFD analysis of mine fire smoke spread and reverse flow conditions.

Fernández-Alaiz, F., Castañón, A. M., Gómez-Fernández, F., & Bascompta, M. J. A. S. (2020). Mine fire behavior under different ventilation conditions: real-scale tests and CFD modeling. 10(10), 3380.

Hansen, R. (2018). Fire statistics from the mining industry in New South Wales, Queensland and Western Australia. Brisbane: The University of Queensland.

Hu, Y., Liu, X., Wang, F., & Cheng, C. (2012). An overview of agent-based evacuation models for building fires. Proceedings of 2012 9th IEEE International Conference on Networking, Sensing and Control,

Hu, Y., Wang, F., & Liu, X. (2014). A CPSS Approach for Emergency Evacuation in Building Fires. IEEE Intelligent Systems, 29(3), 48-52. https://doi.org/10.1109/MIS.2014.38

Hwang, C. C., & Edwards, J. C. (2001). CFD Modeling Of Smoke Reversal. Proceedings of The International Conference on Engineered Fire Protection Design, ...Applying Fire Science to Fire Protection Problems, San Francisco, CA, June 11-15, 2001. Bethesda, MD: Society of Fire Protection Engineers, Inc., 2001 Jun; :376-387, Bethesda, MD.

Kuligowski, E. D. (2008). Modeling human behavior during building fires.

Li, C., Li, J., Hu, L., & Hou, D. (2015). Visualization and simulation model of underground mine fire disaster based on Cellular Automata. Applied Mathematical Modelling, 39(15), 4351-4364. https://doi.org/https://doi.org/10.1016/j.apm.2014.12.051

Li, J. S. M., & Chow, W. K. (2003). Numerical studies on performance evaluation of tunnel ventilation safety systems. Tunnelling and Underground Space Technology, 18(5), 435-452. https://doi.org/https://doi.org/10.1016/S0886-7798(03)00023-3

Li, Y. Z., & Ingason, H. (2012). The maximum ceiling gas temperature in a large tunnel fire. Fire Safety Journal, 48, 38-48.

Mossberg, A., Nilsson, D., & Wahlqvist, J. J. F. S. J. (2021). Evacuation elevators in an underground metro station: A Virtual Reality evacuation experiment. 120, 103091.

Nguyen, M. H., Ho, T. V., & Zucker, J.-D. (2013). Integration of smoke effect and blind evacuation strategy (SEBES) within fire evacuation simulation. Simulation Modelling Practice and Theory, 36, 44-59.

NIOSH. (2021). Mine Disasters by Accident Type, 1839-2021 Retrieved Accessed May 22, 2023 from https://wwwn.cdc.gov/NIOSH-Mining/MMWC/MineDisasters/AccidentType

Poon, L. S. J. F. S. S. (1994). EvacSim: a simulation model of occupants with behavioural attributes in emergency evacuation of high-rise building fires. 4, 681-692.

Salami , O. B., Xu, G., Kumar, A. R., & Pushparaj, R. I. (2023). Underground mining fire hazards and the optimization of emergency evacuation strategies (EES): The issues, existing methodology and limitations, and way forward. Process Safety and Environmental Protection, 177, 617-634. https://doi.org/https://doi.org/10.1016/j.psep.2023.07.012

Shen, T.-S. (2005). ESM: a building evacuation simulation model. Building and Environment, 40(5), 671-680. https://doi.org/https://doi.org/10.1016/j.buildenv.2004.08.029

Stewart, C. (2021). Challenges and solutions in the development of the VentFIRE mine network fire simulator. In Mine Ventilation (pp. 300-308). CRC Press.

Tan, L., Hu, M., & Lin, H. (2015). Agent-based simulation of building evacuation: Combining human behavior with predictable spatial accessibility in a fire emergency. Information Sciences, 295, 53-66.

Tang, W., Yuan, L., Bahrami, D., & Rowland, J. (2021). Water spray suppression of leaked oil fires: A numerical study. In Mine Ventilation (pp. 309-316). CRC Press.

Yuan, J.-P., Fang, Z., Yin, Z.-C., Lo, S.-M. J. T. J. y. H. G. J. o. C., Architectural, & Engineering, E. (2009). Combined network model for occupant evacuation in building fires. 31(2).

Yuan, L., & Smith, A. C. (2015). Numerical modeling of water spray suppression of conveyor belt fires in a large-scale tunnel. Process Safety and Environmental Protection, 95, 93-101. https://doi.org/https://doi.org/10.1016/j.psep.2015.02.018

Zhu, Y., Wang, D., Shao, Z., Xu, C., Zhu, X., Qi, X., & Liu, F. (2019). A statistical analysis of coalmine fires and explosions in China. Process Safety and Environmental Protection, 121, 357-366. https://doi.org/https://doi.org/10.1016/j.psep.2018.11.013

VITA

Salami received in PhD in Mining Engineering from Missouri University of Science and Technology in May 2024. Prior to that, he obtained a bachelor's degree in Mining Engineering with first class honors from the Federal University of Technology Akure, Nigeria in 2016 and a Master graduate certificate in oil and gas field development Engineering from the Xian University of Petroleum in 2020. As a PhD researcher at Missouri S&T under the mentorship of Dr Guang Xu, Salami continued to demonstrate excellence. He published eight articles, and delivered more than fifteen technical presentations on a variety of research findings from his work in the Ventilation, Safety, and Health Lab. Apart from wining more than forty academic awards so far in his career, Salami was a member of many professional organizations including the Honor Society of Geosciences (Sigma Gamma Epsilon), Scientific Research Honor Society (Sigma Xi), American Exploration and Mining Association, Society of Mining Metallurgy and Exploration, International society of Rock Mechanics, and Canadian Institute of Mining and Metallurgy. His future endeavor cuts across mining innovations, energy sustainability, and critical minerals development.